Microtubules in cell migration, morphogenesis and metabolism: Making the connections

Microtubuli in celmigratie, morfogenese en metabolisme: Het maken van verbindingen
(met een samenvatting in het Nederlands)

Proefschrift

ter verkrijging van de graad van doctor aan de Universiteit Utrecht op gezag van de rector magnificus, prof. dr. G.J. van der Zwaan, ingevolge het besluit van het college voor promoties in het openbaar te verdedigen op woensdag 29 november 2017 des middags te 4.15 uur

door

Ivar Noordstra

geboren op 21 mei 1989 te Genemuiden

Promotor: Prof. dr. A.S. Akhmanova

ISBN: 978-90-393-6865-7

The studies described in this thesis were performed at the division of Cell Biology at the Faculty of Science of Utrecht University in Utrecht, The Netherlands.

Main cover by Aron Noordstra: Pencil and watercolor painting reflecting how minor events could lead to major morphogenetic changes.

Photo CV by Julia-fotografie

Layout by Ivar Noordstra

Printed by Gildeprint

“He who wonders discovers that this is in itself a wonder.”

Maurits Cornelis Escher

Table of contents

Chapter 1	General introduction	9
Chapter 2	Linking cortical microtubule attachment and exocytosis	27
Chapter 3	Mesenchymal cell invasion requires cooperative regulation of persistent microtubule growth by SLAIN2 and CLASP1	49
Chapter 4	Control of apico-basal epithelial polarity by the microtubule minus-end-binding protein CAMSAP3 and spectraplakin ACF7	99
Chapter 5	Focal adhesion-associated protein complexes function as docking platforms for insulin granules in pancreatic β-cells	131
Chapter 6	General discussion	153
Addendum	Summary	170
	Nederlandse samenvatting	172
	Curriculum Vitae	175
	List of publications	176
	Dankwoord	177

1

General introduction

Ivar Noordstra[1]

[1]Cell Biology, Faculty of Science, Utrecht University, 3584 CH Utrecht, The Netherlands

1

General introduction

Cells are the basic structural, functional, and biological units of all known living organisms. They were discovered in 1665 by an Englishman, Robert Hooke, who observed a thin slice of cork under a simple microscope. The many small box-like structures reminded him of small rooms called "cells" in which Christian monks lived and meditated. More than 350 years later cells are often referred to as "the building blocks of life". While the number of cells in plants and animals varies from species to species, the human body is made up of around thirty trillion cells which all have their own specialized functions. In order to fulfill these functions, spatial organization of cells is tightly regulated by many different structures and mechanisms. In this thesis we focus on the role of microtubules, major cytoskeletal elements, in cell migration, morphogenesis and metabolism, all of which are essential processes that rely on tightly controlled maintenance of cell polarity.

Cell polarity

Cell polarity refers to a fundamental property of eukaryotic cells, in which cellular components and structures are organized in an asymmetric fashion. This tightly controlled organization enables the cells to fulfill specialized functions. Migrating cells are a classic example of being highly polarized. Cell migration is a process essential for a variety of biological processes ranging from embryonic development to inflammatory response and wound repair. In addition, it drives the development of metastatic cancer. Migrating cells display a front-rear polarity axis in which the leading edge protrudes and binds the extracellular matrix followed by the detachment and retraction of the trailing edge (Etienne-Manneville, 2008) (Figure 1A). Also epithelial cells, which line the surface of the animal body and internal cavities, are famous for their polarity. They adhere to one another through tight junctions, adherens junctions and desmosomes thereby forming a highly specialized and protective layer. Epithelial layers exhibit apico-basal polarity defined by the apical membrane facing the outside surface of the body, and the basolateral surface connecting the cells to surrounding cells and the extracellular matrix (Knust, 2002; Roignot et al., 2013) (Figure 1B). A final example of highly polarized cells are neurons, which receive signals from neighboring cells through their dendrites and propagate action potentials down their axons, resulting in the release of neurotransmitters (Tahirovic and Bradke, 2009) (Figure 1C).

Microtubules

By placing objects containing an intrinsic polarity inside a symmetrical entity, symmetry can be broken. In cells, the role of 'symmetry breaker' is fulfilled by the cytoskeleton, a

network of fibers that provides the cell with structural support and is involved in multiple processes including control of cell shape, organelle anchorage, cell motility, intracellular transport and chromosome segregation. In eukaryotic cells, the cytoskeletal network is composed of three main molecular structures: microtubules, actin filaments and intermediate filaments, which have distinct biological roles and harbor different mechanical properties and dynamics. Here we focus on the microtubule network, which has been shown to be key for breaking symmetry and maintaining cell polarity. Microtubules, which owe their polarity to the asymmetry of their building blocks, have two distinct ends; the minus end and plus end. As microtubules are among the main organizers of cellular polarity, it is not surprising that the organization of both ends is tightly controlled in polarized cells.

The polarity of migrating cells with ruffling leading lamellipodia and contractile rears is reflected by the polarized organization of the underlying microtubule cytoskeleton. The majority of the microtubules are anchored with their minus ends at the centrosome or the Golgi apparatus, major microtubule organizing centers (MTOCs) which are typically positioned between the nucleus and the leading edge. The density of growing microtubule plus ends is higher in the direction of migration (Etienne-Manneville, 2013) (Figure 1A).

The microtubule cytoskeleton of epithelial cells undergoes a dramatic rearrangement during the cellular morphogenesis, in which the cells shift from being unpolarized to an apico-basal polarized organization. In unpolarized cells the microtubule minus ends are clustered in the middle of the cell and the plus ends are pointing towards the cell periphery resulting in a typical astral microtubule array. As cells become polarized, however, the microtubule network changes and becomes arranged along the apico-basal axis, with the minus ends located at the apical side and the plus ends pointing towards the basal cell regions (Bacallao et al., 1989; Troutt and Burnside, 1988) (Figure 1B).

After their final cell division, immature neurons are round unpolarized cells with many of their microtubules anchored at the centrosome. Under the influence of extrinsic signals, the immature neurons start to develop neurites (axon and dendrites), the centrosome becomes inactive, and the microtubule network changes from centrosomal to non-centrosomal (Kuijpers and Hoogenraad, 2011). In mature mammalian neurons, electron microscopy revealed a highly polarized cytoskeletal network with mixed orientation of microtubules in dendrites and a uniform plus-end out orientation in the axon (Baas et al., 1988; Burton, 1988) (Figure 1C).

To understand the function of microtubules in polarity, one has to understand the intrinsic and extrinsic properties that control this phenomenon. Microtubules are long hollow tubes measuring about 25 nm in diameter that stretch throughout the cells cytoplasm. The microtubule wall is constructed from a globular protein called tubulin. Each tubulin molecule is a dimer that consists of two slightly different polypeptide subu-

nits, α-tubulin and β-tubulin, which are attached head to tail into protofilaments. Lateral attachment of the protofilaments gives rise to the typical hollow shape of microtubules, which can be extended by the addition of more α/β-tubulin dimers. Microtubules found in most organisms have thirteen protofilaments, although microtubules composed of fewer or more protofilaments have also been observed (Burton et al., 1975). All protofilaments are arranged in parallel, which gives rise to the intrinsic polarity of microtubules with a fast-growing, highly dynamic plus end and a slow-growing minus end (Akhmanova and Steinmetz, 2015). Despite the structural similarity of α- and β-tubulin, there are some slight differences, resulting in distinct structures at both microtubule ends (Nogales et al., 1998).

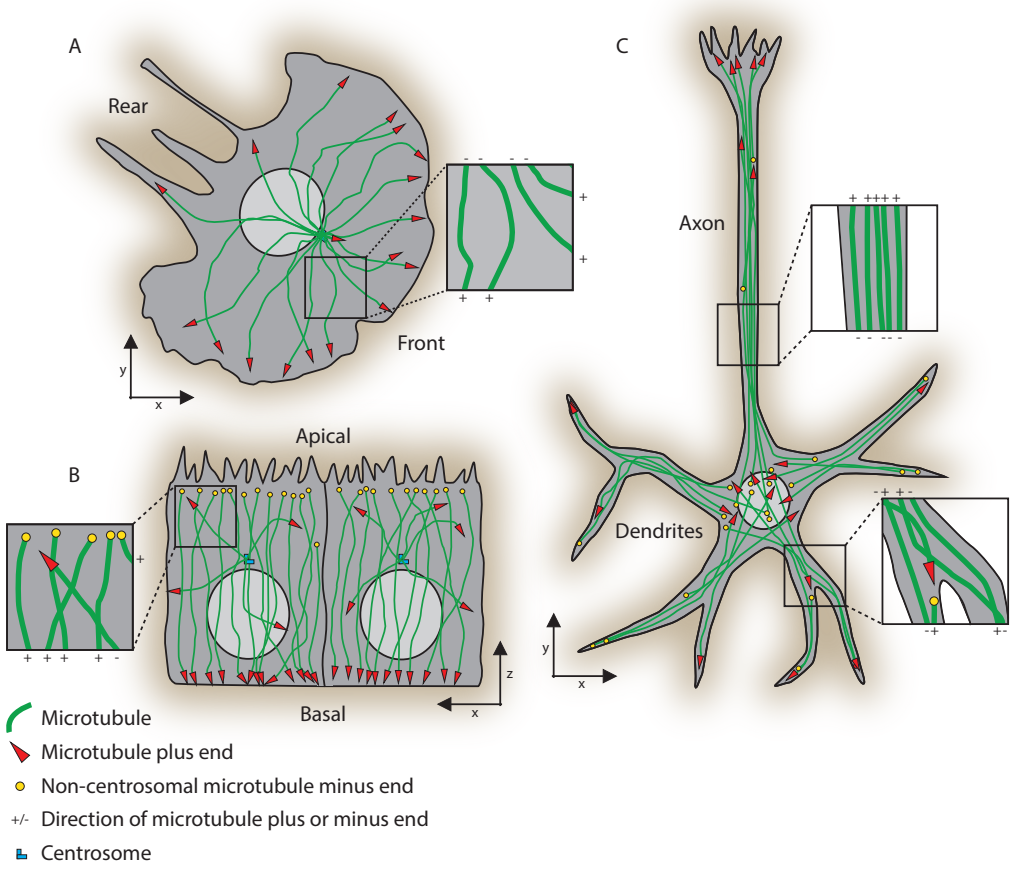

Figure 1. Microtubule organization in different cellular systems
Microtubule organization in **(A)** a migrating cell, **(B)** polarized epithelial cells and **(C)** a neuron.

Microtubule dynamics

The dynamic properties of microtubules enable a cell to quickly respond to environmental and cellular cues. This is powered by the hydrolysis of GTP bound to β-tubulin, which enables microtubules to switch between catastrophes (transition from growth to shrinkage) and rescues (transition from shrinkage to growth). GTP-bound tubulin dimers are incorporated into growing microtubules. After incorporation, the GTP bound to β-tubulin is hydrolyzed to GDP. In a growing microtubule, the addition of GTP-bound tubulin dimers is faster than the hydrolysis from GTP to GDP resulting in a GTP cap, which favors microtubule polymerization. If nucleotide hydrolysis proceeds more rapidly than subunit addition, the GTP cap is lost. GDP bound tubulin dimers reduce the stability of the microtubule tip and the protofilaments curve outwards, resulting in microtubule shrinkage (Akhmanova and Steinmetz, 2015; Desai and Mitchison, 1997).

Microtubule associated proteins

Numerous factors are shown to be involved in the regulation of microtubule dynamics. They can be broadly grouped into microtubule-associated proteins (MAPs) and molecular motor proteins, of which the latter has been shown to be particularly important for cell polarity and will be introduced later. Among the MAPs, the microtubule plus-end tracking proteins (+TIPs), which include structurally and functionally diverse microtubule regulators, are distinguished by their ability to concentrate at growing microtubule ends (Akhmanova and Steinmetz, 2008). Central players among the +TIPs are the members of the end binding (EB) protein family. They autonomously recognize the GTP bound state of growing microtubule ends and thereby recruit a plethora of different binding partners (Bieling et al., 2007; Komarova et al., 2009; Maurer et al., 2012). EBs are shown to reduce catastrophe rates and promote continuous microtubule growth in cells (Komarova et al., 2009; Vitre et al., 2008). Since EBs promote catastrophes *in vitro*, this effect presumably occurs through EB binding partners (Komarova et al., 2009). Over the years many more +TIPs have been found that track microtubule plus ends independently or are linked to plus ends through EBs. The latter fall into two major classes: proteins containing globular cytoskeleton-associated protein-glycine-rich (CAP-Gly) domains and proteins with a short linear motif Ser-any amino acid-Ile-Pro (SxIP) embedded in unstructured positively charged regions. Most +TIPs act as microtubule stabilizers and play additional roles in microtubule capture and signaling, two key processes regulating cell polarity (Akhmanova and Steinmetz, 2008). In addition to +TIPs, a wide range of MAPs has been shown to be associated with the microtubule lattice, thereby controlling microtubule dynamics and organization as well as intracellular transport (Mandelkow and Mandelkow, 1995). Classic examples are MAP2, Tau (Chen et al., 1992), and protein regulator of cytokinesis 1 (PRC1) (Mollinari et al., 2002), which are important for microtubule spacing, bundling and orientation. More recently the field of minus-end

binding proteins (-TIPs) started to emerge. -TIPs, which will be introduced later, have also been shown to play essential roles in controlling microtubule organization and cellular polarity.

Post-translational modifications of tubulin

In addition to MAPs, two different intrinsic properties of microtubules can generate microtubule diversity: expression of different α- and β isoforms, referred to as tubulin isotypes, and posttranslational modifications (PTMs) on α- and β-subunits (Janke, 2014; Song and Brady, 2015). Till now, nine different isotypes have been described for both α- and β-tubulin, and their expression can be cell type specific (Chakraborti et al., 2016). A remarkable number of tubulin PTMs has been found including acetylation of α-tubulin on lysine-40 (L'Hernault and Rosenbaum, 1985; Piperno and Fuller, 1985), the removal of the C-terminal tyrosine from α-tubulin (detyrosination) (Gundersen et al., 1984; Hallak et al., 1977; Thompson, 1977), and the addition of longer or shorter chains of glutamates (glutamylation) (Edde et al., 1990) or glycines (glycylation) (Redeker et al., 1994) to glutamate residues near the C-terminus of both α- and β-tubulin. In addition to these modifications present on tubulins polymerized into microtubules, multiple PTMs were found only on soluble tubulin dimers. PTMs appear to regulate the stability and structure of microtubule assemblies. This regulation might occur through directly affecting microtubule structure or indirectly by regulating the binding of one or more MAPs. Four decades of research revealed that PTMs affect not only microtubule dynamics but also microtubule interactions with other cellular components. As a consequence, there is increasing evidence of tubulin PTMs controlling cell polarity. In particular neuronal polarity strongly relies on PTMs which direct molecular cargoes to specific subcellular regions (Janke and Kneussel, 2010). PTMs were also shown to play a role in organizing the microtubule organization in polarized epithelial cells. For a long time it was known that apico-basally orientated, non-centrosomal microtubules are more stable than the centrosomal microtubules in unpolarized cells (Bartolini and Gundersen, 2006; Bre et al., 1990). Detailed analysis revealed that the morphological transition from unpolarized cells to polarized cells was strongly associated with a substantial decrease in microtubule detyrosination and polyglutamylation, and an increase in microtubule acetylation (Quinones et al., 2011). Whether this is the cause or the result of the change in microtubule stability is a point of debate. However, recent data indicates that microtubules acquire resistance to mechanical stress, thus became more stable upon acetylation (Xu et al., 2017).

Localization and function of microtubule plus- and minus-end associated complexes

As indicated above, positioning of the microtubule ends is essential for obtaining and

maintaining cellular polarity. Since microtubules harbor two distinct ends, different protein complexes have been shown to be involved in linking the ends to specific cellular regions. In most mammalian cell types, microtubule minus ends are nucleated from the centrosome, a widely studied MTOC which is composed of centrioles and the surrounding pericentriolar material (PCM). The PCM consists of multiple proteins that are highly organized (Fu and Glover, 2012; Lawo et al., 2012; Mennella et al., 2012; Sonnen et al., 2012) and together control microtubule nucleation, anchoring and dynamics (Nigg and Raff, 2009; Woodruff et al., 2015). Centrosomal microtubule minus ends are stabilized by γ-tubulin ring complexes (γ-TuRCs), multiprotein ring-shaped complexes that are composed of γ-tubulin and other non-tubulin proteins (Li and Joshi, 1995; Wiese and Zheng, 2000). Since the centrosome is one of the major organizers of microtubules, its positioning controls many important cellular processes including polarity, cell shape regulation, cilia formation and intracellular transport as well as the position of cellular structures, including the mitotic spindle (Tang and Marshall, 2012). In addition to the centrosome, also the Golgi apparatus was shown to be an important MTOC, which functions both as a microtubule nucleation and anchoring site in mammalian cells. Also microtubule nucleation from the Golgi membranes requires the components of the γ-TuRC (Efimov et al., 2007; Rivero et al., 2009). While the Golgi controls the formation of microtubule arrays, microtubules also regulate the organization of the Golgi apparatus. This mainly depends on cytoplasmic dynein-based minus end-directed transport along microtubules (Corthesy-Theulaz et al., 1992). In the absence of microtubules, the Golgi is fragmented and reorganizes into numerous distributed stacks which, nevertheless, remain competent for protein processing and sorting (De Brabander et al., 1977; Rogalski and Singer, 1984). Proper positioning of the Golgi has been linked to multiple polarity associated processes. For example, axon formation in hippocampal neurons occurs at a site faced by the centrosome and Golgi apparatus (de Anda et al., 2005) and migrating fibroblasts reposition their Golgi to the leading edge to face the direction of migration (Kupfer et al., 1982). Although the centrosome and Golgi apparatus can be depicted as the major MTOCs in cells, multiple other nucleation sites have been described (Petry and Vale, 2015). It has been shown that also the nuclear envelope (Robinow and Marak, 1966), chromatin and kinetochores (Heald et al., 1996), and microtubules themselves (Goshima et al., 2008; Janson et al., 2005; Murata et al., 2005) can serve as sites for microtubule nucleation.

As mentioned previously, the γ-TuRC nucleates microtubules and caps their minus ends. However, not all minus-ends are capped with the γ-TuRC, so observations of the γ-TuRC are unlikely to be sufficient for explaining the distribution and behavior of all microtubule minus ends. Recently, a series of studies demonstrated that CAMSAP/Patronin/Nezha family members recognize and regulate microtubule minus ends and control their dynamics in different animal species (Akhmanova and Hoogenraad, 2015;

Goodwin and Vale, 2010; Jiang et al., 2014; Tanaka et al., 2012). Depletion of one or multiple CAMSAP proteins causes a significant loss of non-centrosomal microtubules (Jiang et al., 2014; Nagae et al., 2013; Tanaka et al., 2012) and strongly affects cell polarity in multiple systems. CAMSAP2 knockdown in RPE1 cells perturbed cell migration in a monolayer wound assay. This was explained by a defect in reorientation of the Golgi apparatus towards the wound edge (Jiang et al., 2014; Wu et al., 2016). Interestingly, the non-centrosomal microtubule organization of polarized epithelial cells seems to specifically rely on CAMSAP3 which is localized at the apical domain of the cells (Khanal et al., 2016; Nashchekin et al., 2016; Toya et al., 2016). Depletion of CAMSAP3 affected delivery of cargo destined for the apical membrane (Khanal et al., 2016). RNAi-mediated depletion of specifically CAMSAP2 also led to a significant loss of non-centrosomal microtubules in neurons. As a result, neuronal polarity, axon specification and dendritic branching were strongly affected *in vitro* and *in vivo* (Yau et al., 2014).

The structural differences between the microtubule minus and plus ends facilitate the binding of different protein complexes to either end. As mentioned above, +TIPs are a heterogeneous class of proteins distinguished by their specific accumulation at microtubule plus ends. Multiple +TIPs have been shown to be involved in anchoring microtubule plus ends to different cellular structures. The best-studied microtubule plus-end interaction is the attachment to kinetochores during chromosome alignment and segregation, two key steps of mitosis (Foley and Kapoor, 2013).

A second cellular structure, well known for its interactions with microtubule plus ends, is the cell cortex. Cortical microtubule interactions are facilitated by the cortical microtubule stabilizing complex (CMSC). This multiprotein complex links microtubules to focal adhesions (Bouchet et al., 2016; Lansbergen et al., 2006; van der Vaart et al., 2013), thereby promoting the delivery of exocytotic cargo required for the turnover of focal adhesions (Astro and de Curtis, 2015; Stehbens et al., 2014). In addition, a remarkable number of +TIPs has been shown to interact with IQGAP, a versatile protein that acts as central hub coordinating cytoskeletal organization and membrane trafficking at cortical regions (White et al., 2012). CMSC- as well as IQGAP-mediated cortical microtubule interactions are described in more detail in Chapter 2. Finally, a cytoplasmic dynein based force generating complex links microtubules to the cortex and participates in microtubule network positioning and asymmetric cell divisions (McNally, 2013).

As is the case for the Golgi apparatus, the morphology of the endoplasmic reticulum (ER) strongly relies on microtubules (Gurel et al., 2014). There are two different types of microtubule dependent ER movements: sliding, involving motor based transport along pre-existing stable acytelated microtubules and movement mediated by +TIP-dependent attachment to the growing plus ends of microtubules (Friedman et al., 2010; Grigoriev et al., 2008; Waterman-Storer and Salmon, 1998).

Lastly, multiple +TIPs have been shown to mediate the interaction between mi-

crotubule plus ends and other cytoskeletal structures, including the lattice of microtubules themselves. The latter is mainly driven by plus end-bound microtubule motors that walk on neighboring microtubules (Chen et al., 2014; Doodhi et al., 2014; Mattie et al., 2010). This microtubule guidance was shown to be essential in creating a uniform microtubule polarity in dendrites of fly neurons (Mattie et al., 2010), but could also apply to other systems which depend on a tightly controlled microtubule organization. Direct interactions between microtubule plus ends and actin filaments are mediated by spectraplakins, very large proteins containing microtubule as well as actin binding domains that are involved in a wide range of cellular processes (Suozzi et al., 2012). Recently, spectraplakins were also shown to interact with microtubule minus ends thereby controlling the apico-basal microtubule organization in polarized epithelial cells and focal adhesion turnover during cell migration (Khanal et al., 2016; Nashchekin et al., 2016; Ning et al., 2016). In addition to the spectraplakin-based direct interactions, microtubule plus ends can be linked to actin via multiprotein complexes. In yeast the EB1 homologue Bim1p was shown to recruit the class V myosin Myo2p trough an interaction with Kar9p, thereby forming a protein complex essential for yeast cell polarization (Yin et al., 2000). In vertebrate cells a similar +TIP complex was found composed of EB1, melanophilin and Myosin Va, which mediated the transfer of melanosomes from microtubules to actin (Wu et al., 2005).

Regulation of polarity by microtubules

Microtubules are key in breaking symmetry thereby providing the polarity that is needed for cells to fulfill their dedicated functions in multicellular organisms. As described above, the organization of microtubules is controlled in many different ways ranging from the intrinsic properties of α and β-tubulin to associated proteins that link microtubule ends to well-defined cellular structures. But the question remains how cells employ this cytoskeletal system to create and maintain polarity. One of the major functions of microtubules is to serve as tracks for motor proteins, kinesins and cytoplasmic dynein, which use energy derived from ATP hydrolysis to transport membranes, proteins and mRNA molecules. Kinesins mostly walk to the microtubule plus end (Hirokawa et al., 2009) and dynein walks to the minus end (Roberts et al., 2013). Although there is a single dynein responsible for cytoplasmic transport, 45 mammalian kinesin superfamily (KIF) genes classified into 14 families are known up to date. Many of them have multiple specific regulatory proteins which together cover a whole additional level of polarity control. In addition, motor proteins not only employ microtubules as tracks for transport, but also regulate microtubule dynamics and organization (Drummond, 2011; Laan et al., 2012; Yogev et al., 2017).

Microtubule tips can concentrate signaling molecules, such as Rho GTPase guanine nucleotide exchange factors (GEFs) (Jiang et al., 2012; Rogers et al., 2004) which

are major regulators of actin dynamics (Sit and Manser, 2011). Actin dynamics and in particular the regulation by the Rho GTPases CDC42, Rac and Rho are tightly associated with formation of actin based protrusions and actomyosin contractility. For this reason, local regulation by microtubule plus-end specific signaling platforms has a strong influence on cell morphology and polarity as can be seen in neurons (van Haren et al., 2014) and migrating cells (Etienne-Manneville, 2013).

Finally, microtubules are able to resist compressive loads and generate forces of a few pN, comparable to the forces generated by motor proteins (Brangwynne et al., 2007; Dogterom and Yurke, 1997). Since those forces are sufficient to deform membranes (Fygenson et al., 1997; Laan et al., 2008), microtubules could potentially change cell morphology thereby creating polarity. Interestingly, plasma membrane deformation and protrusion formation, as can been seen in migrating cells, is in general accompanied by a higher microtubule density, and thus higher forces (Wadsworth, 1999). As mentioned above, tubulin PTMs and MAPs have a strong influence on microtubule stability and mechanical properties. Interestingly, several stabilizing MAPs are highly expressed in neurons where microtubules are particularly important for supporting cell protrusions (Kuijpers and Hoogenraad, 2011). However, more detailed cell biological studies will be needed to understand to what extend mechanical properties of microtubules contribute to cell polarity.

Scope of the thesis

Many cellular systems and processes strongly rely on tightly regulated polarity which is maintained by the microtubule cytoskeleton. In this thesis we studied the microtubule-associated molecular mechanisms underlying polarity in different cellular backgrounds including metastatic breast cancer cells, polarized intestinal epithelial cells and insulin producing pancreatic β-cells.

In **Chapter 2**, we provide an overview of mammalian protein complexes that have been shown to participate in cortical microtubule capture and exocytosis, thereby regulating the spatial organization of secretion.

In **Chapter 3**, we describe a specific role for microtubule dynamics in 3D cell migration. We found that in 3D cultured cells, growing microtubules continuously target the outmost tip of migrating cells thereby possibly generating an anterograde force. This force may antagonize cell retraction and thus promote the formation and maintenance of extended cell protrusions. In addition, we show that in 3D, processive microtubule growth was maintained by SLAIN2 and CLASP1, two +TIPs that inhibit microtubule catastrophes and thereby support microtubule load-bearing functions.

In **Chapter 4**, we report that spectraplakin ACF7 is a binding partner of CAMSAP3. We reveal that this interaction is required for the apical localization of CAMSAP3-decorated microtubule minus ends in polarized intestinal epithelial cells.

We also evaluate the effect of the loss of ACF7 and CAMSAP3 on 3D polarized cyst formation and the organization of the apical actin network thereby providing new insights in the molecular mechanisms underlying these processes.

In **Chapter 5**, we examine the multiprotein complexes in pancreatic β-cells that are responsible for the docking of insulin containing granules. We show that these complexes consist of cortical microtubule stabilizing complex subunits and proteins which previously have been demonstrated to be involved in neurotransmitter release at the presynaptic active zone in neurons. We found that, upon increased actomyosin contractility and focal adhesion activation, insulin docking complexes accumulate in the vicinity of focal adhesions, thereby creating potential hotspots for insulin secretion.

In **Chapter 6**, we discuss how microtubules and microtubule associated proteins control cell migration, morphogenesis and metabolism. We combine our work on metastatic breast cancer cells (Chapter 3), polarized epithelia (Chapter 4) and pancreatic β-cells (Chapter 5) and put it in a broader perspective.

References

Akhmanova, A., and C.C. Hoogenraad. 2015. Microtubule minus-end-targeting proteins. Curr Biol. 25:R162-171.Akhmanova, A., and M.O. Steinmetz. 2008. Tracking the ends: a dynamic protein network controls the fate of microtubule tips. Nat Rev Mol Cell Biol. 9:309-322.

Akhmanova, A., and M.O. Steinmetz. 2015. Control of microtubule organization and dynamics: two ends in the limelight. Nat Rev Mol Cell Biol. 16:711-726.

Astro, V., and I. de Curtis. 2015. Plasma membrane-associated platforms: dynamic scaffolds that organize membrane-associated events. Sci Signal. 8:re1.

Baas, P.W., J.S. Deitch, M.M. Black, and G.A. Banker. 1988. Polarity orientation of microtubules in hippocampal neurons: uniformity in the axon and nonuniformity in the dendrite. Proc Natl Acad Sci U S A. 85:8335-8339.

Bacallao, R., C. Antony, C. Dotti, E. Karsenti, E.H. Stelzer, and K. Simons. 1989. The subcellular organization of Madin-Darby canine kidney cells during the formation of a polarized epithelium. J Cell Biol. 109:2817-2832.

Bartolini, F., and G.G. Gundersen. 2006. Generation of noncentrosomal microtubule arrays. J Cell Sci. 119:4155-4163.

Bieling, P., L. Laan, H. Schek, E.L. Munteanu, L. Sandblad, M. Dogterom, D. Brunner, and T. Surrey. 2007. Reconstitution of a microtubule plus-end tracking system in vitro. Nature. 450:1100-1105.

Bouchet, B.P., R.E. Gough, Y.C. Ammon, D. van de Willige, H. Post, G. Jacquemet, A.M. Altelaar, A.J. Heck, B.T. Goult, and A. Akhmanova. 2016. Talin-KANK1 interaction controls the recruitment of cortical microtubule stabilizing complexes to focal adhesions. Elife. 5.

Brangwynne, C.P., F.C. MacKintosh, and D.A. Weitz. 2007. Force fluctuations and polymerization dynamics of intracellular microtubules. Proc Natl Acad Sci U S A. 104:16128-16133.

Bre, M.H., R. Pepperkok, A.M. Hill, N. Levilliers, W. Ansorge, E.H. Stelzer, and E. Karsenti. 1990. Regulation of microtubule dynamics and nucleation during polarization in MDCK II cells. J Cell Biol. 111:3013-3021.

Burton, P.R. 1988. Dendrites of mitral cell neurons contain microtubules of opposite polarity. Brain Res. 473:107-115.

Burton, P.R., R.E. Hinkley, and G.B. Pierson. 1975. Tannic acid-stained microtubules with 12, 13, and 15 protofilaments. J Cell Biol. 65:227-233.

Chakraborti, S., K. Natarajan, J. Curiel, C. Janke, and J. Liu. 2016. The emerging role of the tubulin code: From the tubulin molecule to neuronal function and disease. Cytoskeleton (Hoboken). 73:521-550.

Chen, J., Y. Kanai, N.J. Cowan, and N. Hirokawa. 1992. Projection domains of MAP2 and tau determine spacings between microtubules in dendrites and axons. Nature. 360:674-677.

Chen, Y., M.M. Rolls, and W.O. Hancock. 2014. An EB1-kinesin complex is sufficient to steer microtubule growth in vitro. Curr Biol. 24:316-321.

Corthesy-Theulaz, I., A. Pauloin, and S.R. Pfeffer. 1992. Cytoplasmic dynein participates in the centrosomal localization of the Golgi complex. J Cell Biol. 118:1333-1345.

de Anda, F.C., G. Pollarolo, J.S. Da Silva, P.G. Camoletto, F. Feiguin, and C.G. Dotti. 2005. Centrosome localization determines neuronal polarity. Nature. 436:704-708.

De Brabander, M., J. De May, M. Joniau, and G. Geuens. 1977. Ultrastructural immunocytochemical distribution of tubulin in cultured cells treated with microtubule inhibitors. Cell Biol Int Rep. 1:177-183.

Desai, A., and T.J. Mitchison. 1997. Microtubule polymerization dynamics. Annu Rev Cell Dev Biol. 13:83-117.

Dogterom, M., and B. Yurke. 1997. Measurement of the force-velocity relation for growing microtubules. Science. 278:856-860.

Doodhi, H., E.A. Katrukha, L.C. Kapitein, and A. Akhmanova. 2014. Mechanical and geometrical constraints control kinesin-based microtubule guidance. Curr Biol. 24:322-328.

Drummond, D.R. 2011. Regulation of microtubule

dynamics by kinesins. Semin Cell Dev Biol. 22:927-934.

Edde, B., J. Rossier, J.P. Le Caer, E. Desbruyeres, F. Gros, and P. Denoulet. 1990. Posttranslational glutamylation of alpha-tubulin. Science. 247:83-85.

Efimov, A., A. Kharitonov, N. Efimova, J. Loncarek, P.M. Miller, N. Andreyeva, P. Gleeson, N. Galjart, A.R. Maia, I.X. McLeod, J.R. Yates, 3rd, H. Maiato, A. Khodjakov, A. Akhmanova, and I. Kaverina. 2007. Asymmetric CLASP-dependent nucleation of noncentrosomal microtubules at the trans-Golgi network. Dev Cell. 12:917-930.

Etienne-Manneville, S. 2008. Polarity proteins in migration and invasion. Oncogene. 27:6970-6980.

Etienne-Manneville, S. 2013. Microtubules in cell migration. Annu Rev Cell Dev Biol. 29:471-499.

Foley, E.A., and T.M. Kapoor. 2013. Microtubule attachment and spindle assembly checkpoint signalling at the kinetochore. Nat Rev Mol Cell Biol. 14:25-37.

Friedman, J.R., B.M. Webster, D.N. Mastronarde, K.J. Verhey, and G.K. Voeltz. 2010. ER sliding dynamics and ER-mitochondrial contacts occur on acetylated microtubules. J Cell Biol. 190:363-375.

Fu, J., and D.M. Glover. 2012. Structured illumination of the interface between centriole and peri-centriolar material. Open Biol. 2:120104.

Fygenson, D.K., J.F. Marko, and A. Libchaber. 1997. Mechanisms of microtubule-based membrane extension. Phys Rev Lett. 79.

Goodwin, S.S., and R.D. Vale. 2010. Patronin regulates the microtubule network by protecting microtubule minus ends. Cell. 143:263-274.

Goshima, G., M. Mayer, N. Zhang, N. Stuurman, and R.D. Vale. 2008. Augmin: a protein complex required for centrosome-independent microtubule generation within the spindle. J Cell Biol. 181:421-429.

Grigoriev, I., S.M. Gouveia, B. van der Vaart, J. Demmers, J.T. Smyth, S. Honnappa, D. Splinter, M.O. Steinmetz, J.W. Putney, Jr., C.C. Hoogenraad, and A. Akhmanova. 2008. STIM1 is a MT-plus-end-tracking protein involved in remodeling of the ER. Curr Biol. 18:177-182.

Gundersen, G.G., M.H. Kalnoski, and J.C. Bulinski. 1984. Distinct populations of microtubules: tyrosinated and nontyrosinated alpha tubulin are distributed differently in vivo. Cell. 38:779-789.

Gurel, P.S., A.L. Hatch, and H.N. Higgs. 2014. Connecting the cytoskeleton to the endoplasmic reticulum and Golgi. Curr Biol. 24:R660-672.

Hallak, M.E., A. Rodrigues, H.S. Barra, and R. Caputto. 1977. Release of tyrosine from tyrosinated tubulin. Some common factors that affect this process and the assembly of tubulin. FEBS Lett. 73.

Heald, R., R. Tournebize, T. Blank, R. Sandaltzopoulos, P. Becker, A. Hyman, and E. Karsenti. 1996. Self-organization of microtubules into bipolar spindles around artificial chromosomes in Xenopus egg extracts. Nature. 382:420-425.

Hirokawa, N., Y. Noda, Y. Tanaka, and S. Niwa. 2009. Kinesin superfamily motor proteins and intracellular transport. Nat Rev Mol Cell Biol. 10:682-696.

Janke, C. 2014. The tubulin code: molecular components, readout mechanisms, and functions. J Cell Biol. 206:461-472.

Janke, C., and M. Kneussel. 2010. Tubulin post-translational modifications: encoding functions on the neuronal microtubule cytoskeleton. Trends Neurosci. 33:362-372.

Janson, M.E., T.G. Setty, A. Paoletti, and P.T. Tran. 2005. Efficient formation of bipolar microtubule bundles requires microtubule-bound gamma-tubulin complexes. J Cell Biol. 169:297-308.

Jiang, K., S. Hua, R. Mohan, I. Grigoriev, K.W. Yau, Q. Liu, E.A. Katrukha, A.F. Altelaar, A.J. Heck, C.C. Hoogenraad, and A. Akhmanova. 2014. Microtubule minus-end stabilization by polymerization-driven CAMSAP deposition. Dev Cell. 28:295-309.

Jiang, K., G. Toedt, S. Montenegro Gouveia, N.E. Davey, S. Hua, B. van der Vaart, I. Grigoriev, J. Larsen, L.B. Pedersen, K. Bezstarosti, M. Lince-Faria, J. Demmers, M.O. Steinmetz, T.J. Gibson, and A. Akhmanova. 2012. A Proteome-wide screen for mammalian SxIP motif-containing microtubule plus-end tracking proteins. Curr Biol. 22:1800-1807.

Khanal, I., A. Elbediwy, C. Diaz de la Loza Mdel, G.C. Fletcher, and B.J. Thompson. 2016. Shot and Patronin polarise microtubules to direct

membrane traffic and biogenesis of microvilli in epithelia. J Cell Sci. 129:2651-2659.

Knust, E. 2002. Regulation of epithelial cell shape and polarity by cell-cell adhesion (Review). Mol Membr Biol. 19:113-120.

Komarova, Y., C.O. De Groot, I. Grigoriev, S.M. Gouveia, E.L. Munteanu, J.M. Schober, S. Honnappa, R.M. Buey, C.C. Hoogenraad, M. Dogterom, G.G. Borisy, M.O. Steinmetz, and A. Akhmanova. 2009. Mammalian end binding proteins control persistent microtubule growth. J Cell Biol. 184:691-706.

Kuijpers, M., and C.C. Hoogenraad. 2011. Centrosomes, microtubules and neuronal development. Mol Cell Neurosci. 48:349-358.

Kupfer, A., D. Louvard, and S.J. Singer. 1982. Polarization of the Golgi apparatus and the microtubule-organizing center in cultured fibroblasts at the edge of an experimental wound. Proc Natl Acad Sci U S A. 79:2603-2607.

L'Hernault, S.W., and J.L. Rosenbaum. 1985. Chlamydomonas alpha-tubulin is posttranslationally modified by acetylation on the epsilon-amino group of a lysine. Biochemistry. 24:473-478.

Laan, L., J. Husson, E.L. Munteanu, J.W. Kerssemakers, and M. Dogterom. 2008. Force-generation and dynamic instability of microtubule bundles. Proc Natl Acad Sci U S A. 105:8920-8925.

Laan, L., N. Pavin, J. Husson, G. Romet-Lemonne, M. van Duijn, M.P. Lopez, R.D. Vale, F. Julicher, S.L. Reck-Peterson, and M. Dogterom. 2012. Cortical dynein controls microtubule dynamics to generate pulling forces that position microtubule asters. Cell. 148:502-514.

Lansbergen, G., I. Grigoriev, Y. Mimori-Kiyosue, T. Ohtsuka, S. Higa, I. Kitajima, J. Demmers, N. Galjart, A.B. Houtsmuller, F. Grosveld, and A. Akhmanova. 2006. CLASPs attach microtubule plus ends to the cell cortex through a complex with LL5beta. Dev Cell. 11:21-32.

Lawo, S., M. Hasegan, G.D. Gupta, and L. Pelletier. 2012. Subdiffraction imaging of centrosomes reveals higher-order organizational features of pericentriolar material. Nat Cell Biol. 14:1148-1158.

Li, Q., and H.C. Joshi. 1995. Gamma-tubulin is a minus end-specific microtubule binding protein. J Cell Biol. 131:207-214.

Mandelkow, E., and E.M. Mandelkow. 1995. Microtubules and microtubule-associated proteins. Curr Opin Cell Biol. 7:72-81.

Mattie, F.J., M.M. Stackpole, M.C. Stone, J.R. Clippard, D.A. Rudnick, Y. Qiu, J. Tao, D.L. Allender, M. Parmar, and M.M. Rolls. 2010. Directed microtubule growth, +TIPs, and kinesin-2 are required for uniform microtubule polarity in dendrites. Curr Biol. 20:2169-2177.

Maurer, S.P., F.J. Fourniol, G. Bohner, C.A. Moores, and T. Surrey. 2012. EBs recognize a nucleotide-dependent structural cap at growing microtubule ends. Cell. 149:371-382.

McNally, F.J. 2013. Mechanisms of spindle positioning. J Cell Biol. 200:131-140.

Mennella, V., B. Keszthelyi, K.L. McDonald, B. Chhun, F. Kan, G.C. Rogers, B. Huang, and D.A. Agard. 2012. Subdiffraction-resolution fluorescence microscopy reveals a domain of the centrosome critical for pericentriolar material organization. Nat Cell Biol. 14:1159-1168.

Mollinari, C., J.P. Kleman, W. Jiang, G. Schoehn, T. Hunter, and R.L. Margolis. 2002. PRC1 is a microtubule binding and bundling protein essential to maintain the mitotic spindle midzone. J Cell Biol. 157:1175-1186.

Murata, T., S. Sonobe, T.I. Baskin, S. Hyodo, S. Hasezawa, T. Nagata, T. Horio, and M. Hasebe. 2005. Microtubule-dependent microtubule nucleation based on recruitment of gamma-tubulin in higher plants. Nat Cell Biol. 7:961-968.

Nagae, S., W. Meng, and M. Takeichi. 2013. Non-centrosomal microtubules regulate F-actin organization through the suppression of GEF-H1 activity. Genes Cells. 18:387-396.

Nashchekin, D., A.R. Fernandes, and D. St Johnston. 2016. Patronin/Shot Cortical Foci Assemble the Noncentrosomal Microtubule Array that Specifies the Drosophila Anterior-Posterior Axis. Dev Cell. 38:61-72.

Nigg, E.A., and J.W. Raff. 2009. Centrioles, centrosomes, and cilia in health and disease. Cell. 139:663-678.

Ning, W., Y. Yu, H. Xu, X. Liu, D. Wang, J. Wang, Y. Wang, and W. Meng. 2016. The CAMSAP3-ACF7 Complex Couples Noncentrosomal Microtubules with Actin Filaments to Coordinate Their Dynamics. Dev Cell. 39:61-74.

Nogales, E., S.G. Wolf, and K.H. Downing. 1998. Structure of the alpha beta tubulin dimer by electron crystallography. Nature. 391:199-203.

Petry, S., and R.D. Vale. 2015. Microtubule nucleation at the centrosome and beyond. Nat Cell Biol. 17:1089-1093.

Piperno, G., and M.T. Fuller. 1985. Monoclonal antibodies specific for an acetylated form of alpha-tubulin recognize the antigen in cilia and flagella from a variety of organisms. J Cell Biol. 101:2085-2094.

Quinones, G.B., B.A. Danowski, A. Devaraj, V. Singh, and L.A. Ligon. 2011. The posttranslational modification of tubulin undergoes a switch from detyrosination to acetylation as epithelial cells become polarized. Mol Biol Cell. 22:1045-1057.

Redeker, V., N. Levilliers, J.M. Schmitter, J.P. Le Caer, J. Rossier, A. Adoutte, and M.H. Bre. 1994. Polyglycylation of tubulin: a posttranslational modification in axonemal microtubules. Science. 266:1688-1691.

Rivero, S., J. Cardenas, M. Bornens, and R.M. Rios. 2009. Microtubule nucleation at the cis-side of the Golgi apparatus requires AKAP450 and GM130. EMBO J. 28:1016-1028.

Roberts, A.J., T. Kon, P.J. Knight, K. Sutoh, and S.A. Burgess. 2013. Functions and mechanics of dynein motor proteins. Nat Rev Mol Cell Biol. 14:713-726.

Robinow, C.F., and J. Marak. 1966. A fiber apparatus in the nucleus of the yeast cell. J Cell Biol. 29:129-151.

Rogalski, A.A., and S.J. Singer. 1984. Associations of elements of the Golgi apparatus with microtubules. J Cell Biol. 99:1092-1100.

Rogers, S.L., U. Wiedemann, U. Hacker, C. Turck, and R.D. Vale. 2004. Drosophila RhoGEF2 associates with microtubule plus ends in an EB1-dependent manner. Curr Biol. 14:1827-1833.

Roignot, J., X. Peng, and K. Mostov. 2013. Polarity in mammalian epithelial morphogenesis. Cold Spring Harb Perspect Biol. 5.

Sit, S.T., and E. Manser. 2011. Rho GTPases and their role in organizing the actin cytoskeleton. J Cell Sci. 124:679-683.

Song, Y., and S.T. Brady. 2015. Post-translational modifications of tubulin: pathways to functional diversity of microtubules. Trends Cell Biol. 25:125-136.

Sonnen, K.F., L. Schermelleh, H. Leonhardt, and E.A. Nigg. 2012. 3D-structured illumination microscopy provides novel insight into architecture of human centrosomes. Biol Open. 1:965-976.

Stehbens, S.J., M. Paszek, H. Pemble, A. Ettinger, S. Gierke, and T. Wittmann. 2014. CLASPs link focal-adhesion-associated microtubule capture to localized exocytosis and adhesion site turnover. Nat Cell Biol. 16:561-573.

Suozzi, K.C., X. Wu, and E. Fuchs. 2012. Spectraplakins: master orchestrators of cytoskeletal dynamics. J Cell Biol. 197:465-475.

Tahirovic, S., and F. Bradke. 2009. Neuronal polarity. Cold Spring Harb Perspect Biol. 1:a001644.

Tanaka, N., W. Meng, S. Nagae, and M. Takeichi. 2012. Nezha/CAMSAP3 and CAMSAP2 cooperate in epithelial-specific organization of noncentrosomal microtubules. Proc Natl Acad Sci U S A. 109:20029-20034.

Tang, N., and W.F. Marshall. 2012. Centrosome positioning in vertebrate development. J Cell Sci. 125:4951-4961.

Thompson, W.C. 1977. Post-translational addition of tyrosine to alpha tubulin in vivo in intact brain and in myogenic cells in culture. FEBS Lett. 80:9-13.

Toya, M., S. Kobayashi, M. Kawasaki, G. Shioi, M. Kaneko, T. Ishiuchi, K. Misaki, W. Meng, and M. Takeichi. 2016. CAMSAP3 orients the apical-to-basal polarity of microtubule arrays in epithelial cells. Proc Natl Acad Sci U S A. 113:332-337.

Troutt, L.L., and B. Burnside. 1988. The unusual microtubule polarity in teleost retinal pigment epithelial cells. J Cell Biol. 107:1461-1464.

van der Vaart, B., W.E. van Riel, H. Doodhi, J.T. Kevenaar, E.A. Katrukha, L. Gumy, B.P. Bouchet, I. Grigoriev, S.A. Spangler, K.L. Yu, P.S. Wulf, J. Wu, G. Lansbergen, E.Y. van Battum, R.J. Pasterkamp, Y. Mimori-Kiyosue, J. Demmers, N. Olieric, I.V. Maly, C.C. Hoogenraad, and A. Akhmanova. 2013. CFEOM1-associated kinesin KIF21A is a cortical microtubule growth inhibitor. Dev Cell. 27:145-160.

van Haren, J., J. Boudeau, S. Schmidt, S. Basu, Z. Liu, D. Lammers, J. Demmers, J. Benhari, F. Grosveld, A. Debant, and N. Galjart. 2014. Dy-

namic microtubules catalyze formation of navigator-TRIO complexes to regulate neurite extension. Curr Biol. 24:1778-1785.

Vitre, B., F.M. Coquelle, C. Heichette, C. Garnier, D. Chretien, and I. Arnal. 2008. EB1 regulates microtubule dynamics and tubulin sheet closure in vitro. Nat Cell Biol. 10:415-421.

Wadsworth, P. 1999. Regional regulation of microtubule dynamics in polarized, motile cells. Cell Motil Cytoskeleton. 42:48-59.

Waterman-Storer, C.M., and E.D. Salmon. 1998. Endoplasmic reticulum membrane tubules are distributed by microtubules in living cells using three distinct mechanisms. Curr Biol. 8:798-806.

White, C.D., H.H. Erdemir, and D.B. Sacks. 2012. IQGAP1 and its binding proteins control diverse biological functions. Cell Signal. 24:826-834.

Wiese, C., and Y. Zheng. 2000. A new function for the gamma-tubulin ring complex as a microtubule minus-end cap. Nat Cell Biol. 2.

Woodruff, J.B., O. Wueseke, V. Viscardi, J. Mahamid, S.D. Ochoa, J. Bunkenborg, P.O. Widlund, A. Pozniakovsky, E. Zanin, S. Bahmanyar, A. Zinke, S.H. Hong, M. Decker, W. Baumeister, J.S. Andersen, K. Oegema, and A.A. Hyman. 2015. Centrosomes. Regulated assembly of a supramolecular centrosome scaffold in vitro. Science. 348:808-812.

Wu, J., C. de Heus, Q. Liu, B.P. Bouchet, I. Noordstra, K. Jiang, S. Hua, M. Martin, C. Yang, I. Grigoriev, E.A. Katrukha, A.F. Altelaar, C.C. Hoogenraad, R.Z. Qi, J. Klumperman, and A. Akhmanova. 2016. Molecular Pathway of Microtubule Organization at the Golgi Apparatus. Dev Cell. 39:44-60.

Wu, X.S., G.L. Tsan, and J.A. Hammer, 3rd. 2005. Melanophilin and myosin Va track the microtubule plus end on EB1. J Cell Biol. 171:201-207.

Xu, Z., L. Schaedel, D. Portran, A. Aguilar, J. Gaillard, M.P. Marinkovich, M. Thery, and M.V. Nachury. 2017. Microtubules acquire resistance from mechanical breakage through intralumenal acetylation. Science. 356:328-332.

Yau, K.W., S.F. van Beuningen, I. Cunha-Ferreira, B.M. Cloin, E.Y. van Battum, L. Will, P. Schatzle, R.P. Tas, J. van Krugten, E.A. Katrukha, K. Jiang, P.S. Wulf, M. Mikhaylova, M. Harterink, R.J. Pasterkamp, A. Akhmanova, L.C. Kapitein, and C.C. Hoogenraad. 2014. Microtubule minus-end binding protein CAMSAP2 controls axon specification and dendrite development. Neuron. 82:1058-1073.

Yin, H., D. Pruyne, T.C. Huffaker, and A. Bretscher. 2000. Myosin V orientates the mitotic spindle in yeast. Nature. 406:1013-1015.

Yogev, S., C.I. Maeder, R. Cooper, M. Horowitz, A.G. Hendricks, and K. Shen. 2017. Local inhibition of microtubule dynamics by dynein is required for neuronal cargo distribution. Nat Commun. 8:15063.

2

Linking cortical microtubule attachment and exocytosis

Ivar Noordstra[1] and Anna Akhmanova[1]

F1000Research (2017); 6:469

[1]Cell Biology, Faculty of Science, Utrecht University, 3584 CH Utrecht, The Netherlands

Summary

Exocytosis is a fundamental cellular process whereby secreted molecules are packaged into vesicles that move along cytoskeletal filaments and fuse with the plasma membrane. To function optimally, cells are strongly dependent on precisely controlled delivery of exocytotic cargo. In mammalian cells, microtubules serve as major tracks for vesicle transport by motor proteins, and thus microtubule organization is important for targeted delivery of secretory carriers. Over the years, multiple microtubule-associated and cortical proteins have been discovered that facilitate the interaction between the microtubule plus ends and the cell cortex. In this review, we focus on mammalian protein complexes that have been shown to participate in both cortical microtubule capture and exocytosis, thereby regulating the spatial organization of secretion. These complexes include microtubule plus-end tracking proteins, scaffolding factors, actin-binding proteins, and components of vesicle docking machinery, which together allow efficient coordination of cargo transport and release.

Review

Exocytosis is a secretory trafficking process during which molecules are processed and transported to the cell surface, where they can be either released into the extracellular space or inserted into the plasma membrane. Secretory transport occurs in multiple steps: after budding from the Golgi, exocytotic vesicles travel along cytoskeletal filaments toward the cell periphery, come into contact with tethering factors that can restrain them, and subsequently dock and fuse with the plasma membrane with the aid of soluble NSF attachment protein receptors (SNAREs). Secretion can occur constitutively, to maintain cell homeostasis and provide components of extracellular matrix and cell adhesion structures (constitutive exocytosis). Alternatively, release of specific cargos in many types of differentiated cells can be tightly controlled in both space and time by a variety of signaling pathways (regulated exocytosis). Regulated exocytosis plays an important role in multiple processes, including synaptic neurotransmission, endocrine and paracrine signaling, or the release of hydrolytic enzymes by intestinal cells and leukocytes (Burgess and Kelly, 1987; Wu et al., 2014).

Vesicular transport is facilitated by the cytoskeleton, and in mammalian cells the major tracks for vesicle transport are microtubules, dynamic hollow tube-like structures with an outer diameter of 25 nm and lengths in the order of tens of microns. Microtubules have intrinsic polarity, with fast growing plus ends and slowly growing minus ends. Vesicles are transported along microtubules by two types of motors: kinesins, which are mostly plus-end-directed, and cytoplasmic dynein, which moves to microtubule minus ends.

In order to function optimally, cells rely heavily on a precisely controlled delivery of cargo. To do so, they take advantage of protein complexes that specifically connect membrane trafficking and cytoskeletal organization at the cell cortex. Tethering of microtubule tips, the end points of vesicle transport, to the sites of vesicle fusion can provide efficient routes for secretion. In many types of mammalian cells, microtubule minus ends are clustered at the internally positioned microtubule-organizing centers, the centrosome and the Golgi apparatus (Akhmanova and Hoogenraad, 2015; Conduit et al., 2015; Zhu and Kaverina, 2013), and the secretory trafficking mainly takes place in the direction of microtubule plus ends. It should be noted that in polarized epithelia and in neurons, microtubule minus ends can also be positioned in the vicinity of cell cortex and serve as sites of vesicle delivery. Since the mechanisms responsible for cortical microtubule minus-end tethering are only beginning to be understood (Khanal et al., 2016; Moss et al., 2007; Nashchekin et al., 2016; Ning et al., 2016; Noordstra et al., 2016; Toya et al., 2016), their connections to exocytosis still need to be unraveled.

In contrast, the factors responsible for coordinating the organization of micro-

tubule plus ends and secretion have received much attention. For example, in different types of migrating cells, secretory traffic is preferentially directed toward the leading cell edge (Schmoranzer et al., 2003; Toomre et al., 1999). Such polarization of exocytosis can help to establish and maintain cell asymmetry and provide molecules needed for membrane protrusion. An important function of exocytosis is formation and modification of cell adhesions to extracellular matrix or other cells. In particular, it is well established that microtubule plus ends can be specifically linked to the vicinity of focal adhesions (FAs) to promote their remodeling and thus facilitate efficient cell movement (Small and Kaverina, 2003; Stehbens and Wittmann, 2012).

Complexes responsible for coordinating microtubule plus-end organization and exocytosis consist of molecules localized to microtubule plus ends and cortical proteins, which can participate, often through additional factors, in vesicle tethering and docking. At the cortex, these complexes typically comprise different scaffolds associated with the actin cytoskeleton or directly with the plasma membrane. On microtubules, the major players are microtubule plus-end tracking proteins (+TIPs), a heterogeneous class of proteins distinguished by their specific accumulation at the growing microtubule plus ends (Akhmanova and Steinmetz, 2015; Schuyler and Pellman, 2001). Here, we provide an overview of the mammalian +TIPs involved in cortical microtubule tethering, their associated cortical attachment complexes, and their roles in exocytosis.

+TIPs involved in cortical microtubule capture

Prominent factors that can autonomously recognize growing microtubule ends are the members of end binding (EB) protein family (Bieling et al., 2007; Komarova et al., 2009; Maurer et al., 2012). EBs recruit to microtubule tips a plethora of different binding partners, which fall into two major classes: proteins containing globular cytoskeleton-associated protein-glycine-rich (CAP-Gly) domains and proteins with a short linear motif Ser-any amino acid-Ile-Pro (SxIP) embedded in unstructured positively charged regions (Akhmanova and Steinmetz, 2015). Mammalian +TIPs well known for their involvement in cortical microtubule capture are the CAP-Gly-containing cytoplasmic linker protein of 170 kDa (CLIP-170), p150Glued, the large subunit of the dynein co-factor dynactin, the SxIP proteins CLIP-associating proteins (CLASP1/2) and the tumor suppressor adenomatous polyposis coli (APC).

CLIP-170, the first +TIP to be reported (Perez et al., 1999; Pierre et al., 1992), was proposed to be involved in tethering microtubules to the cell cortex via IQGAP1 (Fukata et al., 2002), a cortical scaffold protein with interesting roles in exocytosis which we will discuss below (Figure 1). In fibroblasts, IQGAP1 recruits CLIP-170-decorated microtubule plus ends to actin filaments at the leading edge during migration (Watanabe et al., 2004). Interestingly, subsequent biochemical studies showed that IQGAP1 appears to act as a cortical hub for multiple +TIPs: for example, it can interact with APC, which

is found in the same protein complex as CLIP-170 (Watanabe et al., 2004) (Figure 1). Upon the depletion of APC, the leading edge localization of IQGAP1 as well as CLIP170 was perturbed and directional migration was affected, suggesting that APC, CLIP170, and IQGAP act in a tripartite complex that mediates cortical anchoring of microtubules during cell movement (Watanabe et al., 2004). Immunoprecipitation experiments from fibroblasts also revealed an interaction between IQGAP1 and CLASP2, which was implicated in polarized cell movement (Watanabe et al., 2009) (Figure 1). Furthermore, a complex of IQGAP1 with SKAP, an SxIP protein originally identified as a +TIP linking kinetochores to spindle microtubules (Fang et al., 2009; Wang et al., 2012), was shown to orchestrate directional migration by coupling dynamic microtubule plus ends to cortical regions in breast cancer cells (Cao et al., 2015) (Figure 1). It should be noted that the evidence for the function of IQGAP1 as a cortical hub for different +TIPs strongly relies on protein interaction data and would profit from additional mechanistic cell biological analyses.

APC, which was shown to directly bind to EB1 (Su et al., 1995), has been implicated in multiple additional cortical microtubule stabilization pathways. *In vivo*, it localizes to actin-rich cortical protrusions where it directly interacts with actin filaments through its C-terminal basic domain (Moseley et al., 2007; Okada et al., 2010). On the basis of *in vitro* experiments, APC was also suggested to play a role in actin nucleation (Okada et al., 2010). Furthermore, APC was shown to stabilize microtubules at the cortex in migrating fibroblasts by acting together with the actin-nucleating factor of the formin family, mDia (Wen et al., 2004). In migrating astrocytes, APC directly interacts with the cortical scaffold protein Dlg1 (Etienne-Manneville et al., 2005), thereby directly linking microtubules to the cortex. The latter interaction is regulated by the kinase GSK3β, which in turn can be phosphorylated by a Par6-PKCζ complex (Etienne-Manneville et al., 2005).

CLASP1 and CLASP2 form another family of major microtubule regulators that accumulate at the microtubule plus ends at the front of migrating cells. The asymmetric CLASP distribution is mediated by their spatially controlled phosphorylation through GSK3β, which reduces their affinity for microtubule plus ends (Akhmanova et al., 2001; Kumar et al., 2009; Watanabe et al., 2009). CLASPs are recruited to the cell cortex by directly interacting with the phosphatidylinositol (3,4,5)-trisphosphate (PIP3)-binding protein LL5β (Lansbergen et al., 2006) (Figure 2). LL5β is part of a large protein assembly tightly linked to FAs, which controls FA turnover (see below). Another SxIP-containing +TIP shown to participate in organizing microtubules in the vicinity of FAs is the APC-binding protein AMER2/FAM123, which is directly linked to the plasma membrane by a phospholipid-binding domain (Jiang et al., 2012; Pfister et al., 2012; Siesser et al., 2012) (Figure 1).

Also, the dynein-dynactin complex represents an important player in microtu-

bule capture at the cortex. In contrast to other +TIPs, which promote lateral microtubule attachments to the cortical sites, cytoplasmic dynein can form end-on attachments and exert forces to position the whole microtubule network in both interphase and mitosis (Dujardin and Vallee, 2002; Laan et al., 2012; McNally, 2013). Though mostly studied during cell division, when secretion is downregulated, cortical dynein was also shown to play a role in microtubule tethering to the plasma membrane in neurons, where it acts together with the neural cell adhesion molecule, and may have a role in stabilization of synapses (Perlson et al., 2013).

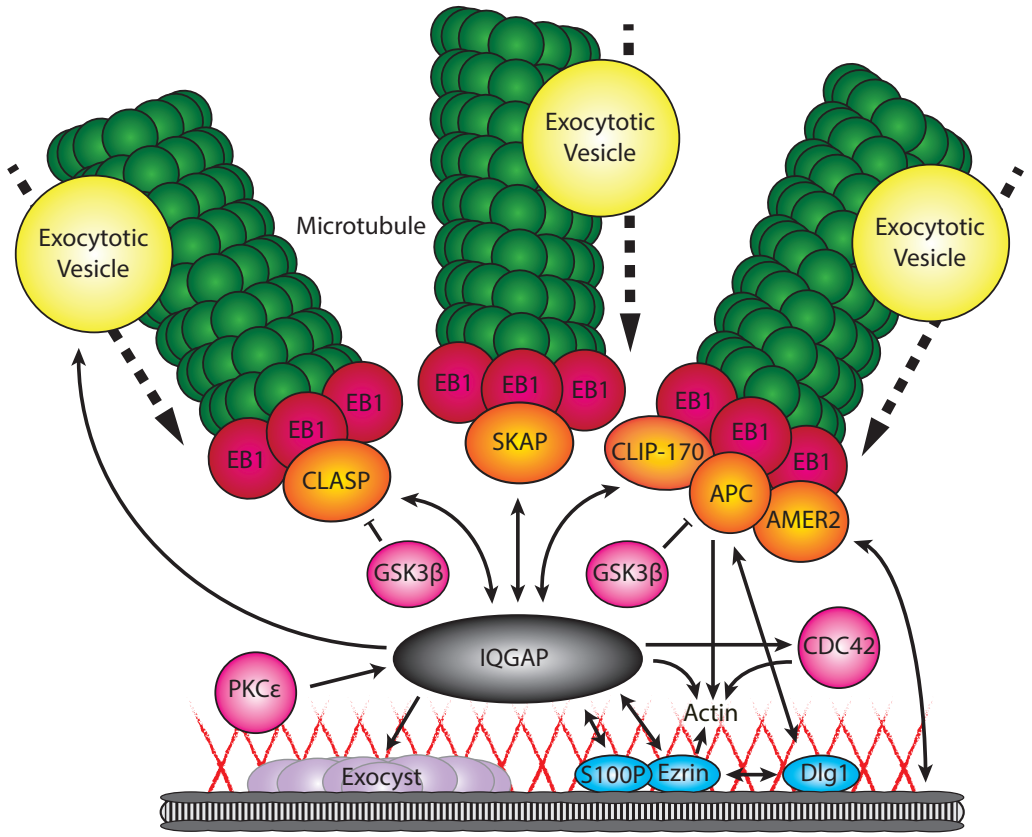

Figure 1. Schematic overview of IQGAP and associated protein functions in cortical microtubule capturing and exocytosis

Through its different domains, IQGAP interacts with a subset of microtubule plus-end tracking proteins (+TIPs) (orange) and cortical proteins (blue), thereby facilitating the microtubule capture at sites with high exocytotic activity. At the same time, IQGAP controls multiple components involved in secretion, including exocytotic vesicle-specific Rab GTPases (yellow), the exocyst complex (purple), and actin (red lines). Single-headed arrow, protein interaction with regulatory function; double-headed arrow, protein interaction facilitating recruitment; bar-headed line, negative regulation; dotted arrow, movement in direction of arrow.

Finally, spectraplakins, a group of very large proteins, have been shown to be involved in cortical microtubule stabilization. Spectraplakins have the ability to directly link microtubules and actin filaments and are involved in a wide range of cellular processes. Despite the presence of only two mammalian genes, a variety of spectraplakin isoforms have been found. This results from the existence of alternative tissue-specific promotors and multiple splice variants (Suozzi et al., 2012). Among them, actin crosslinking factor 7 (ACF7), also known as microtubule actin crosslinking factor 1 (MACF1), has been studied most extensively. Owing to the intrinsic properties of a C-terminal microtubule-binding domain and the presence of an SxIP domain, it can interact with microtubules and specifically accumulate at their ends. At the same time, the N-terminal calponin homology domains mediate the binding to sites rich in actin, such as the cell cortex (Kodama et al., 2003). Depletion of ACF7 was associated with the impaired microtubule growth along F-actin fibers toward FAs, and this significantly affected FA turnover and cell migration (Wu et al., 2008). Cortical recruitment of ACF7 has been connected to the presence of membrane-bound APC, which in turn is regulated by GSK3 (Zaoui et al., 2010), indicating the interplay of multiple pathways in recruiting microtubules to FAs. Recently, ACF7 was also shown to be a key player in linking microtubule minus ends to the apical membrane of polarized epithelial layers through calmodulin-regulated spectrin-associated protein 3 (CAMSAP3) (Khanal et al., 2016; Nashchekin et al., 2016; Noordstra et al., 2016). Interestingly the ACF7-CAMSAP3 interaction was also associated with FA targeting and cell migration (Ning et al., 2016).

Among the numerous links between microtubules and the cell cortex, two broad groups of protein assemblies with clear connections to secretion have emerged—IQGAP-containing complexes and the CLASP- and LL5-containing cortical microtubule stabilization complexes—and these will be discussed in more detail below.

Coordination of cytoskeletal cortical interactions and secretion by IQGAP1

As mentioned above, IQGAP1 interacts with multiple +TIPs, thereby facilitating the capture of microtubules at specific cortical cell regions. At the same time, IQGAP1 plays a role at different steps of the secretory pathway, ranging from actin remodeling to the control of specific membrane trafficking regulators, such as Rab GTPases or the exocyst complex. This functional diversity is based on the presence of multiple domains, including a calponin homology domain, IQGAP-specific repeats, a calmodulin-binding motif, a RasGAP-related domain, and a RasGAP C-terminus, which can mediate binding to a surprisingly broad set of proteins.

IQGAP1 is linked to the cortex via S100P and the plasma membrane- and actin-binding protein ezrin (Heil et al., 2011; Nammalwar et al., 2015) (Figure 1). S100 proteins bind to Ca^{2+} and the interaction between S100P and IQGAP1 is strictly Ca^{2+}-dependent (Heil et al., 2011). Also, ezrin has been shown to bind to Ca^{2+}-bound S100P and

IQGAP1, but since ezrin and IQGAP1 do interact in the absence of Ca^{2+}, this interaction appeared to be S100P-independent (Nammalwar et al., 2015). Both S100P and ezrin co-localize with IQGAP1 in the cortical cell regions, and ezrin depletion reduced the cortical localization of IQGAP1 (Heil et al., 2011; Nammalwar et al., 2015). Interestingly, ezrin also interacts with the APC-binding protein Dlg1 (Lasserre et al., 2010), but it is not known whether APC, Dlg1, IQGAP1, and ezrin can function in the same complex.

IQGAPs are best known as important regulators of actin dynamics. In turn, the actin cytoskeleton plays a major role in regulating all steps of exocytosis. Multiple studies show that the actin network acts as a physical barrier that is removed during exocytosis, allowing vesicles to dock and fuse with the plasma membrane (Eitzen, 2003; Malacombe et al., 2006). Many lines of research also indicate the role of actin in directing vesicles to the fusion sites, regulating the fusion pores and providing the driving force to complete fusion (Masedunskas et al., 2011; Nightingale et al., 2012; Sokac et al., 2006). Undoubtedly, actin regulation is essential for properly functioning exocytotic machinery.

IQGAP1 was initially identified as a target for the Rho GTPases CDC42 and Rac1 (Bashour et al., 1997; Kuroda et al., 1996), two factors involved in actin organization. Despite the name, IQGAP1 displays no GAP activity to the Rho GTPases (Bashour et al., 1997; Brill et al., 1996; Kuroda et al., 1996; McCallum et al., 1996). In fact, it is well established that IQGAP1 inhibits the GTPase activity of CDC42 and Rac1 to stabilize their GTP-bound form (Brill et al., 1996; Hart et al., 1996; Noritake et al., 2004). Accumulated evidence points in the direction of CDC42 being an important regulator of post-Golgi traffic in an actin-dependent manner (Egorov et al., 2009; Salvarezza et al., 2009). Interestingly, the CDC42-IQGAP interaction was directly linked to exocytosis in gastric parietal cells, epithelial cells that are located in the gastric glands of the stomach. In these cells, IQGAP1 and its homologue IQGAP2 are expressed and localized differentially (Chew et al., 2005; Zhou et al., 2003). In contrast to IQGAP1, which localizes to the basolateral regions of the cells, IQGAP2 specifically localizes to the apical plasma membrane, where it interacts with CDC42. This interaction was shown to be essential for polarized secretion (Zhou et al., 2003). Biochemical evidence demonstrated that IQGAP1 can be phosphorylated by the kinase PKCε at its C-terminus, thereby relieving an autoinhibited fold, enhancing the binding of IQGAP1 to active CDC42 (Grohmanova et al., 2004), and leading to attenuation of exocytosis (Rittmeyer et al., 2008). PKCε has also been implicated in exocytosis by playing an essential role in the disassembly of actin filaments following docking and tethering of the vesicles (Mendez et al., 2003; Park et al., 2006; Xue et al., 2009). Since different stages of exocytosis require different actin organizations, these data suggest a dynamic interplay between PKCε, CDC42, and IQGAP in regulating actin dynamics.

In addition to interacting with indirect actin modifiers like the Rho GTPases,

IQGAP1 also binds to a set of proteins that directly organize the actin cytoskeleton, such as the actin-related protein (Arp) 2/3 complex and formins. IQGAP can stimulate Arp2/3-dependent actin polymerization through direct as well as indirect interactions via the activation of neural Wiskott-Aldrich syndrome protein (N-WASp) (Bensenor et al., 2007; Le Clainche et al., 2007). Also, mDia1, an actin-nucleating protein of the formin family, which was implicated in microtubule regulation through APC and other pathways (Bartolini et al., 2012; Eng et al., 2006; Wen et al., 2004), was identified as a binding partner for IQGAP1. IQGAP1 specifically interacts with the Rho-activated form of mDia1 which results in the recruitment of the protein and actin assembly at sites with high exocytotic activity, like the leading edge of migrating cells (Bartolini et al., 2016; Brandt et al., 2007).

Next to Rho GTPases, Rab GTPases also belong to the key regulators of membrane trafficking and exocytosis. Interestingly, Rab27A, a small GTPase that regulates exocytosis of insulin-containing vesicles in pancreatic β cells (Yi et al., 2002), has been shown to form a complex with IQGAP1 (Kimura et al., 2013). Remarkably, not only exocytosis but also endocytosis of insulin secretory membranes, a process essential to maintain a constant cell volume and to allow the reuse of exocytotic machinery, strongly depends on complex formation between Rab27A and IQGAP1. Depletion of IQGAP1 prevented glucose-induced redistribution of Rab27A from the cytosol to the plasma membrane (Kimura et al., 2013). These data suggest that IQGAP1 participates in both endocytosis and exocytosis upon glucose stimulation in β cells. Whether these functions relate in some way to the interactions of IQGAP1 with microtubule-binding proteins is currently unclear, especially as, strikingly, microtubules in β cells restrict, rather than promote, the availability of insulin granules for secretion (Zhu et al., 2015).

IQGAP1 has been shown to associate with the Exo70, Sec3, and Sec8 subunits of the exocyst complex (Rittmeyer et al., 2008; Sakurai-Yageta et al., 2008) (Figure 1), an evolutionarily conserved octameric protein complex, which mediates the tethering of exocytotic vesicles prior to fusion and which is implicated in a wide variety of cellular processes (Martin-Urdiroz et al., 2016). The IQGAP1-exocyst interactions are controlled by CDC42 and RhoA (Rittmeyer et al., 2008; Sakurai-Yageta et al., 2008). Interestingly, depletion of IQGAP1 strongly affected insulin secretion from pancreatic β cells (Rittmeyer et al., 2008) and secretion of matrix metalloproteinases (Sakurai-Yageta et al., 2008), two unrelated cellular processes which both strongly rely on exocytosis and the exocyst complex (Liu et al., 2009; Tsuboi et al., 2005). However, it cannot be excluded that these phenotypes are caused by other functions of IQGAP1 in exocytosis as described above.

Taken together, the existing data suggest that IQGAP1 is an excellent candidate for playing the role of a central hub coordinating cytoskeletal organization and membrane trafficking. However, more detailed biochemical and cell biological studies will

be needed to understand the exact mechanisms underlying its activity and unravel which of the numerous proposed interactions and functions of IQGAP1 are compatible and cooperative and which ones are mutually exclusive.

CLASP- and LL5-associated complexes in microtubule organization and secretion

As mentioned above, CLASPs are among the key players responsible for cortical microtubule targeting. Through the direct interaction with LL5β and its homologue LL5α (Hotta et al., 2010; Lansbergen et al., 2006), they associate with a large protein assembly, which here will be termed cortical microtubule stabilizing complex (CMSC) (Astro et al., 2014; Bouchet et al., 2016a; Lansbergen et al., 2006; van der Vaart et al., 2013) (Figure 2). As discussed below, this complex has been shown to be a regulator of FA turnover and is tightly clustered at the rims of FAs, although it does not spatially overlap with them (Astro et al., 2014; Astro et al., 2016; Bouchet et al., 2016a; Lansbergen et al., 2006; van der Vaart et al., 2013). LL5s are PIP3-binding proteins, and their membrane recruitment as well as the localization of the whole CMSC can be influenced by PI3 kinase activity (Lansbergen et al., 2006; Paranavitane et al., 2003). Recently, Prickle1, a protein known for its role in planar cell polarity, was shown to participate in the LL5β-dependent accumulation of CLASPs in close proximity to FAs at retracting cell edges, thus controlling FA disassembly and cell motility (Lim et al., 2016).

CMSC contains several scaffolding proteins, including the SAM domain containing proteins liprin-α1 and -β1, a coiled coil adaptor ELKS (also known as ERC1, for ELKS/RAB6-interacting/CAST family member 1), and the ankyrin repeat protein KANK1. Liprin-α1 and -β1 were initially identified as interacting partners of the protein tyrosine phosphatase LAR (Serra-Pages et al., 1995), a transmembrane protein that is involved in axon guidance (Johnson and Van Vactor, 2003) and in the maintenance of excitatory synapses in hippocampal neurons (Dunah et al., 2005). However, it is unknown whether LAR homologues are present and have a functional role in CMSCs. Liprin-α1 directly interacts with ELKS (Ko et al., 2003). Both ELKS and the members of the liprin-α family are major components of the cytomatrix at the active zone (CAZ), the principal site of Ca^{2+}-dependent exocytosis of neurotransmitters at neuronal synapses; these proteins thus have complex roles in neurotransmission across different animal species (Gundelfinger and Fejtova, 2012; Spangler and Hoogenraad, 2007; Sudhof, 2012). Importantly, CMSC and CAZ have many non-overlapping components; for example, CAZ does not contain either LL5 or KANK homologues and does not appear to be directly connected to microtubules. In addition to coordinating the trafficking of neurotransmitter-containing vesicles at the CAZ, liprin-α1 was shown to be a key component of the molecular machinery underlying the internalization of fibronectin and recycling of fibronectin-bound α5β1-integrin to basolateral membranes in endothelial cells, a process essential for defining and maintaining cell polarity (Mana et al., 2016).

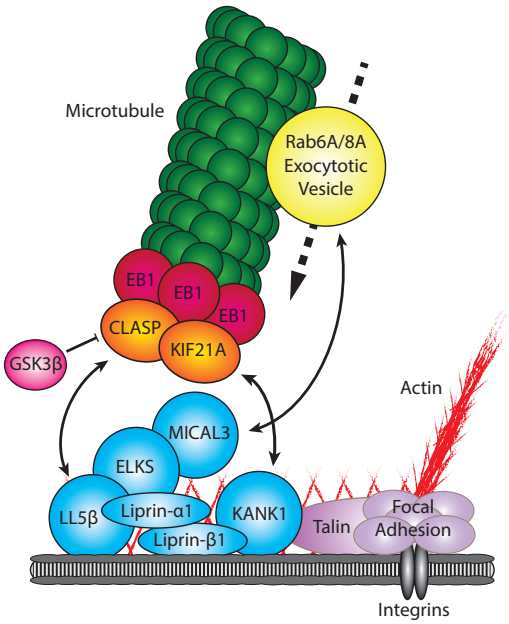

Figure 2. Schematic overview of the cortical microtubule stabilizing complex (CMSC) and associated proteins involved in microtubule capture and exocytosis

The CMSC (blue) captures microtubules through direct interactions with a specific subset of microtubule plus-end tracking proteins (+TIPs) (orange). CMSC components are found in the proximity of focal adhesions (purple), where they regulate microtubule-mediated focal adhesion turnover. Furthermore, the CMSC has been shown to directly interact with Rab6A/Rab8A-positive vesicles (yellow), thereby facilitating secretion. Double-headed arrow, protein interaction facilitating recruitment; bar-headed line, negative regulation; dotted arrow, movement in direction of arrow.

CMSCs are linked to FAs by KANK1, which directly interacts with talin, the core FA protein (Bouchet et al., 2016a) (Figure 2). KANK1 also binds to liprin-β1, and the inhibition of either the liprin-β1-KANK1 or the KANK1-talin binding disrupts the CMSC localization around FAs and cortical microtubule capture around FAs (Bouchet et al., 2016a). How a direct interaction between an FA component and a CMSC component can lead to their non-overlapping localization next to each other is currently a mystery. KANK2, a KANK1 homologue, also localizes as a tight "belt" around FAs and interacts with talin (Sun et al., 2016). Interestingly, it suppresses mechanical force transmission across activated integrins by interfering with F-actin binding (Sun et al., 2016). The fact that talin might interact with KANK1 and actin in a mutually exclusive manner could explain why KANKs localize to the periphery of FAs and not to their actin-associated core. It is possible that KANK1 bound to the FA periphery acts as a "seed" for CMSC assembly through multivalent interactions between its scaffolding components (Astro and de Curtis, 2015; Bouchet et al., 2016a). In addition to coupling the CMSCs to FAs, KANK1 recruits to the cortex the kinesin-4 family member KIF21A. This plus-end-directed motor protein strongly inhibits both microtubule growth and catastrophes at the cell cortex, thus cooperating with CLASPs in promoting cortical microtubule stability (van der Vaart et al., 2013).

ELKS is a ubiquitously expressed adaptor, which can be recruited to the plasma membrane by both LL5s and liprin-α1 (Ko et al., 2003; Lansbergen et al., 2006). The effect of ELKS depletion on the microtubule organization is relatively mild because ELKS does not bind to microtubules and is not essential for the cortical localization of

LL5β or CLASPs but rather plays a scaffolding role by concentrating cortical clusters of LL5β and CLASPs at the cell periphery (Lansbergen et al., 2006). However, ELKS has been shown to be a central player in constitutive exocytosis (Grigoriev et al., 2007). It directly interacts with all isoforms of the small GTPase Rab6 (Rab6A, Rab6A′, and Rab6B) (Monier et al., 2002), an abundantly expressed Rab GTPase that strongly decorates the Golgi apparatus and cytoplasmic vesicles (Del Nery et al., 2006; Martinez et al., 1997; Martinez et al., 1994). Although these vesicles were originally believed to be responsible for COPI-independent transport to the Golgi (Girod et al., 1999; White et al., 1999), detailed imaging studies demonstrated that in fact they predominantly fuse with the plasma membrane and thus represent carriers of constitutive secretion (Grigoriev et al., 2007).

Rab6A-positive vesicles immobilize and fuse at the cortical FA-associated sites containing LL5β, and ELKS depletion causes strong accumulation of Rab6A-positive vesicles at the cell periphery because although their exit from the Golgi and microtubule-based transport are not perturbed, their docking and fusion are inhibited (Grigoriev et al., 2007). The underlying mechanism is not entirely clear. Similar to CAZ components, ELKS-containing complexes might promote the interaction between SNAREs located on the vesicles and the plasma membrane; however, it is currently unclear whether there is a direct connection between SNAREs and ELKS. Furthermore, in addition to the direct binding to ELKS, Rab6 also controls the recruitment to exocytotic vesicles of another Rab GTPase, Rab8A. Rab8A is a well-known player in exocytosis (Ang et al., 2003; Hattula et al., 2006; Huber et al., 1993; Sato et al., 2007). Interestingly, Rab8A interacts with ELKS-positive cortical sites through the binding partner of ELKS, MICAL3 (Grigoriev et al., 2011), a multidomain oxidative enzyme which can promote disassembly of actin filaments and potentially remodel other protein complexes and also act as a scaffold (Giridharan and Caplan, 2014; Liu et al., 2016; Terman et al., 2002).

In migrating cells, CMSCs are strongly clustered around the FAs at the leading cell edge and promote their disassembly (Lansbergen et al., 2006; Stehbens et al., 2014). Microtubules anchored by CLASPs in the vicinity of FAs serve as tracks for transport of exocytotic Rab6-positive vesicles. Secretory trafficking delivers to the cell surface membrane type 1 metalloprotease (MT1-MMP), which can degrade the extracellular matrix around FAs, resulting in integrin detachment, loss of tension, and FA turnover (Stehbens et al., 2014). These observations help to explain why liprin-α1, liprin-β1, LL5β, and ELKS promote invasive behavior and internalization of integrins in breast cancer cells (Asperti et al., 2009; Astro et al., 2011; Astro et al., 2014; Astro et al., 2016; Chiaretti et al., 2016). Importantly, MT1-MMP delivery and integrin recycling also strongly depend on endosomal trafficking, which requires microtubules (Castro-Castro et al., 2016; Paul et al., 2015). How exactly endosome trafficking connects to CMSC components deserves further investigation. Finally, it should be noted that in three-dimensional matrix

invasion assays, the major function of cortical microtubule stabilization by CLASPs and possibly also their partners might be not only to direct vesicle traffic but also to mechanically support long protrusions that mesenchymal cells extend in three dimensions to penetrate between the matrix fibers (Bouchet et al., 2016b).

LL5β and ELKS were also shown to concentrate at podosomes, actin-rich dynamic structures which can remodel the extracellular matrix (Proszynski and Sanes, 2013); and CLASPs, together with a plus-end-directed kinesin-3 KIF1C, were shown to regulate podosome formation (Efimova et al., 2014). Interestingly, podosome-like structures ("synaptic podosomes") are also formed at neuromuscular junctions (NMJs) undergoing remodeling during postnatal stages of development, and LL5β, which strongly localizes to regions of high density of acetylcholine receptors at the NMJ, has been implicated in this process (Kishi et al., 2005; Proszynski et al., 2009; Proszynski and Sanes, 2013). At the NMJ, the complexes of LL5β and CLASPs were shown to capture microtubule plus ends and in this way create a route for the delivery of vesicles containing acetylcholine receptors to the postsynaptic membrane (Basu et al., 2015; Basu et al., 2014; Schmidt et al., 2012). It is currently unknown whether ELKS participates in the regulation of the fusion of acetylcholine receptor-containing carriers with the plasma membrane, but this possibility seems quite likely, given the involvement of ELKS in secretion and the observation that ELKS is present at the NMJ (Tokoro et al., 2007). Taken together, these data show that CMSCs or complexes related to them in composition regulate both microtubule organization and secretion in different types of undifferentiated as well as differentiated cells.

Conclusions and future directions

Microtubules play an essential role in exocytosis by serving as tracks for motor proteins that transport secretory carriers. The best studied mammalian cell models so far include migrating mesenchymal cells, in which a surprisingly diverse set of molecules is responsible for attaching and stabilizing microtubules to cortical sites close to the leading cell edge. An important unresolved question is whether the different complexes described so far, such as CMSCs and IQGAP-linked cortical assemblies, represent cooperating or redundant pathways or whether *in vivo* they act in the same or different cell and tissue settings. Addressing this question will require systematic analysis of all major players using the same cellular models and also exploring their expression and interactions in tissues. Relevant in this respect is the analysis of tissue-specific isoforms of the investigated proteins. For example, whereas IQGAP1 was extensively studied, much less is known about its homologues IQGAP2, which is enriched in the liver and stomach, and IQGAP3, which is mainly found in brain and lung tissue (Wang et al., 2007). Their domain composition is highly similar to that of IQGAP1 and given their specific expression in tissues with high exocytotic activity, they are interesting candidates for having

profound but undiscovered roles in exocytosis.

Another interesting set of questions concerns the involvement of the discussed complexes in regulated secretion. There are strong data showing that many of the factors described above are important for regulated exocytosis. For example, ELKS and liprin-α are well-known players in neurotransmitter release in neurons and also are required for exocytotic release of inflammatory mediators by mast cells upon induction of allergic responses (Nomura et al., 2009). ELKS was also found to coincide with the docking and fusion sites of insulin in a pancreatic β-cell line; consistent with this observation, ELKS clusters show significant overlap with the clusters of the SNARE syntaxin 1, and ELKS depletion strongly affected insulin exocytosis (Ohara-Imaizumi et al., 2005). However, as indicated above, the connections between CMSC components and SNAREs require further elucidation. Furthermore, microtubule plus ends do not appear to be directly connected to the sites of exocytosis in neurons or β cells. It is possible that microtubules are linked to secretory sites when relatively rapid transport of newly synthesized proteins from the Golgi apparatus is functionally important. Direct microtubule-based delivery might not be essential when an excess of secretory cargo is available or when extensive local recycling of secreted molecules takes place, as is the case in neurons. In some cell types, such as pancreatic β cells, microtubules may even be used to sequester rather than deliver secretory cargo (Zhu et al., 2015). Investigating the diversity of the mechanisms responsible for vesicle delivery and fusion represents an exciting subject for future research.

References

Akhmanova, A., and C.C. Hoogenraad. 2015. Microtubule minus-end-targeting proteins. Curr Biol. 25:R162-171.

Akhmanova, A., C.C. Hoogenraad, K. Drabek, T. Stepanova, B. Dortland, T. Verkerk, W. Vermeulen, B.M. Burgering, C.I. De Zeeuw, F. Grosveld, and N. Galjart. 2001. Clasps are CLIP-115 and -170 associating proteins involved in the regional regulation of microtubule dynamics in motile fibroblasts. Cell. 104:923-935.

Akhmanova, A., and M.O. Steinmetz. 2015. Control of microtubule organization and dynamics: two ends in the limelight. Nat Rev Mol Cell Biol. 16:711-726.

Ang, A.L., H. Folsch, U.M. Koivisto, M. Pypaert, and I. Mellman. 2003. The Rab8 GTPase selectively regulates AP-1B-dependent basolateral transport in polarized Madin-Darby canine kidney cells. J Cell Biol. 163:339-350.

Asperti, C., V. Astro, A. Totaro, S. Paris, and I. de Curtis. 2009. Liprin-alpha1 promotes cell spreading on the extracellular matrix by affecting the distribution of activated integrins. J Cell Sci. 122:3225-3232.

Astro, V., C. Asperti, M.G. Cangi, C. Doglioni, and I. de Curtis. 2011. Liprin-alpha1 regulates breast cancer cell invasion by affecting cell motility, invadopodia and extracellular matrix degradation. Oncogene. 30:1841-1849.

Astro, V., S. Chiaretti, E. Magistrati, M. Fivaz, and I. de Curtis. 2014. Liprin-alpha1, ERC1 and LL5 define polarized and dynamic structures that are implicated in cell migration. J Cell Sci. 127:3862-3876.

Astro, V., and I. de Curtis. 2015. Plasma membrane-associated platforms: dynamic scaffolds that organize membrane-associated events. Sci Signal. 8:re1.

Astro, V., D. Tonoli, S. Chiaretti, S. Badanai, K. Sala, M. Zerial, and I. de Curtis. 2016. Liprin-alpha1 and ERC1 control cell edge dynamics by promoting focal adhesion turnover. Sci Rep. 6:33653.

Bartolini, F., L. Andres-Delgado, X. Qu, S. Nik, N. Ramalingam, L. Kremer, M.A. Alonso, and G.G. Gundersen. 2016. An mDia1-INF2 formin activation cascade facilitated by IQGAP1 regulates stable microtubules in migrating cells. Mol Biol Cell. 27:1797-1808.

Bartolini, F., N. Ramalingam, and G.G. Gundersen. 2012. Actin-capping protein promotes microtubule stability by antagonizing the actin activity of mDia1. Mol Biol Cell. 23:4032-4040.

Bashour, A.M., A.T. Fullerton, M.J. Hart, and G.S. Bloom. 1997. IQGAP1, a Rac- and Cdc42-binding protein, directly binds and cross-links microfilaments. J Cell Biol. 137:1555-1566.

Basu, S., S. Sladecek, I. Martinez de la Pena y Valenzuela, M. Akaaboune, I. Smal, K. Martin, N. Galjart, and H.R. Brenner. 2015. CLASP2-dependent microtubule capture at the neuromuscular junction membrane requires LL5beta and actin for focal delivery of acetylcholine receptor vesicles. Mol Biol Cell. 26:938-951.

Basu, S., S. Sladecek, H. Pemble, T. Wittmann, J.A. Slotman, W. van Cappellen, H.R. Brenner, and N. Galjart. 2014. Acetylcholine receptor (AChR) clustering is regulated both by glycogen synthase kinase 3beta (GSK3beta)-dependent phosphorylation and the level of CLIP-associated protein 2 (CLASP2) mediating the capture of microtubule plus-ends. J Biol Chem. 289:30857-30867.

Bensenor, L.B., H.M. Kan, N. Wang, H. Wallrabe, L.A. Davidson, Y. Cai, D.A. Schafer, and G.S. Bloom. 2007. IQGAP1 regulates cell motility by linking growth factor signaling to actin assembly. J Cell Sci. 120:658-669.

Bieling, P., L. Laan, H. Schek, E.L. Munteanu, L. Sandblad, M. Dogterom, D. Brunner, and T. Surrey. 2007. Reconstitution of a microtubule plus-end tracking system in vitro. Nature. 450:1100-1105.

Bouchet, B.P., R.E. Gough, Y.C. Ammon, D. van de Willige, H. Post, G. Jacquemet, A.M. Altelaar, A.J. Heck, B.T. Goult, and A. Akhmanova. 2016a. Talin-KANK1 interaction controls the recruitment of cortical microtubule stabilizing complexes to focal adhesions. Elife. 5.

Bouchet, B.P., I. Noordstra, M. van Amersfoort, E.A. Katrukha, Y.C. Ammon, N.D. Ter Hoeve,

L. Hodgson, M. Dogterom, P.W.B. Derksen, and A. Akhmanova. 2016b. Mesenchymal Cell Invasion Requires Cooperative Regulation of Persistent Microtubule Growth by SLAIN2 and CLASP1. Dev Cell. 39:708-723.

Brandt, D.T., S. Marion, G. Griffiths, T. Watanabe, K. Kaibuchi, and R. Grosse. 2007. Dia1 and IQGAP1 interact in cell migration and phagocytic cup formation. J Cell Biol. 178:193-200.

Brill, S., S. Li, C.W. Lyman, D.M. Church, J.J. Wasmuth, L. Weissbach, A. Bernards, and A.J. Snijders. 1996. The Ras GTPase-activating-protein-related human protein IQGAP2 harbors a potential actin binding domain and interacts with calmodulin and Rho family GTPases. Mol Cell Biol. 16:4869-4878.

Burgess, T.L., and R.B. Kelly. 1987. Constitutive and regulated secretion of proteins. Annu Rev Cell Biol. 3:243-293.

Cao, D., Z. Su, W. Wang, H. Wu, X. Liu, S. Akram, B. Qin, J. Zhou, X. Zhuang, G. Adams, C. Jin, X. Wang, L. Liu, D.L. Hill, D. Wang, X. Ding, and X. Yao. 2015. Signaling Scaffold Protein IQGAP1 Interacts with Microtubule Plus-end Tracking Protein SKAP and Links Dynamic Microtubule Plus-end to Steer Cell Migration. J Biol Chem. 290:23766-23780.

Castro-Castro, A., V. Marchesin, P. Monteiro, C. Lodillinsky, C. Rosse, and P. Chavrier. 2016. Cellular and Molecular Mechanisms of MT1-MMP-Dependent Cancer Cell Invasion. Annu Rev Cell Dev Biol. 32:555-576.

Chew, C.S., C.T. Okamoto, X. Chen, and H.Y. Qin. 2005. IQGAPs are differentially expressed and regulated in polarized gastric epithelial cells. Am J Physiol Gastrointest Liver Physiol. 288:G376-387.

Chiaretti, S., V. Astro, E. Chiricozzi, and I. de Curtis. 2016. Effects of the scaffold proteins liprin-alpha1, beta1 and beta2 on invasion by breast cancer cells. Biol Cell. 108:65-75.

Conduit, P.T., A. Wainman, and J.W. Raff. 2015. Centrosome function and assembly in animal cells. Nat Rev Mol Cell Biol. 16:611-624.

Del Nery, E., S. Miserey-Lenkei, T. Falguieres, C. Nizak, L. Johannes, F. Perez, and B. Goud. 2006. Rab6A and Rab6A' GTPases play non-overlapping roles in membrane trafficking. Traffic. 7:394-407.

Dujardin, D.L., and R.B. Vallee. 2002. Dynein at the cortex. Curr Opin Cell Biol. 14:44-49.

Dunah, A.W., E. Hueske, M. Wyszynski, C.C. Hoogenraad, J. Jaworski, D.T. Pak, A. Simonetta, G. Liu, and M. Sheng. 2005. LAR receptor protein tyrosine phosphatases in the development and maintenance of excitatory synapses. Nat Neurosci. 8:458-467.

Efimova, N., A. Grimaldi, A. Bachmann, K. Frye, X. Zhu, A. Feoktistov, A. Straube, and I. Kaverina. 2014. Podosome-regulating kinesin KIF1C translocates to the cell periphery in a CLASP-dependent manner. J Cell Sci. 127:5179-5188.

Egorov, M.V., M. Capestrano, O.A. Vorontsova, A. Di Pentima, A.V. Egorova, S. Mariggio, M.I. Ayala, S. Tete, J.L. Gorski, A. Luini, R. Buccione, and R.S. Polishchuk. 2009. Faciogenital dysplasia protein (FGD1) regulates export of cargo proteins from the golgi complex via Cdc42 activation. Mol Biol Cell. 20:2413-2427.

Eitzen, G. 2003. Actin remodeling to facilitate membrane fusion. Biochim Biophys Acta. 1641:175-181.

Eng, C.H., T.M. Huckaba, and G.G. Gundersen. 2006. The formin mDia regulates GSK3beta through novel PKCs to promote microtubule stabilization but not MTOC reorientation in migrating fibroblasts. Mol Biol Cell. 17:5004-5016.

Etienne-Manneville, S., J.B. Manneville, S. Nicholls, M.A. Ferenczi, and A. Hall. 2005. Cdc42 and Par6-PKCzeta regulate the spatially localized association of Dlg1 and APC to control cell polarization. J Cell Biol. 170:895-901.

Fang, L., A. Seki, and G. Fang. 2009. SKAP associates with kinetochores and promotes the metaphase-to-anaphase transition. Cell Cycle. 8:2819-2827.

Fukata, M., T. Watanabe, J. Noritake, M. Nakagawa, M. Yamaga, S. Kuroda, Y. Matsuura, A. Iwamatsu, F. Perez, and K. Kaibuchi. 2002. Rac1 and Cdc42 capture microtubules through IQGAP1 and CLIP-170. Cell. 109:873-885.

Giridharan, S.S., and S. Caplan. 2014. MICAL-family proteins: Complex regulators of the actin cytoskeleton. Antioxid Redox Signal. 20:2059-2073.

Girod, A., B. Storrie, J.C. Simpson, L. Johannes, B.

Goud, L.M. Roberts, J.M. Lord, T. Nilsson, and R. Pepperkok. 1999. Evidence for a COP-I-independent transport route from the Golgi complex to the endoplasmic reticulum. Nat Cell Biol. 1:423-430.

Grigoriev, I., D. Splinter, N. Keijzer, P.S. Wulf, J. Demmers, T. Ohtsuka, M. Modesti, I.V. Maly, F. Grosveld, C.C. Hoogenraad, and A. Akhmanova. 2007. Rab6 regulates transport and targeting of exocytotic carriers. Dev Cell. 13:305-314.

Grigoriev, I., K.L. Yu, E. Martinez-Sanchez, A. Serra-Marques, I. Smal, E. Meijering, J. Demmers, J. Peranen, R.J. Pasterkamp, P. van der Sluijs, C.C. Hoogenraad, and A. Akhmanova. 2011. Rab6, Rab8, and MICAL3 cooperate in controlling docking and fusion of exocytotic carriers. Curr Biol. 21:967-974.

Grohmanova, K., D. Schlaepfer, D. Hess, P. Gutierrez, M. Beck, and R. Kroschewski. 2004. Phosphorylation of IQGAP1 modulates its binding to Cdc42, revealing a new type of rho-GTPase regulator. J Biol Chem. 279:48495-48504.

Gundelfinger, E.D., and A. Fejtova. 2012. Molecular organization and plasticity of the cytomatrix at the active zone. Curr Opin Neurobiol. 22:423-430.

Hart, M.J., M.G. Callow, B. Souza, and P. Polakis. 1996. IQGAP1, a calmodulin-binding protein with a rasGAP-related domain, is a potential effector for cdc42Hs. EMBO J. 15:2997-3005.

Hattula, K., J. Furuhjelm, J. Tikkanen, K. Tanhuanpaa, P. Laakkonen, and J. Peranen. 2006. Characterization of the Rab8-specific membrane traffic route linked to protrusion formation. J Cell Sci. 119:4866-4877.

Heil, A., A.R. Nazmi, M. Koltzscher, M. Poeter, J. Austermann, N. Assard, J. Baudier, K. Kaibuchi, and V. Gerke. 2011. S100P is a novel interaction partner and regulator of IQGAP1. J Biol Chem. 286:7227-7238.

Hotta, A., T. Kawakatsu, T. Nakatani, T. Sato, C. Matsui, T. Sukezane, T. Akagi, T. Hamaji, I. Grigoriev, A. Akhmanova, Y. Takai, and Y. Mimori-Kiyosue. 2010. Laminin-based cell adhesion anchors microtubule plus ends to the epithelial cell basal cortex through LL5alpha/beta. J Cell Biol. 189:901-917.

Huber, L.A., S. Pimplikar, R.G. Parton, H. Virta, M. Zerial, and K. Simons. 1993. Rab8, a small GTPase involved in vesicular traffic between the TGN and the basolateral plasma membrane. J Cell Biol. 123:35-45.

Jiang, K., G. Toedt, S. Montenegro Gouveia, N.E. Davey, S. Hua, B. van der Vaart, I. Grigoriev, J. Larsen, L.B. Pedersen, K. Bezstarosti, M. Lince-Faria, J. Demmers, M.O. Steinmetz, T.J. Gibson, and A. Akhmanova. 2012. A Proteome-wide screen for mammalian SxIP motif-containing microtubule plus-end tracking proteins. Curr Biol. 22:1800-1807.

Johnson, K.G., and D. Van Vactor. 2003. Receptor protein tyrosine phosphatases in nervous system development. Physiol Rev. 83:1-24.

Khanal, I., A. Elbediwy, C. Diaz de la Loza Mdel, G.C. Fletcher, and B.J. Thompson. 2016. Shot and Patronin polarise microtubules to direct membrane traffic and biogenesis of microvilli in epithelia. J Cell Sci. 129:2651-2659.

Kimura, T., M. Yamaoka, S. Taniguchi, M. Okamoto, M. Takei, T. Ando, A. Iwamatsu, T. Watanabe, K. Kaibuchi, T. Ishizaki, and I. Niki. 2013. Activated Cdc42-bound IQGAP1 determines the cellular endocytic site. Mol Cell Biol. 33:4834-4843.

Kishi, M., T.T. Kummer, S.J. Eglen, and J.R. Sanes. 2005. LL5beta: a regulator of postsynaptic differentiation identified in a screen for synaptically enriched transcripts at the neuromuscular junction. J Cell Biol. 169:355-366.

Ko, J., M. Na, S. Kim, J.R. Lee, and E. Kim. 2003. Interaction of the ERC family of RIM-binding proteins with the liprin-alpha family of multidomain proteins. J Biol Chem. 278:42377-42385.

Kodama, A., I. Karakesisoglou, E. Wong, A. Vaezi, and E. Fuchs. 2003. ACF7: an essential integrator of microtubule dynamics. Cell. 115:343-354.

Komarova, Y., C.O. De Groot, I. Grigoriev, S.M. Gouveia, E.L. Munteanu, J.M. Schober, S. Honnappa, R.M. Buey, C.C. Hoogenraad, M. Dogterom, G.G. Borisy, M.O. Steinmetz, and A. Akhmanova. 2009. Mammalian end binding proteins control persistent microtubule growth. J Cell Biol. 184:691-706.

Kumar, P., K.S. Lyle, S. Gierke, A. Matov, G. Danuser, and T. Wittmann. 2009. GSK3beta phosphorylation modulates CLASP-microtubule association and lamella microtubule attachment. J Cell

Biol. 184:895-908.

Kuroda, S., M. Fukata, K. Kobayashi, M. Nakafuku, N. Nomura, A. Iwamatsu, and K. Kaibuchi. 1996. Identification of IQGAP as a putative target for the small GTPases, Cdc42 and Rac1. J Biol Chem. 271:23363-23367.

Laan, L., N. Pavin, J. Husson, G. Romet-Lemonne, M. van Duijn, M.P. Lopez, R.D. Vale, F. Julicher, S.L. Reck-Peterson, and M. Dogterom. 2012. Cortical dynein controls microtubule dynamics to generate pulling forces that position microtubule asters. Cell. 148:502-514.

Lansbergen, G., I. Grigoriev, Y. Mimori-Kiyosue, T. Ohtsuka, S. Higa, I. Kitajima, J. Demmers, N. Galjart, A.B. Houtsmuller, F. Grosveld, and A. Akhmanova. 2006. CLASPs attach microtubule plus ends to the cell cortex through a complex with LL5beta. Dev Cell. 11:21-32.

Lasserre, R., S. Charrin, C. Cuche, A. Danckaert, M.I. Thoulouze, F. de Chaumont, T. Duong, N. Perrault, N. Varin-Blank, J.C. Olivo-Marin, S. Etienne-Manneville, M. Arpin, V. Di Bartolo, and A. Alcover. 2010. Ezrin tunes T-cell activation by controlling Dlg1 and microtubule positioning at the immunological synapse. EMBO J. 29:2301-2314.

Le Clainche, C., D. Schlaepfer, A. Ferrari, M. Klingauf, K. Grohmanova, A. Veligodskiy, D. Didry, D. Le, C. Egile, M.F. Carlier, and R. Kroschewski. 2007. IQGAP1 stimulates actin assembly through the N-WASP-Arp2/3 pathway. J Biol Chem. 282:426-435.

Lim, B.C., S. Matsumoto, H. Yamamoto, H. Mizuno, J. Kikuta, M. Ishii, and A. Kikuchi. 2016. Prickle1 promotes focal adhesion disassembly in cooperation with the CLASP-LL5beta complex in migrating cells. J Cell Sci. 129:3115-3129.

Liu, J., P. Yue, V.V. Artym, S.C. Mueller, and W. Guo. 2009. The role of the exocyst in matrix metalloproteinase secretion and actin dynamics during tumor cell invadopodia formation. Mol Biol Cell. 20:3763-3771.

Liu, Q., F. Liu, K.L. Yu, R. Tas, I. Grigoriev, S. Remmelzwaal, A. Serra-Marques, L.C. Kapitein, A.J. Heck, and A. Akhmanova. 2016. MICAL3 Flavoprotein Monooxygenase Forms a Complex with Centralspindlin and Regulates Cytokinesis. J Biol Chem. 291:20617-20629.

Malacombe, M., M.F. Bader, and S. Gasman. 2006. Exocytosis in neuroendocrine cells: new tasks for actin. Biochim Biophys Acta. 1763:1175-1183.

Mana, G., F. Clapero, E. Panieri, V. Panero, R.T. Bottcher, H.Y. Tseng, F. Saltarin, E. Astanina, K.I. Wolanska, M.R. Morgan, M.J. Humphries, M.M. Santoro, G. Serini, and D. Valdembri. 2016. PPFIA1 drives active alpha5beta1 integrin recycling and controls fibronectin fibrillogenesis and vascular morphogenesis. Nat Commun. 7:13546.

Martin-Urdiroz, M., M.J. Deeks, C.G. Horton, H.R. Dawe, and I. Jourdain. 2016. The Exocyst Complex in Health and Disease. Front Cell Dev Biol. 4:24.

Martinez, O., C. Antony, G. Pehau-Arnaudet, E.G. Berger, J. Salamero, and B. Goud. 1997. GTP-bound forms of rab6 induce the redistribution of Golgi proteins into the endoplasmic reticulum. Proc Natl Acad Sci U S A. 94:1828-1833.

Martinez, O., A. Schmidt, J. Salamero, B. Hoflack, M. Roa, and B. Goud. 1994. The small GTP-binding protein rab6 functions in intra-Golgi transport. J Cell Biol. 127:1575-1588.

Masedunskas, A., M. Sramkova, L. Parente, K.U. Sales, P. Amornphimoltham, T.H. Bugge, and R. Weigert. 2011. Role for the actomyosin complex in regulated exocytosis revealed by intravital microscopy. Proc Natl Acad Sci U S A. 108:13552-13557.

Maurer, S.P., F.J. Fourniol, G. Bohner, C.A. Moores, and T. Surrey. 2012. EBs recognize a nucleotide-dependent structural cap at growing microtubule ends. Cell. 149:371-382.

McCallum, S.J., W.J. Wu, and R.A. Cerione. 1996. Identification of a putative effector for Cdc42Hs with high sequence similarity to the RasGAP-related protein IQGAP1 and a Cdc42Hs binding partner with similarity to IQGAP2. J Biol Chem. 271:21732-21737.

McNally, F.J. 2013. Mechanisms of spindle positioning. J Cell Biol. 200:131-140.

Mendez, C.F., I.B. Leibiger, B. Leibiger, M. Hoy, J. Gromada, P.O. Berggren, and A.M. Bertorello. 2003. Rapid association of protein kinase C-epsilon with insulin granules is essential for insulin exocytosis. J Biol Chem. 278:44753-44757.

Monier, S., F. Jollivet, I. Janoueix-Lerosey, L. Johannes, and B. Goud. 2002. Characterization of novel Rab6-interacting proteins involved in endosome-to-TGN transport. Traffic. 3:289-297.

Moseley, J.B., F. Bartolini, K. Okada, Y. Wen, G.G. Gundersen, and B.L. Goode. 2007. Regulated binding of adenomatous polyposis coli protein to actin. J Biol Chem. 282:12661-12668.

Moss, D.K., G. Bellett, J.M. Carter, M. Liovic, J. Keynton, A.R. Prescott, E.B. Lane, and M.M. Mogensen. 2007. Ninein is released from the centrosome and moves bi-directionally along microtubules. J Cell Sci. 120:3064-3074.

Nammalwar, R.C., A. Heil, and V. Gerke. 2015. Ezrin interacts with the scaffold protein IQGAP1 and affects its cortical localization. Biochim Biophys Acta. 1853:2086-2094.

Nashchekin, D., A.R. Fernandes, and D. St Johnston. 2016. Patronin/Shot Cortical Foci Assemble the Noncentrosomal Microtubule Array that Specifies the Drosophila Anterior-Posterior Axis. Dev Cell. 38:61-72.

Nightingale, T.D., D.F. Cutler, and L.P. Cramer. 2012. Actin coats and rings promote regulated exocytosis. Trends Cell Biol. 22:329-337.

Ning, W., Y. Yu, H. Xu, X. Liu, D. Wang, J. Wang, Y. Wang, and W. Meng. 2016. The CAMSAP3-ACF7 Complex Couples Noncentrosomal Microtubules with Actin Filaments to Coordinate Their Dynamics. Dev Cell. 39:61-74.

Nomura, H., T. Ohtsuka, S. Tadokoro, M. Tanaka, and N. Hirashima. 2009. Involvement of ELKS, an active zone protein, in exocytotic release from RBL-2H3 cells. Cell Immunol. 258:204-211.

Noordstra, I., Q. Liu, W. Nijenhuis, S. Hua, K. Jiang, M. Baars, S. Remmelzwaal, M. Martin, L.C. Kapitein, and A. Akhmanova. 2016. Control of apico-basal epithelial polarity by the microtubule minus-end-binding protein CAMSAP3 and spectraplakin ACF7. J Cell Sci. 129:4278-4288.

Noritake, J., M. Fukata, K. Sato, M. Nakagawa, T. Watanabe, N. Izumi, S. Wang, Y. Fukata, and K. Kaibuchi. 2004. Positive role of IQGAP1, an effector of Rac1, in actin-meshwork formation at sites of cell-cell contact. Mol Biol Cell. 15:1065-1076.

Ohara-Imaizumi, M., T. Ohtsuka, S. Matsushima, Y. Akimoto, C. Nishiwaki, Y. Nakamichi, T. Kikuta, S. Nagai, H. Kawakami, T. Watanabe, and S. Nagamatsu. 2005. ELKS, a protein structurally related to the active zone-associated protein CAST, is expressed in pancreatic beta cells and functions in insulin exocytosis: interaction of ELKS with exocytotic machinery analyzed by total internal reflection fluorescence microscopy. Mol Biol Cell. 16:3289-3300.

Okada, K., F. Bartolini, A.M. Deaconescu, J.B. Moseley, Z. Dogic, N. Grigorieff, G.G. Gundersen, and B.L. Goode. 2010. Adenomatous polyposis coli protein nucleates actin assembly and synergizes with the formin mDia1. J Cell Biol. 189:1087-1096.

Paranavitane, V., W.J. Coadwell, A. Eguinoa, P.T. Hawkins, and L. Stephens. 2003. LL5beta is a phosphatidylinositol (3,4,5)-trisphosphate sensor that can bind the cytoskeletal adaptor, gamma-filamin. J Biol Chem. 278:1328-1335.

Park, Y.S., E.M. Hur, B.H. Choi, E. Kwak, D.J. Jun, S.J. Park, and K.T. Kim. 2006. Involvement of protein kinase C-epsilon in activity-dependent potentiation of large dense-core vesicle exocytosis in chromaffin cells. J Neurosci. 26:8999-9005.

Paul, N.R., G. Jacquemet, and P.T. Caswell. 2015. Endocytic Trafficking of Integrins in Cell Migration. Curr Biol. 25:R1092-1105.

Perez, F., G.S. Diamantopoulos, R. Stalder, and T.E. Kreis. 1999. CLIP-170 highlights growing microtubule ends in vivo. Cell. 96:517-527.

Perlson, E., A.G. Hendricks, J.E. Lazarus, K. Ben-Yaakov, T. Gradus, M. Tokito, and E.L. Holzbaur. 2013. Dynein interacts with the neural cell adhesion molecule (NCAM180) to tether dynamic microtubules and maintain synaptic density in cortical neurons. J Biol Chem. 288:27812-27824.

Pfister, A.S., M.V. Hadjihannas, W. Rohrig, A. Schambony, and J. Behrens. 2012. Amer2 protein interacts with EB1 protein and adenomatous polyposis coli (APC) and controls microtubule stability and cell migration. J Biol Chem. 287:35333-35340.

Pierre, P., J. Scheel, J.E. Rickard, and T.E. Kreis. 1992. CLIP-170 links endocytic vesicles to microtubules. Cell. 70:887-900.

Proszynski, T.J., J. Gingras, G. Valdez, K. Krzewski,

and J.R. Sanes. 2009. Podosomes are present in a postsynaptic apparatus and participate in its maturation. Proc Natl Acad Sci U S A. 106:18373-18378.

Proszynski, T.J., and J.R. Sanes. 2013. Amotl2 interacts with LL5beta, localizes to podosomes and regulates postsynaptic differentiation in muscle. J Cell Sci. 126:2225-2235.

Rittmeyer, E.N., S. Daniel, S.C. Hsu, and M.A. Osman. 2008. A dual role for IQGAP1 in regulating exocytosis. J Cell Sci. 121:391-403.

Sakurai-Yageta, M., C. Recchi, G. Le Dez, J.B. Sibarita, L. Daviet, J. Camonis, C. D'Souza-Schorey, and P. Chavrier. 2008. The interaction of IQGAP1 with the exocyst complex is required for tumor cell invasion downstream of Cdc42 and RhoA. J Cell Biol. 181:985-998.

Salvarezza, S.B., S. Deborde, R. Schreiner, F. Campagne, M.M. Kessels, B. Qualmann, A. Caceres, G. Kreitzer, and E. Rodriguez-Boulan. 2009. LIM kinase 1 and cofilin regulate actin filament population required for dynamin-dependent apical carrier fission from the trans-Golgi network. Mol Biol Cell. 20:438-451.

Sato, T., S. Mushiake, Y. Kato, K. Sato, M. Sato, N. Takeda, K. Ozono, K. Miki, Y. Kubo, A. Tsuji, R. Harada, and A. Harada. 2007. The Rab8 GTPase regulates apical protein localization in intestinal cells. Nature. 448:366-369.

Schmidt, N., S. Basu, S. Sladecek, S. Gatti, J. van Haren, S. Treves, J. Pielage, N. Galjart, and H.R. Brenner. 2012. Agrin regulates CLASP2-mediated capture of microtubules at the neuromuscular junction synaptic membrane. J Cell Biol. 198:421-437.

Schmoranzer, J., G. Kreitzer, and S.M. Simon. 2003. Migrating fibroblasts perform polarized, microtubule-dependent exocytosis towards the leading edge. J Cell Sci. 116:4513-4519.

Schuyler, S.C., and D. Pellman. 2001. Microtubule "plus-end-tracking proteins": The end is just the beginning. Cell. 105:421-424.

Serra-Pages, C., N.L. Kedersha, L. Fazikas, Q. Medley, A. Debant, and M. Streuli. 1995. The LAR transmembrane protein tyrosine phosphatase and a coiled-coil LAR-interacting protein co-localize at focal adhesions. EMBO J. 14:2827-2838.

Siesser, P.F., M. Motolese, M.P. Walker, D. Goldfarb, K. Gewain, F. Yan, R.M. Kulikauskas, A.J. Chien, L. Wordeman, and M.B. Major. 2012. FAM123A binds to microtubules and inhibits the guanine nucleotide exchange factor ARHGEF2 to decrease actomyosin contractility. Sci Signal. 5:ra64.

Small, J.V., and I. Kaverina. 2003. Microtubules meet substrate adhesions to arrange cell polarity. Curr Opin Cell Biol. 15:40-47.

Sokac, A.M., C. Schietroma, C.B. Gundersen, and W.M. Bement. 2006. Myosin-1c couples assembling actin to membranes to drive compensatory endocytosis. Dev Cell. 11:629-640.

Spangler, S.A., and C.C. Hoogenraad. 2007. Liprin-alpha proteins: scaffold molecules for synapse maturation. Biochem Soc Trans. 35:1278-1282.

Stehbens, S., and T. Wittmann. 2012. Targeting and transport: how microtubules control focal adhesion dynamics. J Cell Biol. 198:481-489.

Stehbens, S.J., M. Paszek, H. Pemble, A. Ettinger, S. Gierke, and T. Wittmann. 2014. CLASPs link focal-adhesion-associated microtubule capture to localized exocytosis and adhesion site turnover. Nat Cell Biol. 16:561-573.

Su, L.K., M. Burrell, D.E. Hill, J. Gyuris, R. Brent, R. Wiltshire, J. Trent, B. Vogelstein, and K.W. Kinzler. 1995. APC binds to the novel protein EB1. Cancer Res. 55:2972-2977.

Sudhof, T.C. 2012. The presynaptic active zone. Neuron. 75:11-25.

Sun, Z., H.Y. Tseng, S. Tan, F. Senger, L. Kurzawa, D. Dedden, N. Mizuno, A.A. Wasik, M. Thery, A.R. Dunn, and R. Fassler. 2016. Kank2 activates talin, reduces force transduction across integrins and induces central adhesion formation. Nat Cell Biol. 18:941-953.

Suozzi, K.C., X. Wu, and E. Fuchs. 2012. Spectraplakins: master orchestrators of cytoskeletal dynamics. J Cell Biol. 197:465-475.

Terman, J.R., T. Mao, R.J. Pasterkamp, H.H. Yu, and A.L. Kolodkin. 2002. MICALs, a family of conserved flavoprotein oxidoreductases, function in plexin-mediated axonal repulsion. Cell. 109:887-900.

Tokoro, T., S. Higa, M. Deguchi-Tawarada, E. Inoue, I. Kitajima, and T. Ohtsuka. 2007. Localization of the active zone proteins CAST, ELKS,

and Piccolo at neuromuscular junctions. Neuroreport. 18:313-316.

Toomre, D., P. Keller, J. White, J.C. Olivo, and K. Simons. 1999. Dual-color visualization of trans-Golgi network to plasma membrane traffic along microtubules in living cells. J Cell Sci. 112 (Pt 1):21-33.

Toya, M., S. Kobayashi, M. Kawasaki, G. Shioi, M. Kaneko, T. Ishiuchi, K. Misaki, W. Meng, and M. Takeichi. 2016. CAMSAP3 orients the apical-to-basal polarity of microtubule arrays in epithelial cells. Proc Natl Acad Sci U S A. 113:332-337.

Tsuboi, T., M.A. Ravier, H. Xie, M.A. Ewart, G.W. Gould, S.A. Baldwin, and G.A. Rutter. 2005. Mammalian exocyst complex is required for the docking step of insulin vesicle exocytosis. J Biol Chem. 280:25565-25570.

van der Vaart, B., W.E. van Riel, H. Doodhi, J.T. Kevenaar, E.A. Katrukha, L. Gumy, B.P. Bouchet, I. Grigoriev, S.A. Spangler, K.L. Yu, P.S. Wulf, J. Wu, G. Lansbergen, E.Y. van Battum, R.J. Pasterkamp, Y. Mimori-Kiyosue, J. Demmers, N. Olieric, I.V. Maly, C.C. Hoogenraad, and A. Akhmanova. 2013. CFEOM1-associated kinesin KIF21A is a cortical microtubule growth inhibitor. Dev Cell. 27:145-160.

Wang, S., T. Watanabe, J. Noritake, M. Fukata, T. Yoshimura, N. Itoh, T. Harada, M. Nakagawa, Y. Matsuura, N. Arimura, and K. Kaibuchi. 2007. IQGAP3, a novel effector of Rac1 and Cdc42, regulates neurite outgrowth. J Cell Sci. 120:567-577.

Wang, X., X. Zhuang, D. Cao, Y. Chu, P. Yao, W. Liu, L. Liu, G. Adams, G. Fang, Z. Dou, X. Ding, Y. Huang, D. Wang, and X. Yao. 2012. Mitotic regulator SKAP forms a link between kinetochore core complex KMN and dynamic spindle microtubules. J Biol Chem. 287:39380-39390.

Watanabe, T., J. Noritake, M. Kakeno, T. Matsui, T. Harada, S. Wang, N. Itoh, K. Sato, K. Matsuzawa, A. Iwamatsu, N. Galjart, and K. Kaibuchi. 2009. Phosphorylation of CLASP2 by GSK-3beta regulates its interaction with IQGAP1, EB1 and microtubules. J Cell Sci. 122:2969-2979.

Watanabe, T., S. Wang, J. Noritake, K. Sato, M. Fukata, M. Takefuji, M. Nakagawa, N. Izumi, T. Akiyama, and K. Kaibuchi. 2004. Interaction with IQGAP1 links APC to Rac1, Cdc42, and actin filaments during cell polarization and migration. Dev Cell. 7:871-883.

Wen, Y., C.H. Eng, J. Schmoranzer, N. Cabrera-Poch, E.J. Morris, M. Chen, B.J. Wallar, A.S. Alberts, and G.G. Gundersen. 2004. EB1 and APC bind to mDia to stabilize microtubules downstream of Rho and promote cell migration. Nat Cell Biol. 6:820-830.

White, J., L. Johannes, F. Mallard, A. Girod, S. Grill, S. Reinsch, P. Keller, B. Tzschaschel, A. Echard, B. Goud, and E.H. Stelzer. 1999. Rab6 coordinates a novel Golgi to ER retrograde transport pathway in live cells. J Cell Biol. 147:743-760.

Wu, L.G., E. Hamid, W. Shin, and H.C. Chiang. 2014. Exocytosis and endocytosis: modes, functions, and coupling mechanisms. Annu Rev Physiol. 76:301-331.

Wu, X., A. Kodama, and E. Fuchs. 2008. ACF7 regulates cytoskeletal-focal adhesion dynamics and migration and has ATPase activity. Cell. 135:137-148.

Xue, R., Y. Zhao, L. Su, F. Ye, and P. Chen. 2009. PKC epsilon facilitates recovery of exocytosis after an exhausting stimulation. Pflugers Arch. 458:1137-1149.

Yi, Z., H. Yokota, S. Torii, T. Aoki, M. Hosaka, S. Zhao, K. Takata, T. Takeuchi, and T. Izumi. 2002. The Rab27a/granuphilin complex regulates the exocytosis of insulin-containing dense-core granules. Mol Cell Biol. 22:1858-1867.

Zaoui, K., K. Benseddik, P. Daou, D. Salaun, and A. Badache. 2010. ErbB2 receptor controls microtubule capture by recruiting ACF7 to the plasma membrane of migrating cells. Proc Natl Acad Sci U S A. 107:18517-18522.

Zhou, R., Z. Guo, C. Watson, E. Chen, R. Kong, W. Wang, and X. Yao. 2003. Polarized distribution of IQGAP proteins in gastric parietal cells and their roles in regulated epithelial cell secretion. Mol Biol Cell. 14:1097-1108.

Zhu, X., R. Hu, M. Brissova, R.W. Stein, A.C. Powers, G. Gu, and I. Kaverina. 2015. Microtubules Negatively Regulate Insulin Secretion in Pancreatic beta Cells. Dev Cell. 34:656-668.

Zhu, X., and I. Kaverina. 2013. Golgi as an MTOC: making microtubules for its own good. Histochem Cell Biol. 140:361-367.

3

Mesenchymal cell invasion requires cooperative regulation of persistent microtubule growth by SLAIN2 and CLASP1

Benjamin P. Bouchet[1*], Ivar Noordstra[1*], Miranda van Amersfoort[2], Eugene A. Katrukha[1], York-Christoph Ammon[1], Natalie D. ter Hoeve[2], Louis Hodgson[3], Marileen Dogterom[4], Patrick W.B. Derksen[2] and Anna Akhmanova[1]

Developmental Cell (2016); 39:708-723.

*Authors contributed equally

[1]Cell Biology, Faculty of Science, Utrecht University, 3584 CH Utrecht, The Netherlands
[2]Department of Pathology, University Medical Center Utrecht, Heidelberglaan 100, 3584 CX Utrecht, The Netherlands
[3]Department of Anatomy and Structural Biology, Gruss-Lipper Biophotonics Center, Albert Einstein College of Medicine, Bronx, NY 10461, USA
[4]Department of Bionanoscience, Kavli Institute of Nanoscience, Delft University of Technology, Lorentzweg 1, 2628 CJ Delft, The Netherlands

Summary

Microtubules regulate signaling, trafficking, and cell mechanics, but the respective contribution of these functions to cell morphogenesis and migration in 3D matrices is unclear. Here, we report that the microtubule plus-end tracking protein (+TIP) SLAIN2, which suppresses catastrophes, is not required for 2D cell migration but is essential for mesenchymal cell invasion in 3D culture and in a mouse cancer model. We show that SLAIN2 inactivation does not affect Rho GTPase activity, trafficking, and focal adhesion formation. However, SLAIN2-dependent catastrophe inhibition determines microtubule resistance to compression and pseudopod elongation. Another +TIP, CLASP1, is also needed to form invasive pseudopods because it prevents catastrophes specifically at their tips. When microtubule growth persistence is reduced, inhibition of depolymerization is sufficient for pseudopod maintenance but not remodeling. We propose that catastrophe inhibition by SLAIN2 and CLASP1 supports mesenchymal cell shape in soft 3D matrices by enabling microtubules to perform a load-bearing function.

Introduction

The ability to move through a three-dimensional (3D) matrix is a physiological feature found in many differentiated cell types and in developmental precursors (Friedl and Gilmour, 2009; Lam and Huttenlocher, 2013; Nakaya and Sheng, 2008). Besides its role in tissue morphogenesis and immune surveillance, cell invasion is also associated with metastasis in solid cancers (Chaffer and Weinberg, 2011). Importantly, cell migration modes in 3D matrices are determined by cell shape characteristics (Friedl and Gilmour, 2009). In particular, mesenchymal cell motility, found in fibroblasts, endothelial cells, embryonic cells undergoing epithelial-mesenchymal transition (EMT), and invasive tumors, requires formation of long pseudopods (Cheung et al., 2013; Clark and Vignjevic, 2015; Friedl and Gilmour, 2009; Grinnell and Petroll, 2010; Petrie and Yamada, 2015).

The importance of microtubules (MTs) for mesenchymal pseudopod elongation in soft matrices has been known since the 1980s (Grinnell et al., 2003; Tomasek and Hay, 1984). Numerous studies showed that the destruction or perturbation of the MT network by MT-targeting agents (MTAs) abolishes pseudopod-based invasion (Kikuchi and Takahashi, 2008; Lee et al., 2015; Martins and Kolega, 2012; Oyanagi et al., 2012; Pourroy et al., 2006; Rhee et al., 2007; Tran et al., 2009). However, the molecular mechanisms responsible for the ability of MTs to support mesenchymal cell protrusions in soft matrices are yet to be established.

Until now, the mechanical involvement of the cytoskeleton in cell invasion was mostly linked to actin and its regulators (Kikuchi and Takahashi, 2008; Kutys and Yamada, 2014; Sahai and Marshall, 2003; Sanz-Moreno and Marshall, 2010; Wilson et al., 2013). In contrast, MTs are viewed as signaling and trafficking platforms that modulate cell shape by indirectly regulating Rho guanosine triphosphatases (GTPases), substrate adhesion, and polarity (Etienne-Manneville, 2013; Gierke and Wittmann, 2012; Petrie and Yamada, 2015; Rhee et al., 2007). Depletion of the plus-end tracking protein (+TIP) EB1 caused invasion defects in hepatocyte growth factor-stimulated canine epithelial cells (Gierke and Wittmann, 2012). EB1 controls the recruitment of a broad variety of other +TIPs involved in MT polymerization and depolymerization, their interaction with various cellular structures, transport, and signaling (Akhmanova and Steinmetz, 2015). The mechanistic basis for the involvement of EB1 in pseudopod protrusion thus needs to be elucidated.

Several studies introduced the idea that MTs can mechanically contribute to cell morphogenesis (Brangwynne et al., 2006; Dennerll et al., 1988; Fygenson et al., 1997a; Matrone et al., 2010; Wang et al., 2001; Winckler and Solomon, 1991). The tensegrity model suggests that the ability of MTs to withstand compression at the cell cortex controls cell shape in soft 3D matrices (Ingber, 2003). However, a limitation to such a func-

tion is that the dynamic MT tips in proximity of the cell cortex are expected to undergo force-induced catastrophes (Janson et al., 2003; Laan et al., 2008). An important question is thus whether physiological mechanisms of catastrophe regulation are compatible with a load-bearing function of MTs in 3D cell morphogenesis.

Here, we identify the +TIP and catastrophe inhibitor SLAIN2 (van der Vaart et al., 2011) as an essential factor for mesenchymal cell invasion both *in vitro* and in a mouse tumor model. This function is independent of the regulation of Rho GTPase activity, vesicle transport, and focal adhesion formation but rather underlies the resistance of dynamic MT plus ends to compression. We show that SLAIN2, as well as another +TIP, CLASP1, enable mesenchymal cells to form long invasive pseudopods by promoting highly persistent MT growth at their tips. When persistent MT growth is perturbed, suppression of MT depolymerization is sufficient for the maintenance but not for the remodeling of invasive pseudopods. Based on experimental data and computer simulations, we discuss the implications of these findings for the mechanical role of dynamic MTs in cell invasion and their relevance in cancer therapeutics.

Results

SLAIN2-dependent inhibition of MT catastrophes is required for mesenchymal cell invasion

To test how the regulation of MT growth affects mesenchymal cell invasion, we used cancer cells from different origins (MDA-MB-231, HT-1080) and non-tumor human mammary cells carrying an inducible EMT system based on doxycycline-controlled expression of ZEB1 (Zhang et al., 2015) (Figures S1A and S1B). These three cell models displayed invasive properties when grown in a soft collagen I-based 3D matrix with characteristic long invasive pseudopods at their leading edge (Figure 1A). We previously showed that the +TIP SLAIN2 inhibits MT catastrophes specifically in interphase cells by promoting EB1-dependent recruitment of the polymerase ch-TOG to MT plus ends (van der Vaart et al., 2011). To test the importance of this mechanism for cell invasion, we inactivated SLAIN2 by RNA-interference-mediated knockdown or expression of a dominant negative mutant, SLAIN2-N (SL2-N), which binds ch-TOG but not to EB1 (Figures 1B and 1C) (van der Vaart et al., 2011). As we showed before, these treatments induced a loss of ch-TOG from MT plus ends (Figure S1C) and reduced MT growth rate and persistence (Figures S1D and S1E; Movie S1). A similar MT growth defect was observed by depleting ch-TOG (Figures S1D–S1F), confirming the notion that the effect of SLAIN2 depletion on MT dynamics is due to the reduction of ch-TOG localization at MT plus ends. Loss of SLAIN2 function did not affect cell-cycle progression or localization of other +TIPs, such as CLIP-170 and CLASP1, to MT plus ends (Figures 1D and S1G). Although MTs showed highly interrupted growth, they still formed a morphologically normal network, the density of which was similar to control cells at the leading edge (Figures 1E, 1F, and S1H).

SLAIN2-depleted cells spread and migrated normally on a stiff 2D matrix consisting of collagen I-coated coverslips (Figures 1F, S2A, and S2B; Movie S2). However, inside soft collagen I gels (2 mg/mL), loss of SLAIN2 function caused a dramatic change in cell morphology, as the cells completely failed to form long invasive pseudopods (Figures 1G–1I and Movie S2). This defect was due to the inability of SLAIN2-depleted cells to elongate their protrusions, while protrusion initiation was unaffected (Figures S2C and S2D). Importantly, the difference between the effect of SLAIN2 depletion in 2D and 3D was not associated with the differential subcellular localization of SLAIN2, as it tracked all growing MT plus ends both on stiff 2D and in soft 3D matrices (Figure S1I). Consistently, the extent of MT dynamics perturbation by SLAIN2 inactivation was the same in soft 3D gels as on stiff 2D substrates, and MTs penetrated pseudopod tips in a similar fashion in control and SLAIN2-depleted cells (Figures S1D, S1E, and 1G).

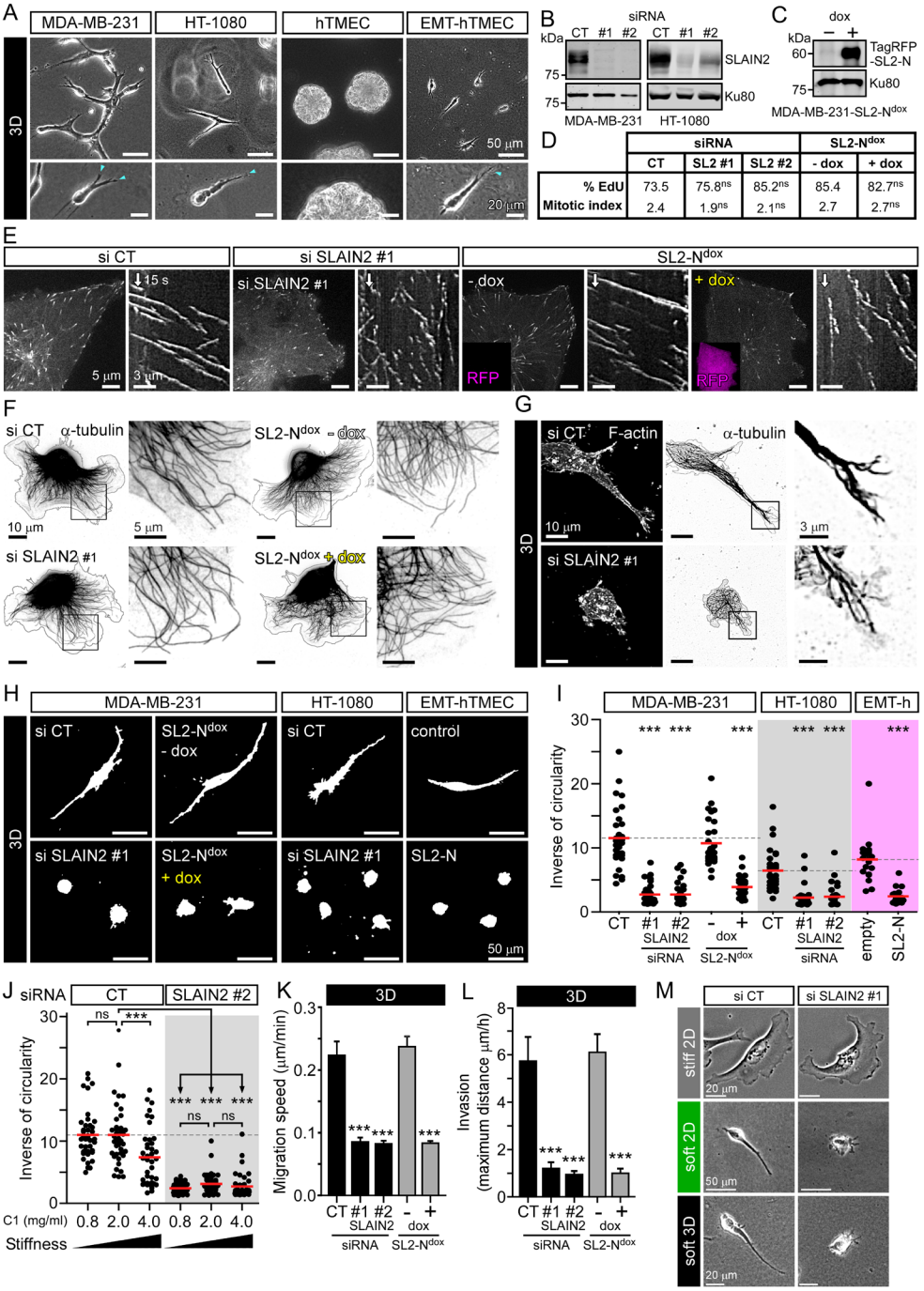

Figure 1. SLAIN2 is required for mesenchymal cell invasion

(A) Morphology of cancer and non-cancer mesenchymal cells grown in collagen I-based 3D matrices. MDA-MB-231, HT-1080, and untransformed human mammary epithelial cells converted to mesenchymal cells by EMT (EMT-hTMEC, 4 days in 3D, compared with control cells hTMEC, 16 days in 3D); blue arrowheads indicate invasive pseudopods at the leading edge. **(B and C)**

Western blot analysis of SLAIN2 depletion by two independent siRNAs (#1 and #2) compared with control siRNA (CT) in MDA-MB-231 and HT-1080 cells (B), and doxycycline-induced expression (dox) of the TagRFP-T-tagged dominant negative SLAIN2 mutant (SL2-N) in MDA-MB-231 cells (MDA-MB-231-SL2-Ndox) (C). **(D)** S-phase progression and cell division assessed by 5-ethynyl-2′-deoxyuridine (EdU) incorporation, expressed in percentage, and mitotic index in MDA-MB-231 cells treated as in (B) and (C). **(E)** Changes in MT dynamics in MDA-MB-231 cells treated as in (B) and (C) and illustrated by live fluorescence images and kymographs of EB3-GFP. **(F and G)** MT network in 2D- and 3D-grown MDA-MB-231 cells treated as in (B) and (C); immunofluorescence staining of α-tubulin and cell outline (gray line). **(H and I)** Effect of SLAIN2 inactivation on invasive cell morphology of 3D-grown cells (H) and corresponding quantification of cell elongation (I); EMT-hTMECs were transduced with the empty vector or TagRFP-T-tagged dominant negative SLAIN2-N. **(J)** Quantification of SLAIN2-depleted MDA-MB-231 cell elongation in collagen I (C1) gels of different concentrations. **(K and L)** Migration speed (K) and maximum invasion distance (L) of 3D-cultured cells treated as in (B) and (C). **(M)** Comparison of cell morphology on 2D stiff matrix (collagen I-coated glass), on top of 2D soft matrix (2 mg/mL collagen I gel) or inside 3D soft matrix (2 mg/mL collagen I gel) using phase-contrast imaging. Bar plots are presented as mean ± SEM. Red line denotes the mean. In all plots, ***$p < 0.001$, Mann-Whitney U test; ns, no significant difference with control. See also Figures S1 and S2; Movies S1 and S2.

Matrix stiffness can influence MT stability and their ability to activate Rho to control cell contractility (Heck et al., 2012). Based on previous studies, we defined collagen I concentration ranging from 0.8 to 4 mg/mL as conditions providing either more compliant or stiffer 3D matrices (Heck et al., 2012; Petrie et al., 2012; Wolf et al., 2013). Neither softening nor stiffening of the matrix rescued pseudopod defects induced by SLAIN2 depletion that we observed in 2-mg/mL collagen I cultures (Figure 1J). In fact, stiffening significantly reduced pseudopod elongation in control cells (Figure 1J), possibly by activating Rho-dependent contractility (Heck et al., 2012) or providing excessive adhesion ligand.

The loss of pseudopods in SLAIN2-depleted cells correlated with strong suppression of invasive properties (Figures 1K and 1L; Movie S2). Importantly, SLAIN2-depleted cells were also unable to extend protrusions when cultured on top of a soft collagen matrix (Figures 1M, S2E, and S2F); however, despite their small size, the 2D motility of these cells was not impaired compared with control cells (Figures S2G and S2H). This indicates that SLAIN2 is required for cell elongation in soft environments independently of their dimensionality, but is only essential for motility in the 3D situation. Depletion of ch-TOG had the same effects as SLAIN2 inactivation on interphase cell morphology in soft 3D matrices and similarly suppressed invasiveness (Figures S2I–S2L). These results show that the SLAIN2/ch-TOG axis determines pseudopod elongation in a soft environment without affecting MT network integrity, and this function is essential for mesenchymal motility of cells embedded in 3D matrices.

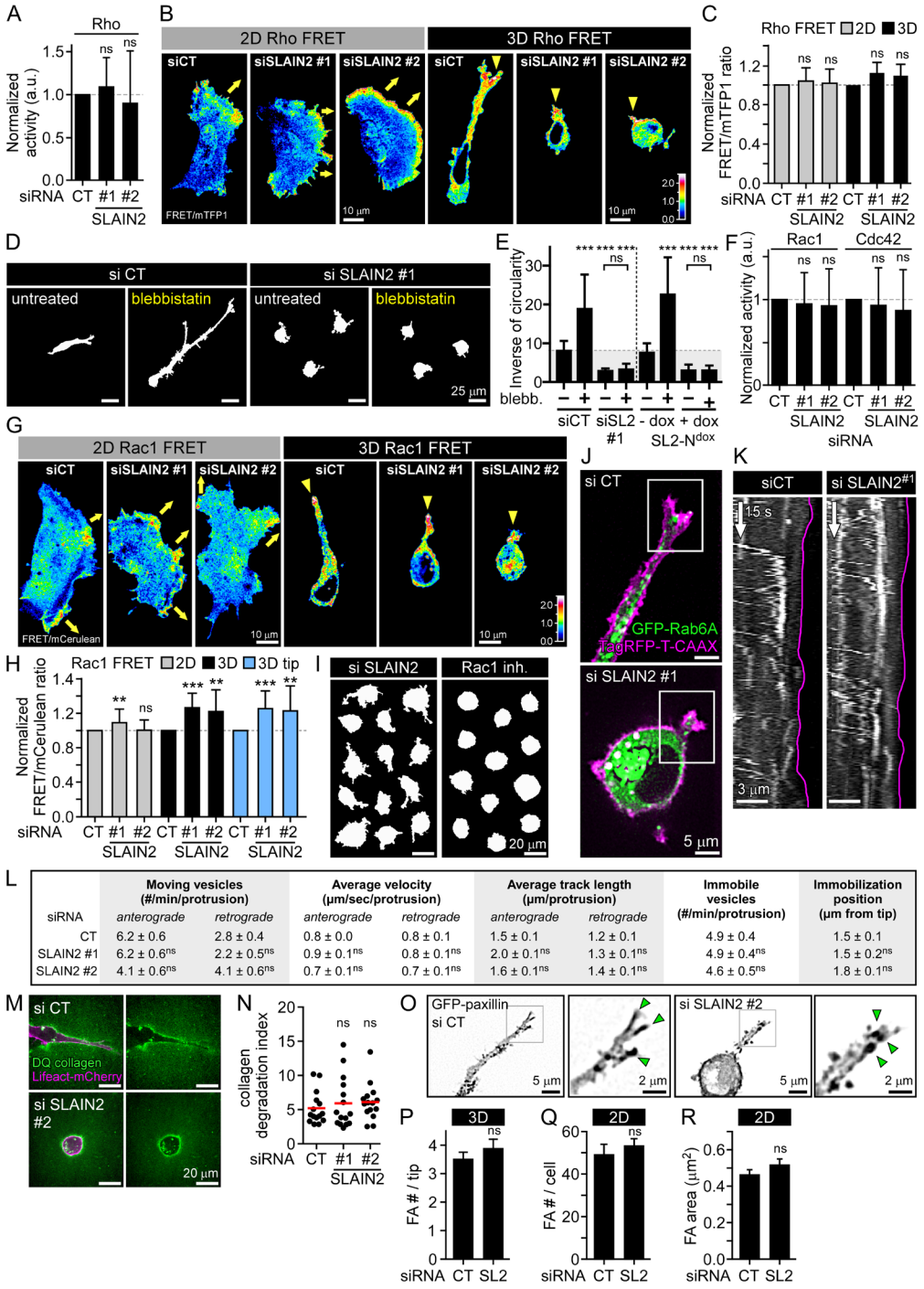

siRNA	Moving vesicles (#/min/protrusion) anterograde	Moving vesicles (#/min/protrusion) retrograde	Average velocity (µm/sec/protrusion) anterograde	Average velocity (µm/sec/protrusion) retrograde	Average track length (µm/protrusion) anterograde	Average track length (µm/protrusion) retrograde	Immobile vesicles (#/min/protrusion)	Immobilization position (µm from tip)
CT	6.2 ± 0.6	2.8 ± 0.4	0.8 ± 0.0	0.8 ± 0.1	1.5 ± 0.1	1.2 ± 0.1	4.9 ± 0.4	1.5 ± 0.1
SLAIN2 #1	6.2 ± 0.6^{ns}	2.2 ± 0.5^{ns}	0.9 ± 0.1^{ns}	0.8 ± 0.1^{ns}	2.0 ± 0.1^{ns}	1.3 ± 0.1^{ns}	4.9 ± 0.4^{ns}	1.5 ± 0.2^{ns}
SLAIN2 #2	4.1 ± 0.6^{ns}	4.1 ± 0.6^{ns}	0.7 ± 0.1^{ns}	0.7 ± 0.1^{ns}	1.6 ± 0.1^{ns}	1.4 ± 0.1^{ns}	4.6 ± 0.5^{ns}	1.8 ± 0.1^{ns}

Figure 2. Effect of SLAIN2 inactivation in Rho GTPase activity, exocytotic transport, collagenolysis, and focal adhesions

(A) Rho activation assay in control and SLAIN2-depleted cells. Error bars denote SD. **(B and C)** Ratiometric representation (B) and measurement (C) of Rho biosensor activation from FRET im-

aging 2D- and 3D-grown cells depleted for SLAIN2. Yellow arrows, migration direction in 2D; yellow arrowheads, pseudopod tip-localized active Rho. Error bars denote SEM. **(D and E)** Effects of myosin II inhibition by blebbistatin (blebb.) on invasive morphology of 3D-grown cells (D) and quantification of cell elongation (E), Error bars denote SEM. **(F)** Rac1 and Cdc42 activation assays in SLAIN2-depleted cells. Error bars denote SD. **(G and H)** Ratiometric representation (G) and measurement (H) of Rac1 biosensor activation from FRET imaging in 2D- and 3D-grown cells depleted for SLAIN2 (3D tip, 5 µm). Yellow arrows and arrowheads as in (B). Error bars denote SEM. **(I)** Comparison of the effects of Rac1 inactivation (NSC23766 inhibitor, inh.) to SLAIN2 inactivation (siRNA) on pseudopod formation. **(J and K)** Transport of exocytotic vesicles marked with GFP-Rab6A in SLAIN2-depleted cells grown in 3D and expressing the membrane marker TagRFP-T-CAAX. Fluorescence images (J) and kymographs (K) showing Rab6A vesicle localization and dynamics in 3D-grown pseudopods (purple line, pseudopod tip). **(L)** Quantification of GFP-Rab6A localization and dynamics at pseudopod tips (5 µm) in SLAIN2-depleted cells (#, number). **(M and N)** Collagenolysis visualized by live fluorescence imaging of DQ collagen in Lifeact-mCherry expressing cells depleted for SLAIN2 and grown in 3D for 2 days (M) and corresponding quantification of collagen degradation (N). Red bar denotes the mean. **(O and P)** Focal adhesion formation visualized by live fluorescence imaging of GFP-paxillin in SLAIN2-depleted cells grown in 3D (O) and corresponding quantification of focal adhesion number (FA #) in pseudopod tips (P). Green arrowheads, cell tip-localized focal adhesions; error bars denote SEM. **(Q and R)** Quantification of focal adhesion number per cell (Q) and area (R) in SLAIN2-depleted cells grown on a stiff 2D matrix. Error bars denote SEM. In all plots, $^{**}p < 0.01$ and $^{***}p < 0.001$, Mann-Whitney U test. ns, no significant difference with control. See also Movie S3.

SLAIN2 depletion does not impair the activity of Rho GTPases, exocytotic transport, collagenolysis, or adhesion formation

MT disassembly increases cell contractility by upregulating Rho and myosin II, and reduces cell protrusion by downregulating Rac1 (Etienne-Manneville, 2013). However, using biochemical and Förster resonance energy transfer (FRET) sensor-based analysis in 2D and 3D cultures, we found that after SLAIN2 knockdown, Rho activity was not upregulated and localized normally at the leading cell edges in 2D and cell protrusions in 3D (Figures 2A–2C). Furthermore, although myosin II inhibition induced strong elongation of control cells in 3D, it completely failed to rescue formation of invasive pseudopods after SLAIN2 inactivation (Figures 2D and 2E). This indicates that Rho- and myosin II-dependent contraction did not cause the elongation defects in SLAIN2-depleted cells. The overall activities of Rac1 and Cdc42 were unchanged, and FRET biosensor imaging showed that Rac1 activity was neither reduced nor mislocalized in SLAIN2-depleted cells (Figures 2F–2H). In fact, Rac1 inhibition blocked cell elongation in 3D but also caused the loss of small protrusions, while these could still be observed in SLAIN2-depleted cells (Figure 2I). Thus Rac1 downregulation was not responsible for defects in protrusion elongation caused by SLAIN2 inactivation.

Next, we assessed MT-based transport in SLAIN2-depleted cells by imaging in 3D cultures the trafficking of exocytotic vesicles marked with GFP-Rab6A (Figures 2J and 2K; Movie S3). We found that vesicle direction, speed, track length, and tip targeting

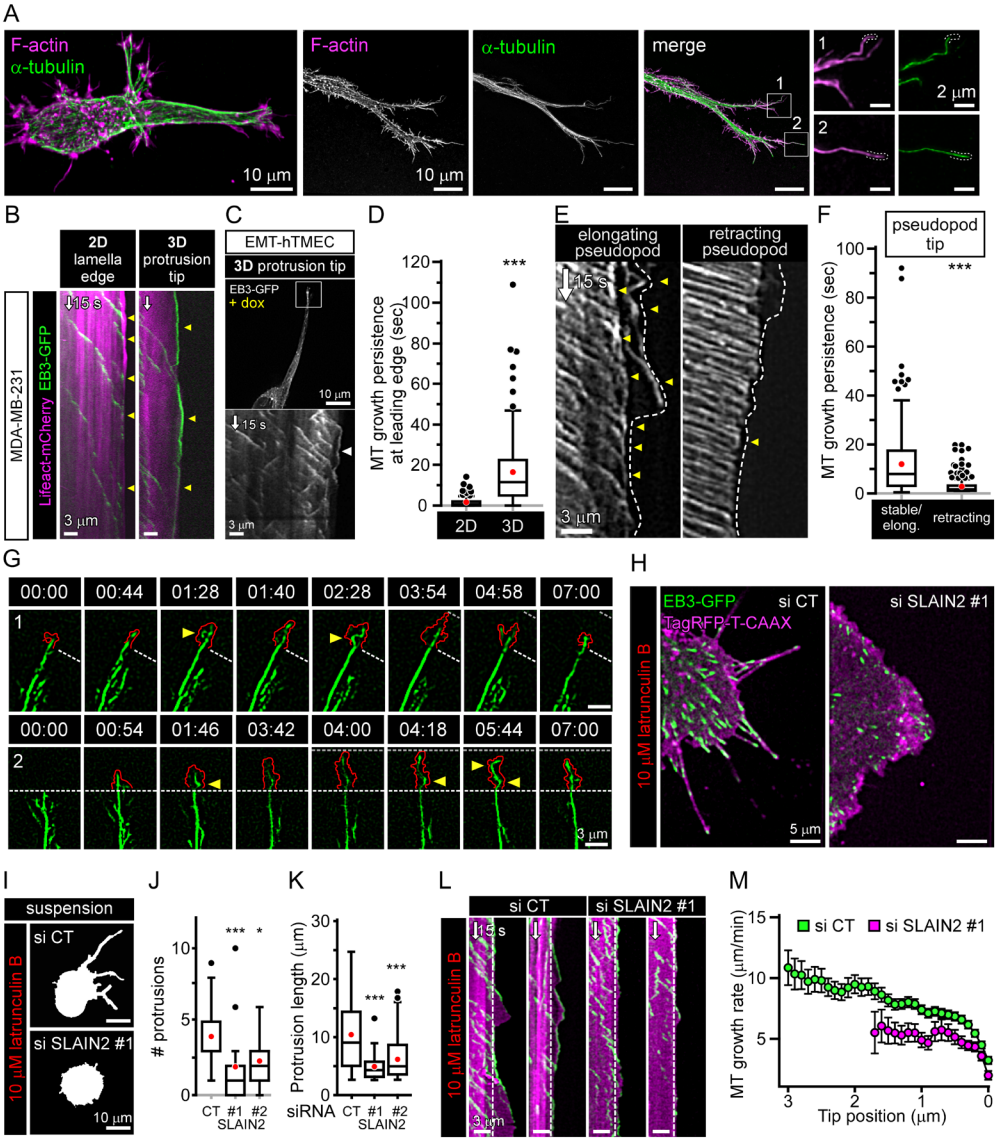

Figure 3. MT behavior at the tips of cell protrusions

(A) Organization of MTs in invasive pseudopods visualized by immunofluorescence staining of α-tubulin (F-actin staining, phalloidin). **(B and C)** Persistence of MT growth at invasive pseudopod tips of mesenchymal cells grown in 3D. Fluorescence imaging and kymographs of EB3-GFP in invasive pseudopod tips of MDA-MB-231 cells (B) (compared with 2D lamella edge) and untransformed human mammary epithelial cells converted to mesenchymal phenotype by ZEB1 expression (C). Arrowheads indicate MT growth persistence at the cell edge. **(D)** Quantification of MT growth persistence at the leading edge (5 μm) in 3D (pseudopod) compared with 2D (lamella). **(E and F)** Kymographs (E) and quantification (F) of MT growth persistence at the tips of elongating and retracting pseudopods. Arrowheads as in (B) and (C). **(G)** Fluorescence time-lapse images of β-tubulin-GFP at the tip of invasive pseudopods (1, 2). Red line, protrusion edge marked by TagRFP-T-CAAX; white dashed line, edge position at the beginning of the protrusive event; gray

dashed line, edge outermost position during the protrusive event; arrowheads, MT buckling at pseudopod tips. **(H–M)** Cell membrane deformation by growing MT ends in SLAIN2-depleted cells treated with latrunculin B. Fluorescence images of EB3-GFP and TagRFP-T-CAAX in adherent cells (H), cell morphology (I), and quantification of protrusions formed in cells that were kept in suspension to exclude the effects of cell adhesion on protrusion formation (J and K) (#, number). Kymographs of EB3-GFP and TagRFP-T-CAAX fluorescence in cell protrusions in adherent cells (L; white dashed line, lamella edge) and deceleration profiles of growing MT ends as a function of distance to the outermost tip position (M). Error bars denote SEM. Box plots indicate the 25th percentile (bottom boundary), median (middle line), mean (red dots), 75th percentile (top boundary), nearest observations within 1.5 times the interquartile range (whiskers), and outliers (black dots). In all plots, $*p < 0.05$ and $***p < 0.001$, Mann-Whitney U test. See also Movies S4 and S5.

in pseudopods were not affected by SLAIN2 inactivation (Figures 2K–2L and Movie S3). This is consistent with the presence of morphologically normal MT network in these conditions (Figures 1F and 1G). In agreement with normal exocytotic trafficking, we also found no impairment of collagenolysis (Figures 2M and 2N). Furthermore, using GFP-paxillin imaging in 3D cultures as previously described (Gierke and Wittmann, 2012; Harunaga and Yamada, 2011; Kubow et al., 2013), we found no evidence of focal adhesion impairment in SLAIN2-depleted cells in either 3D or 2D cultures (Figures 2O–2R). We conclude that Rho GTPase activity, vesicle transport, matrix degradation, and focal adhesions were not affected in a way that could explain cell elongation defects in soft matrix-grown SLAIN2-deficient cells.

SLAIN2 promotes MT-dependent membrane deformation

To test a more mechanical explanation for the SLAIN2 phenotype in 3D, we investigated whether MTs are subjected to compressive forces at pseudopod cortex. We found that growing MT ends were in very close contact with invasive pseudopod tips (Figures 3A–3C). Interestingly, EB3-GFP comets persisted much longer at the tips of pseudopods of cells grown in soft 3D matrix than at the edges of lamella spreading on top of stiff 2D matrices (Figures 3B–3D and Movie S4). A similar behavior was observed for GFP-SLAIN2 comets (Figure S1I), indicating that the differences in MT dynamics at the cell cortex in 2D and 3D were not due to differential SLAIN2 recruitment. MT persistence at the cortex was specific for elongating, but not retracting pseudopods (Figures 3E and 3F). Next, we performed whole MT imaging using β-tubulin-GFP in extending pseudopods in 3D and observed extensive MT buckling at pseudopod tips (20/20 cells; 2.3 ± 0.2 buckling events/min at the tip [10 μm]), indicating that MT growth at these sites is associated with compression (Brangwynne et al., 2006) (Figure 3G and Movie S5). Importantly, protrusion tip dynamics consisted of alternating short-scale (3–5 μm) lamella-based extensions and retractions, which both correlated with MT buckling (Figure 3G and Movie S5).

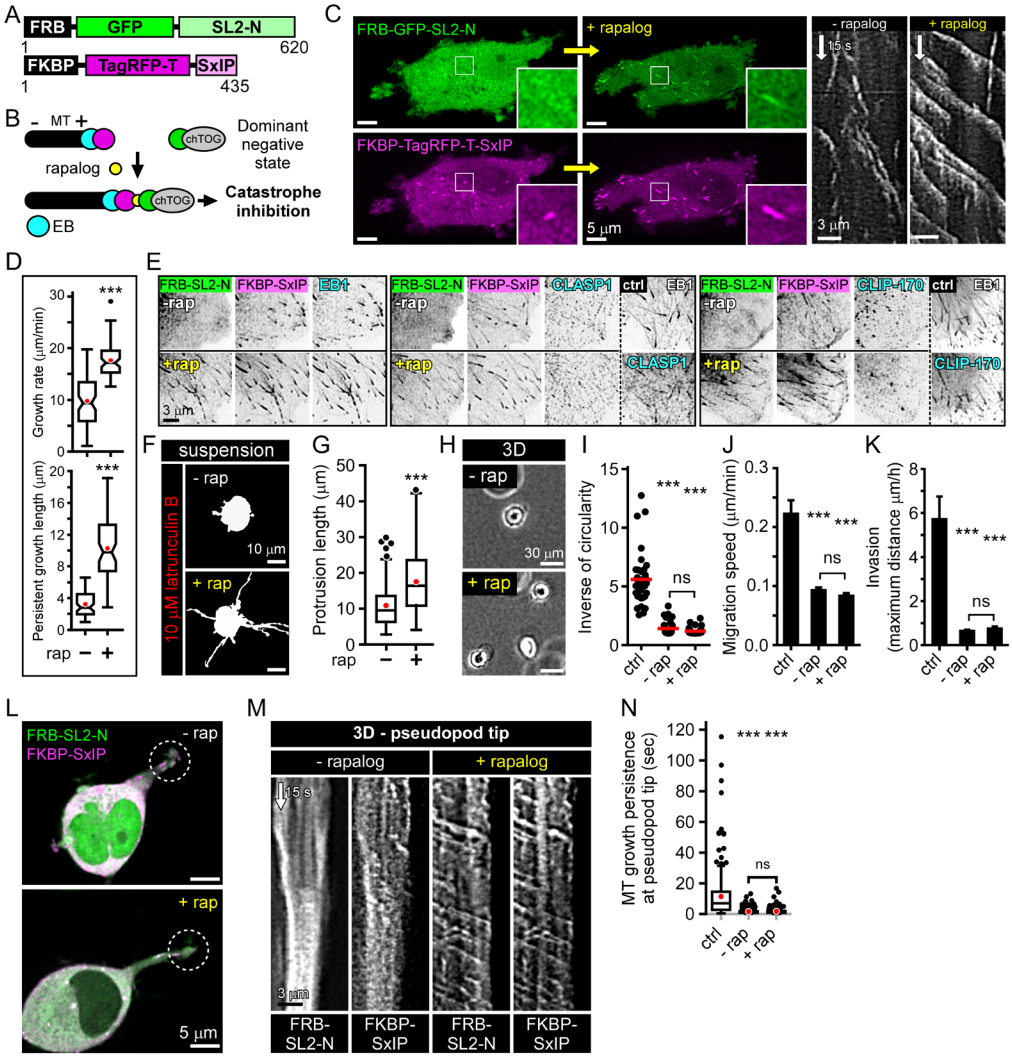

Figure 4. SLAIN2-ch-TOG complex is insufficient to promote MT persistence at pseudopod tips and invasion

(A and B) Fusion protein design (A) and principle (B) of the chemical dimerization-based rescue of SLAIN2-driven MT growth. Without rapalog, the SxIP peptide (purple) binds to end-binding protein (EB) (blue) at MT plus ends, while the SLAIN2-N mutant (SL2-N, green) has a dominant negative effect because it prevents ch-TOG recruitment to MT plus ends; upon the addition of rapalog (yellow), SL2-N heterodimerizes with the SxIP peptide and recruits ch-TOG to plus ends. Overexpressed SxIP peptide competes with the endogenous +TIPs for EB binding. **(C)** Fluorescence images of the proteins depicted in (A), before and after rapalog addition; kymographs of FKBP-TagRFP-T-SxIP are shown on the right. **(D)** MT dynamics parameters in cells treated as shown in (C), before and after rapalog (rap) addition. **(E)** +TIP localization visualized by immunofluorescence staining in cells treated as shown in (C), before and after rapalog addition and compared with control (ctrl). **(F and G)** Cell membrane deformation by growing MT ends in cells in suspension treated as shown in (C), with or without rapalog and treated with latrunculin B. **(H–K)** Phase-contrast images (H), morphology quantification (I), migration speed (J), and inva-

sion (K) in 3D-grown cells treated as in (C) and compared with control cells. Error bars denote SEM. **(L–N)** Live fluorescence images (L) of proteins described in (A) in 3D-grown cells treated as in (C), corresponding kymographs (M), and quantification of MT growth persistence at pseudopods tips (5 µm area) compared with control cells (N). Dashed-line circles, pseudopod tip regions used for making the kymographs. Box plots are presented as in Figure 3; notches, 95% confidence interval of the median. In all plots, *** < 0.001, Mann-Whitney U test. ns, no significant difference with control. See also Movie S6.

We next set out to examine more directly the effect of SLAIN2 inactivation on MT resistance to compression. For this, we performed F-actin depolymerization assays, in which dynamic MTs push the membrane to form thin elongated protrusions (Figure 3H). In these conditions, cell membrane deformation correlates with the ability of MTs to withstand compression mostly driven by isometric plasma membrane tension (Wang et al., 2001; Whipple et al., 2007). Upon F-actin depolymerization in control cells, long protrusions were formed. Growing MT ends gradually decelerated and stalled at protrusion tips as they stopped elongating, as can be expected for MTs growing under load (Janson et al., 2003) (Figures 3H–3M). In SLAIN2-depleted cells, only very short and much less numerous protrusions were formed, and this correlated with slower MT growth and much quicker stalling (Figures 3H–3M). These data suggest that SLAIN2 enhances resistance of growing MTs to compression.

MT persistence at pseudopod tips and mesenchymal invasion require cooperation of SLAIN2 with other +TIPs

Next, we set out to test whether SLAIN2/ch-TOG-driven MT growth could support pseudopod elongation independently of other +TIPs. We designed an assay based on inducible binding of two protein domains, FRB and FKBP, upon the addition of a rapamycin analog (rapalog) (Pollock et al., 2000). The ch-TOG-binding fragment SLAIN2-N (SL2-N) was fused to FRB, and an EB1-binding motif SxIP (Honnappa et al., 2009) was fused to FKBP (Figures 4A and 4B). As expected, in the absence of rapalog, SL2-N acted as a dominant negative mutant and suppressed MT growth (Figures 1 and 4B–4D), while the SxIP peptide competed with other +TIPs for the binding to EB1 (Duellberg et al., 2014; van der Vaart et al., 2011) and displaced them from MT tips (Figure 4E). Upon rapalog addition, SL2-N was recruited to MT plus ends, and processive MT growth was restored (Figures 4B–4D and Movie S6). Importantly, the localization of CLASP1 and CLIP-170 to MT plus ends was still abolished (Figure 4E), because unlike the full-length SLAIN2 (van der Vaart et al., 2011), the SL2-N-SxIP module does not bind to these proteins. Strikingly, rapalog addition rescued plasma membrane deformation by growing MTs in the absence of F-actin (Figures 4F and 4G), but not the pseudopod formation or cell invasion in soft matrices (Figures 4H–4K). We found that, in contrast

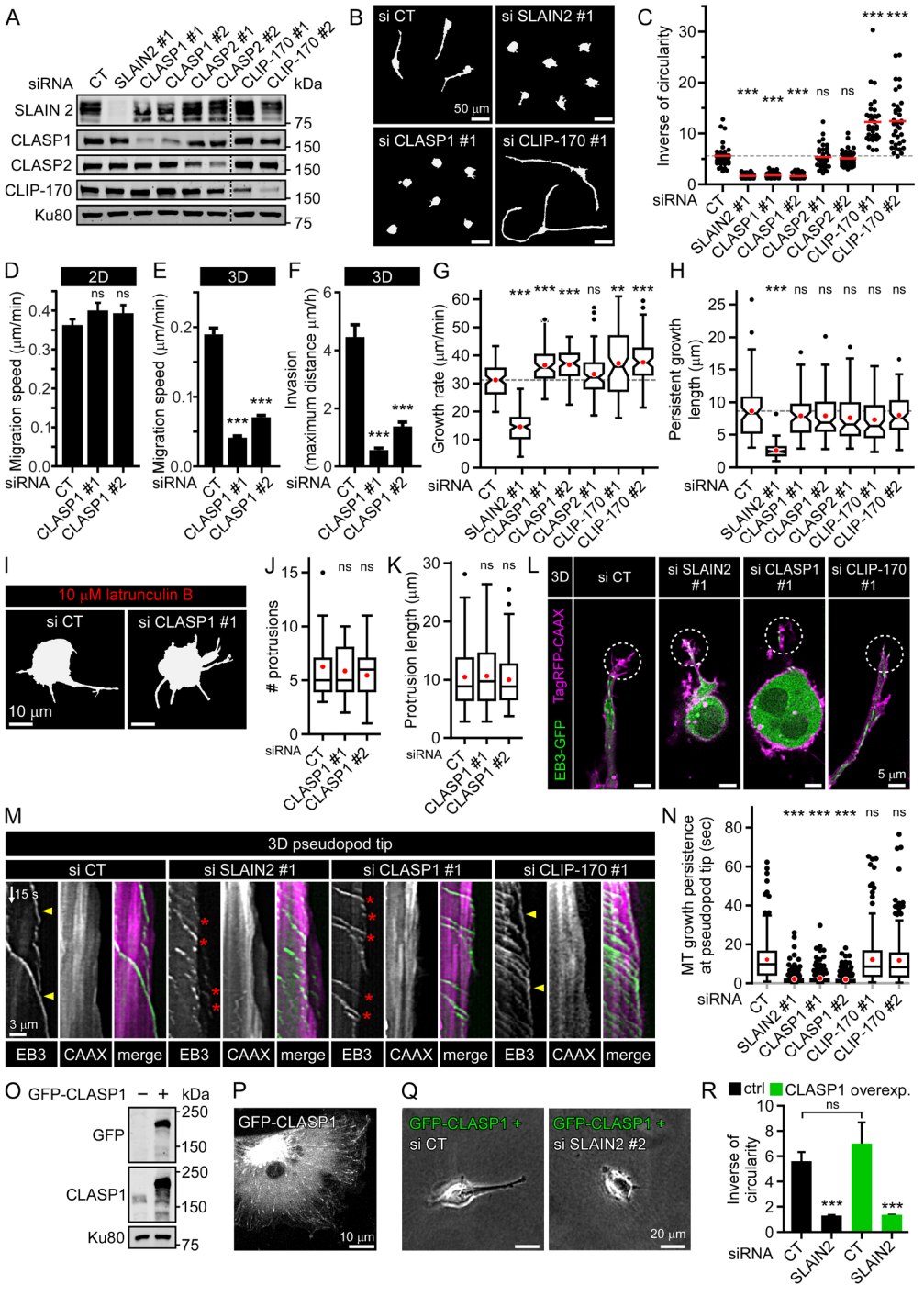

Figure 5. CLASP1 Is required for mesenchymal cell invasion and MT persistence at pseudopod tips

(A) Western blot analysis of SLAIN2, CLASP1, CLASP2, and CLIP-170 depletion by siRNA in MDA-MB-231 cells. **(B and C)** Cell morphology in a 3D matrix (B) and corresponding quantification of

elongation (C) in cells treated as in (A). **(D–F)** Migration speed in 2D (D) or 3D matrix (E) and invasion (F) in CLASP1-depleted cells. Error bars denote SEM. **(G and H)** MT dynamics parameters in cells treated as in (A). **(I–K)** Cell membrane deformation by growing MTs in CLASP1-depleted cells treated with latrunculin B in suspension. Cell morphology in suspension (I) and quantification of protrusion number (#) (J) and length (K). **(L–N)** Live fluorescence images (L) of EB3-GFP and TagRFP-CAAX in 3D-grown cells treated as in (A), corresponding kymographs (M), and quantification of MT growth persistence at pseudopods tips (5 µm area) (N). Dashed-line circles, pseudopod tip regions used for making kymographs. In (M), events of persistent MT growth at pseudopod tips are indicated with yellow arrowheads and MT catastrophes at pseudopod tips by red asterisks. **(O)** Western blot analysis of GFP-CLASP1 overexpression compared with endogenous expression of CLASP1 in MDA-MB-231 cells. **(P)** Live fluorescence image of overexpressed GFP-CLASP1 in MDA-MB-231 cells. **(Q and R)** Phase-contrast images (Q) of GFP-CLASP1 overexpressing cells as in (O), depleted for SLAIN2 and grown in 3D, and corresponding morphology analysis compared with control cells (R). Error bars denote SEM. Box plots are presented as in Figure 3. In all plots, $^{**}p < 0.01$ and $^{***}p < 0.001$, Mann-Whitney U test. ns, no significant difference with control. See also Movie S7.

to MT polymerization in the cytoplasm, MT growth persistence at pseudopod tips was not rescued by rapalog addition (Figures 4L–4N). Hence, the EB1/SLAIN2/ch-TOG complex is sufficient to drive processive growth of MTs in the cytoplasm and increases their load-bearing capacity, allowing them to push plasma membrane in the absence of F-actin. However, additional +TIPs are needed to prevent catastrophe at the actin-rich cell cortex and support pseudopod elongation in soft matrices.

CLASP1 is required for the elongation of invasive pseudopods and MT growth persistence at their tips

To search for factors cooperating with SLAIN2 in promoting pseudopod elongation, we tested the requirement of several +TIPs including CLASP1, CLASP2, and CLIP-170 for maintaining mesenchymal cell shape in 3D and found that CLASP2 knockdown by ~60%–70% had no effect and CLIP-170 knockdown promoted cell elongation (Figures 5A–5C). However, similar to SLAIN2 inactivation, CLASP1 knockdown abolished pseudopod elongation, 3D cell motility, and invasiveness without affecting 2D cell motility (Figures 5A–5F). Importantly, this phenotype was not due to an increase of MT catastrophe frequency in internal cell regions (Figure 5H), in agreement with our previous analysis (Mimori-Kiyosue et al., 2005). MTs in CLASP1-depleted cells could also efficiently form membrane protrusions after F-actin depolymerization (Figures 5I–5K). However, CLASP1 depletion dramatically increased catastrophe frequency specifically at pseudopod tips (Figures 5L–5N and Movie S7). Of note, a moderate overexpression of GFP-CLASP1, which was insufficient to cause MT bundling, could not rescue pseudopod elongation defects induced by SLAIN2 depletion in soft 3D matrices (Figures 5O–5R). Together, these results suggest that mesenchymal cell elongation in soft 3D

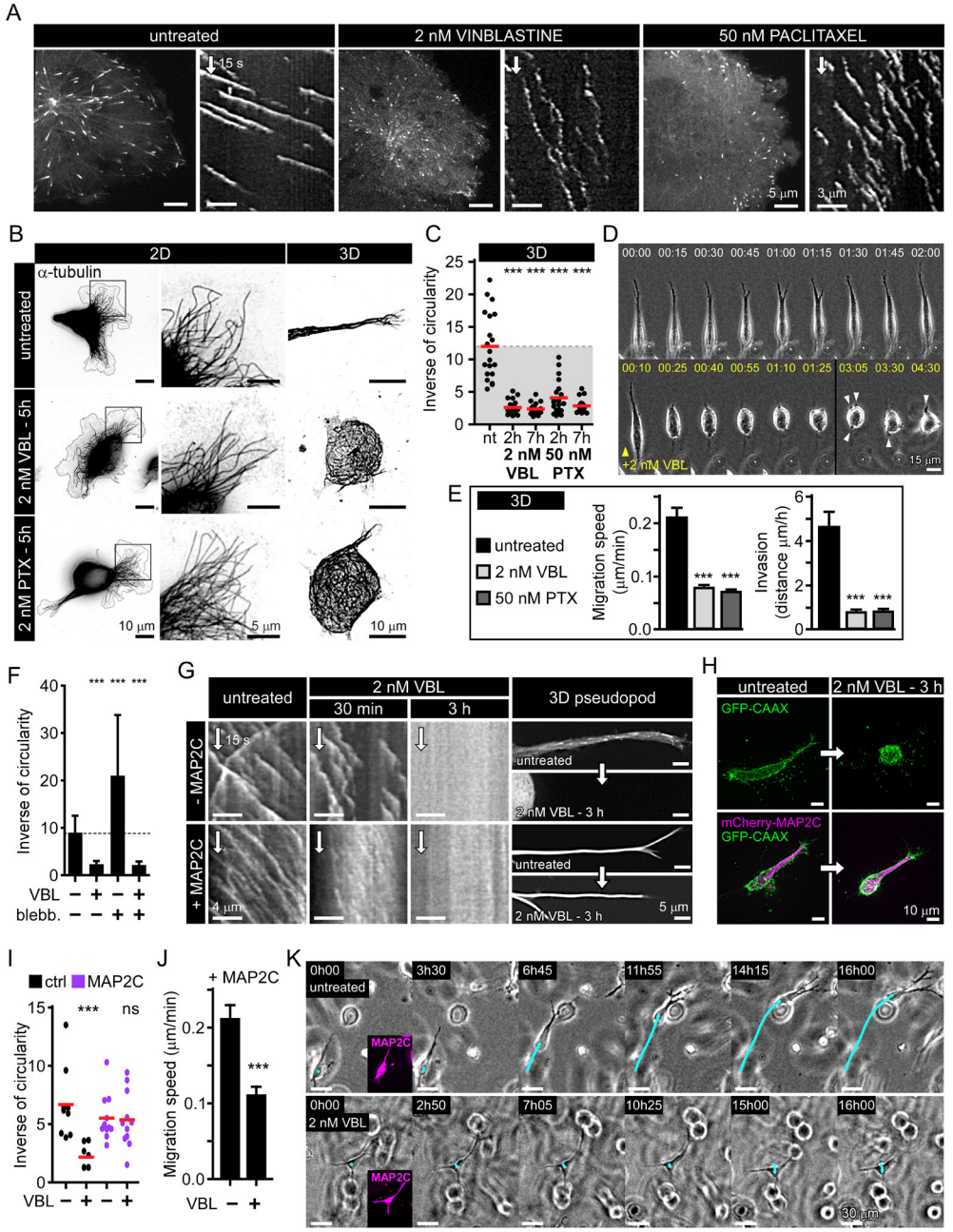

Figure 6. Inhibition of MT depolymerization is sufficient for invasive pseudopod maintenance
(A) Catastrophe induction by low doses of vinblastine (VBL) and paclitaxel (PTX) illustrated by live fluorescence images and kymographs of EB3-GFP in MDA-MB-231 cells. **(B)** MT network maintenance in 2D- and 3D-grown cells treated as in (A), illustrated by immunofluorescence staining of α-tubulin. **(C)** Quantification of invasive morphology of 3D-grown cells treated as in (A). **(D)** Phase-contrast images from time-lapse recording of mesenchymal cells migrating in a 3D matrix and treated when indicated by vinblastine as in (A). Arrowheads indicate the formation of

small pseudopods that fail to elongate. **(E)** Migration speed and invasion of mesenchymal cells grown in 3D and treated as in (A). **(F)** Effect of myosin II inhibition (blebb., blebbistatin) on invasive morphology of cells treated as in (A). **(G)** Effect of MAP2C expression on the maintenance of invasive pseudopods when MT growth persistence is attenuated. Kymographs show EB3-GFP dynamics in cells treated as indicated, and panels on the right show invasive pseudopods before and after treatment; in +MAP2C condition; images are mCherry-MAP2C fluorescence. **(H and I)** Invasive morphology (H) and its quantification (I) in 3D-grown mesenchymal cells before and after attenuation of persistent MT growth by vinblastine as in (A), with or without MAP2C expression. **(J and K)** 3D migration speed (J) and invasive behavior (K) of MAP2C-expressing cells treated as in (A). Bar plots are presented as mean ± SEM. Red line denotes the mean. In all plots, ***p < 0.001, Mann-Whitney U test. ns, no significant difference with control. See also Figure S3; Movies S8, S9, and S10.

matrices requires the cooperation of CLASP1 with SLAIN2/ch-TOG to inhibit MT catastrophes in pseudopod tips.

MT persistence at the tips of invasive pseudopods controls their maintenance

We next set out to test whether MT persistence at protrusion tips is sufficient for preventing pseudopod retraction in the absence of MT growth. We used two different MTAs, vinblastine and paclitaxel, which, although they have opposing effects on MT dynamics at high concentrations, lead to a mild catastrophe induction at low doses (Mohan et al., 2013), similar to the effect of SLAIN2 inactivation (Figures 6A , S3A, and S3B; Movie S8). Importantly, in these conditions MT network, +TIP localization, and 2D cell spreading and motility were preserved (Figures 6B and S3C–S3E), as was also the case after SLAIN2 depletion.

Low-dose MTA treatments caused rapid retraction of invasive pseudopods and suppressed 3D motility (Figures 6C–6E and Movie S9), and while small pseudopods were still formed, they failed to elongate (Figure 6D and Movie S9), very similar to SLAIN2 inactivation. Increased myosin II-based contractility could not explain cell rounding in these conditions, since blebbistatin treatment failed to rescue cell elongation, again similarly to what we found in SLAIN2-depleted cells (Figure 6F). Focal adhesions and vesicle transport were maintained during cell retraction, and their perturbations could thus not explain the loss of long pseudopods (Figure S3F and Movie S10).

Strikingly, the expression of MT-stabilizing proteins MAP2C and Tau was sufficient to prevent pseudopod retraction in the absence of persistent MT growth (Figures 6G–6I and S3G). Cell motility was normal in MAP2C- and Tau-expressing cells (Figures 6J and 6K). However, after MT growth inhibition by MTA treatment, pseudopods could not remodel and 3D motility was blocked despite the fact that the invasive cell shape was maintained (Figures 6J and 6K). These data indicate that prevention of MT depolymerization at pseudopod tips is sufficient for pseudopod maintenance, but MT growth is essential for cell shape changes and, thus, cell movement in 3D.

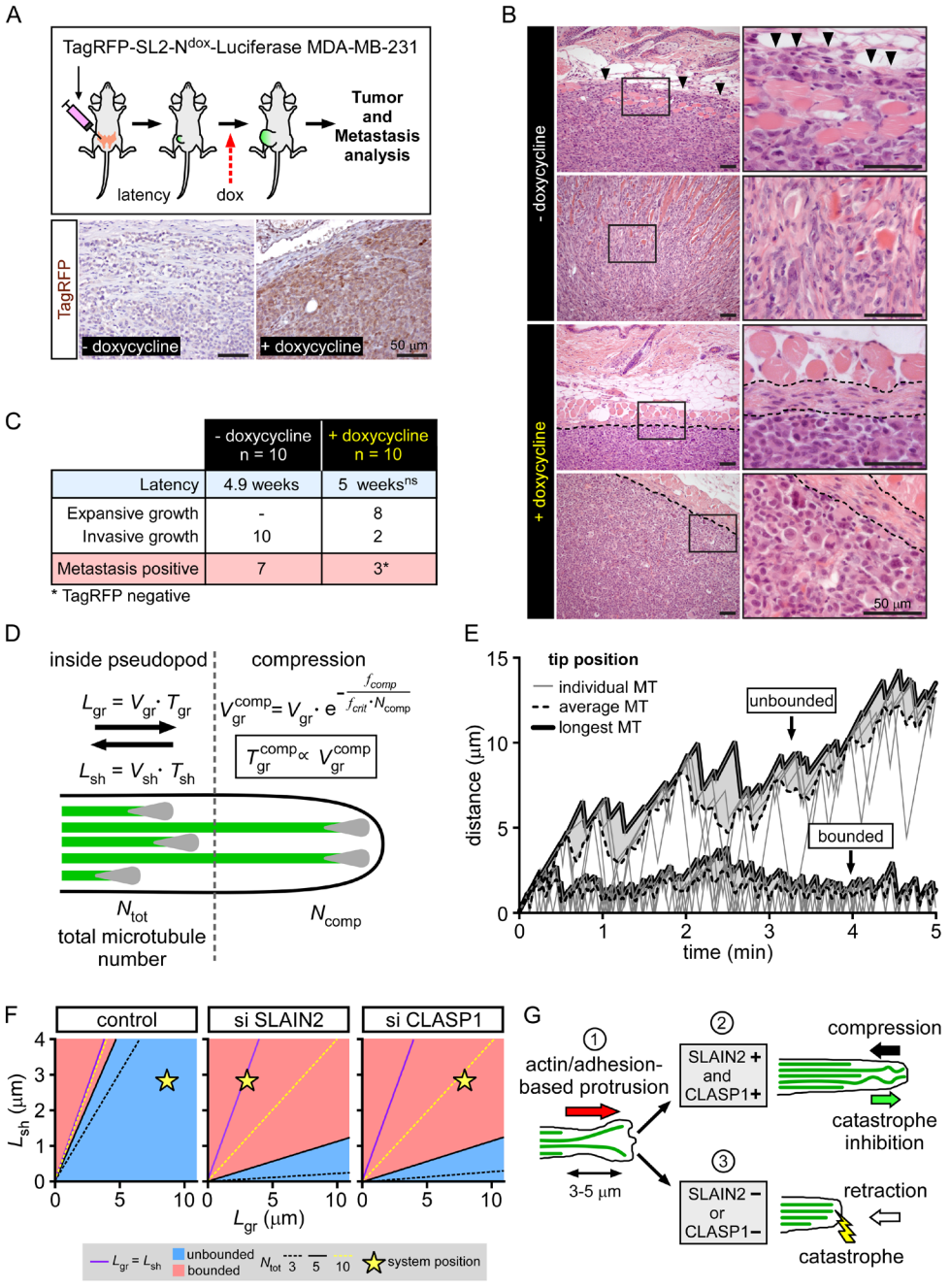

Figure 7. Interphase-specific attenuation of SLAIN2/ch-TOG-Driven MT growth suppresses tumor invasion in mice

(A) Luciferase-expressing MDA-MB-231 cells carrying a doxycycline-controlled expression construct for TagRFP-tagged dominant negative SLAIN2 mutant (SL2-N) were orthotopically transplanted into recipient mice. When tumor volume exceeded 1,000 mm3 or upon detection of metastases by bioluminescence imaging the mice were euthanized, and tumors and metastases

were further analyzed by anatomic pathology evaluation. Bottom panel, immunohistochemical staining of TagRFP in primary tumors from mice treated or untreated with doxycycline. **(B)** H&E staining in primary tumors from the mice transplanted and treated as explained in (A). Note that highly invasive control cells infiltrate the striated subcutaneous muscle layer (arrowheads). Doxycycline-treated mice: in the left panels, dotted line indicates primary tumor margin; in the right panels, dotted lines indicate clear and intact demarcation of the dermal/epidermal basement membrane. **(C)** Latency, primary tumor growth classification, and metastasis evaluation in mice transplanted and treated as explained in (A). ns, not significant (t test). **(D)** Schematic representation of the model. MT dynamic instability parameters are different for MTs deep inside pseudopods and those compressed against the extending edge. See Supplemental Experimental Procedures for details. **(E)** Examples of simulations corresponding to the "bounded" (bottom) and "unbounded" (top) growth. Thick solid lines depict the growing edge of the pseudopod defined by the longest MT. Gray area marks the distance between the edge and the average MT length. Thin gray lines correspond to individual MTs. **(F)** Parametric diagrams corresponding to the control condition, SLAIN2 depletion, and CLASP depletion. For x axis Lgr = Vgr.Tgr and for y axis Lsh = Vsh.Tsh. Purple line marks a boundary between the "bounded" and "unbounded" growth in case of unconstrained MT growth. Blue areas correspond to the "unbounded" growth regime in the presence of the cell cortex for Ntot = 5. Dashed lines mark transition boundaries for the Ntot = 3 (black) and Ntot = 10 (yellow). Star indicates state of the system in each condition. **(G)** Proposed model for the role of MT growth persistence in pseudopod elongation in soft matrix. The leading edge is formed by the tip of a pseudopod that elongates via a succession of short small-amplitude protrusions driven by actin and matrix adhesion (1). When both SLAIN2 and CLASP1 are present (2), growing MTs persist at the pseudopod tip, where they resist compression and counteract retraction. Pseudopod tip is stabilized and can undergo a new cycle of protrusion/stabilization. When SLAIN2 or CLASP1 are inactivated (3), MTs engaged in the newly formed protrusion undergo catastrophe due to unknown factors and are unable to counteract retraction. The pseudopod fails to maintain the newly formed protrusion and retracts. See also Figure S4.

Interphase-specific induction of MT catastrophe by SLAIN2 inactivation suppresses tumor invasion *in vivo*

We next sought to test whether MT catastrophe inhibition by SLAIN2 is relevant for *in vivo* cell invasion. For this purpose, we orthotopically transplanted in mice luciferase-expressing MDA-MB-231 cells expressing the TagRFP-tagged dominant negative SLAIN2-N mutant under the control of doxycycline (n = 20, Figure 7A). Upon detection of palpable tumors (100 mm3), we started doxycycline administration in ten mice and monitored tumor growth and metastasis by luciferase-based bioluminescence imaging (Figure 7A). SLAIN2-N expression was efficiently induced *in vivo* (Figure 7A) and strikingly prevented invasive growth ($p < 0.001$), resulting in expansive tumors with clearly defined borders that were confined to the mammary fat pad (Figures 7B and 7C). No significant differences were observed in tumor latency ($p = 0.894$; Figure 7C). While we detected occasional small lung metastases in three out of ten doxycycline-treated mice, they consisted of cells that did not express the dominant negative SLAIN2-N mu-

tant (Figures 7C and S4A). Thus, interphase-specific induction of MT catastrophe by SLAIN2 ablation abolishes invasiveness of mesenchymal cells *in vivo* and is a potent strategy to prevent mammary tumor invasion and metastatic outgrowth.

Theoretical model of invasive pseudopod growth as a function of MT growth persistence

To model how changes in MT growth persistence can affect pseudopod elongation, we performed Monte Carlo simulations based on previous studies (Dogterom and Leibler, 1993; Janson et al., 2003; Laan et al., 2008). In our model, we assumed that a compressive load, a feature that reduces growth speed and induces catastrophe (Janson et al., 2003), is applied to MTs that are longer than the average length of all MTs in the bundle (Figure 7D). We also assumed that catastrophe depends on the intrinsic resistance of individual MTs to the opposing force and the total number of MTs sharing the load (Laan et al., 2008).

The simulations showed that MT bundles can be either in "unbounded" or "bounded" growth regimes (Figure 7E), as described earlier (Dogterom and Leibler, 1993; Janson et al., 2003), the latter state being associated with the inability to support pseudopod elongation. Parametric diagrams show that a compressive force reduces the area of polymerization parameters corresponding to the unbounded growth regime (see Figure 7F); this reduction only depends on the number of MTs and their resistance to the opposing force. Consistent with experimental data, the control system remains in the unbounded state in the presence of force (blue area), whereas SLAIN2- and CLASP1-depleted systems are in the bounded regime (Figures 7F, S4B, and S4C). Moreover, this model predicts that contrarily to SLAIN2 depletion, doubling of the number of MTs in a CLASP1-depleted situation could potentially bring the system back into an unbounded state (Figure 7F). However, CLASP depletion actually tends to decrease rather than increase MT density (Mimori-Kiyosue et al., 2005), which would bring the system to a bounded regime according to our simulation. Altogether, these simulations support the idea that growth persistence of MT bundles under load is a crucial factor in soft matrix-based protrusion growth.

Discussion

Our study revealed that MT growth persistence at the cell cortex is necessary for the invasive shape and 3D motility of mesenchymal cells *in vitro* and *in vivo*. We found that an increase in MT catastrophes at pseudopod tips does not prevent pseudopod initiation but blocks pseudopod elongation, and when cells are embedded in a 3D environment this leads to a block of motility, likely because cells are unable to form distant adhesion sites to pull themselves through the matrix.

In 2D cultures the destruction of the MT network inhibits Rac1, therefore reducing protrusion, and upregulates myosin II-based contractility via Rho (Krendel et al., 2002; Waterman-Storer et al., 1999). In soft 3D matrices complete MT destruction causes pseudopod retraction, which cannot be rescued by myosin II inhibition, and it was proposed that this defect is due to Rac1 inactivation (Grinnell et al., 2003; Rhee et al., 2007). Our non-destructive approach shows that catastrophe induction by SLAIN2 or ch-TOG inactivation, or low-dose MTA treatments, causes an equally strong loss of invasive pseudopods. We demonstrate that this effect is not due to upregulated Rho and myosin II activities, downregulation of Rac1, or mislocalization of those GTPases, likely because MTs are preserved in these conditions. Cell spreading and migration in 2D, which critically depend on Rho GTPase activity and localization, are consistently unaffected by SLAIN2 inactivation. Hence, a morphogenetic function of MTs in soft matrices relies on a specific aspect of their dynamics that is mechanistically distinct from Rho GTPase regulation.

Focal adhesions control cell shape, are formed in soft 3D matrices (Harunaga and Yamada, 2011), and depend on integrin trafficking and matrix proteases (Friedl and Alexander, 2011; Jacquemet et al., 2013; Stehbens and Wittmann, 2012). Previously, invasive pseudopod defects caused by EB1 depletion were linked to altered myosin II activity, MT penetration in pseudopods, focal adhesion, and vesicle trafficking (Gierke and Wittmann, 2012). This phenotype likely reflects the perturbation of multiple mechanisms controlled by the large numbers of +TIPs that depend on EB1 for MT association (Akhmanova and Steinmetz, 2015). Here, by inactivating SLAIN2 alone, we show that increasing catastrophe frequency without affecting +TIP localization, MT density at pseudopod tips, vesicle trafficking, matrix degradation, or focal adhesions is sufficient to block pseudopod-based cell invasion.

We find that invasive pseudopod tips display highly persistent growth of MTs associated with their buckling. Buckling indicates compression, possibly generated by myosin II-based actin contraction and flow (Brangwynne et al., 2006; Gupton et al., 2002; Wang et al., 2001), membrane tension (Elbaum et al., 1996; Fygenson et al., 1997a; Fygenson et al., 1997b), MT growth itself (Dogterom and Yurke, 1997), or a combination

of these factors. In fact, we observed frequent short-scale retractions of pseudopod tips associated with MT buckling, and given the limited matrix adhesion in soft 3D matrices (Harunaga and Yamada, 2011), compression of the cytoskeleton is expected (Ingber, 2003).

To analyze MT resistance to compression, we examined the ability of cells to extend membrane protrusions after actin disassembly, and found that SLAIN2/ch-TOG-driven growth persistence was essential for this process while other EB1-associated +TIPs were likely dispensable. However, in the presence of actin, additional factors were necessary to prevent catastrophes, possibly due to a different biochemical environment of the actin-rich cortex or higher forces exerted at pseudopod extremities. We identified one such factor as CLASP1, which contributes to catastrophe suppression by acting specifically at pseudopod tips. CLASP1 is a well-studied MT-stabilizing protein and a rescue factor (Al-Bassam and Chang, 2011; Mimori-Kiyosue et al., 2005). CLASP1 depletion induced catastrophes only at the cell cortex, which is in line with the previously described local function of CLASPs at the leading cell edge (Akhmanova et al., 2001; Wittmann and Waterman-Storer, 2005). It is possible that CLASP1 partners such as LL5β or +TIPs acting in the same complexes, such as spectraplakins (Drabek et al., 2006; Lansbergen et al., 2006), also participate in regulating MT dynamics in pseudopods. Local differences between the localization and activity of CLASP1 or its partners might explain the differences in MT growth persistence between protruding and retracting pseudopods. The crosstalk between MTs and actin could also play an important role, especially as the actin organization in 2D and 3D is different, with 3D cells lacking prominent actin-based structures such as stress fibers and large lamellae. Differences in actomyosin-based retrograde flow, which can affect MT dynamics (Gupton et al., 2002; Waterman-Storer and Salmon, 1997), might explain why MTs grow more persistently at pseudopod tips in 3D than at the edges of lamella in 2D.

Interestingly, our data emphasize the fundamental difference between neurons and 3D-grown mesenchymal cells in the dependence of their shape on MT growth. SLAIN2 inactivation caused only limited defects in axon elongation (van der Vaart et al., 2011), and in fact low doses of paclitaxel can even promote axon outgrowth (Witte et al., 2008). Neurons express many stabilizing MT-associated proteins (MAPs), which can counteract neurite retraction when MT growth is perturbed. In contrast, the ability of mesenchymal cells to make long protrusions and move in 3D critically depends on dynamic MTs. Interestingly, we show that introducing neuronal MAPs makes mesenchymal cells less sensitive to retraction caused by MT growth perturbations, although processive MT growth is still needed for their 3D motility.

Together with our computational modeling, our experimental data suggest that catastrophe inhibition promotes a load-bearing role for MTs during cell elongation in soft matrix. We propose a model in which SLAIN2/ch-TOG and CLASP1, by reducing

catastrophe frequency at the cortex, allow MTs to support a part of the compression generated by cellular prestress in soft matrices (Ingber, 2003). Accordingly in mesenchymal cell invasion, while actin and matrix adhesion drive elongation, MTs can bear the load to oppose cell retraction (Figure 7G). We propose that this mechanism is important on top of or within soft matrices, but not on stiff matrices, where the substrate itself, in combination with strong cell adhesion to the matrix, can serve as a mechanical element to prevent cell retraction. In agreement with this view, perturbation of persistent MT growth on top of a soft 2D gel strongly impaired cell spreading. However, this did not inhibit cell motility because cells could essentially "roll over," even though their protrusions were small. In contrast, within a 3D gel the inability to elongate pseudopods inhibited the capacity of cells to form distant adhesions, making them immotile. Taken together, these data indicate that the importance of MT dynamics for making cell protrusions depends on matrix stiffness, while the importance of long protrusions for cell movement depends on substrate dimensionality. While our data support a "mechanical" model of MT-dependent control of cell shape, we cannot rule out potential alternative pathways involving either signaling or trafficking, which might connect MT growth persistence to pseudopod elongation in soft matrices.

Interphase rather than mitosis has been proposed to be the major target of MTAs in cancer therapy (Komlodi-Pasztor et al., 2011; Mitchison, 2012). In parallel, targeting interphase cell migration could be a very potent anti-metastatic strategy in invasive cancers (Cheung and Ewald, 2014; Palmer et al., 2011). Our finding that SLAIN2 inactivation in cancer cells inhibits tumor invasion and metastasis in an interphase-specific manner has major implications for cancer therapeutics. It supports the idea that anti-metastatic action of MTAs relates to their anti-migratory effects in interphase cells. It also suggests that SLAIN2 itself is a potential target for metastatic cancer treatment that can be further studied using the tools developed in this study.

Experimental procedures

Cell lines and 3D culture

MDA-MB-231 cells were obtained from J. Martens (Erasmus MC Rotterdam, the Netherlands) and cultured respectively in DMEM supplemented with 10% fetal calf serum (FCS). HT-1080 cells were a gift of K. Wolf (Radboud University Nijmegen, the Netherlands) and were cultured in DMEM supplemented with 10% FCS. Clonal versions of the original MDA-MB-231 cell line were selected according to their high invasiveness in 3D matrix. Primary human mammary epithelial cells (HMECs) were purchased from Lonza and cultured in MEGM (MEBM and supplement). HEK293T cells were cultured in DMEM supplemented with 10% FCS. hTERT-immortalized HMECs (hTMECs) were generated by viral transduction of hTERT in HMECs using the pBABEhygro-hTERT plasmid and 50 mg/mL hygromycin selection. 3D cultures of MDA-MB-231, HT-1080, and doxycycline-treated EMThTMEC cells were set up by cell suspension seeding in 2 mg/mL rat tail collagen I gels neutralized according to manufacturer protocol; for stiffness-related experiments, collagen concentration was changed as mentioned. EMT-hTMEC 3D culture without doxycycline was performed in Matrigel or a mix of Matrigel with neutralized collagen I, and growth-arrested acini were obtained within 10–20 days as previously described (Seton-Rogers et al., 2004). 2D cultures were set up either on non-coated or collagen I-coated coverslips (12 M HCl wash, poly-D-lysine coating in borate buffer [1.24 g of boric acid, 1.9 g of sodium tetraborate, 400 mL of milliQ water, pH 8.5] and 500 mg/mL collagen I coating).

Live-cell imaging

Fluorescence imaging of 2D and 3D live cultures was performed on a Nikon spinning disk-based confocal imaging station described in Supplemental Experimental Procedures using a stage-top incubator INUBG2E-ZILCS (Tokai Hit) for 37C/5% CO2 incubation and 37C lens heating. Simultaneous two-color imaging was performed using the DV2 two-channel simultaneous-imaging system (Photometrics) equipped with the dichroic filter 565dcxr (Chroma). 2D imaging was performed using Nikon Apo TIRF 1003 numerical aperture (NA) 1.49 oil, Plan Apo VC 603 NA 1.4, or Plan Fluor 403 NA 1.3 objectives. 3D imaging was performed using a Nikon Apo LWD lS 403 NA 1.15 water-immersion objective eventually combined with the Nikon Ti intermediate 1.53 magnification lens.

Mouse experiments

All animal experiments were approved by the Utrecht University Animal Experimental Committee (DEC-ABC no. 2014.III.08.075). The fourth (inguinal) mammary

gland from female RAG2 immunodeficient mice (Gimeno et al., 2004) was exposed and approximately 106 MDA-MB-231 cells expressing luciferase and carrying doxycycline-inducible expression of SLAIN2-N were injected using a 50-mL Hamilton syringe. Buprenorphine (Temgesic), 100 mL (0.03 mg/mL) was injected subcutaneously as analgesic treatment. Tumor growth was measured using a digital caliper (Mitutoyo) on a weekly basis. Upon development of palpable tumors, mice were switched from a standard diet to doxycycline-containing chow (A153D00201; Sniff) for the remainder of the experiment. Luciferase-based bioluminescence of primary tumor and metastases was monitored as previously described (Schackmann et al., 2011). Mice were euthanized when tumor volume exceeded 1,000 mm3 or when bioluminescence imaging revealed metastases.

Author contributions

B.P.B., I.N., M.D., P.W.B.D., and A.A. designed the experiments and wrote the paper. B.P.B., I.N., Y.-C. A., M.v.A., and N.D.t.H. conducted the experiments and analyzed the data. E.A.K. analyzed data in Figure 3M. B.P.B., E.A.K., and M.D. conceived the theoretical model; E.A.K. developed the model and carried out the computer-based simulations. L.H. generated reagents.

Acknowledgements

We are grateful to Dr. I. Grigoriev for assistance with microscopy; J. van der Beek and J. Bertram for help with cloning and 3D cultures; L. Kapitein and G. Koenderink for critically reading the manuscript; and R. Weinberg, M. Sixt, R. Wedlich-Söldner, Y. Mimori-Kiyosue, K. Jiang, L. Cassimeris, I. Barde, D. Trono, J. E. Mertz, O. Pertz, S. Vogel, M. Davidson, D. Piston, P. Schätzle, C. Hoogenraad, E. Bindels, E. Soler, J. Martens, S. Royle, and K. Wolf for the gift of reagents. This work was supported by the Netherlands Organisation for Scientific Research (NWO) through an ALW-VICI grant 865.08.002 and ALW Open Program grant 822.02.002 to A.A., European Research Council (ERC) Synergy Grant 609822 to M.D. and A.A., Marie Skłodowska-Curie Actions Innovative Training Network PolarNet 675407 , Fondation pour la Recherche Médicale and Marie Curie International Intra-European Fellowship to B.P.B., NWO/ZonMW-VIDI 016.096.318 to P.W.D., and Foundation Vrienden UMC Utrecht (11.081), the Dutch Cancer Society (KWF-UU-2011-5230 and KWF-UU-2014-7201), and National Cancer Institute grant CA181838 to L.H.

References

Akhmanova, A., C.C. Hoogenraad, K. Drabek, T. Stepanova, B. Dortland, T. Verkerk, W. Vermeulen, B.M. Burgering, C.I. De Zeeuw, F. Grosveld, and N. Galjart. 2001. Clasps are CLIP-115 and -170 associating proteins involved in the regional regulation of microtubule dynamics in motile fibroblasts. Cell. 104:923-935.

Akhmanova, A., and M.O. Steinmetz. 2015. Control of microtubule organization and dynamics: two ends in the limelight. Nat Rev Mol Cell Biol. 16:711-726.

Al-Bassam, J., and F. Chang. 2011. Regulation of microtubule dynamics by TOG-domain proteins XMAP215/Dis1 and CLASP. Trends Cell Biol. 21:604-614.

Brangwynne, C.P., F.C. MacKintosh, S. Kumar, N.A. Geisse, J. Talbot, L. Mahadevan, K.K. Parker, D.E. Ingber, and D.A. Weitz. 2006. Microtubules can bear enhanced compressive loads in living cells because of lateral reinforcement. J Cell Biol. 173:733-741.

Chaffer, C.L., and R.A. Weinberg. 2011. A perspective on cancer cell metastasis. Science. 331:1559-1564.

Cheung, K.J., and A.J. Ewald. 2014. Invasive leader cells: metastatic oncotarget. Oncotarget. 5:1390-1391.

Cheung, K.J., E. Gabrielson, Z. Werb, and A.J. Ewald. 2013. Collective invasion in breast cancer requires a conserved basal epithelial program. Cell. 155:1639-1651.

Clark, A.G., and D.M. Vignjevic. 2015. Modes of cancer cell invasion and the role of the microenvironment. Curr Opin Cell Biol. 36:13-22.

Dennerll, T.J., H.C. Joshi, V.L. Steel, R.E. Buxbaum, and S.R. Heidemann. 1988. Tension and compression in the cytoskeleton of PC-12 neurites. II: Quantitative measurements. J Cell Biol. 107:665-674.

Dogterom, M., and S. Leibler. 1993. Physical aspects of the growth and regulation of microtubule structures. Phys Rev Lett. 70:1347-1350.

Dogterom, M., and B. Yurke. 1997. Measurement of the force-velocity relation for growing microtubules. Science. 278:856-860.

Drabek, K., M. van Ham, T. Stepanova, K. Draegestein, R. van Horssen, C.L. Sayas, A. Akhmanova, T. Ten Hagen, R. Smits, R. Fodde, F. Grosveld, and N. Galjart. 2006. Role of CLASP2 in microtubule stabilization and the regulation of persistent motility. Curr Biol. 16:2259-2264.

Duellberg, C., M. Trokter, R. Jha, I. Sen, M.O. Steinmetz, and T. Surrey. 2014. Reconstitution of a hierarchical +TIP interaction network controlling microtubule end tracking of dynein. Nat Cell Biol. 16:804-811.

Elbaum, M., D. Kuchnir Fygenson, and A. Libchaber. 1996. Buckling microtubules in vesicles. Phys Rev Lett. 76:4078-4081.

Etienne-Manneville, S. 2013. Microtubules in cell migration. Annu Rev Cell Dev Biol. 29:471-499.

Friedl, P., and S. Alexander. 2011. Cancer invasion and the microenvironment: plasticity and reciprocity. Cell. 147:992-1009.

Friedl, P., and D. Gilmour. 2009. Collective cell migration in morphogenesis, regeneration and cancer. Nat Rev Mol Cell Biol. 10:445-457.

Fygenson, D.K., M. Elbaum, B. Shraiman, and A. Libchaber. 1997a. Microtubules and vesicles under controlled tension. Phys. Rev. E 55:850-859.

Fygenson, D.K., J.F. Marko, and A. Libchaber. 1997b. Mechanisms of microtubule-based membrane extension. Phys Rev Lett. 79:4497-4500.

Gierke, S., and T. Wittmann. 2012. EB1-recruited microtubule +TIP complexes coordinate protrusion dynamics during 3D epithelial remodeling. Curr Biol. 22:753-762.

Gimeno, R., K. Weijer, A. Voordouw, C.H. Uittenbogaart, N. Legrand, N.L. Alves, E. Wijnands, B. Blom, and H. Spits. 2004. Monitoring the effect of gene silencing by RNA interference in human CD34+ cells injected into newborn RAG2-/-gammac-/- mice: functional inactivation of p53 in developing T cells. Blood. 104:3886-3893.

Grinnell, F., C.H. Ho, E. Tamariz, D.J. Lee, and G. Skuta. 2003. Dendritic fibroblasts in three-dimensional collagen matrices. Mol Biol Cell. 14:384-395.

Grinnell, F., and W.M. Petroll. 2010. Cell motility

and mechanics in three-dimensional collagen matrices. Annu Rev Cell Dev Biol. 26:335-361.

Gupton, S.L., W.C. Salmon, and C.M. Waterman-Storer. 2002. Converging populations of f-actin promote breakage of associated microtubules to spatially regulate microtubule turnover in migrating cells. Curr Biol. 12:1891-1899.

Harunaga, J.S., and K.M. Yamada. 2011. Cell-matrix adhesions in 3D. Matrix Biol. 30:363-368.

Heck, J.N., S.M. Ponik, M.G. Garcia-Mendoza, C.A. Pehlke, D.R. Inman, K.W. Eliceiri, and P.J. Keely. 2012. Microtubules regulate GEF-H1 in response to extracellular matrix stiffness. Mol Biol Cell. 23:2583-2592.

Honnappa, S., S.M. Gouveia, A. Weisbrich, F.F. Damberger, N.S. Bhavesh, H. Jawhari, I. Grigoriev, F.J. van Rijssel, R.M. Buey, A. Lawera, I. Jelesarov, F.K. Winkler, K. Wuthrich, A. Akhmanova, and M.O. Steinmetz. 2009. An EB1-binding motif acts as a microtubule tip localization signal. Cell. 138:366-376.

Ingber, D.E. 2003. Tensegrity I. Cell structure and hierarchical systems biology. J Cell Sci. 116:1157-1173.

Jacquemet, G., M.J. Humphries, and P.T. Caswell. 2013. Role of adhesion receptor trafficking in 3D cell migration. Curr Opin Cell Biol. 25:627-632.

Janson, M.E., M.E. de Dood, and M. Dogterom. 2003. Dynamic instability of microtubules is regulated by force. J Cell Biol. 161:1029-1034.

Kikuchi, K., and K. Takahashi. 2008. WAVE2- and microtubule-dependent formation of long protrusions and invasion of cancer cells cultured on three-dimensional extracellular matrices. Cancer Sci. 99:2252-2259.

Komlodi-Pasztor, E., D. Sackett, J. Wilkerson, and T. Fojo. 2011. Mitosis is not a key target of microtubule agents in patient tumors. Nat Rev Clin Oncol. 8:244-250.

Krendel, M., F.T. Zenke, and G.M. Bokoch. 2002. Nucleotide exchange factor GEF-H1 mediates cross-talk between microtubules and the actin cytoskeleton. Nat Cell Biol. 4:294-301.

Kubow, K.E., S.K. Conrad, and A.R. Horwitz. 2013. Matrix microarchitecture and myosin II determine adhesion in 3D matrices. Curr Biol. 23:1607-1619.

Kutys, M.L., and K.M. Yamada. 2014. An extracellular-matrix-specific GEF-GAP interaction regulates Rho GTPase crosstalk for 3D collagen migration. Nat Cell Biol. 16:909-917.

Laan, L., J. Husson, E.L. Munteanu, J.W. Kerssemakers, and M. Dogterom. 2008. Force-generation and dynamic instability of microtubule bundles. Proc Natl Acad Sci U S A. 105:8920-8925.

Lam, P.Y., and A. Huttenlocher. 2013. Interstitial leukocyte migration in vivo. Curr Opin Cell Biol. 25:650-658.

Lansbergen, G., I. Grigoriev, Y. Mimori-Kiyosue, T. Ohtsuka, S. Higa, I. Kitajima, J. Demmers, N. Galjart, A.B. Houtsmuller, F. Grosveld, and A. Akhmanova. 2006. CLASPs attach microtubule plus ends to the cell cortex through a complex with LL5beta. Dev Cell. 11:21-32.

Lee, M.H., P.H. Wu, D. Gilkes, I. Aifuwa, and D. Wirtz. 2015. Normal mammary epithelial cells promote carcinoma basement membrane invasion by inducing microtubule-rich protrusions. Oncotarget. 6:32634-32645.

Martins, G.G., and J. Kolega. 2012. A role for microtubules in endothelial cell protrusion in three-dimensional matrices. Biol Cell. 104:271-286.

Matrone, M.A., R.A. Whipple, K. Thompson, E.H. Cho, M.I. Vitolo, E.M. Balzer, J.R. Yoon, O.B. Ioffe, K.C. Tuttle, M. Tan, and S.S. Martin. 2010. Metastatic breast tumors express increased tau, which promotes microtentacle formation and the reattachment of detached breast tumor cells. Oncogene. 29:3217-3227.

Mimori-Kiyosue, Y., I. Grigoriev, G. Lansbergen, H. Sasaki, C. Matsui, F. Severin, N. Galjart, F. Grosveld, I. Vorobjev, S. Tsukita, and A. Akhmanova. 2005. CLASP1 and CLASP2 bind to EB1 and regulate microtubule plus-end dynamics at the cell cortex. J Cell Biol. 168:141-153.

Mitchison, T.J. 2012. The proliferation rate paradox in antimitotic chemotherapy. Mol Biol Cell. 23:1-6.

Mohan, R., E.A. Katrukha, H. Doodhi, I. Smal, E. Meijering, L.C. Kapitein, M.O. Steinmetz, and A. Akhmanova. 2013. End-binding proteins sensitize microtubules to the action of microtubule-targeting agents. Proc Natl Acad Sci U S A. 110:8900-8905.

Nakaya, Y., and G. Sheng. 2008. Epithelial to mesenchymal transition during gastrulation: an embryological view. Dev Growth Differ. 50:755-766.

Oyanagi, J., T. Ogawa, H. Sato, S. Higashi, and K. Miyazaki. 2012. Epithelial-mesenchymal transition stimulates human cancer cells to extend microtubule-based invasive protrusions and suppresses cell growth in collagen gel. PLoS One. 7:e53209.

Palmer, T.D., W.J. Ashby, J.D. Lewis, and A. Zijlstra. 2011. Targeting tumor cell motility to prevent metastasis. Adv Drug Deliv Rev. 63:568-581.

Petrie, R.J., N. Gavara, R.S. Chadwick, and K.M. Yamada. 2012. Nonpolarized signaling reveals two distinct modes of 3D cell migration. J Cell Biol. 197:439-455.

Petrie, R.J., and K.M. Yamada. 2015. Fibroblasts Lead the Way: A Unified View of 3D Cell Motility. Trends Cell Biol. 25:666-674.

Pollock, R., R. Issner, K. Zoller, S. Natesan, V.M. Rivera, and T. Clackson. 2000. Delivery of a stringent dimerizer-regulated gene expression system in a single retroviral vector. Proc Natl Acad Sci U S A. 97:13221-13226.

Pourroy, B., S. Honore, E. Pasquier, V. Bourgarel-Rey, A. Kruczynski, C. Briand, and D. Braguer. 2006. Antiangiogenic concentrations of vinflunine increase the interphase microtubule dynamics and decrease the motility of endothelial cells. Cancer Res. 66:3256-3263.

Rhee, S., H. Jiang, C.H. Ho, and F. Grinnell. 2007. Microtubule function in fibroblast spreading is modulated according to the tension state of cell-matrix interactions. Proc Natl Acad Sci U S A. 104:5425-5430.

Sahai, E., and C.J. Marshall. 2003. Differing modes of tumour cell invasion have distinct requirements for Rho/ROCK signalling and extracellular proteolysis. Nat Cell Biol. 5:711-719.

Sanz-Moreno, V., and C.J. Marshall. 2010. The plasticity of cytoskeletal dynamics underlying neoplastic cell migration. Curr Opin Cell Biol. 22:690-696.

Schackmann, R.C., M. van Amersfoort, J.H. Haarhuis, E.J. Vlug, V.A. Halim, J.M. Roodhart, J.S. Vermaat, E.E. Voest, P. van der Groep, P.J. van Diest, J. Jonkers, and P.W. Derksen. 2011. Cytosolic p120-catenin regulates growth of metastatic lobular carcinoma through Rock1-mediated anoikis resistance. J Clin Invest. 121:3176-3188.

Seton-Rogers, S.E., Y. Lu, L.M. Hines, M. Koundinya, J. LaBaer, S.K. Muthuswamy, and J.S. Brugge. 2004. Cooperation of the ErbB2 receptor and transforming growth factor beta in induction of migration and invasion in mammary epithelial cells. Proc Natl Acad Sci U S A. 101:1257-1262.

Stehbens, S., and T. Wittmann. 2012. Targeting and transport: how microtubules control focal adhesion dynamics. J Cell Biol. 198:481-489.

Tomasek, J.J., and E.D. Hay. 1984. Analysis of the role of microfilaments and microtubules in acquisition of bipolarity and elongation of fibroblasts in hydrated collagen gels. J Cell Biol. 99:536-549.

Tran, T.A., L. Gillet, S. Roger, P. Besson, E. White, and J.Y. Le Guennec. 2009. Non-anti-mitotic concentrations of taxol reduce breast cancer cell invasiveness. Biochem Biophys Res Commun. 379:304-308.

van der Vaart, B., C. Manatschal, I. Grigoriev, V. Olieric, S.M. Gouveia, S. Bjelic, J. Demmers, I. Vorobjev, C.C. Hoogenraad, M.O. Steinmetz, and A. Akhmanova. 2011. SLAIN2 links microtubule plus end-tracking proteins and controls microtubule growth in interphase. J Cell Biol. 193:1083-1099.

Wang, N., K. Naruse, D. Stamenovic, J.J. Fredberg, S.M. Mijailovich, I.M. Tolic-Norrelykke, T. Polte, R. Mannix, and D.E. Ingber. 2001. Mechanical behavior in living cells consistent with the tensegrity model. Proc Natl Acad Sci U S A. 98:7765-7770.

Waterman-Storer, C.M., and E.D. Salmon. 1997. Actomyosin-based retrograde flow of microtubules in the lamella of migrating epithelial cells influences microtubule dynamic instability and turnover and is associated with microtubule breakage and treadmilling. J Cell Biol. 139:417-434.

Waterman-Storer, C.M., R.A. Worthylake, B.P. Liu, K. Burridge, and E.D. Salmon. 1999. Microtubule growth activates Rac1 to promote lamellipodial protrusion in fibroblasts. Nat Cell Biol. 1:45-50.

Whipple, R.A., A.M. Cheung, and S.S. Martin. 2007. Detyrosinated microtubule protrusions in suspended mammary epithelial cells promote re-

attachment. Exp Cell Res. 313:1326-1336.

Wilson, K., A. Lewalle, M. Fritzsche, R. Thorogate, T. Duke, and G. Charras. 2013. Mechanisms of leading edge protrusion in interstitial migration. Nat Commun. 4:2896.

Winckler, B., and F. Solomon. 1991. A role for microtubule bundles in the morphogenesis of chicken erythrocytes. Proc Natl Acad Sci U S A. 88:6033-6037.

Witte, H., D. Neukirchen, and F. Bradke. 2008. Microtubule stabilization specifies initial neuronal polarization. J Cell Biol. 180:619-632.

Wittmann, T., and C.M. Waterman-Storer. 2005. Spatial regulation of CLASP affinity for microtubules by Rac1 and GSK3beta in migrating epithelial cells. J Cell Biol. 169:929-939.

Wolf, K., M. Te Lindert, M. Krause, S. Alexander, J. Te Riet, A.L. Willis, R.M. Hoffman, C.G. Figdor, S.J. Weiss, and P. Friedl. 2013. Physical limits of cell migration: control by ECM space and nuclear deformation and tuning by proteolysis and traction force. J Cell Biol. 201:1069-1084.

Zhang, P., Y. Sun, and L. Ma. 2015. ZEB1: at the crossroads of epithelial-mesenchymal transition, metastasis and therapy resistance. Cell Cycle. 14:481-487.

Supplemental figures

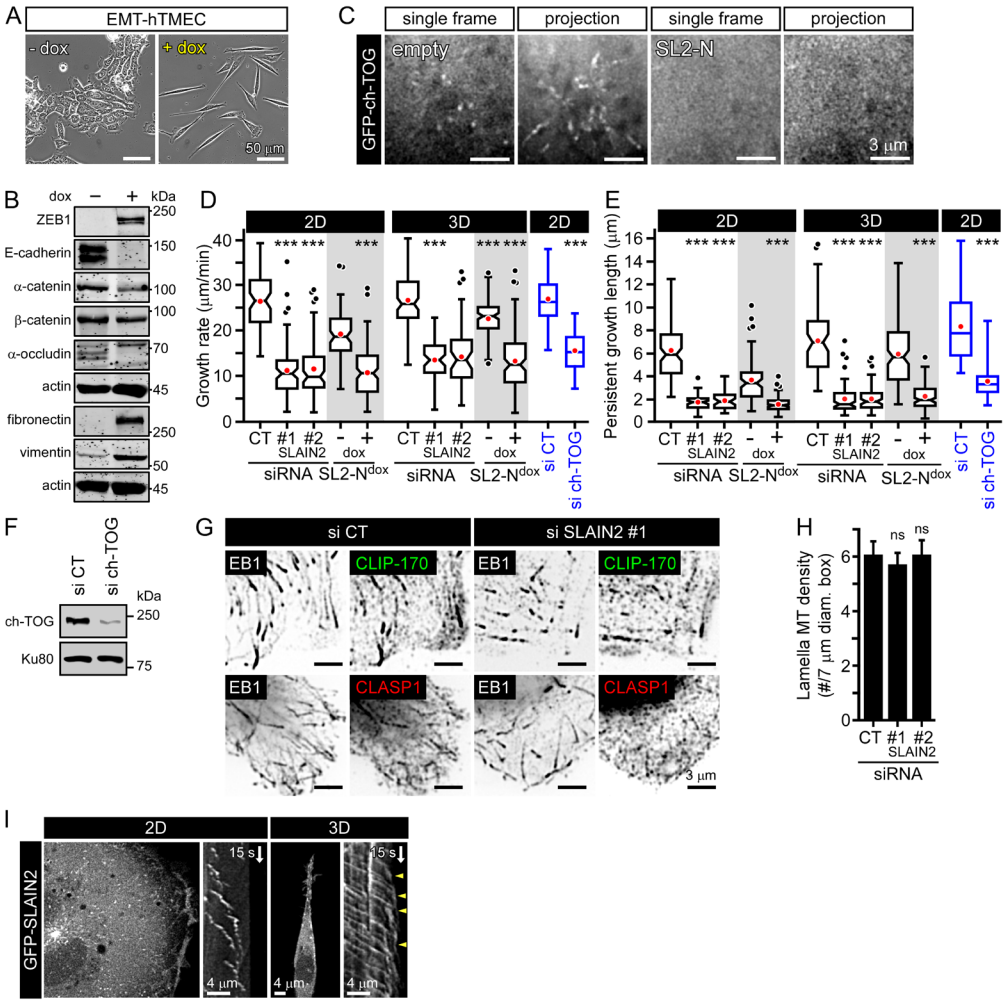

Figure S1, related to Figure 1. Effects of SLAIN2 and ch-TOG depletion on MT dynamics
(A) Phase contrast images of non-tumor human mammary epithelial cells (hTMEC) converted into mesenchymal cells by doxycycline-induced (dox, 4 days) expression of ZEB1 (EMT-hTMEC). **(B)** Western blot analysis of epithelial (E-cadherin, α- and β-catenin, α-occludin) and mesenchymal markers (fibronectin, vimentin) in cells shown in (A). **(C)** Single frames and maximum intensity projections of GFP-ch-TOG live fluorescence image series acquired at 2 frames per second for 1 minute in HT-1080 cells co-transfected with either empty TagRFP or TagRFP-SL2-N vector. Ch-TOG comets are visible in control but not in TagRFP-SL2-N transfected cells. (D and E) MT growth rate **(D)** and persistent growth length **(E)** in MDA-MB-231 cells depleted of SLAIN2 by two independent siRNAs (#1 and #2), expressing a doxycycline-inducinble (dox) construct for the TagRFP-T-tagged dominant negative SLAIN2 mutant (SL2-N), or depleted of ch-TOG using siRNA. Cells were grown on 2D or in 3D matrix, as indicated. Box plots indicate the 25th percentile (bottom boundary), median (middle line), mean (red dots), 75th percentile (top boundary), near-

est observations within 1.5 times the interquartile range (whiskers), 95% confidence interval of the median (notches) and outliers (black dots). **(F)** Western blot analysis of siRNA-mediated ch-TOG depletion in MDA-MB-231 cells. **(G)** Analysis of +TIP localization in SLAIN2-depleted MDA-MB-231 cells by immunofluorescence staining of EB1, CLIP-170 and CLASP1. **(H)** MT density in the lamella of SLAIN2-depleted MDA-MB-231 cells grown in 2D. **(I)** Live fluorescence images and kymographs of GFP-SLAIN2 in HT-1080 cells grown on collagen I-based stiff 2D or in 3D soft matrices. Arrowheads, MT growth persistence at the cell edge. Bar plots are presented as mean ±SEM. In all plots, ns, no significant difference with control; ***, P<0.001, Mann-Whitney U test. See also movie S1

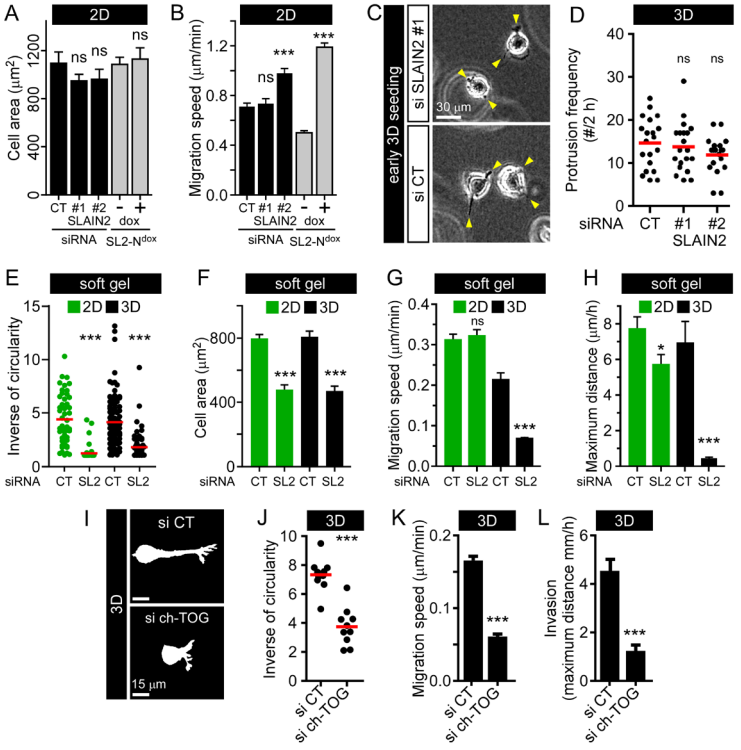

Figure S2, related to Figure 1. Effects of SLAIN2 and ch-TOG depletion on cell morphology and migration in soft 3D matrices

(A and B) Cell spreading (A) and migration speed (B) in 2D cultures of SLAIN2-depleted MDA-MB-231 cells. **(C and D)** Phase contrast images (C) and analysis of protrusion frequency (D) in SLAIN2-depleted MDA-MB-231 cells embedded (3D) in collagen I-based soft matrix for 2 hours. Arrowheads, protrusions. **(E-H)** Cell elongation (E), cell area (F), migration speed (G) and net displacement (H) of SLAIN2-depleted MDA-MB-231 cells grown either on top (2D) or within (3D) a collagen I-based soft matrix. **(I-L)** Cell morphology masks (I) and the corresponding quantification (J), migration speed (K) and invasion (L) of ch-TOG depleted MDA-MB-231 cells blocked in interphase by a 2 day-treatment with 2 mM thymidine; cells were grown in 3D matrix. Bar plots are presented as mean ±SEM; in scatter plots, red bar: mean. In all plots, ns, no significant difference with control; ***, P<0.001, Mann-Whitney U test. See also movie S2

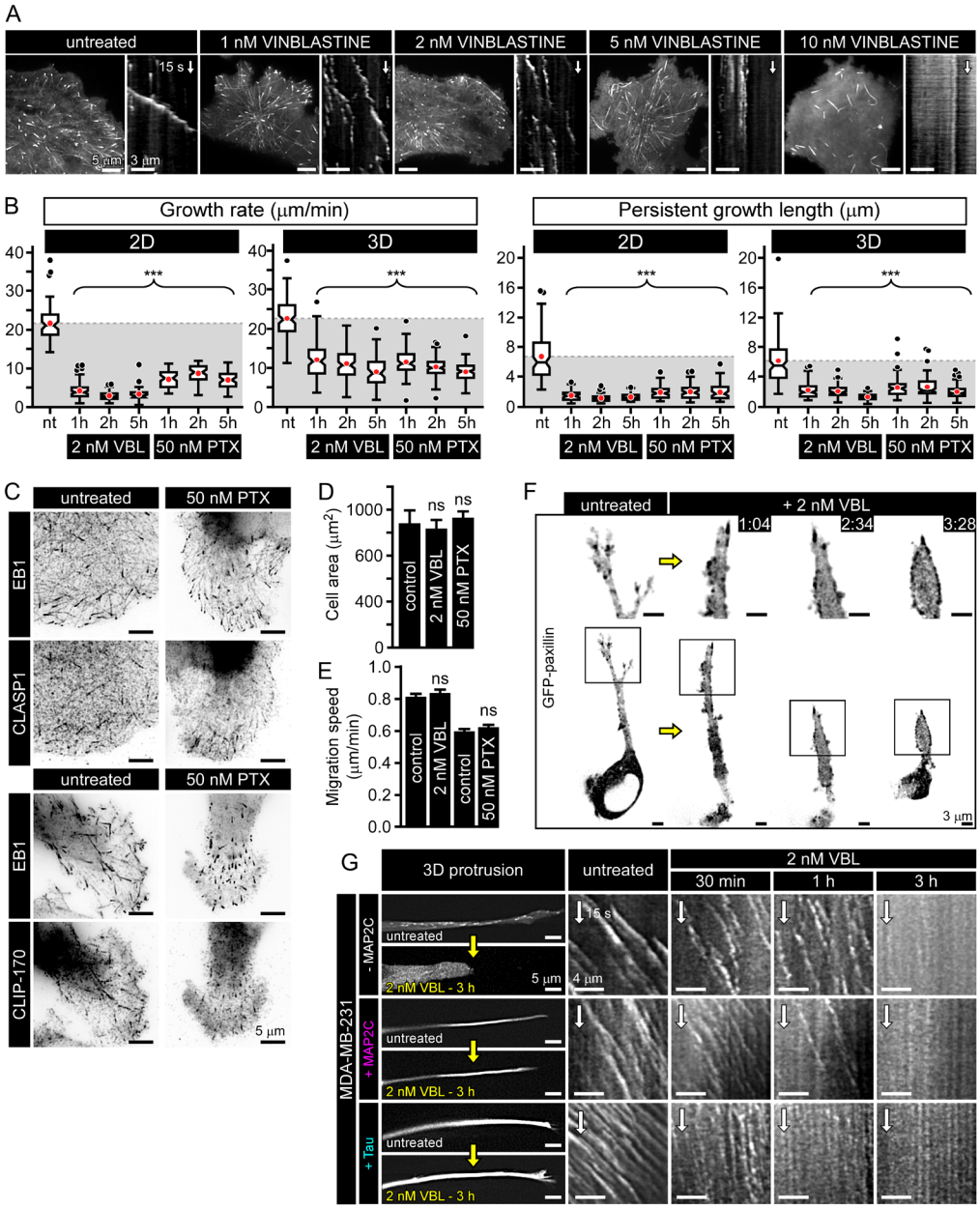

Figure S3, related to Figure 6. Effects of low doses of vinblastine and paclitaxel on MT dynamics, +TIP localization, cell morphology and migration in 2D, and invasive pseudopod maintenance and focal adhesions in 3D

(A) Live fluorescence images of EB3-GFP and corresponding kymographs in cells treated with vinblastine as indicated. **(B)** MT dynamics parameters in 2D- or 3D-grown MDA-MB-231 cells treated as indicated (VBL, vinblastine; PTX, paclitaxel). Box plots are presented as in Fig. S1. **(C)** Immunofluorescence staining for EB1, CLASP1 and CLIP-170 in cells treated as indicated. **(D and E)** Cell spreading (D) and migration speed (E) in 2D-grown cells treated as indicated. **(F)** Focal adhesions in invasive pseudopods visualized by confocal fluorescence imaging of GFP-paxillin

in 3D grown cells treated as indicated (time, h:min). **(G)** Effect of MAP2C and Tau expression on invasive pseudopod maintenance when MT growth persistence is attenuated. Kymographs show EB3-GFP dynamics in cells treated as indicated. Panels on the right show invasive pseudopods before and after treatment; in +MAP2C and +Tau conditions, images illustrate mCherry-MAP2C and mCherry-Tau fluorescence, respectively. See also Movies S8 and S10.

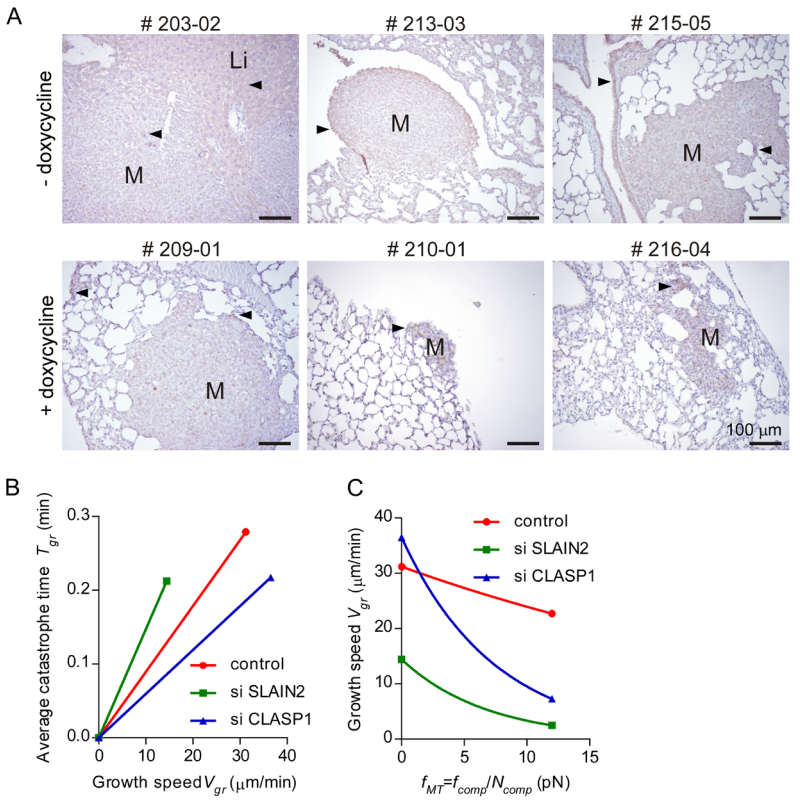

Figure S4, related to Figure 7. SLAIN2 requirement for metastatic outgrowth in mammary tumor and simulation of MT force-velocity dependence

(A) Immunohistochemical staining for TagRFP in metastases from mice orthotopically transplanted with luciferase-expressing MDA-MB-231 cells carrying a doxycycline-controlled SL2-N expression cassette. Shown are lung and liver metastases from control mice (mice #203-02, 213-03, 215-05; top panels) or lung metastases from the 3 doxycycline-treated mice found positive for metastasis (mice # 209-01, 210-01, 216-04; bottom panels). M= metastasis; Li = liver tissue. Note the absence of specific TagRFP staining in the metastases from the doxycycline-treated mice. Black arrowheads depict non-specific staining in liver or lung epithelial cells. Bar represents 100 µm. **(B)** Linear dependence of the average catastrophe time on the growth rate for individual MTs used in the theoretical model. Experimental data are taken from Fig. 5G, N. **(C)** Fitting of force-velocity dependence for different conditions using two reference points: in the absence and in the presence of compressive force.

Supplemental experimental procedures

Constructs and siRNAs

The pLVX-IRES-Hygro (pLVIH) and pLVX-IRES-Neo (pLVIN) vectors were constructed by cloning respectively the IRES-hygromycin resistance cassette from the pBabe-hTERT-Hygro plasmid (R. Weinberg, Whitehead Institute, Cambridge, USA; Addgene #1773) and the IRES-neomycin resistance cassette from the pQCXIN plasmid (Clontech) into the pLVX-IRES-Puro plasmid (pLVIP, Clontech). The EB3-GFP coding sequence (Stepanova et al., 2003) was inserted into pBABE-Zeo (R. Weinberg Whitehead Institute, USA; Addgene #1766) and pLVIH plasmids to generate the pBabe-Zeo-EB3-GFP and pLVIH-EB3-GFP plasmids. The Lifeact-mCherry coding sequence (Riedl et al., 2008) (a gift of M. Sixt, IST Austria, and R. Wedlich-Söldner, University of Münster, Germany) was inserted into pLNCX2 plasmid (Clontech) to generate the pLN-Lifeact-mCherry plasmid. The H2B-GFP coding sequence (pBOS-H2BGFP; BD Pahramingen) was cloned into pLNCX2 to generate the pLN-H2B-GFP plasmid. The CAAX coding sequence (Lansbergen et al., 2006) was cloned into the pEGFP-C2 plasmid (Clontech) to generate the pEGFP-C2-CAAX plasmid or into the pTagRFP-T-C1 plasmid (a gift of Y. Mimori-Kiyosue, RIKEN CDB, Kobe, Japan) to generate the TagRFP-T-CAAX cassette subsequently cloned into pLVIP resulting in the pLVIP-TagRFP-T-CAAX plasmid. The β-tubulin-GFP coding sequence (kindly provided by K. Jiang, Utrecht University, the Netherlands) was cloned into pLVIP to generate the pLVIP-β-tubulin-GFP plasmid. The Tet-responsive transactivator (rtTA2sM2) coding sequence from the pSIN-TRE-mSEAP-hPGK-rtTA2sM2 plasmid (pSIN-TRE-rtTA; a gift of I.Barde and D. Trono, EPFL, Switzerland) (Barde et al., 2006) was cloned into pLVIP to generate the rtTA2sM2-IRES-Puro cassette subsequently cloned into pSIN-TRE-rtTA resulting in the all-in-one pSIN-TRE-rtTA-IRES-Puro plasmid carrying a doxycycline-inducible expression cassette and a separate constitutive expression cassette for rtTA2sM2 and puromycin resistance. The human ZEB1 coding sequence from the pcDNA4hismaxCZEB1 plasmid (a gift of J. E. Mertz, McArdle Laboratory for Cancer Research, Madison, USA) (Ellis et al., 2010) was cloned into pLVX-Tight-Puro (Clontech) and pSIN-TRE-rtTA-IRES-Puro plasmids to generate the pLVX-TP-ZEB1 and pSIN-TRE-rIP-ZEB1 plasmids, respectively. The pEGFP-C1-SLAIN2 plasmid was previously described (van der Vaart et al., 2011) and the coding sequence of the human SLAIN2 protein N-terminus (SLAIN2-N, amino acids 1-267) (van der Vaart et al., 2011) was cloned into pTagRFP-T-C1 to generate the pTagRFP-T-SLAIN2-N plasmid. The re-

sulting TagRFP-T-SLAIN2-N cassette was cloned into pSIN-TRE-rtTA-IRES-Puro and pQCXIN to generate the pSIN-TRE-rIP-RFP-SLAIN2-N and pQCXIN-RFP-SLAIN2-N plasmids, respectively. The Rho biosensor coding plasmid pLenti-RhoA2G is a gift of O. Pertz, University of Basel, Switzerland (Addgene plasmid # 40179). The Rac1 biosensor coding sequence from the pTriEX-His-Myc4-Rac1-biosensor plasmid (Moshfegh et al., 2014) was cloned into pLVIN to generate the pLVIN-Rac1-bs plasmid. The pC5V (Cerulean-5-Venus), pCerulean-C1 and pmVenus-C1 plasmids were purchased from Addgene (# 26394, S. Vogel; # 54604, M. Davidson and D. Piston; # 5465, M. Davidson). The GFP-Rab6A coding sequence (Grigoriev et al., 2007) was cloned into pQCXIN to generate the pQCXIN-GFP-Rab6A plasmid. The pQC-GFP-paxillin was previously described (Bouchet et al., 2011). The FRB and SLAIN2-N coding sequences from respectively the pC_4-R_HE (ARGENT™) and pTagRFP-T-SLAIN2-N plasmids were cloned into pEGFP-C2 plasmid, and the resulting FRB-GFP-SLAIN2-N cassette was subsequently cloned into pLVIP to generate the pLVIP-FRB-GFP-SLAIN2-N plasmid. The FKBP-TagRFP-T-MACF18LZ coding sequence (Honnappa et al., 2009) (a gift of P. Schätzle, Utrecht University, the Netherlands) was cloned into pLVIN to generate the pLVIN-FKBP-TagRFP-T-SxIP plasmid. The GFP-CLASP1α (Akhmanova et al., 2001) was cloned into pLVIH to generate the pLVIH-GFP-CLASP1 plasmid. The pmCherry-MAP2C and pmCherry-4R-Tau plasmids were a gift of C. Hoogenraad, Utrecht University, the Netherlands. The pLVX-Tet-On Advanced plasmid and the lentiviral Lenti-X HTX Packaging vector mix were purchased from Clontech. The retroviral packaging vector pCL-Ampho was kindly provided by E. Bindels, Erasmus MC, The Netherlands. The lentiviral packaging vectors psPAX2 and pMD2.G were kindly provided by E. Soler, Erasmus MC, the Netherlands. The GFP-ch-TOG vector pBrain-GFP-ch-TOGKDP-shch-TOG simultaneously expressing an shRNA for depleting human ch-TOG and a GFP-tagged ch-TOG rescue construct was a gift of S. Royle (Warwick Medical School, UK) (Gutierrez-Caballero et al., 2015). Individual siRNAs targeting SLAIN2, ch-TOG, CLASP1, CLASP2 and CLIP-170, and luciferase targeting control siRNA were previously described (Lansbergen et al., 2006; Mimori-Kiyosue et al., 2005; van der Vaart et al., 2011). For experiments based on ch-TOG depletion, 2 mM thymidine was added one day after siRNA transfection and 2 days prior to imaging in order to block cells in interphase and avoid mitosis-related cell rounding. In ch-TOG- and CLASP-depleted 3D cultures, mitotic cells were excluded from morphology and migration analysis using H2B-GFP fluorescence imaging to monitor chromosome condensation.

Antibodies and cell culture reagents

The rat monoclonal antibody against tyrosinated α-tubulin (YL1/2) was purchased from Abcam. Mouse monoclonal antibodies against the following proteins were used: α-tubulin (DM1A), fibronectin (FN-3E2), vimentin (V9) and phospho-tyrosine (Sig-

ma-Aldrich); E-cadherin (36/E-Cadherin), α-catenin (5/a-catenin), β-catenin (14/Beta-Catenin), α-occludin (19/Occludin), Ku80 (7/Ku80) and EB1 (BD Biosciences); actin (C4) (Merck-Millipore); Rho, Rac1 and Cdc42 (Cytoskeleton); GFP (Roche). We used rabbit polyclonal antibody against ZEB1 (Bethyl Laboratories), SLAIN1/2 (van der Vaart et al., 2011), ch-TOG (a gift from L. Cassimeris, Lehigh University), CLASP1 (Mimori-Kiyosue et al., 2005), CLIP-170 and CLASP2 (Akhmanova et al., 2001), EB3 (Stepanova et al., 2003) and TagRFP (Evrogen). Note that the anti-SLAIN1/2 antibody used here also recognizes SLAIN1, but the depletion of SLAIN2 alone was sufficient to strongly decrease the total SLAIN signal, indicating that SLAIN1, which is predominantly neuronal (van der Vaart et al., 2012), does not contribute significantly to the SLAIN2 pool in the investigated cells.

Alexa Fluor 405-, Alexa Fluor 488- and Alexa Fluor 594-conjugated goat antibodies against rat, rabbit and mouse were purchased from Life Technologies. For Western blotting, IRDye 800CW-conjugated goat antibody against rabbit IgG and IRDye 680LT-conjugated goat antibody against mouse IgG were purchased from Li-Cor Biosciences.

Rat tail collagen Type I (high concentration) for soft 3D culture was purchased from Corning and bovine dermis pepsin-extracted collagen I solution for stiff 2D culture was purchased from Advanced BioMatrix (PureCol). Stiffness of rat tail collagen I gels was defined based on previous publications using an identical preparation method, similar invasive cell lines and elastic modulus measurement (Heck et al., 2012; Wolf et al., 2013). Phenol red-free Matrigel was purchased from BD Biosciences. For collagenolysis assay, fluorescein conjugated DQ collagen (type I from bovine skin, Life Technologies) was prepared according to the manufacturer's instructions and mixed at a final concentration of 25 μg/ml with the gel preparation. Collagenolysis was observed by confocal imaging 2 days after seeding. DMEM, MEBM and supplement (human EGF, insulin, hydrocortisone, bovine pituitary extract, gentamicin and amphotericin-B) and trypsin neutralizing solution were purchased from Lonza. DMEM/F12 and RPMI 1640 were purchased from Life Technologies.

We used the following chemicals, reagents and drugs: Alexa Fluor 594- and Alexa Fluor 488-conjugated phalloidin and G418 (Geneticin) (Life Technologies); puromycin and hygromycin (InvivoGen); thymidine, vinblastine sulfate, ROCK1 inhibitor Y-27632, sodium borohydride ($NaBH_4$), DAPI, Triton X-100, Tween 20, bovine serum albumin (BSA), poly-HEMA and doxycycline hydrochloride solution (Sigma-Aldrich); polybrene and Rac1 inhibitor NSC23766 (Merck-Millipore); paclitaxel and blebbistatin (Enzo Life Sciences); polyethyleneimine "Max" (MaxPEI) (Polysciences); latrunculin B (Santa Cruz Biotechnology); Rapalog (Clontech); Vectashield (Vector Laboratories); paraformaldehyde (16%) and glutaraldehyde (10%) (Electron Microscopy Sciences); poly-D-lysine (MP Biomedicals).

Click-iT EdU Cell Proliferation assay was purchased from Life Technologies, performed according to manufacturer's instructions and analyzed on 10-20 independent fields of view (~100-500 cells per condition). FuGENE6 Transfection Reagent (cDNA) was purchased from Roche. HiPerFect Transfection Reagent (siRNA) was purchased from Qiagen. Amaxa Cell Line Nucleofector Kit V was purchased from Lonza. Multi-well glass bottom and slide chambers were purchased from Thermo Scientific. Rac1/Cdc42 and Rho activation assay kits were purchased from Cytoskeleton and used according to the manufacturer's instructions in sparse cell cultures stimulated with fresh 10% FCS-containing medium 3 hours before lysis (n = 5-6 independent experiments); 800 μg of pre-cleared whole cell lysis were incubated with 15 μg of Rhotekin-RBD (Rho) or 10 μg of PAK-PBD (Rac1) beads and input was as indicated in Figure 3.

Transfection, lentiviral infection and cell line selection

Lentivirus packaging was performed by MaxPEI-based co-transfection of HEK293T cells with psPAX2, pMD2.G and the lentiviral vector of interest. In the case of non-self-inactivated vectors (pLVX-based vector, Clontech), the vector of interest was co-transfected with the Lenti-X HTX packaging mix. Retrovirus packaging was performed by co-transfection of HEK293T cells with pCL-Ampho vector with the retroviral vector of interest. Supernatant of packaging cells was harvested up to 72 hours after transfection, 0.45 μm-filtered and incubated with a PEG 6000-based precipitation solution overnight at 4°C. After precipitation, virus was concentrated up to 100 times by centrifugation and dissolution in 1X phosphate buffered saline (PBS). Target cells were incubated for 4 hours in complete medium supplemented with 8 μg/ml polybrene before infection. Medium was replaced 24-48 hours after infection and eventual antibiotics for selection were added.

Clonal MDA-MB-231 stable lines expressing the following combinations of tagged proteins were established by infection using the plasmids and viruses described above, antibiotics selection (2 μg/ml puromycin; 500-750 μg/ml G418) and/or limiting dilution-based subcloning: Lifeact-mCherry, EB3-GFP, Lifeact-mCherry and EB3-GFP, H2B-GFP, TagRFP-T-CAAX and β-tubulin-GFP, doxycycline-inducible TagRFP-T-SLAIN2-N, TagRFP-T-CAAX and GFP-Rab6A', FRB-GFP-SLAIN2-N and FKBP-TagRFP-T-SxIP, and GFP-paxillin. Clonal HT-1080 stable lines expressing the following tagged proteins were established by infection using the plasmids and viruses described above, using antibiotics selection (2 μg/ml puromycin; 600 μg/ml G418) and/or limiting dilution-based subcloning: Rho biosensor, Rac1 biosensor and EB3-GFP. Clonal hTMECs stable lines expressing the following combinations of proteins were established by infection using the plasmids and viruses described above, antibiotics selection (0.5 μg/ml puromycin; 100-200 μg/ml G418) and/or limiting dilution-based subcloning: EB3-GFP, doxycycline-inducible ZEB1, EB3-GFP and doxycycline-inducible ZEB1,

and doxycycline-inducible ZEB1 and constitutive TagRFP-T-SLAIN2-N. hTMEC clones carrying ZEB1-inducible expression (hTMEC-ZEB1^{dox}) were selected based on ZEB1 expression level analyzed by Western blotting and efficient and sustained EMT characterized by morphology and Western blotting-based analysis of epithelial and mesenchymal markers after 0.5-1 μg/ml doxycycline treatment.

Transient overexpression of Cerulean, mVenus, C5V, mCherry-MAP2C and GFP-CAAX, or mCherry-4R-Tau was achieved by FuGENE6-based transfection in HT-1080 cells and Amaxa Cell Line Nucleofector Kit V-based nucleofection in MDA-MB-231 cells, 24-48 hours prior imaging and according to manufacturer instructions. Transfection of 5-10 nM siRNA in MDA-MB-231 and HT-1080 cells was performed using HiPerFect according to manufacturer's instructions.

Working solutions of vinblastine and paclitaxel were freshly prepared for each experiment and diluted in DMSO and complete medium. ROCK1 inhibitor Y-27632 was used at 10 μM, myosin II inhibitor blebbistatin was used at 50 μM, Rac1 inhibitor NSC23766 was used at 200 μM, latrunculin B was used at 10 μM and rapalog was used at 100 nM. Inhibitors were either added to the culture medium for short-term treatment and/or mixed with the gel for long treatment in 3D cultures.

Fluorescent staining, microscopy of fixed samples and analysis

For immunofluorescence staining of α-tubulin and F-actin in 2D cultures, cells were first extracted for 30 seconds at room temperature (RT) with 0.2 % Triton X-100 in cytoskeleton stabilizing buffer (CSB; 60 mM PIPES, 20 mM HEPES, 1 mM $MgCl_2$, 4 mM EGTA, 100 mg/ml sucrose), fixed in 2% PFA/0.1% glutaraldehyde in CSB for 10 minutes, permeabilized in 0.2% Triton X-100 for 15 minutes at RT, blocked in 1% BSA diluted in 1X PBS supplemented with 0.05% Tween 20. Samples were then sequentially incubated at RT with mouse monoclonal antibody against α-tubulin, Alexa Fluor 488-conjugated goat antibodies against mouse IgG, and 2 μg/ml DAPI/1:200 Alexa Fluor 594-conjugated phalloidin and after the final wash, dried and mounted in Vectashield. Cell area in 2D cultures was measured in 10-17 cells. Lamella MT density was performed using ImageJ in images of α-tubulin staining by manual counting, using a 7 μm-diameter region of interest (n=25, 5 cells). For immunofluorescence staining of focal adhesions, cells were fixed in 4% PFA for 15 minutes, permeabilized in 0.2% Triton X-100 for 5 minutes at RT, blocked in 1% BSA diluted in 1X PBS supplemented with 0.05% Tween 20, sequentially incubated at RT with mouse monoclonal antibody against phospho-tyrosine, Alexa Fluor 488-conjugated goat antibodies against mouse IgG and Alexa Fluor 594-conjugated phalloidin. For quantification of focal adhesion in 3D, phospho-tyrosine clusters larger than 0.1 μm^2 were manually counted and measured using ImageJ (n=8 cells). For focal adhesion quantification in 2D, phospho-tyrosine clusters larger than 0.1 μm^2 were counted using particle analyzer in ImageJ (n=14 cells).

For immunofluorescence staining of α-tubulin and F-actin in 3D cultures, cells were incubated with 0.5% Triton X-100/0.1% glutaraldehyde CSB pre-extraction buffer at 37°C for 5 minutes, fixed in 0.3% glutaraldehyde diluted in 1X PBS for 10 minutes at RT, rinsed in 1X PBS, permeabilized for 30-45 minutes at RT in 0.5-0.7% Triton X-100 diluted in 1X PBS and blocked 30 minutes at RT in 1% BSA diluted in 1X IF wash solution (10X stock; 38.00 g NaCl 9.38 g Na_2HPO_4, 2.07 g NaH_2PO_4, 2.5 g NaN_3, 10 ml Triton X-100, 2.5 ml Tween-20, 500 ml MilliQ water, pH 7.4). Glutaraldehyde was quenched 1-3 times for 5 minutes using 2.5 mg/ml $NaBH_4$ diluted in permeabilizing solution. Incubation with the rat monoclonal antibody against tyrosinated α-tubulin was performed for 3 hours at RT or overnight at 4°C. Alternatively, incubation with mouse monoclonal antibodies against α-tubulin was used and 2% PFA/0.1% glutaraldehyde was used for fixation. Secondary antibody, DAPI, and Alexa Fluor 488 or 594-conjugated phalloidin incubations were performed as described above. Multi-well supports were dismounted, 3D gel plugs were dried at RT, covered with Vectashield and coverslip, incubated overnight at RT and the resulting sample was sealed with nail polish.

2D Samples were imaged using widefield fluorescence illumination on a Nikon Eclipse 80i upright microscope equipped with a CoolSNAP HQ^2 CCD camera (Photometrics), an Intensilight C-HGFI precentered fiber illuminator (Nikon), ET-DAPI, ET-EGFP and ET-mCherry filters (Chroma), controlled by Nikon NIS Br software and using a Plan Apo VC 100x NA 1.4 oil, Plan Apo VC 60x NA 1.4 oil or a Plan Fluor 20x MI NA 0.75 oil objective (Nikon). For presentation, images were adjusted for brightness and processed by Gaussian blur and Unsharp mask filter using ImageJ 1.47v (NIH). For cell area measurement, Alexa Fluor 594-conjugated phalloidin images were processed for threshold to reveal the cell edge, and the binary cell mask obtained was selected and measured using ImageJ 1.47v.

3D samples were imaged by confocal fluorescence microscopy on a Nikon Eclipse Ti microscope equipped with a perfect focus system (PFS, Nikon), a spinning disk-based confocal scanner unit (CSU-X1-A1, Yokogawa), an Evolve 512 EMCCD camera (Photometrics) attached to a 2.0X intermediate lens (Edmund Optics), a super high pressure mercury lamp (C-SHG1, Nikon), a Roper Scientific custom-made set of Stradus 405 nm (100 mW, Vortran), Calypso 491 nm (100 mW, Cobolt) and Jive 561 nm (100 mW, Cobolt) lasers, a set of ET-BFP2, ET-EGFP, ET-mCherry and ET-EGFP-mCherry filters (Chroma) for widefield fluorescence observation, a set of ET460/50m, ET525/50m or ET535/30m (green), ET630/75m (red) and ET-EGFP/mCherry filters (Chroma) for spinning disk-based confocal imaging and a motorized stage MS-2000-XYZ with Piezo Top Plate (ASI). The microscope setup was controlled by MetaMorph 7.7.11.0. Images were acquired using Plan Fluor 10x NA 0.3 air, Plan Fluor 20x MI NA 0.75 oil, Plan Apochromat λ 60x NA 1.4 oil and Plan Apo VC 60x NA 1.4 oil objectives.

Z-series images of fluorescent staining of α-tubulin, F-actin and DQ collagen

in 3D cultures were acquired using 0.2 μm-step confocal-based scan (50-145 z-planes) and were presented as maximum projections adjusted for brightness and eventually processed by Gaussian blur and unsharp mask filter using ImageJ 1.47v or deconvolved using Huygens Software 4.4.0p9 (SVI). Images of DQ collagen with Lifeact-mCherry or TagRFP-CAAX were acquired similarly and single planes are displayed. Collagen degradation index was calculated using DQ collagen fluorescence images processed by Gaussian blur and background subtraction using ImageJ. It represents the ratio of pixel intensity sum in the first 5 μm away from the cell body to the same value in the next 5 μm recorded by 10 pixel-wide selection lines (Plot profile)(n=15, 5 cells).

Cell circularity and area in 3D or on-top cultures was measured on maximum projection of z-series images when the z distribution of the cell body did not span the average z dimension of a completely rounded cell (approximately 20 μm) to limit z-related bias in morphology analysis (n = 10-35 cells). Binary cell mask obtained after thresholding was analyzed using ImageJ 1.47v for circularity.

Live cell imaging and analysis

Kymograph-based analysis of MT plus end dynamics was carried out using cells stably expressing EB3-GFP as previously described (van der Vaart et al., 2011) using a 1 μm cut-off for a growth event and Kymograph ImageJ plugin (A. Seitz, EPFL, Switzerland, http://biop.epfl.ch/TOOL_KYMOGRAPH.html). For the dataset presented, 44-176 growth events were analyzed in 5-20 cells. For presentation, images were adjusted for brightness and processed by Gaussian blur and unsharp mask filter using ImageJ 1.47v. For the analysis of growing MT plus end residence within 5 μm from the cell edge, 2-channel kymographs (EB3-GFP/ Lifeact-mCherry or TagRFP-T-CAAX,) were used. Only the MT growth events starting and finishing within the time of the recording and displaying a velocity ranging from 2-fold slower than average to ~0 μm/min (stationary comet) were classified as residence events and subsequently quantified for duration (n = 124-309, 11-29 cells). For β-tubulin-GFP/TagRFP-T-CAAX imaging and MT buckling analysis, images were acquired by confocal fluorescence at one optimal z-plane, adjusted for brightness, processed by Gaussian blur, background subtraction and unsharp mask filter using ImageJ 1.47v.

Load-bearing capacity of MTs at the cell cortex in the absence of F-actin was analyzed in two ways. First, adherent cells were treated with latrunculin B followed by immediate simultaneous fluorescence imaging of EB3-GFP and TagRFP-T-CAAX on the spinning disk-based confocal imaging station described above (n = 24-32 cells). To build distributions of EB3-GFP comet velocity during protrusion formation, we used kymograph-based analysis. Two-channel kymographs (EB3-GFP, TagRFP-T-CAAX) were built along a line traced at the estimated average position of the protrusion using the ImageJ plugin KymoResliceWide (https://github.com/ekatrukha/KymoResliceWide). Only

EB3-GFP comets, which were localized to protrusion tips and the position of which correlated with the elongation of the protrusion were analyzed. Individual growth events were manually traced using segmented line tool of ImageJ. The resulting coordinates (x, t) were imported into Matlab and analyzed using a custom written script. Instantaneous velocity extracted from the slope of each segment within a tracing was assigned to the corresponding protrusion length. All growth episodes were inversely ranked with the end position being assigned to the zero coordinate and the start position assigned to the maximum protrusion length value. Corresponding MT growth rate as a function of its relative position to the tip of the protrusion at maximum length was sampled at 0.1 μm intervals and presented as a multiple event average per bin. To facilitate the comparison between control and SLAIN2-depleted cells, data points from protrusion length >3 μm were excluded from analysis. Alternatively, MT ability to push cortical membrane in the absence of F-actin was analyzed by counting (n = 15 cells) and measuring (n = 29-145) cortical protrusions (length cut-off, 2.5 μm) formed in cells treated for 15 minutes with latrunculin B and cultured on a poly-HEMA-treated non-adherent support. Measurements were performed on masks obtained from maximum projection of z-series of 1 μm-step confocal fluorescence images of TagRFP-CAAX expressing cells.

FRET-based analysis of Rho and Rac1 activity was performed on clonal HT-1080 cells lines described above and stably expressing the previously described Rho single chain biosensor (Fritz et al., 2013) or Rac1 single chain biosensor (Moshfegh et al., 2014). Fluorescence imaging of Rho and Rac1 biosensors was performed on the spinning disk-based confocal imaging station described above implemented with a ET-ECFP/EYFP filter (Chroma), a Stradus 445 nm (80mW, Vortran) laser for excitation of mTFP1 (Rho biosensor) and mCerulean (Rac1 biosensor), a dichroic filter T505lpxr equipping the DV2 device for simultaneous blue and yellow fluorescence imaging and a Di01-T442/514/647 emission filter (Semrock). Biosensor probe distribution was monitored by mTFP1/mCerulean fluorescence imaging upon 445 nm excitation, compared to mVenus fluorescence upon 445 nm excitation (FRET) and used to detect eventual aggregation/sequestration-related artefacts. To minimize cell motion-related artefacts, mTFP1/mCerulean and mVenus emission upon 445nm excitation were recorded simultaneously using the DV2 device. Manual alignment of the DV2 mirrors was performed to reduce as much as possible misalignment-related artefacts in the FRET/mTFP1 or mCerulean fluorescence ratio calculation and spatial distribution. When necessary, further adjustment was performed using split images and ratiometric result obtained from a custom written ImageJ macro. The standards Cerulean (pmCerulean-C1), mVenus (pmVenus-C1) and positive control C5V (pC5V) (Koushik et al., 2006) were imaged with the same setup in transiently transfected HT-1080 cells. Using thresholding on the FRET image, a cell mask was determined and applied to the 32-bit FRET/mTFP1 or mCerulean ratiometric image to measure mean ratio value within each cell. For presentation purpos-

es, the 32-bit ratiometric image was submitted to Gaussian blur, a 16 color-lookup table was applied and a 8-bit color calibration bar is displayed. For 2D cultures, single plane confocal images were acquired at the ventral cell cortex (n = 40 cells). In 3D cultures, single plane confocal images were acquired at position allowing maximal measurement of Rho (n = 10) or Rac1 (n = 17) activity over the cell body including pseudopods and later processed using thresholding to exclude both outside of the cell and nucleus from the analysis. 2D and 3D cultures were respectively imaged using a Plan Fluor 40x NA 1.3 and Apo LWD λS 40x NA 1.15 with a supplementary image series using an extra 1.5x magnification before projection on the camera chip for 3D protrusion tip analysis.

Rab6A-GFP vesicle dynamics within 5 µm of the pseudopod tip was analyzed on kymographs from 3D confocal imaging (n = 12-13 cells; 112-162 moving towards the tip; 50-73 vesicles moving towards the cell body; 121-128 immobile vesicles). GFP-paxillin images were used for focal adhesion counting at the tip of live cells grown in 3D (n=8, 4 cells).

Phase contrast and wide field fluorescence live cell imaging were performed on a Nikon Ti equipped with a perfect focus system (PFS, Nikon), a super high pressure mercury lamp (C-SHG1, Nikon), Lambda SC Smart Shutter controllers (Sutter), a Plan Apochromat DM 20x NA 0.75 (Ph2) or a Plan Fluor DLL 10x NA 0.3 (Ph1), a ET-mCherry filter (Chroma), a CoolSNAP HQ^2 CCD camera (Photometrics), a motorized stage MS-2000-XYZ with Piezo Top Plate (ASI) and a stage top incubator INUG2E-ZILCSD-DV (Tokai Hit) for 37°C/5% CO2 incubation. The microscope setup was controlled by the open source microscopy software Micro-Manager. Processing with Gaussian blur and Unsharp mask filter using ImageJ 1.47v was used for presentation. Red fluorescent images were subjected to background subtraction and adjusted for brightness before the overlay with phase contrast images. Alternatively, phase contrast and widefield fluorescence live cell imaging were performed using the BioStation CT (Nikon) equipped with a 2/3-inch cooled CCD camera, a high-intensity red LED for phase contrast imaging, and a 460-490 nm LED and a GFP-3035B filter block (Semrock) for green fluorescence imaging. Cell migration speed and distance from starting point were analyzed in 5 minute interval/1.5 hour long (2D) or 15 minute interval/20 hours long (3D; on-top) time-lapse recordings (n = 21-114 cells) using the MTtrackJ plugin v1.5.0 in ImageJ 1.47v. Inverse of circularity and cell area in soft 3D vs soft 2D matrices (n = 48-108), CLASP1-overexpressing vs control cells (n=12) and rapalog-based rescue (n = 37-44) were analyzed on phase contrast images. Protrusion frequency in SLAIN2-depleted cells (Fig. S2D) was analyzed by manual counting using phase contrast time-lapse recording of 3D cultures started one hour after 3D seeding and performed for 2 hours (n=19-20 cells).

Immunohistochemistry in mouse tissues

Tissues were isolated and fixed in 4% formalin. Tissues were cut into 4 µm sections,

dehydrated, and stained with hematoxylin and eosin. For immunohistochemical stainings, fixed sections were rehydrated and incubated with rabbit anti-TagRFP antibody (1:200). Endogenous peroxidases were blocked with 3% H_2O_2 followed by incubation with HRP-conjugated secondary anti-rabbit antibodies (Immunologic). Substrate was developed with DAB (DAKO). Imaging was performed using a Nikon Eclipse E800 microscope mounted with a Nikon digital camera DXM1200.

Model for the collective dynamics of MTs in pseudopods

Dynamics of MT bundles inside pseudopods was modeled using Monte Carlo simulations written in Matlab (version 2011b, Natick, MA, USA) similar to previous studies (Dogterom and Leibler, 1993; Janson et al., 2003; Laan et al., 2008). The total number of MTs N_{tot} was constant during each simulation, but varied from 3 to 10 for different conditions. MT growth and shrinkage were considered as deterministic processes with defined velocities, whereas catastrophe and rescue events of individual MTs were treated as random processes. The main parameters of dynamic instability were the growth V_{gr} and shrinkage V_{sh} rates, and the average catastrophe T_{gr} and rescue T_{sh} times. Growth rate and average catastrophe time for each condition were obtained from the experimental measurements of the dynamics of EB3 comets inside pseudopods (Fig. 5G,H). For the shrinking rate and average rescue time we selected previously measured values of 20 μm/min and 0.14 min correspondingly (Kapoor and Panda, 2012). Each MT in the bundle started to grow at zero length in the "semi-infinite" geometry and switched between growing and shrinking phases. If the length of a MT was zero, it automatically switched to the growth phase. The final output of simulations was a set of MT lengths over discrete time sequences

$$L_i(t_j),\ i \in [1, N_{tot}],\ t_j = j \cdot dt,\ t \in [0, T]$$

where dt is the time step and T is the total observation time. The length and growth velocity of the MT bundle were defined as the length and velocity of the longest MT in the bundle.

We assumed that the average catastrophe time depends linearly on the growth rate (Janson et al., 2003) and used the measured values of V_{gr} and T_{gr} far from the edge of the protrusion (in the absence of load, Fig. 5G,H) to calculate the corresponding coefficient of proportionality for each condition (Fig. S4B). MTs longer than the average MT length in the bundle were supposed to resist the compressive load (accounting for the round shape of the tip of protrusion), which led to a decrease of their growth rate. We assumed a simplified functional form for the force-velocity dependence

$$V_g\ (f_{comp}) = V_g\ (0) \exp\left(-\frac{f_{comp}}{f_{crit} N_{comp}} \right)$$

where f_{comp} is the total compressive force generated at the edge of the pseudopod, Ncomp is the total number of MTs sharing the load, $V_{gr}(0)$ is the growth rate far from the edge (in the absence of compressive force) and f_{crit} is characteristic "resistance force" of individual MT (Dogterom and Yurke, 1997). To estimate f_{crit} for each condition, we assumed that on average N_{tot}=5 and N_{comp} = 0.5*N_{tot} and that the total force f_{comp} experienced by the pseudopod is around 30 pN, i.e. on average each load-bearing MT experiences a force of 12 pN (Bornschlogl et al., 2013; Farrell et al., 2013; Koster et al., 2005; Pontes et al., 2011). Knowing characteristics of individual MT dynamics in the absence of force (f_{MT}=0, Fig. 5G,H) and under the estimated load (f_{MT} ~12 pN, Fig. 5N) allowed us to find the value of f_{crit} by fitting (Fig. S4C). As a result we obtained values of 37.7 pN for the control, 6.8 pN for the SLAIN2 siRNA and 7.4 pN for the CLASP1 siRNA conditions (Fig. S4C). These values are much higher than those measured previously *in vitro* (Dogterom and Yurke, 1997), which might hint at a more efficient force generation by MTs growing under *in vivo* conditions. However, the high f_{crit} value for the control condition might be an overestimate, since the number of microtubules sharing the load might be different for different conditions. Shrinkage was assumed to be force-independent.

All simulations were performed with the time step dt=0.1 s for the total time of T=20 min. To validate the model and map parameter space, we first performed simulations in the absence of the "compressed" state. In this case, the model becomes equivalent to the published earlier (Dogterom and Leibler, 1993). The simulation reproduced regimes of "unbounded" and "bounded" growth with a sharp transition taking place along the line $L_{gr}=L_{sh}$, where $L_{gr}=V_{gr}T_{gr}$ and $L_{sh}=V_{sh}T_{sh}$ (Fig. 7E, and see the purple line Fig. 7F). For this reason, we chose these two combinations as the main parameters to build the system's parametric diagrams. For each simulation in the "unbounded" mode, we calculated the average pseudopod/bundle length at current time as $\max(L_i(t_j))_i$ and fitted its time sequence with linear function to estimate the average velocity of pseudopod growth. With fixed value of L_{gr} the rate of pseudopod extension depended linearly on the value of L_{sh} (or vice versa), while moving deeper into the "unbounded" region of the parametric diagram, confirming the results obtained in (Dogterom and Leibler, 1993). After the introduction of a "compressed" state, the overall behavior of the model did not change. It showed regimes of "unbounded" and "bounded" growth and the same linear dependence of MT bundle/protrusion growth velocity on the main parameters. The main difference was that the position of the border separating two dynamic modes had changed. We calculated the new position of the separation border on the parametric diagram numerically, using stochastic simulations of MT bundle described above. It is challenging to distinguish the difference between "bounded" and "unbounded" regimes in the area of parameters near the separation border due to highly stochastic behavior of the bundle (Fig. 7E). To avoid this ambiguity, we measured average protrusion/bundle growth velocity "deep" inside the "unbounded" growth area, where processive growth

of the MT bundle is highly pronounced and its rate can be calculated precisely. We used five different values of L_{sh} (while keeping the L_{gr}, constant) and measured from the simulation the average bundle/protrusion velocity, which usually was in the range 1-10 μm/min. Since the growth rate of the MT bundle depends on the L_{sh} linearly, we were able to get the value of L_{sh}^{crit} located at the separation border between "bounded" and "unbounded" states (corresponding to the zero growth rate of the bundle) from a linear fit. This procedure was repeated five times and after averaging we got the value of L_{sh}^{crit} for the constant L_{gr} on the parametric diagram. The same search of L_{sh}^{crit} was repeated for the range of L_{gr} values, composing the final separation border between two regimes on parametric diagram.

As an independent verification of the model, we calculated the pseudopod extension rate at the point of the parametric diagram corresponding to the control condition. Simulations gave the value of 5.4 μm/min that is very close to the values of 3-6 μm/min observed in the experimental data.

Supplemental references

Akhmanova, A., C.C. Hoogenraad, K. Drabek, T. Stepanova, B. Dortland, T. Verkerk, W. Vermeulen, B.M. Burgering, C.I. De Zeeuw, F. Grosveld, and N. Galjart. 2001. Clasps are CLIP-115 and -170 associating proteins involved in the regional regulation of microtubule dynamics in motile fibroblasts. Cell. 104:923-935.

Barde, I., M.A. Zanta-Boussif, S. Paisant, M. Leboeuf, P. Rameau, C. Delenda, and O. Danos. 2006. Efficient control of gene expression in the hematopoietic system using a single Tet-on inducible lentiviral vector. Mol.Ther. 13:382-390.

Bornschlogl, T., S. Romero, C.L. Vestergaard, J.F. Joanny, G.T. Van Nhieu, and P. Bassereau. 2013. Filopodial retraction force is generated by cortical actin dynamics and controlled by reversible tethering at the tip. Proc Natl Acad Sci U S A. 110:18928-18933.

Bouchet, B.P., F. Fauvet, G. Grelier, C.M. Galmarini, and A. Puisieux. 2011. p21(Cip1) regulates cell-substrate adhesion and interphase microtubule dynamics in untransformed human mammary epithelial cells. Eur.J.Cell Biol. 90:631-641.

Dogterom, M., and S. Leibler. 1993. Physical aspects of the growth and regulation of microtubule structures. Phys Rev Lett. 70:1347-1350.

Dogterom, M., and B. Yurke. 1997. Measurement of the force-velocity relation for growing microtubules. Science. 278:856-860.

Ellis, A.L., Z. Wang, X. Yu, and J.E. Mertz. 2010. Either ZEB1 or ZEB2/SIP1 can play a central role in regulating the Epstein-Barr virus latent-lytic switch in a cell-type-specific manner. J.Virol. 84:6139-6152.

Farrell, B., F. Qian, A. Kolomeisky, B. Anvari, and W.E. Brownell. 2013. Measuring forces at the leading edge: a force assay for cell motility. Integr Biol (Camb). 5:204-214.

Fritz, R.D., M. Letzelter, A. Reimann, K. Martin, L. Fusco, L. Ritsma, B. Ponsioen, E. Fluri, S. Schulte-Merker, J. van Rheenen, and O. Pertz. 2013. A versatile toolkit to produce sensitive FRET biosensors to visualize signaling in time and space. Sci Signal. 6:rs12.

Grigoriev, I., D. Splinter, N. Keijzer, P.S. Wulf, J. Demmers, T. Ohtsuka, M. Modesti, I.V. Maly, F. Grosveld, C.C. Hoogenraad, and A. Akhmanova. 2007. Rab6 regulates transport and targeting of exocytotic carriers. Dev.Cell. 13:305-314.

Gutierrez-Caballero, C., S.G. Burgess, R. Bayliss, and S.J. Royle. 2015. TACC3-ch-TOG track the growing tips of microtubules independently of clathrin and Aurora-A phosphorylation. Biology open. 4:170-179.

Heck, J.N., S.M. Ponik, M.G. Garcia-Mendoza, C.A. Pehlke, D.R. Inman, K.W. Eliceiri, and P.J. Keely. 2012. Microtubules regulate GEF-H1 in response to extracellular matrix stiffness. Mol. Biol.Cell. 23:2583-2592.

Honnappa, S., S.M. Gouveia, A. Weisbrich, F.F. Damberger, N.S. Bhavesh, H. Jawhari, I. Grigoriev, F.J. van Rijssel, R.M. Buey, A. Lawera, I. Jelesarov, F.K. Winkler, K. Wuthrich, A. Akhmanova, and M.O. Steinmetz. 2009. An EB1-binding motif acts as a microtubule tip localization signal. Cell. 138:366-376.

Janson, M.E., M.E. de Dood, and M. Dogterom. 2003. Dynamic instability of microtubules is regulated by force. J Cell Biol. 161:1029-1034.

Kapoor, S., and D. Panda. 2012. Kinetic stabilization of microtubule dynamics by indanocine perturbs EB1 localization, induces defects in cell polarity and inhibits migration of MDA-MB-231 cells. Biochem Pharmacol. 83:1495-1506.

Koster, G., A. Cacciuto, I. Derenyi, D. Frenkel, and M. Dogterom. 2005. Force barriers for membrane tube formation. Phys Rev Lett. 94:068101.

Koushik, S.V., H. Chen, C. Thaler, H.L. Puhl, 3rd, and S.S. Vogel. 2006. Cerulean, Venus, and VenusY67C FRET reference standards. Biophys J. 91:L99-L101.

Laan, L., J. Husson, E.L. Munteanu, J.W. Kerssemakers, and M. Dogterom. 2008. Force-generation and dynamic instability of microtubule bundles. Proc Natl Acad Sci U S A. 105:8920-8925.

Lansbergen, G., I. Grigoriev, Y. Mimori-Kiyosue, T. Ohtsuka, S. Higa, I. Kitajima, J. Demmers, N. Galjart, A.B. Houtsmuller, F. Grosveld, and A. Akhmanova. 2006. CLASPs attach microtubule

plus ends to the cell cortex through a complex with LL5beta. Dev.Cell. 11:21-32.

Mimori-Kiyosue, Y., I. Grigoriev, G. Lansbergen, H. Sasaki, C. Matsui, F. Severin, N. Galjart, F. Grosveld, I. Vorobjev, S. Tsukita, and A. Akhmanova. 2005. CLASP1 and CLASP2 bind to EB1 and regulate microtubule plus-end dynamics at the cell cortex. J.Cell Biol. 168:141-153.

Moshfegh, Y., J.J. Bravo-Cordero, V. Miskolci, J. Condeelis, and L. Hodgson. 2014. A Trio-Rac1-Pak1 signalling axis drives invadopodia disassembly. Nat Cell Biol. 16:574-586.

Pontes, B., N.B. Viana, L.T. Salgado, M. Farina, V. Moura Neto, and H.M. Nussenzveig. 2011. Cell cytoskeleton and tether extraction. Biophys J. 101:43-52.

Riedl, J., A.H. Crevenna, K. Kessenbrock, J.H. Yu, D. Neukirchen, M. Bista, F. Bradke, D. Jenne, T.A. Holak, Z. Werb, M. Sixt, and R. Wedlich-Soldner. 2008. Lifeact: a versatile marker to visualize F-actin. Nat.Methods. 5:605-607.

Stepanova, T., J. Slemmer, C.C. Hoogenraad, G. Lansbergen, B. Dortland, C.I. De Zeeuw, F. Grosveld, C.G. van, A. Akhmanova, and N. Galjart. 2003. Visualization of microtubule growth in cultured neurons via the use of EB3-GFP (end-binding protein 3-green fluorescent protein). J.Neurosci. 23:2655-2664.

van der Vaart, B., M.A. Franker, M. Kuijpers, S. Hua, B.P. Bouchet, K. Jiang, I. Grigoriev, C.C. Hoogenraad, and A. Akhmanova. 2012. Microtubule plus-end tracking proteins SLAIN1/2 and ch-TOG promote axonal development. J.Neurosci. 32:14722-14728.

van der Vaart, B., C. Manatschal, I. Grigoriev, V. Olieric, S.M. Gouveia, S. Bjelic, J. Demmers, I. Vorobjev, C.C. Hoogenraad, M.O. Steinmetz, and A. Akhmanova. 2011. SLAIN2 links microtubule plus end-tracking proteins and controls microtubule growth in interphase. J.Cell Biol. 193:1083-1099.

Wolf, K., L.M. Te, M. Krause, S. Alexander, R.J. Te, A.L. Willis, R.M. Hoffman, C.G. Figdor, S.J. Weiss, and P. Friedl. 2013. Physical limits of cell migration: Control by ECM space and nuclear deformation and tuning by proteolysis and traction force. J.Cell Biol. 201:1069-1084.

4

Control of apico-basal epithelial polarity by the microtubule minus-end-binding protein CAMSAP3 and spectraplakin ACF7

Ivar Noordstra[1], Qingyang Liu[1], Wilco Nijenhuis[1], Shasha Hua[1], Kai Jiang[1], Matthijs Baars[1], Sanne Remmelzwaal[1], Maud Martin[1], Lukas C. Kapitein[1] and Anna Akhmanova[1]

Journal of Cell Science (2016); 129:4278-4288

[1]Cell Biology, Faculty of Science, Utrecht University, 3584 CH Utrecht, The Netherlands

Summary

The microtubule cytoskeleton regulates cell polarity by spatially organizing membrane trafficking and signaling processes. In epithelial cells, microtubules form parallel arrays aligned along the apico–basal axis, and recent work has demonstrated that the members of CAMSAP/Patronin family control apical tethering of microtubule minus ends. Here, we show that in mammalian intestinal epithelial cells, the spectraplakin ACF7 (also known as MACF1) specifically binds to CAMSAP3 and is required for the apical localization of CAMSAP3-decorated microtubule minus ends. Loss of ACF7 but not of CAMSAP3 or its homolog CAMSAP2 affected the formation of polarized epithelial cysts in three-dimensional cultures. In short-term epithelial polarization assays, knockout of CAMSAP3, but not of CAMSAP2, caused microtubule re-organization into a more radial centrosomal array, redistribution of Rab11-positive (also known as Rab11A) endosomes from the apical cell surface to the pericentrosomal region and inhibition of actin brush border formation at the apical side of the cell. We conclude that ACF7 is an important regulator of apico–basal polarity in mammalian intestinal cells and that a radial centrosome-centered microtubule organization can act as an inhibitor of epithelial polarity.

Introduction

Microtubules regulate cell polarity by serving as rails for intracellular transport and by controlling organelle positioning and signaling. Although in many types of cultured cells microtubules form a radial array, in polarized epithelial cells, microtubules are arranged along the apico–basal axis, with the minus ends located at the apical side (Akhmanova and Hoogenraad, 2015; Bartolini and Gundersen, 2006; Dammermann et al., 2003). This non-centrosomal microtubule organization can be controlled by the relocalization of γ-tubulin-binding centrosomal microtubule-anchoring proteins, such as ninein, to non-centrosomal apical sites (Moss et al., 2007) and by proteins that bind to microtubule minus ends independently of γ-tubulin. The most notable example of the latter are the members of calmodulin-regulated spectrin-associated protein (CAMSAP)/Patronin family, which can recognize and decorate free microtubule minus ends and protect non-centrosomal microtubules from depolymerization (Goodwin and Vale, 2010; Hendershott and Vale, 2014; Jiang et al., 2014; Tanaka et al., 2012). Recent work in worms has demonstrated that a ninein homolog and Patronin can act both redundantly and non-redundantly in organizing non-centrosomal arrays in different cell types (Wang et al., 2015).

In mammalian cells, the minus-end-binding protein CAMSAP3 (also known as Nezha or Marshalin) was initially shown to interact with components of adherens junctions and to anchor microtubule minus ends at these sites (Meng et al., 2008). CAMSAP3 is also very abundant in supporting cells of the organ of Corti, a specialized type of epithelial cell with extremely dense microtubule bundles that are anchored at centrosomal and non-centrosomal microtubule-organizing centers at the cell cortex (Takahashi et al., 2016; Zheng et al., 2013). Similar to other CAMSAP/Patronin-family members, CAMSAP3 has a C-terminal conserved domain, the CKK, as well as several coiled-coil regions and an N-terminal calponin homology domain, the function of which is currently unknown (Akhmanova and Hoogenraad, 2015; Baines et al., 2009). Through the CKK domain and the adjacent positively charged microtubule-binding regions, CAMSAP3, as well as its homolog CAMSAP2 recognize and decorate polymerizing microtubule minus ends, forming stretches of stabilized microtubule lattice that can serve as ‘seeds’ for non-centrosomal microtubule outgrowth (Jiang et al., 2014). Recent work shows that CAMSAP3 is an important factor in organizing apico–basal microtubule arrays in enterocytes, where it strongly localizes to the apical cell cortex and tethers microtubule minus ends (Toya et al., 2016). Mice homozygous for the C-terminal truncation of CAMSAP3, in which the CKK domain is lost, are viable but show increased lethality at early postnatal stages (Toya et al., 2016). Intestinal epithelial cells of those mice could still polarize and form a normal brush border, in spite of the fact that the microtubules were disorganized, and the nuclei and Golgi membranes mispositioned

(Toya et al., 2016). Experiments in Caco-2 cells, a human intestinal cancer cell line, have demonstrated that the first coiled-coil region of CAMSAP3 is involved in recruitment of CAMSAP3-bound microtubule minus ends to the apical side (Toya et al., 2016). In CAMSAP1, this coiled-coil region was shown to bind to spectrin (King et al., 2014). Whether the apical localization of CAMSAP3, indeed, depends on spectrin or some other proteins has not been determined.

Here, we set out to investigate the mechanism of CAMSAP3 recruitment to the apical side of epithelial cells. We found that CAMSAP3, but not CAMSAP2, interacts with the spectraplakin ACF7, also known as MACF1 (Karakesisoglou et al., 2000; Kodama et al., 2003; Wu et al., 2008), and that ACF7 depletion leads to the release of CAMSAP3-decorated microtubule stretches from the apical cell surface. ACF7, CAMSAP2 and CAMSAP3 were not essential for the distribution of early cell polarity markers in two-dimensional (2D) cultures; however, loss of ACF7 but not of the two CAMSAP proteins affected the formation of epithelial cysts in 3D cultures, indicating that ACF7 plays a more profound role in epithelial polarity than the CAMSAP proteins. Loss of CAMSAP3 led to more centrosome-centered microtubule organization, and this affected the organization of the actin cytoskeleton at the apical side of the cell, probably owing to mislocalization of recycling endosomes that are positive for Rab11A, which are an important component in apical polarity and brush border formation in intestinal cells (Bryant et al., 2010; Dhekne et al., 2014; Knowles et al., 2015; Overeem et al., 2015; Sobajima et al., 2014). Taken together, our study identifies ACF7 as an important regulator of apico–basal polarity in mammalian intestinal cells and demonstrates the importance of non-centrosomal microtubule organization for efficient epithelial cell polarization.

Results

Visualization of localization and dynamics of CAMSAP3 in polarized epithelial cells using GFP-knock-in cells

To facilitate visualization of CAMSAP3 in Caco-2 cells, we have generated a homozygous knock-in line in which the endogenous CAMSAP3 protein was tagged with GFP (Figure 1A). In agreement with previous publications (Meng et al., 2008; Tanaka et al., 2012; Toya et al., 2016), in this cell line, CAMSAP3–GFP localized to microtubule ends, colocalized with endogenous CAMSAP2 and was concentrated at the apical side of polarized Caco-2 monolayers (Figures 1B–1D). Upon microtubule depolymerization through nocodazole treatment, no apical CAMSAP3 stretches were detected, indicating that the apical recruitment of CAMSAP3 strongly depends on the presence of microtubules (Figure 1E). We next used fluorescence recovery after photobleaching (FRAP) assays to investigate the turnover of CAMSAP3–GFP at the apical side of polarized Caco-2 monolayers. We found that in 1-day-old Caco-2 monolayers, a ~75% recovery of CAMSAP3–GFP signals at the apical surface occurred within ~15 min (Figures 1F and 1G). This recovery was associated with movements of unbleached CAMSAP3–GFP-labeled microtubule minus ends into the photobleached area (Figures 1F and 1H). Interestingly, ~15 min after photobleaching in 5-day-old monolayers, the CAMSAP3–GFP signal at the apical surface recovered only to ~40% (Figures 1F and 1G). The mobility of CAMSAP3–GFP stretches in older cultures was much lower (Figure 1H), indicating that the apical cytoskeleton undergoes maturation on a scale of several days, resulting in immobilization of CAMSAP3 stretches.

When Caco-2 cells were cultured in Matrigel, they formed cysts, as described previously (Jaffe et al., 2008). Already at the two-cell stage, GFP–CAMSAP3 colocalized with apical markers, such as atypical protein kinase C (aPKC), and the area of enhanced actin accumulation, which was located at the membrane interface between the two daughter cells, as shown previously (Jaffe et al., 2008) (Figure 1I). After 4 days in 3D culture, GFP–CAMSAP3 strongly accumulated at the apical side (Figure 1J). In such polarized cysts, microtubules were aligned along the apico–basal axis (Figure 1K).

We never observed any accumulation of GFP–CAMSAP3 at the cell–cell junctions in either 2D or 3D cultures, which is in line with the observations in mouse intestine but contradicts the data previously obtained by immunostaining of CAMSAP3 in Caco-2 cells (Meng et al., 2008; Toya et al., 2016). Our data are thus in full agreement with the role of CAMSAP3 in apical microtubule organization but provide no support for CAMSAP3 function at the adherens junctions.

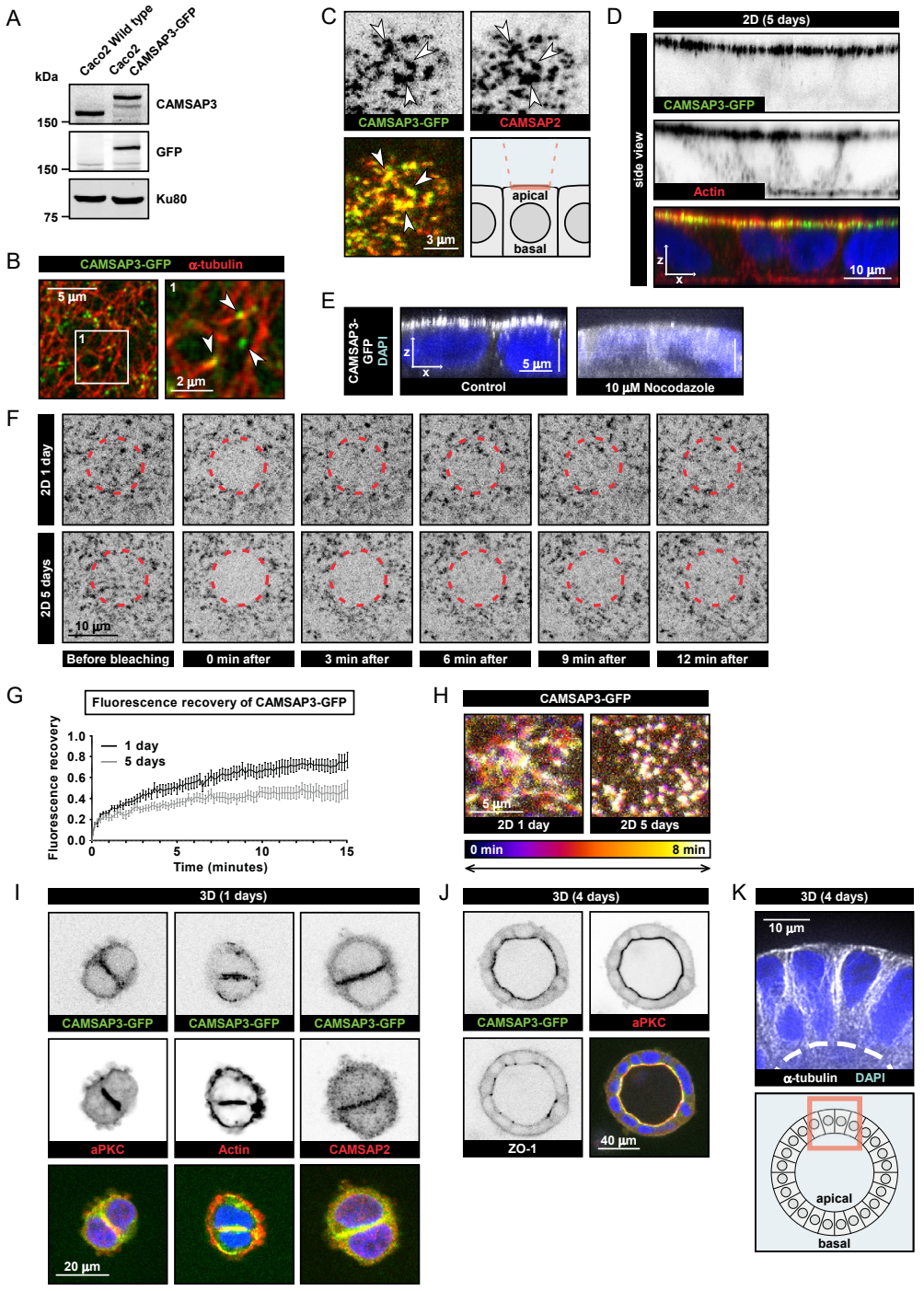

Figure 1. Visualization of localization and dynamics of CAMSAP3 in polarized epithelial cells using CAMSAP3–GFP knock-in cells

(A) Western blot analysis of extracts of wild-type and CAMSAP3–GFP knock-in Caco-2 cells. **(B)** Staining for α-tubulin (red) in CAMSAP3–GFP (green) knock-in Caco-2 cells. White arrowheads

indicate CAMSAP3 signal at microtubule ends. The area imaged is indicated in the schematic in C. **(C)** Staining of CAMSAP2 (red) in CAMSAP3–GFP (green) knock-in Caco-2 cells. White arrowheads indicate the same positions in different panels. Image area is indicated by red rectangle in the scheme. **(D)** Side view of CAMSAP3–GFP (green) knock-in Caco-2 monolayer stained for actin (red) and DNA (blue). **(E)** Side view of control and nocodazole-treated CAMSAP3–GFP (white) knock-in Caco-2 monolayers stained for DNA (blue). **(F)** FRAP analysis of CAMSAP3–GFP at the apical side of a Caco-2 monolayer either 1 or 5 days after reaching a confluent state. Red circle indicates photobleached region. The area imaged is indicated in the schematic in C. **(G)** Average normalized fluorescence intensity graphs after photobleaching as described in E. Error bars, s.e.m. **(H)** Motility representation of CAMSAP3–GFP stretches. Images are presented as maximum projections of 8-min movies with an interval of 10 s (48 frames). Image colors indicate time points (see gradient). The area imaged is indicated in the schematic in C. **(I)** Staining for actin, aPKC, CAMSAP2 (red) and DNA (blue) in 1-day-old 3D cultures of CAMSAP3–GFP (green) knock-in Caco-2 cells. **(J)** Staining of aPKC (red), ZO-1 (white) and DNA (blue) in 4-day- old 3D cultures of CAMSAP3–GFP (green) knock-in Caco-2 cells. **(K)** Staining for α-tubulin (white) and DNA (blue) in 4-day-old 3D cultures of Caco-2 cells. Apical cell surface is indicated by a white stippled line. Image area is indicated by a red square in the scheme.

ACF7 binds to CAMSAP3 and participates in its apical recruitment

We reasoned that the capture and stable association of CAMSAP3 stretches at the apical surface is caused by the presence of a binding partner. To identify CAMSAP3-interacting proteins, we performed streptavidin pull-down assays from HEK293T cells that co-expressed biotinylation (Bio) and GFP-tagged CAMSAP3 and the biotinylated ligase BirA, and analyzed the isolated proteins by performing mass spectrometry (Jiang et al., 2014). The highest scoring hit in this screen was the spectraplakin ACF7 (Figure 2A), whereas no peptides that were derived from spectrin, which has been previously reported to bind to CAMSAP1 (King et al., 2014), were found. Whether this was owing to the absence of appropriate spectrin isoforms in HEK293T cells, the biochemical procedure used or the lack of interaction between CAMSAP3 and spectrin is unclear.

Immunostaining showed colocalization of GFP–CAMSAP3 with the puncta of endogenous ACF7 at the apical side of Caco-2 monolayers (Figure 2B). However, in contrast to CAMSAP3, which was only located apically, ACF7 was spread throughout the cytoplasm (Figure 2D). As an alternative model of enterocyte polarity, we used the LS174T-W4 cell line, in which the activation of LKB1 kinase through doxycycline-induced expression of the adapter protein STRAD (also known as STRADA) is sufficient to induce polarization and formation of microvilli on one side of the cell in the absence of cell–cell contacts (Baas et al., 2004). In doxycycline-treated LS174T-W4 cells, both endogenous and GFP-tagged CAMSAP3 colocalized with endogenous ACF7 beneath the polarized regions of actin enrichment (Figure 2C), supporting complex formation between CAMSAP3 and ACF7.

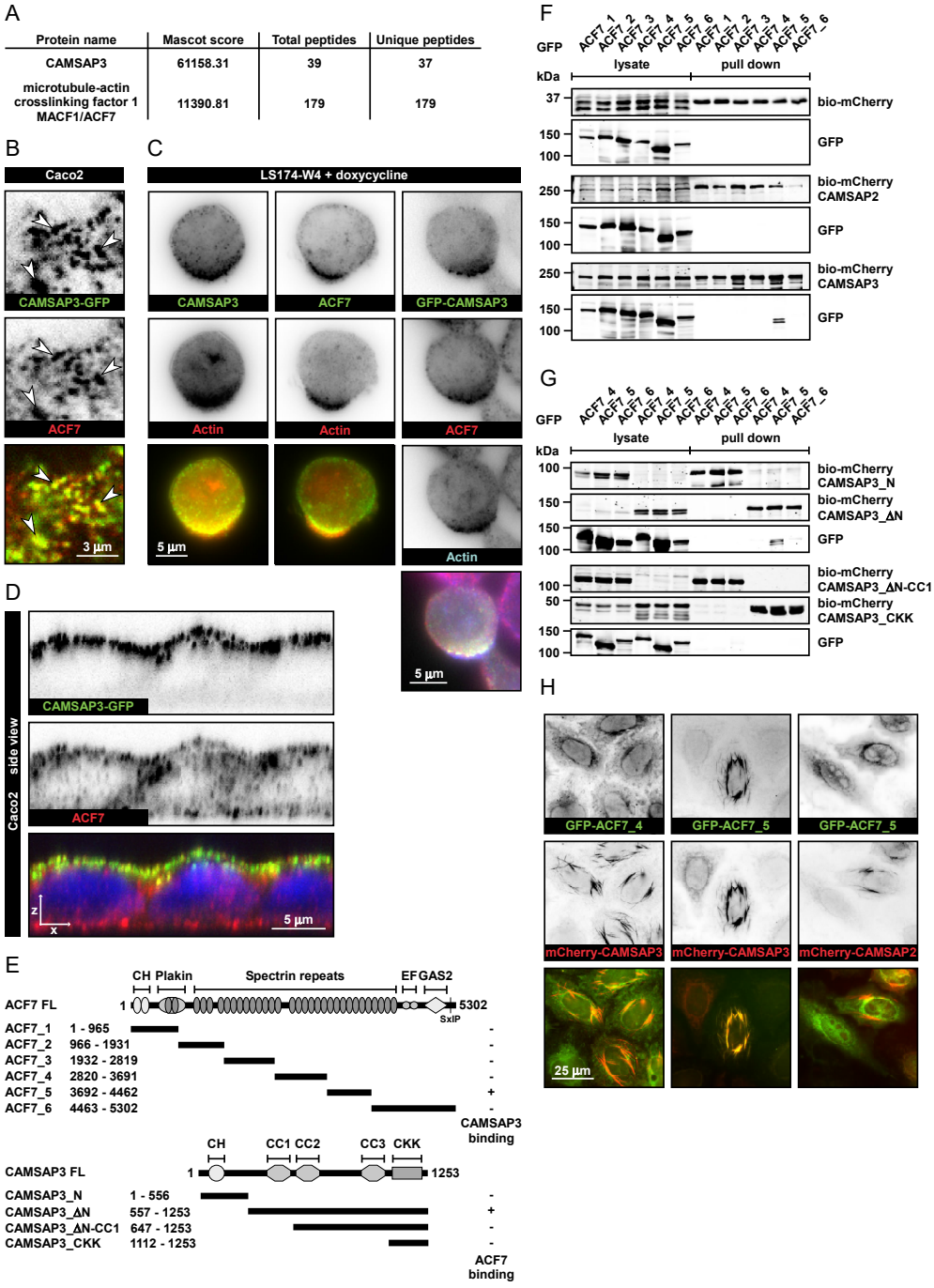

Figure 2. CAMSAP3 interacts with ACF7

(A) Identification of ACF7 as a binding partner of CAMSAP3 by mass-spectrometry-based analysis of a streptavidin pull-down assay with the extracts of HEK293T cells expressing biotinylation-tagged CAMSAP3 and BirA. **(B)** Staining of ACF7 (red) in CAMSAP3–GFP (green) knock-in Caco-2 cells. White arrowheads indicate the same positions in different panels. The area imaged

is indicated in Fig. 1C. **(C)** Staining of different markers in polarized LS174-W4 cells after doxycycline treatment. Left column, staining of CAMSAP3 (green) and actin (red); middle column, staining of ACF7 (green) and actin (red); right column, staining of ACF7 (red) and actin (blue) in a GFP–CAMSAP3-expressing cell. **(D)** Side view of CAMSAP3–GFP (green) knock-in Caco-2 monolayer stained for ACF7 (red) and DNA (blue). **(E)** Domain organization of ACF7 and CAMSAP3, and the deletion mutants used to study protein binding sites and a summary of experimental results indicating protein interactions. FL, full length; CH, calponin homology domain; EF, EF-hand; GAS2, growth-arrest-specific protein 2 domain; CC, coiled-coil domain. **(F)** Streptavidin pull-down assays from HEK293T cells expressing different GFP-tagged ACF7 fragments, BirA and Bio–mCherry, Bio–mCherry–CAMSAP2 or Bio–mCherry–CAMSAP3. **(G)** Streptavidin pull-down assays from HEK293T cells expressing different GFP-tagged ACF7 fragments, BirA and different Bio–mCherry-tagged CAMSAP3 fragments. **(H)** Transiently transfected HeLa cells co-expressing GFP–ACF7 fragments (green) and mCherry–CAMSAP2 or mCherry–CAMSAP3 (red).

We next investigated the interaction between CAMSAP3 and ACF7 biochemically. ACF7 is a very large protein (~5000 amino acids) containing an N-terminal actin-binding calponin homology domain, a plakin domain, 30 spectrin repeats, EF-hand motifs that could mediate Ca^{2+} binding, a microtubule-binding GAS2-related domain and the EB1-binding SxIP motif (Karakesisoglou et al., 2000; Kodama et al., 2003; Wu et al., 2008) (Figure 2E). Because the full-length ACF7 is difficult to efficiently express in cells, we generated GFP-tagged ACF7 fragments covering the whole ACF7 protein. We performed streptavidin pull-down assays from HEK293T cells co-expressing these fragments together with biotin ligase BirA and CAMSAP2 or CAMSAP3 tagged with an mCherry and biotinylation tag (Bio–mCherry), or just the Bio–mCherry protein as a negative control. We found that CAMSAP3, but not CAMSAP2, specifically bound to the ACF7 fragment encompassing spectrin repeats 20–26 (fragment ACF7_5, Figure 2F). Deletion mapping further showed that the coiled-coil region 1 (CC1) of CAMSAP3, which has been previously implicated in the apical localization of the protein (Toya et al., 2016), was essential for this interaction (Figure 2G).

The binding between CAMSAP3 and ACF7 was confirmed by performing colocalization experiments in HeLa cells. Overexpression of CAMSAP3 and CAMSAP2 caused strong bundling of microtubules, and CAMSAP3, but not CAMSAP2, could specifically recruit fragment ACF7_5 to these microtubule bundles (Figure 2H). Furthermore, we found that endogenous ACF7 was recruited to microtubule bundles that had been induced through overexpression of full-length CAMSAP3 and of the CAMSAP3 deletion mutant that lacked the calponin homology domain, but not of the CAMSAP3 deletion mutants that lacked the CC1 region (Figure S1). Taken together, these data indicate that CAMSAP3 and ACF7 interact with each other and can cooperate in binding to microtubules. Deletion mapping showed that the CC1 region of CAMSAP3 and a specific spectrin-repeat region of ACF7 are required for the interaction.

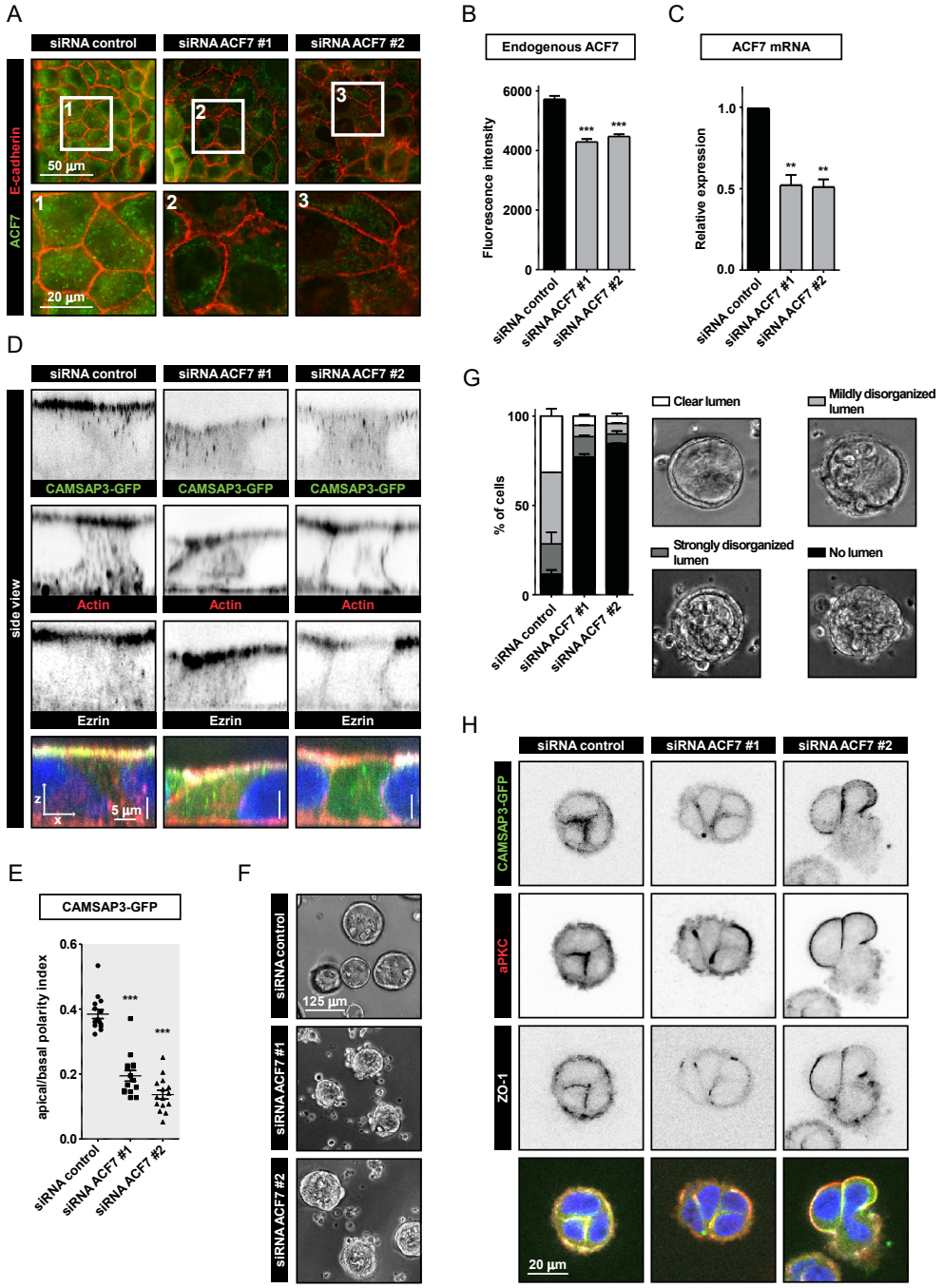

Figure 3. Knockdown of ACF7 perturbs epithelial polarity and CAMSAP3 distribution
(A) Staining of ACF7 (green) and E-cadherin (red) in Caco-2 cells transfected with control siRNA or siRNA against ACF7. **(B)** Quantification of fluorescence intensity of endogenous ACF7 staining in cells treated as described in A. siRNA control, n=78; siRNA ACF7 #1, n=73; siRNA ACF7 #2, n=63; ***P<0.001; Mann–Whitney U-test; error bars, s.e.m. **(C)** qPCR analysis of ACF7 mRNA expres-

sion in cells treated as described in A. ACF7 expression was calculated relative to that under the control condition using two different primer pairs and after normalization to two housekeeping genes. siRNA control, n=12; siRNA ACF7 #1, n=12; siRNA ACF7 #2, n=12; **P<0.01; paired t-test; error bars, s.e.m. **(D)** Side view of CAMSAP3–GFP (green) knock-in Caco-2 monolayer stained for actin (red), ezrin (white) and DNA (blue) and transfected with siRNAs as described in A. **(E)** Quantification of CAMSAP3–GFP localization presented as the apical–basal polarity index [(apical fluorescence intensity/basal fluorescence intensity)−1]. Cells were transfected with siRNAs as described in A. siRNA control, n=15; siRNA ACF7 #1, n=15; siRNA ACF7 #2, n=15; ***P<0.001; Mann–Whitney U-test. Single data points are plotted. Horizontal line, mean; error bars, s.e.m. **(F)** 3D cyst formation 1 day after dense seeding of Caco-2 cells treated as described in A. **(G)** Quantification of 3D cyst formation of cells shown in F. siRNA control, n=200; siRNA ACF7 #1, n=236; siRNA ACF7 #2, n=139; error bars, s.e.m. **(H)** Staining of aPKC (red), ZO-1 (white) and DNA (blue) in CAMSAP3–GFP (green) knock-in Caco-2 cells seeded in a 3D matrix and transfected with siRNA as described in A.

We next investigated whether ACF7 participates in the apical recruitment of CAMSAP3. ACF7 was depleted with two different small interfering (si)RNAs, and the efficiency of depletion was confirmed by immunofluorescence staining and real-time PCR (Figures 3A–3C). Although actin enrichment was still observed at the apical side of ACF7-depleted Caco-2 monolayers, both the apical localization and the total number of CAMSAP3–GFP stretches were very strongly reduced, indicating that ACF7 regulates the localization as well as the formation or stability of CAMSAP3-decorated microtubule stretches (Figures 3D and 3E). In contrast, other early polarity markers, such as ezrin, aPKC and zonula occludens 1 (ZO-1; also known as TJP1) were still apically located in 2D cultures of ACF7-depleted cells (Figure 3D; Figure S2A). Also, the height of polarized monolayers was not significantly affected in the absence of ACF7 (Figure S2B). Further, in line with the fact that ACF7 depletion reduced the abundance of CAMSAP3-decorated microtubule stretches, we found an increase, albeit a mild one, in the number of centrosomal microtubules, indicating that ACF7 contributes to some extent to the maintenance of a non-centrosomal microtubule network (Figures S2C and S2D).

To further address the effect of ACF7 knockdown, we analyzed cyst formation in 3D cultures. To accelerate lumen formation in Caco-2 cysts in order to make 3D analysis compatible with a transient protein depletion protocol, we used dense Caco-2 3D cultures and, after the initial cyst formation, treated them with cholera toxin, which strongly stimulates lumen formation by inducing cAMP signaling (Jaffe et al., 2008). Under these conditions, we found a clear well-formed or mildly disorganized lumen in ~75% of cysts that had been treated with control siRNAs, whereas after ACF7 depletion, only 10% of the cysts developed normally, and cysts completely lacking the lumen were prevalent (Figures 3F and 3G). Analysis of early (3–4 cell) 3D cultures showed that

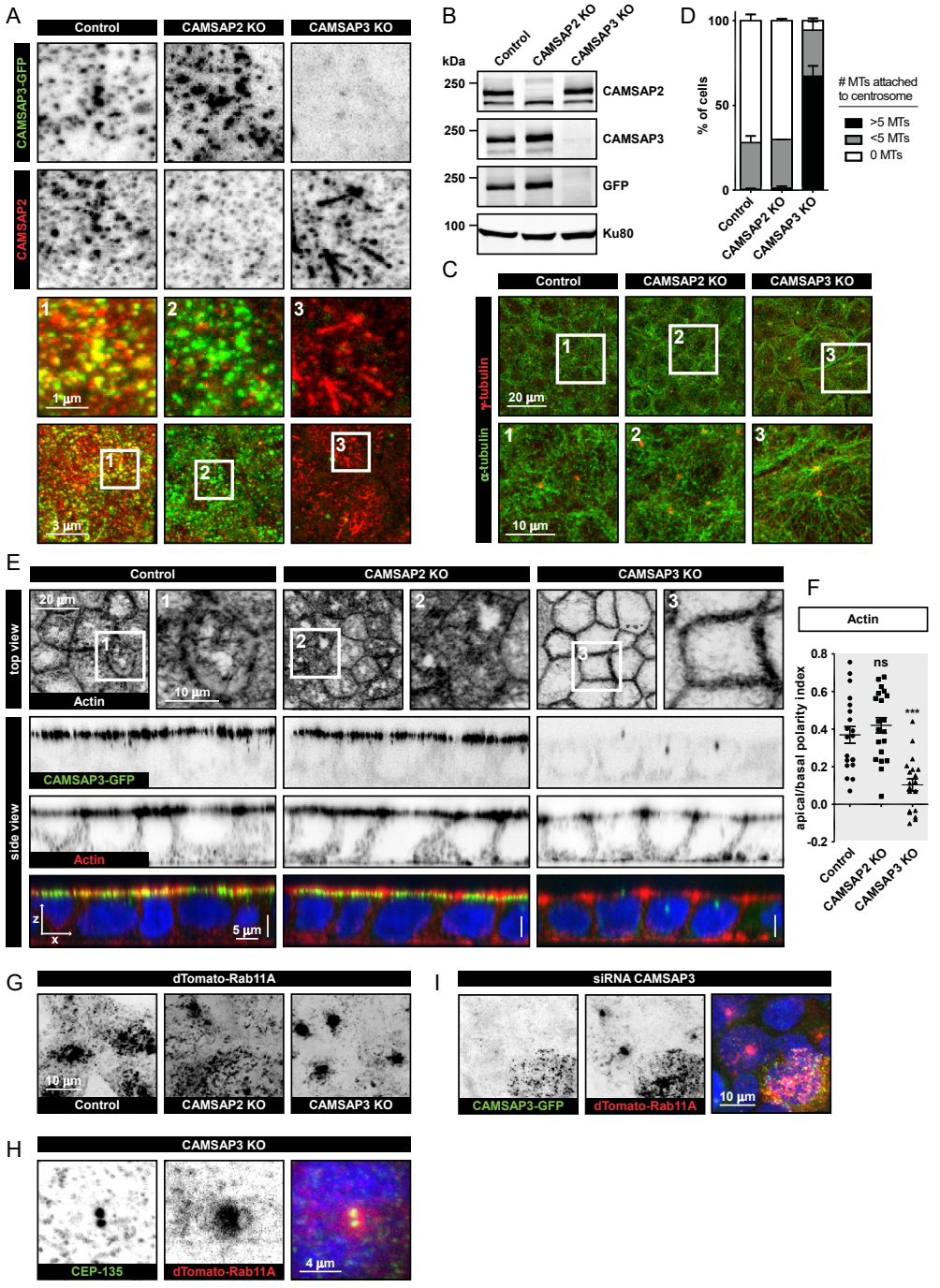

Figure 4. Knockout of CAMSAP3 perturbs the distribution of Rab11A-positive endosomes and apical actin organization

(A) CAMSAP3–GFP (green, knock-in) and CAMSAP2 (red, staining) in control, and CAMSAP2- and CAMSAP3-knockout (KO) cells. **(B)** Western blot analysis of control, and of CAMSAP2- and CAMSAP3-knockout cell extracts. **(C)** Staining of microtubules (green, α-tubulin) and centro-

somes (red, γ-tubulin) in the control and knockout cells described in A. **(D)** Quantification of microtubule organization, presented as the number of microtubules attached to the centrosome. Quantification is based on the staining shown in C. Numbers of analyzed cells: control, n=196; CAMSAP2 KO, n=195; CAMSAP3 KO, n=122; error bars, s.e.m.; #, number; MTs, microtubules. **(E)** Top view: staining of actin in the control or knockout cells shown in A. Side view: side view of a monolayer of control or knockout cells described in A showing CAMSAP3–GFP knock-in, (green), actin (red, staining) and DNA (blue, staining). **(F)** Quantification of actin localization presented as the apical–basal polarity index [(apical fluorescent intensity/basal fluorescent intensity)−1] in the control or knockout cells described in A. Control, n=20; CAMSAP2 KO, n=20; CAMSAP3 KO, n=20; ***P<0.001; ns, no significant difference with control; Mann–Whitney U-test. Single data points are plotted. Horizontal line, mean; error bars, s.e.m. **(G)** Distribution of endosomes visualized with stably expressed dTomato–Rab11A in the control and knockout cells described in A. **(H)** Staining of centrosomes (CEP135, green) in dTomato–Rab11A-expressing CAMSAP3-knockout cells. **(I)** CAMSAP3–GFP (green, knock-in) and dTomato–Rab11A (red, stably expressed) in Caco-2 cells transfected with siRNA against CAMSAP3.

although the apical polarity markers localized to intercellular junctions in control cells, as described previously (Jaffe et al., 2008), they were mislocalized in ACF7-knockdown cells (Figure 3H).

We conclude that although ACF7 depletion does not cause mislocalization of all polarity markers in 2D cultures, it does lead to the loss of apical localization of CAMSAP3. When embedded in a 3D matrix, the distribution of all investigated polarity markers and cyst formation were strongly affected by ACF7 depletion, indicating that distinct mechanisms with differential sensitivities to ACF7 levels control the ability of cells to polarize in 2D and 3D cultures.

CAMSAP3 knockout leads to Rab11A mislocalization and inhibition of apical actin brush border formation

We next set out to address the effects of the loss of CAMSAP2 and CAMSAP3 on epithelial polarity. Using CRISPR-Cas9 technology, we knocked out CAMSAP2 or CAMSAP3 genes in the CAMSAP3-GFP knock-in cell line (Figures 4A and 4B). Apical CAMSAP3–GFP signals were unperturbed in CAMSAP2-knockout cells, whereas in CAMSAP3-knockout cells, CAMSAP2 stretches became longer, as described previously (Tanaka et al., 2012) (Figure 4A). CAMSAP-decorated microtubule stretches are generated through microtubule polymerization from the minus end, and the stretches formed in the presence of CAMSAP3 and CAMSAP2 are likely to be shorter than those formed in the presence of CAMSAP2 alone, because CAMSAP3 is a more efficient inhibitor of microtubule minus-end growth than CAMSAP2 (Jiang et al., 2014). Microtubule organization was not visibly changed in CAMSAP2-knockout cells, but a more centrosome-centered array was observed in CAMSAP3-knockout cells, in line with the findings of a previous study (Tanaka et al., 2012) (Figures 4C and 4D).

Next, we analyzed polarity in CAMSAP2- and CAMSAP3-knockout clones. In 2D cultures, junctional ZO-1 and E-cadherin, as well as the early markers of apical polarity aPKC and ezrin, were unperturbed (Figures S3A and S3B). When cultured in 3D, two out of three CAMSAP2-knockout clones and three out of three CAMSAP3-knockout clones formed morphologically normal cysts (Figures S3C and S3D). Because two CAMSAP2-knockout lines could form morphologically normal cysts, we think that the morphological abnormalities in the third clone were due to secondary mutations. This conclusion was confirmed by siRNA-mediated depletion of CAMSAP2, CAMSAP3 or both CAMSAPs simultaneously (Figure S3E). In addition, CAMSAP2- and CAMSAP3-knockout clones showed no defects in the recruitment of the apical markers aPKC and ZO-1 in early 3D cysts (Figure S3F). We conclude that CAMSAP2 and CAMSAP3 are not required for the formation of lumen-containing 3D cysts, indicating that the strongly affected cyst formation in ACF7-depleted cells is unlikely to be due to CAMSAP3 mislocalization.

We then focused on late markers of epithelial polarity that are associated with the ability of the cells to form a brush border. Apical accumulation of actin and the phosphorylated form of ezrin, an actin-binding protein important for the formation of brush border (Dhekne et al., 2014; Overeem et al., 2015; Viswanatha et al., 2012) was unaffected in CAMSAP2-knockout cells (Figures 4E and 4F; Figure S3A), even though the same cell line showed abnormalities in cyst morphology in 3D culture (Figures S3C and S3D; CAMSAP2 KO #1). This result indicates that the ability of cells to form 3D cysts and to localize actin regulators does not necessarily correlate.

Strikingly, in CAMSAP3-knockout cells, the apical accumulation of actin and phosphorylated ezrin was concentrated around the cell–cell junctions and reduced in the central part of the cell (Figures 4E and 4F; Figure S3A). Previous work has shown that during brush border formation, the apical actin cytoskeleton is strongly regulated by signaling and/or trafficking processes that are dependent on the apical accumulation of Rab11A-positive recycling endosomes (Dhekne et al., 2014; Knowles et al., 2015; Overeem et al., 2015; Sobajima et al., 2014). We analyzed the distribution of Rab11A endosomes by using cells that had been stably transfected with a construct for doxycycline-inducible expression of dTomato–Rab11A. Strikingly, in control and CAMSAP2-knockout cells, Rab11A endosomes were distributed under the apical surface, whereas in CAMSAP3-knockout cells they displayed a single focus of accumulation, which coincided with the centrosome (Figures 4G and 4H; Figure S3G). In fact, the fluorescence intensity of the Rab11A clusters in CAMSAP3-knockout cells appeared to be ~5-fold higher than the fluorescence intensity of apically located Rab11A vesicles in control cells, revealing a very strong clustering of endosomes (Figure S3G). This result was confirmed in cells in which CAMSAP3 had been depleted using siRNA: in these cells, the formation of a single centrally located Rab11A cluster strongly correlated

with the efficiency of CAMSAP3 knockdown (Figure 4I). We also analyzed Rab11A in ACF7-knockdown cells and found that the endosomes were equally distributed over the cell, indicating defects in the apical targeting (Figure S3G). However, actin still accumulated at the apical surface of ACF7-depleted cells (Figure 3D), suggesting that clustering of Rab11A endosomes in the middle part of the cell is more deleterious for actin organization than their random distribution.

Our data support the notion that the localization of Rab11A endosomes strongly correlates with the position of microtubule minus ends, in line with the idea that it is controlled by cytoplasmic dynein (Horgan et al., 2010; Khanal et al., 2016; Riggs et al., 2007). When the microtubule array becomes more radial, Rab11A endosomes accumulate in the central part of the cell, and the formation of apical actin-rich structures is inhibited.

Discussion

In this study, we showed that the spectraplakin ACF7 is a binding partner of CAMSAP3 and that it is required for regulating the abundance and apical localization of CAMSAP3-decorated microtubule stretches. While this paper was in preparation, the Drosophila homologues of CAMSAP3 and ACF7, Patronin and Shortstop (Shot), respectively, were demonstrated to be present in the same apical complex and cooperate with each other, as well as an apical form of spectrin, in organizing apico–basal microtubule arrays in fly epithelia (Khanal et al., 2016) and in early fly embryos (Nashchekin et al., 2016). These findings are also consistent with earlier work in flies, which has demonstrated the importance of Shot for microtubule minus-end organization during tubulogenesis of the embryonic salivary glands (Booth et al., 2014). ACF7 appears to act upstream of CAMSAP3 as a cortical recruitment factor but, given that it has a microtubule-interacting domain, it is also likely to synergize with CAMSAP3 to some extent for microtubule binding and stabilization. We note that the accumulation of CAMSAP3 at the apical cortex occurred in the form of microtubule stretches and thus depended on the presence of intact microtubules. This is similar to the recruitment of CAMSAP2 to the Golgi membranes, where binding of CAMSAP2-decorated microtubule minus ends but not of the cytosolic CAMSAP2 was observed (Wu et al., 2016). It is possible that the presence of multiple CAMSAP molecules on the same microtubule is required for efficient binding to intracellular structures such as the Golgi and the actin-rich cortex by increasing avidity.

Because ACF7 does not show an exclusively apical localization in Caco-2 cells, an additional pathway ensuring tethering of CAMSAP3-decorated stretches specifically to the apical surface must exist. It is possible that, similar to flies, a specific apical isoform of spectrin might be involved; this would mean that the same region of CAMSAP3, the CC1, mediates apical localization by binding to two different proteins. Alternatively, some signaling pathway restricting CAMSAP3 binding to microtubules at the apical cell side might be involved. Interesting in this respect is our observation that CAMSAP3-decorated microtubule stretches become less mobile during monolayer maturation, suggesting that as epithelial cells differentiate, more numerous connections between these stretches and the cortical cytoskeleton are formed, or the cortical cytoskeleton itself becomes less dynamic. It is also important to note that analysis of 3D cysts showed that ACF7 depletion has a stronger impact on cell polarity than loss of CAMSAP proteins, indicating that ACF7 performs additional CAMSAP-independent functions during epithelial polarization.

Furthermore, our data showed that the knockout of CAMSAP3 affected apical actin organization, probably because the more centrosomal microtubule system in

CAMSAP3-knockout cells prevents apical accumulation of Rab11A endosomes. How can these results be reconciled with the presence of a normal brush border in mice expressing nonfunctional CAMSAP3 (Toya et al., 2016)? The most likely explanation is the gradual centrosome inactivation observed during long-term differentiation of epithelial cells. In line with this idea, in CAMSAP3-knockout mice, microtubules in epithelial cells become disorganized but do not form a radial pattern (Toya et al., 2016). A disorganized non-centrosomal array is likely to delay but not to block apical localization of Rab11A endosomes or other yet unknown polarity factors that are transported towards microtubule minus ends. In contrast, the presence of a centrosome seems to act in a dominant-negative manner, by sequestering these factors in the central part of the cell. In line with this idea, actin accumulation at the apical side was inhibited more strongly in CAMSAP3-knockout cells, in which Rab11A endosomes were clustered, than in ACF7-knockdown cells, in which the endosomes were distributed throughout the cell. These data suggest that although the centrosome can promote cell polarization under certain conditions (Bornens, 2012), in epithelial cells it acts as a polarity inhibitor and its microtubule-anchoring activity must be suppressed to allow the cells to efficiently complete their polarization program.

Experimental procedures

Cell culture and transfection

Caco-2 cells were obtained from Alpha Yap (University of Queensland, Australia) (Ratheesh et al., 2012) and cultured in Dulbecco's modified Eagle's medium supplemented with 10% fetal calf serum (FCS). LS174-W4 cells (Baas et al., 2004) were obtained from Johannes L. Bos (UMC Utrecht, The Netherlands) and cultured in RPMI supplemented with 10% FCS. HEK293T cells were obtained from American Type Culture Collection (ATCC) and cultured in DMEM supplemented with 10% FCS. The cell lines were routinely checked for mycoplasma contamination using LT07-518 Mycoalert assay (Lonza). The identity of the cell lines was monitored by immunofluorescence-staining-based analysis with multiple markers. To grow a polarized monolayer of epithelial cells, Caco-2 cells were cultured for 5 days after reaching a fully confluent monolayer. 3D cultures of Caco-2 cells were generated by seeding cells on top (lumen formation assay) or within (3D immunofluorescence staining) 9.7 mg/ml Matrigel (Corning). One day after seeding, cells were treated with 100 ng/ml cholera toxin (Sigma-Aldrich).

FuGENE 6 (Promega) was used to transfect different plasmids into Caco-2 and LS174T-W4 cells. Polyethylenimine (PEI, Polysciences) was used to transfect HEK293T cells for streptavidin pull-down assays. HiPerFect (Qiagen) was used to transfect Caco-2 cells with siRNAs at 20 nM. Corresponding experiments were performed 72 h after siRNA transfection.

Streptavidin pull-down assays, western blotting and mass spectrometry

Streptavidin pull down and western blotting were performed as described previously (Jiang et al., 2014). Samples were prepared from pull-down assays of biotinylated proteins from extracts of transfected HEK293T cells using streptavidin beads, as described previously (Jiang et al., 2014), and were resuspended in 10% formic acid with 5% DMSO and were analyzed with an Agilent 1290 Infinity (Agilent Technologies) liquid chromatography instrument, operating in reverse-phase (C18) mode, coupled to a TripleTOF 5600 (AB Sciex) spectrometer. Mass spectrometry spectra (350–1250 m/z) were acquired in high-resolution mode (R>30,000), whereas tandem mass spectrometry (MS2) spectra were acquired in high-sensitivity mode (R>15,000). Raw files were processed using Proteome Discoverer 1.4 (version 1.4.0.288, Thermo Scientific, Bremen, Germany). The database search was performed using Mascot (version 2.4.1, Matrix Science, UK) against a SwissProt database (taxonomy human). Carbamidomethylation of cysteines was set as a fixed modification and oxidation of methionine was set as a variable modification. Trypsin was specified as the enzyme and up to two missed cleavages were allowed. Data filtering was performed using percolator, resulting in 1% false

discovery rate (FDR). Additional filters were: search engine rank 1, peptide confidence high and ion score >20.

Generation of Caco-2 knock-in and knockout lines

Caco-2 CAMSAP3–GFP knock-in in CAMSAP-knockout cells were generated by using CRISPR–Cas9 technology (Ran et al., 2013). The Caco-2 CAMSAP3–GFP knock-in line was generated by transfecting the cells with the pSpCas9(BB)-2A-Puro (PX459) vector (Addgene, #62988) bearing the appropriate targeting sequence (5′-ACCGCCCG-GGTGGGGCTATT-3′) and the donor plasmid. Caco-2 CAMSAP-knockout cell lines were generated by transfecting the cells with PX459 vector bearing appropriate targeting sequences (CAMSAP2: 5′-CATGATCGATACCCTCATGA-3′; CAMSAP3: 5′-GTACGATTTCTCGCGGGCCA-3′).

To establish clonal stable knock-in and knockout lines, cells were subjected to selection with 20 μg/ml puromycin for 3 days. After selection, cells were allowed to recover in normal medium for 5 days, and the efficiency of knock-in or knockout was checked by immunofluorescence staining. Depending on the efficiency, 20–100 individual clones were isolated and characterized by immunofluorescence staining.

Protein domain prediction, constructs and siRNAs

Protein domains were predicted using the web-based simple modular architecture research tool (SMART) (Letunic et al., 2015; Schultz et al., 1998). Full-length ACF7 was purchased from Promega Kazusa Genome Technologies (pFN21AE0600). ACF7 constructs were amplified by performing PCR and cloned into pEGFP-C2 (Clontech). Bio–mCherry–CAMSAP2, bio–mCherry–CAMSAP3 and GFP–CAMSAP3 have been described previously (Jiang et al., 2014). Deletion mutants were cloned by using PCR-based strategies.

Gibson assembly was used to assemble a pUC19-based CAMSAP3–GFP knock-in donor plasmid. Primers used to amplify the 5′ homology arm were: 5′-CCTTGGCCCCTCTGCACATA-3′ and 5′-TTTGGGGGTGCCGCCGCC-3′. Primers used to amplify the 3′ homology arm were: 5′-CCCCACCCGGGCGGTCCA-3′ and 5′-TTAGTCCTAAGCCTGGGAAGC-3′.

pSIN-TRE-rtTA-IRES-Hygro-iLID-dTomato-Rab11A was constructed from pSIN-TRE-rtTA-IRES-Puro (kindly provided by Benjamin Bouchet, Utrecht University, The Netherlands) by replacing the puromycin-resistance cassette with the hygromycin-resistance cassette from pCDNA5-FRT-TO (Invitrogen) and encodes amino acids 2–216 human Rab11A (derived from GFP–Rab11A WT, a gift from Richard Pagano, Mayo Clinic College of Medicine, Rochester, MN; Addgene plasmid #12674), N-terminally fused to the light-sensitive dimerization module iLID (derived from pLL7.0:Venus-iLID-Mito, a gift from Brian Kuhlman, University of North Carolina, Chapel Hill,

NC; Addgene plasmid #60413) and dTomato.

siRNAs targeting the following sequences were purchased from Sigma-Aldrich: ACF7 #1, 5′-TTGCAGCAGGTGAATGGAC-3′; ACF7 #2, 5′-CCAAAGTGACTT-GAAGGAT-3′ (Drabek et al., 2006); CAMSAP2, 5′-GTACTGGATAAATAAGGTA-3′ (Jiang et al., 2014); CAMSAP3, 5′-GCATTCTGGAGGAAATTGA-3′; and control targeting luciferase, 5′-CGTACGCGGAATACTTCGA-3′ (Dambournet et al., 2011).

Antibodies, drugs and chemicals

Rat monoclonal antibody against tyrosinated α-tubulin (clone YL1/2) was purchased from Abcam (#ab6160). Mouse polyclonal antibody against ACF7 was purchased from Abnova (#H00023499-A01). Mouse monoclonal antibodies against the following proteins were used: CAMSAP3 (#SAB4200415) and γ-tubulin (#T5326) (Sigma-Aldrich); Ku80 (#611360), ZO-1 (#610966), E-cadherin (#610181), mCherry (#632543) (Clontech) and ezrin (#610602) (BD Biosciences). Rabbit polyclonal antibodies against the following proteins were used: GFP (#ab290, Abcam); CAMSAP2 (#NBP1-21402 Novus, #17880-1-AP Proteintech); aPKC (#H00023499-A01, Santa Cruz); Actin (#20-33) and CEP135 (#SAB4503685) (Sigma-Aldrich); phosphorylated ERM (#3141, Cell Signaling); E-cadherin (Alpha Yap, University of Queensland, Australia). Alexa-Fluor-405- (#A-31553 and #A-31556), Alexa-Fluor-488- (#A27023 and #A-11034), Alexa-Fluor-594- (#A-11032, #R37117 and #A-11007) and Alexa-Fluor-647- (#A-21235) conjugated goat antibodies against mouse, rabbit and rat were purchased from Life Technologies. For Western blotting, IRDye-800CW-conjugated goat antibody against mouse and rabbit IgG (#P/N 925-32210 and #P/N 925-32211) and IRDye-680LT-conjugated goat antibody against mouse and rabbit IgG (#P/N 925-68020 and #P/N 925-68021) were purchased from Li-Cor Biosciences. See Table S1 for the antibody dilutions used.

Alexa-Fluor-594-conjugated phalloidin was purchased from Life Technologies (#A12381). Doxycycline was purchased from Sigma-Aldrich and used at a concentration of 1 μg/ml. Nocodazole was purchased from Sigma-Aldrich and used at a concentration of 10 μM. Cell were treated with nocodazole for 2 h prior to fixation.

Lentiviral infection and cell line selection

Lentivirus packaging was performed by using MaxPEI-based co-transfection of HEK293T cells with psPAX2, pMD2.G and the lentiviral vector pSIN-TRE-rtTA-IRES-Hygro-iLID-dTomato-RAB11A. Supernatant of packaging cells was harvested up to 72 h of transfection, filtered through a 0.45-μm filter and incubated with a polyethylene glycol (PEG)-6000-based precipitation solution overnight at 4°C. After precipitation, virus was concentrated up to 100× by centrifugation and dissolution in 1× phosphate buffered saline (PBS). Target cells were incubated for 4 h in complete medium supplemented with 8 μg/ml polybrene before infection. To establish clonal Caco-2 stable lines carrying

doxycycline-inducible dTomato–Rab11A, medium was replaced 24–48 h after infection and 100 µg/ml hygromycin (Invitrogen) was added.

Immunofluorescence staining of fixed samples

For immunofluorescent staining of 2D cultures, cells were fixed with either 4% PFA for 20 min at room temperature (ezrin, CEP135, phosphorylated ERM, phalloidin) or −20°C MeOH for 10 min (α-tubulin, CAMSAP2, aPKC, ZO-1, ACF7, CAMSAP3, actin, E-cadherin, γ-tubulin) followed by permeabilization with 0.2% Triton X-100 for 2 min. Next, samples were blocked with 1% BSA diluted in 1× PBS supplemented with 0.05% Tween-20 for 45 min and sequentially incubated with primary antibodies for 1 h and fluorescently labeled secondary antibodies for 45 min. Finally, samples were washed, dried and mounted in DAPI-containing Vectashield (Vector laboratories).

For immunofluorescence staining of 3D cultures, cells were fixed with 4% PFA for 20 min at room temperature, rinsed with 1× PBS with glycine (10× stock: 38.00 g NaCl, 9.38 g Na_2HPO_4, 2.07 g NaH_2PO_4, 37.50 g glycine in 500 ml milliQ water, pH 7.4) followed by permeabilization with 0.5% Triton X-100 in 1× PBS with glycine for 20 min. Next, samples were blocked with 1% BSA diluted in 1× immunofluorescence wash buffer (10× stock: 38.00 g NaCl, 9.38 g Na_2HPO_4, 2.07 g NaH_2PO_4, 2.5 g NaN_2, 10 ml Triton X-100, 2.5 ml Tween-20 in 500 ml milliQ water, pH 7.4) for 45 min and sequentially incubated with primary antibodies for 2 h at 37°C and fluorescently labeled secondary antibodies for 1.5 h at room temperature. Finally, samples were washed and mounted in DAPI-containing Vectashield.

Microscopy and image analysis

2D confluent monolayers and 3D cultures were imaged by using confocal fluorescence illumination on a Nikon Eclipse Ti microscope equipped with a perfect focus system (PFS, Nikon), a spinning-disc-based confocal scanner unit (CSU-X1-A1, Yokogawa), an Evolve 512 EMCCD camera (Photometrics) attached to a 2.0× intermediate lens (Edmund Optics), a super-high-pressure mercury lamp (C-SHG1, Nikon), a Roper Scientific custom-made set of Stradus 405-nm (100 mW, Vortran), Calypso 491-nm (100 mW, Cobolt) and Jive 561-nm (100 mW, Cobolt) lasers, a set of ET-BFP2, ET-EGFP, ET-mCherry and ET-EGFP-mCherry filters (Chroma) for wide-field fluorescence observation, a set of ET460/50m, ET525/50m or ET535/30m (green), ET630/75m (red) and ET-EGFP/mCherry filters (Chroma) for spinning-disc-based confocal imaging and a motorized stage MS-2000-XYZ with Piezo Top Plate (ASI). The microscope setup was controlled by MetaMorph 7.7.11.0 software. Images were acquired using Plan Fluor 10× NA 0.3 air, Plan Fluor 20× MI NA 0.75 oil, Plan Apochromat λ 60× NA 1.4 oil and Plan Apo VC 60× NA 1.4 oil objectives. This system was also used for FRAP experiments using the iLas2 system (Roper Scientific).

z-series images of 2D confluent layers were acquired using a 0.1-µm-step confocal-based scan. Side views were reconstructed by projecting maximum fluorescence intensities of 50×0.11-µm side view slices. The apical–basal polarity index was determined by using side views as described above in the following equation:

$$\frac{Fa}{Fb} - 1$$

in which F_a is the fluorescent intensity in the upper one-third of the side view corrected for the area and F_b is the fluorescence intensity in the lower two-thirds of the side view corrected for the area. For presentation, images were adjusted for brightness using ImageJ 1.50b. FRAP measurements were performed by bleaching a 8.8-µm-diameter circle in the apical side of a cell monolayer followed by 15 min of imaging with a frame interval of 10 s.

Phase contrast images were acquired on a Nikon Ti instrument equipped with a perfect focus system (PFS, Nikon), a super-high-pressure mercury lamp (C-SHG1, Nikon), Lambda SC Smart Shutter controllers (Sutter), a Plan Apochromat DM 20× NA 0.75 (Ph2) or a Plan Fluor DLL 10× NA 0.3 (Ph1), an ET-mCherry filter (Chroma), a CoolSNAP HQ^2 CCD camera (Photometrics), a motorized stage MS-2000-XYZ with Piezo Top Plate (ASI) and a stage top incubator INUG2E-ZILCSD-DV (Tokai Hit) for 37°C under 5% CO^2. The microscope setup was controlled by the open source microscopy software Micro-manager.

To determine protein knockdown efficiency by immunofluorescence staining, cells were imaged on a Nikon Eclipse 80i upright microscope equipped with a CoolSNAP HQ^2 CCD camera (Photometrics), an Intensilight C-HGFI precentered fiber illuminator (Nikon), ET-DAPI, ET-EGFP and ET-mCherry filters (Chroma), controlled by Nikon NIS Br software and using a Plan Apo VC 100× NA 1.4 oil, Plan Apo VC 60× NA 1.4 oil or a Plan Fluor 20× MI NA 0.75 oil objective (Nikon). For knockdown efficiency tests, fluorescence intensity was measured per cell and corrected for the cell surface area using ImageJ 1.50b.

Microtubule organization in CAMSAP-knockout lines was imaged by confocal fluorescence illumination on a Leica TCS SP8 STED3X SMD FLIM Super Resolution instrument and confocal microscope equipped with adaptive focus control, a filter-free Spectral Leica SP detector and HyD detector, a 405-nm DMOD and a fully tunable supercontinuum white laser (470 to 670 nm). Images were acquired using a HC PL APO Cs2 100×1.40 oil objective. z-series were acquired using 0.16-µm- (Control) and 0.22-µm- (CAMSAP2 and CAMSAP3 knockout) step confocal-based scan. Images are presented as maximum projections and were adjusted for brightness using ImageJ 1.50b.

RT-PCR and quantitative PCR analysis

Total RNA was extracted from Caco-2 cells using Trizol reagent (Thermo Fisher Scientific) and used as a template for reverse transcription (RT-PCR) with random hexamer primers (Thermo Fisher Scientific). After DNase treatment (Thermo Fisher Scientific), cDNA was submitted to quantitative real-time (q)PCR using Sybrgreen technology (Applied Biosystems) on a ViiA7 apparatus (Applied Biosystems). Two ACF7 and two reference gene (HPRT1 and GAPDH) primer pairs were used to quantify ACF7relative expression following siRNA transfection using the ΔΔCt method. Primer sequences were as followed: ACF7 #1, 5′- GGTCCTCTCAGGCATCAAAC-3′, 5′-AGTTTCACCTGTCGCTGCTT-3′; ACF7 #2, 5′-TGCACTCATTCACCGATACC-3′, 5′-CCCAGTCTTTCTGCCACTTC-3′; HPRT1, 5′-TGCAGACTTTGCTTTCCTTGGTCAGG-3′, 5′-CCAACACTTCGTGGGGTCCTTTTCA-3′; GAPDH, 5′-CTTCGCTCTCTGCTCCTCCTGTTCG-3′, 5′-ACCAGGCGCCCAATACGACCAAAT-3′.

Statistical analysis

All experiments were conducted at least twice. Statistical analysis was performed using GraphPad Prism 5.

Author contributions

I.N., L.C.K. and A.A. designed experiments and wrote the paper. A.A. coordinated the project. I.N., Q.L., M.B., S.R. and M.M. generated tools and performed the experiments, W.N., S.H. and K.J. generated tools.

Acknowledgements

We thank J. L. Bos (UMC Utrecht, The Netherlands), A. Yap (University of Queensland, Australia), B. Bouchet (Utrecht University, The Netherlands), R. Pagano (Mayo Clinic College of Medicine, Rochester, MN), B. Kuhlman (University of North Carolina, Chapel Hill, NC) for the gifts of materials, and J. Demmers (Erasmus MC, Rotterdam, The Netherlands) for performing mass spectrometry analysis.

References

Akhmanova, A., and C.C. Hoogenraad. 2015. Microtubule minus-end-targeting proteins. Curr Biol. 25:R162-171.

Baas, A.F., J. Kuipers, N.N. van der Wel, E. Batlle, H.K. Koerten, P.J. Peters, and H.C. Clevers. 2004. Complete polarization of single intestinal epithelial cells upon activation of LKB1 by STRAD. Cell. 116:457-466.

Baines, A.J., P.A. Bignone, M.D. King, A.M. Maggs, P.M. Bennett, J.C. Pinder, and G.W. Phillips. 2009. The CKK domain (DUF1781) binds microtubules and defines the CAMSAP/ssp4 family of animal proteins. Mol Biol Evol. 26:2005-2014.

Bartolini, F., and G.G. Gundersen. 2006. Generation of noncentrosomal microtubule arrays. J Cell Sci. 119:4155-4163.

Booth, A.J., G.B. Blanchard, R.J. Adams, and K. Roper. 2014. A dynamic microtubule cytoskeleton directs medial actomyosin function during tube formation. Dev Cell. 29:562-576.

Bornens, M. 2012. The centrosome in cells and organisms. Science. 335:422-426.

Bryant, D.M., A. Datta, A.E. Rodriguez-Fraticelli, J. Peranen, F. Martin-Belmonte, and K.E. Mostov. 2010. A molecular network for de novo generation of the apical surface and lumen. Nat Cell Biol. 12:1035-1045.

Dambournet, D., M. Machicoane, L. Chesneau, M. Sachse, M. Rocancourt, A. El Marjou, E. Formstecher, R. Salomon, B. Goud, and A. Echard. 2011. Rab35 GTPase and OCRL phosphatase remodel lipids and F-actin for successful cytokinesis. Nat Cell Biol. 13:981-988.

Dammermann, A., A. Desai, and K. Oegema. 2003. The minus end in sight. Curr Biol. 13:R614-624.

Dhekne, H.S., N.H. Hsiao, P. Roelofs, M. Kumari, C.L. Slim, E.H. Rings, and S.C. van Ijzendoorn. 2014. Myosin Vb and Rab11a regulate phosphorylation of ezrin in enterocytes. J Cell Sci. 127:1007-1017.

Drabek, K., M. van Ham, T. Stepanova, K. Draegestein, R. van Horssen, C.L. Sayas, A. Akhmanova, T. Ten Hagen, R. Smits, R. Fodde, F. Grosveld, and N. Galjart. 2006. Role of CLASP2 in microtubule stabilization and the regulation of persistent motility. Curr Biol. 16:2259-2264.

Goodwin, S.S., and R.D. Vale. 2010. Patronin regulates the microtubule network by protecting microtubule minus ends. Cell. 143:263-274.

Hendershott, M.C., and R.D. Vale. 2014. Regulation of microtubule minus-end dynamics by CAMSAPs and Patronin. Proc Natl Acad Sci U S A. 111:5860-5865.

Horgan, C.P., S.R. Hanscom, R.S. Jolly, C.E. Futter, and M.W. McCaffrey. 2010. Rab11-FIP3 links the Rab11 GTPase and cytoplasmic dynein to mediate transport to the endosomal-recycling compartment. J Cell Sci. 123:181-191.

Jaffe, A.B., N. Kaji, J. Durgan, and A. Hall. 2008. Cdc42 controls spindle orientation to position the apical surface during epithelial morphogenesis. J Cell Biol. 183:625-633.

Jiang, K., S. Hua, R. Mohan, I. Grigoriev, K.W. Yau, Q. Liu, E.A. Katrukha, A.F. Altelaar, A.J. Heck, C.C. Hoogenraad, and A. Akhmanova. 2014. Microtubule minus-end stabilization by polymerization-driven CAMSAP deposition. Dev Cell. 28:295-309.

Karakesisoglou, I., Y. Yang, and E. Fuchs. 2000. An epidermal plakin that integrates actin and microtubule networks at cellular junctions. J Cell Biol. 149:195-208.

Khanal, I., A. Elbediwy, C. Diaz de la Loza Mdel, G.C. Fletcher, and B.J. Thompson. 2016. Shot and Patronin polarise microtubules to direct membrane traffic and biogenesis of microvilli in epithelia. J Cell Sci. 129:2651-2659.

King, M.D., G.W. Phillips, P.A. Bignone, N.V. Hayes, J.C. Pinder, and A.J. Baines. 2014. A conserved sequence in calmodulin regulated spectrin-associated protein 1 links its interaction with spectrin and calmodulin to neurite outgrowth. J Neurochem. 128:391-402.

Knowles, B.C., V.G. Weis, S. Yu, J.T. Roland, J.A. Williams, G.S. Alvarado, L.A. Lapierre, M.D. Shub, N. Gao, and J.R. Goldenring. 2015. Rab11a regulates syntaxin 3 localization and microvillus assembly in enterocytes. J Cell Sci.

128:1617-1626.

Kodama, A., I. Karakesisoglou, E. Wong, A. Vaezi, and E. Fuchs. 2003. ACF7: an essential integrator of microtubule dynamics. Cell. 115:343-354.

Letunic, I., T. Doerks, and P. Bork. 2015. SMART: recent updates, new developments and status in 2015. Nucleic Acids Res. 43:D257-260.

Meng, W., Y. Mushika, T. Ichii, and M. Takeichi. 2008. Anchorage of microtubule minus ends to adherens junctions regulates epithelial cell-cell contacts. Cell. 135:948-959.

Moss, D.K., G. Bellett, J.M. Carter, M. Liovic, J. Keynton, A.R. Prescott, E.B. Lane, and M.M. Mogensen. 2007. Ninein is released from the centrosome and moves bi-directionally along microtubules. J Cell Sci. 120:3064-3074.

Nashchekin, D., A.R. Fernandes, and D. St Johnston. 2016. Patronin/Shot Cortical Foci Assemble the Noncentrosomal Microtubule Array that Specifies the Drosophila Anterior-Posterior Axis. Dev Cell. 38:61-72.

Overeem, A.W., D.M. Bryant, and I.S.C. van. 2015. Mechanisms of apical-basal axis orientation and epithelial lumen positioning. Trends Cell Biol. 25:476-485.

Ran, F.A., P.D. Hsu, J. Wright, V. Agarwala, D.A. Scott, and F. Zhang. 2013. Genome engineering using the CRISPR-Cas9 system. Nat Protoc. 8:2281-2308.

Ratheesh, A., G.A. Gomez, R. Priya, S. Verma, E.M. Kovacs, K. Jiang, N.H. Brown, A. Akhmanova, S.J. Stehbens, and A.S. Yap. 2012. Centralspindlin and alpha-catenin regulate Rho signalling at the epithelial zonula adherens. Nat Cell Biol. 14:818-828.

Riggs, B., B. Fasulo, A. Royou, S. Mische, J. Cao, T.S. Hays, and W. Sullivan. 2007. The concentration of Nuf, a Rab11 effector, at the microtubule-organizing center is cell cycle regulated, dynein-dependent, and coincides with furrow formation. Mol Biol Cell. 18:3313-3322.

Schultz, J., F. Milpetz, P. Bork, and C.P. Ponting. 1998. SMART, a simple modular architecture research tool: identification of signaling domains. Proc Natl Acad Sci U S A. 95:5857-5864.

Sobajima, T., S. Yoshimura, T. Iwano, M. Kunii, M. Watanabe, N. Atik, S. Mushiake, E. Morii, Y. Koyama, E. Miyoshi, and A. Harada. 2014. Rab11a is required for apical protein localisation in the intestine. Biol Open. 4:86-94.

Takahashi, S., V.J. Mui, S.K. Rosenberg, K. Homma, M.A. Cheatham, and J. Zheng. 2016. Cadherin 23-C Regulates Microtubule Networks by Modifying CAMSAP3's Function. Sci Rep. 6:28706.

Tanaka, N., W. Meng, S. Nagae, and M. Takeichi. 2012. Nezha/CAMSAP3 and CAMSAP2 cooperate in epithelial-specific organization of noncentrosomal microtubules. Proc Natl Acad Sci U S A. 109:20029-20034.

Toya, M., S. Kobayashi, M. Kawasaki, G. Shioi, M. Kaneko, T. Ishiuchi, K. Misaki, W. Meng, and M. Takeichi. 2016. CAMSAP3 orients the apical-to-basal polarity of microtubule arrays in epithelial cells. Proc Natl Acad Sci U S A. 113:332-337.

Viswanatha, R., P.Y. Ohouo, M.B. Smolka, and A. Bretscher. 2012. Local phosphocycling mediated by LOK/SLK restricts ezrin function to the apical aspect of epithelial cells. J Cell Biol. 199:969-984.

Wang, S., D. Wu, S. Quintin, R.A. Green, D.K. Cheerambathur, S.D. Ochoa, A. Desai, and K. Oegema. 2015. NOCA-1 functions with gamma-tubulin and in parallel to Patronin to assemble non-centrosomal microtubule arrays in C. elegans. Elife. 4:e08649.

Wu, J., C. de Heus, Q. Liu, B.P. Bouchet, I. Noordstra, K. Jiang, S. Hua, M. Martin, C. Yang, I. Grigoriev, E.A. Katrukha, A.F. Altelaar, C.C. Hoogenraad, R.Z. Qi, J. Klumperman, and A. Akhmanova. 2016. Molecular Pathway of Microtubule Organization at the Golgi Apparatus. Dev Cell. 39:44-60.

Wu, X., A. Kodama, and E. Fuchs. 2008. ACF7 regulates cytoskeletal-focal adhesion dynamics and migration and has ATPase activity. Cell. 135:137-148.

Zheng, J., D. Furness, C. Duan, K.K. Miller, R.M. Edge, J. Chen, K. Homma, C.M. Hackney, P. Dallos, and M.A. Cheatham. 2013. Marshalin, a microtubule minus-end binding protein, regulates cytoskeletal structure in the organ of Corti. Biol Open. 2:1192-1202.

Supplemental figures

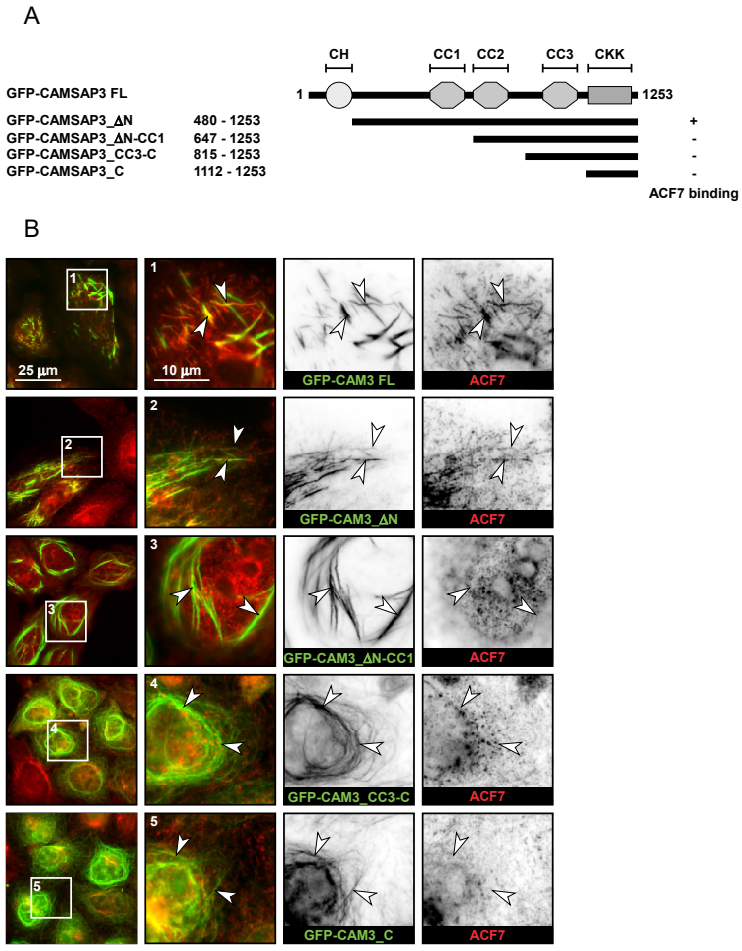

Figure S1. Endogenous ACF7 is recruited to CAMSAP3-induced microtubule bundles in a manner dependent on the CC1 region of CAMSAP3

(A) Domain organization of GFP-CAMSAP3 deletion mutants used to study binding to ACF7 and a summary of detected interactions. FL, full length, CH, calponin homology domain. **(B)** HeLa cells transiently expressing GFP-CAMSAP3 fragments (as in A, green) and stained for ACF7 (red). White arrowheads indicate the same positions in different panels.

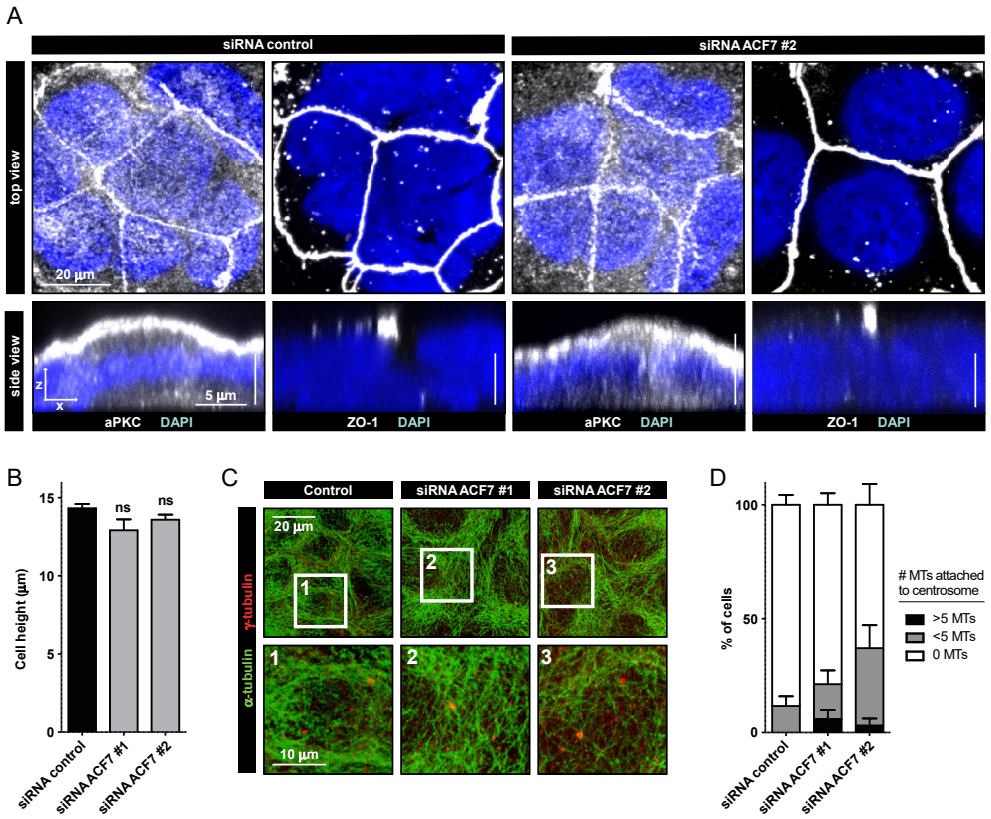

Figure S2. ACF7 depletion does not affect general polarity in 2D monolayer culture
(A) Staining of aPKC, ZO-1 (white) and DNA (blue) in Caco-2 cells transfected with control or ACF7 siRNAs. Both top and side views are shown. **(B)** Quantification of cell height of Caco-2 cells transfected with control or ACF7 siRNAs. Control, n=36; siRNA ACF7 #1, n=36; siRNA ACF7 #2, n=36; ns, not significant; MannWhitney U test; Error bars, SEM. **(C)** Staining of microtubules (green, α-tubulin) and centrosomes (red, ɣ-tubulin) in Caco-2 cells transfected with control or ACF7 siRNAs. **(D)** Quantification of microtubule organization presented as a number of microtubules attached to the centrosome. Quantification based on staining shown in (C). Number of analyzed cells: control, n=41; siRNA ACF7 #1, n=38; siRNA ACF7 #2, n=60; Error bars, SEM; #, number; MTs, microtubules.

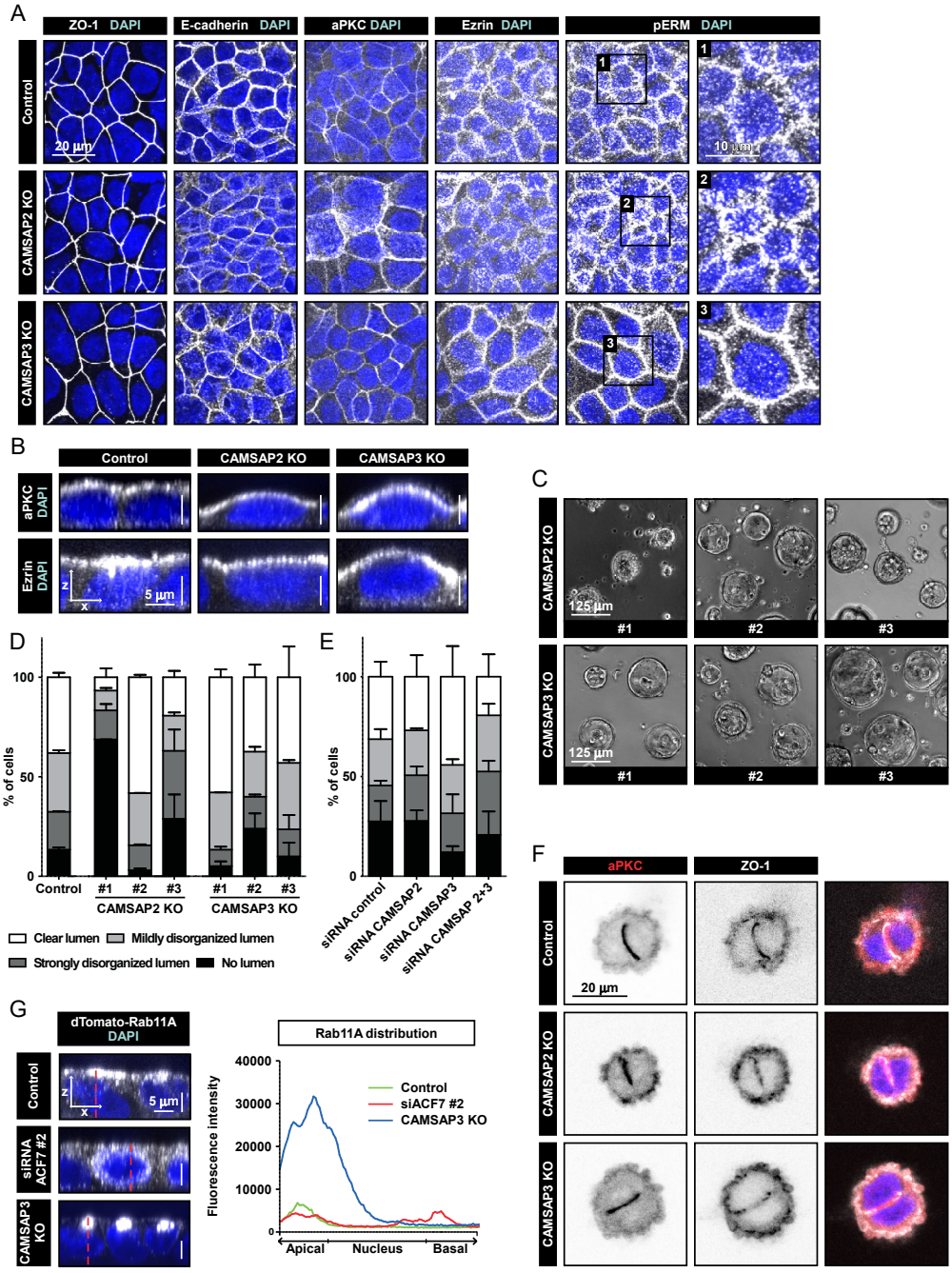

Figure S3. Formation of 3D cysts and the distribution of polarity markers in control, CAMSAP2 and CAMSAP3 knockout cells

(A) Staining for ZO-1, E-cadherin, aPKC, ezrin en pERM (white) and DNA (blue) in control, CAMSAP2 and CAMSAP2 knockout (KO) cells. **(B)** Side view of aPKC, ezrin (white) and DNA (blue) staining in cells as in (A). **(C)** 3D cyst formation 1 day after dense seeding of different CAMSAP2 and CAMSAP3 knockout clones. **(D)** Quantification of 3D cyst formation of cells in (C). Control,

n=200; CAMSAP2 KO #1, n=172; CAMSAP2 KO #2, n=245; CAMSAP2 KO #3, n=143; CAMSAP3 KO #1, n=173; CAMSAP3 KO #2, n=204; CAMSAP3 KO #3, n=213. **(E)** Quantification of 3D cyst formation of Caco-2 cells transfected with siRNA targeting CAMSAP2, CAMSAP3 or CAMSAP2 and 3 simultaneously. siRNA control, n=320; siRNA CAMSAP2, n=226; siRNA CAMSAP3, n=316; siRNA CAMSAP2+3, n=252. **(F)** Staining of aPKC (red), ZO-1 (white) and DNA (blue) in cells as in (A) seeded in a 3D matrix. **(G)** Side view of dTomato-Rab11A (white) and DNA (blue) in control cells, cells transfected with siRNA targeting ACF7 and CAMSAP3 knockout cells. dTomato-Rab11A intensity profiles along the line indicated in red are plotted in the graph.

Supplemental table

Primary antibodies

Target	Source	Dilution	Company	Catalog number
Tyrosinated α-tubulin	Rat	IF 1:300	Abcam	#ab6160
mCherry	Mouse	WB 1:1000	Clontech	#632543
ACF7	Mouse	IF 1:400	Abnova	#H00023499-A01
CAMSAP3	Mouse	IF 1:200 WB 1:1000	Sigma-Aldrich	#SAB4200415
ɣ-tubulin	Mouse	IF 1:100	Sigma-Aldrich	#T5326
Ku80	Mouse	WB 1:2000	BD Biosciences	#611360
ZO-1	Mouse	IF 1:500	BD Biosciences	#610966
E-cadherin	Mouse	IF 1:500	BD Biosciences	#610181
Ezrin	Mouse	IF 1:500	BD Biosciences	#610602
GFP	Rabbit	WB 1:1000	Abcam	#ab290
CAMSAP2	Rabbit	IF 1:300	Novus	#NBP1-21402
CAMSAP2	Rabbit	WB 1:1000	Proteintech	#17880-1-AP
aPKC	Rabbit	IF 1:300	Santa Cruz	#H00023499-A01
Actin	Rabbit	IF 1:200	Sigma-Aldrich	#20-33
CEP135	Rabbit	IF 1:300	Sigma-Aldrich	#SAB4503685
Phosphorylated ERM	Rabbit	IF 1:500	Cell Signaling	#3141
E-cadherin	Rabbit	IF 1:1000	Gift from A. Yap	-

IF: Immunofluorescence staining
WB: Western blot

Secondary antibodies

All secondary antibodies used for immunofluorescence staining were diluted 1:300
All secondary antibodies used for western blot were diluted 1:15000

5

Focal adhesion-associated protein complexes function as docking platforms for insulin granules in pancreatic β-cells

Ivar Noordstra[1], Bastiaan J. Viergever[1], Ká Lou Yu[1], Eugene A. Katrukha[1] and Anna Akhmanova[1]

Manuscript in preparation

[1]Cell Biology, Faculty of Science, Utrecht University, 3584 CH Utrecht, The Netherlands

Summary

High blood glucose levels stimulate pancreatic β-cells to secrete insulin. Efficient secretion depends on the remodeling of actin and focal adhesions, resulting in the activation of the ERK/MAPK signaling pathway and the release of insulin. In this study, we show that the glucose dependent activation of focal adhesions also leads to the recruitment of insulin docking complexes to focal adhesion-rich cortical areas. The insulin docking complexes are composed of cortical microtubule stabilizing complex subunits and proteins involved in the exocytosis of neurotransmitters at the active zone of the neuronal presynapse. Glucose independent activation of the Rho/Rho kinase (ROCK) signaling pathway through nocodazole-induced microtubule depolymerization phenocopied the effect of glucose stimulation on insulin docking complex recruitment. In contrast, inhibition of ROCK or its downstream target myosin II completely abolished recruitment of the insulin docking complex, indicating that focal adhesion-specific relocalization of these complexes depends on the activation of the Rho/ROCK signaling pathway and enhanced actomyosin contractility. Our results provide new insights in the molecular machinery underlying the exocytosis of insulin from pancreatic β-cells.

Introduction

Blood glucose levels are tightly monitored by specialized cells in the pancreas. Pancreatic β-cells respond to elevated glucose levels by an increase in intracellular ATP/ADP ratios, closure of ATP-sensitive K^+ channels (Ashcroft et al., 1984; Cook and Hales, 1984), membrane depolarization, opening of voltage-gated Ca^{2+} channels (Satin and Cook, 1985), activation of exocytotic machinery and secretion of insulin (Meglasson and Matschinsky, 1986; Prentki and Matschinsky, 1987). Subsequently, insulin stimulates glucose uptake and conversion in different tissues including the liver and muscle cells. Malfunctioning of one of these steps can lead to diabetes type II, a major worldwide health problem, which affects increasingly large numbers of patients.

Over the years, different studies revealed a biphasic pattern of insulin secretion upon glucose stimulation, which is caused by the presence and release of two physically separated insulin pools (Curry et al., 1968; Grodsky et al., 1970; O'Connor et al., 1980; Rorsman et al., 2000). The first phase of insulin release takes place within five to ten minutes and is provided by a pool of pre-docked vesicles (Barg et al., 2001; Daniel et al., 1999; Olofsson et al., 2002). The second phase, which starts after approximately 10 minutes and declines after blood glucose levels drop, depends on newly formed vesicles and vesicles that are initially kept away from the membrane (Orci et al., 1972; Seino et al., 2011). The actual docking and fusion of insulin vesicles at the membrane of pancreatic β-cells is a complicated and tightly regulated process with a plethora of different molecules involved.

ELKS and its homologue CAST have been shown to function as one of the major scaffold proteins at the presynaptic active zone of neurons (Hida and Ohtsuka, 2010). The active zone is the principal site of Ca^{2+} dependent exocytosis of neurotransmitters. It is a specialized region of the plasma membrane where tethering, docking and fusion of synaptic vesicles take place. Although the process of neurotransmitter release (milliseconds) is much faster than insulin secretion (minutes), the molecular machinery underlying exocytosis in both systems partially overlaps (Gundelfinger and Fejtova, 2012; Sudhof, 2012). Importantly, ELKS has also been shown to participate in the docking and fusion of insulin vesicles in pancreatic β-cells. Total internal reflection microscopy (TIRF) imaging of single insulin granule motion showed that insulin fusion events often occur on ELKS clusters, and the depletion of ELKS strongly inhibited glucose stimulated insulin secretion (GSIS) (Ohara-Imaizumi et al., 2005).

Detailed analysis revealed that ELKS is a ubiquitously expressed adaptor protein which is member of a large protein assembly known as the cortical microtubule stabilizing complex (CMSC) (Astro and de Curtis, 2015; Noordstra and Akhmanova, 2017). Within this complex it directly interacts with Liprin-α1, a key scaffold protein of

the active zone, and LL5β, a PIP3-binding protein responsible for the recruitment of the CMSC to the membrane (Ko et al., 2003; Lansbergen et al., 2006). As the name suggests, the CMSC stabilizes microtubules at the cortical regions of the cell, specifically in the vicinity of focal adhesions (FAs) through an interaction of the CMSC protein KANK1 and the FA adhesion protein Talin (Bouchet et al., 2016).

In this study we focus on the molecular machinery that underlies the docking of insulin vesicles upon glucose stimulation in the pancreatic β-cell line INS-1E and isolated murine pancreatic islets. We show that insulin vesicles accumulate on CMSC patches that also contain exocytosis-related proteins found in the presynaptic active zone. Upon glucose stimulation, these patches relocalize and accumulate around FAs in a myosin II dependent fashion, thereby forming potential insulin docking and secretion platforms which could strongly influence the levels of insulin secretion.

Results

Insulin vesicles dock on protein complexes composed of CMSC and presynaptic active zone proteins

In order to study the molecular mechanisms underlying docking and fusion of insulin granules, we used the rat pancreatic β-cell line INS-1E (Asfari et al., 1992; Merglen et al., 2004). Immunostaining showed that at moderate glucose levels (11 mM), when insulin is slowly and steadily secreted (Merglen et al., 2004), insulin granules are excluded from actin-rich areas (Figure 1A). This is consistent with previous findings, which showed that actin prevents insulin docking, thereby regulating insulin secretion levels and maintaining glucose homeostasis (Arous and Halban, 2015; Orci et al., 1972). We found that in addition to exclusion from actin fibers, insulin vesicles dock at specific patches (Figure 1B). Interestingly, these patches are marked by the PIP3-binding protein LL5β (Figures 1B and 1C), which is known to be responsible for linking the CMSC to the membrane (Lansbergen et al., 2006; van der Vaart et al., 2013) and which participates in organizing sites of exocytosis in different cell types (Noordstra and Akhmanova, 2017). We next used immunostaining to visualize different members of the complex including the scaffold proteins ELKS, Liprin-α1, Liprin-β1 and KANK1, a protein responsible for linking the CMSC to FAs (Bouchet et al., 2016). All of the indicated proteins localize to the same cortical regions (Figure 1D), suggesting that they form a complex which is involved in the docking of insulin vesicles.

ELKS, as well as Liprin-α1 and Liprin-β1, are key scaffold proteins involved in secretion of neurotransmitters at the active zone of the presynapse (Gundelfinger and Fejtova, 2012; Hida and Ohtsuka, 2010; Sudhof, 2012). Interestingly, although the process of neurotransmitter release is much faster than insulin release from pancreatic β-cells (milliseconds compared to minutes), both processes rely on active secretion upon the generation of an action potential and the influx of calcium. As previous results revealed the presence of ELKS and the Liprins in insulin docking complexes, we used immunostainings to test whether other proteins found at the presynaptic active zone could be involved in docking of insulin granules. Both RIM1/2 and Bassoon, two major presynaptic scaffold proteins, strongly co-localize with the CMSC (Figure 1E) and insulin (Figure 1F), indicating that there is overlap between the neuronal neurotransmitter release machinery and the proteins involved in docking of insulin granules in pancreatic β-cells.

The CMSC has been shown to stabilize and link microtubules to the cortex trough an interaction between LL5β and CLASP (Lansbergen et al., 2006). Also in pancreatic β-cells, CLASP strongly co-localizes to LL5β patches (Figure 1G), pointing in the direction of cortical microtubule stabilization through a CLASP-LL5β interaction.

Taken together, we show that, in the presence of moderate glucose levels (11

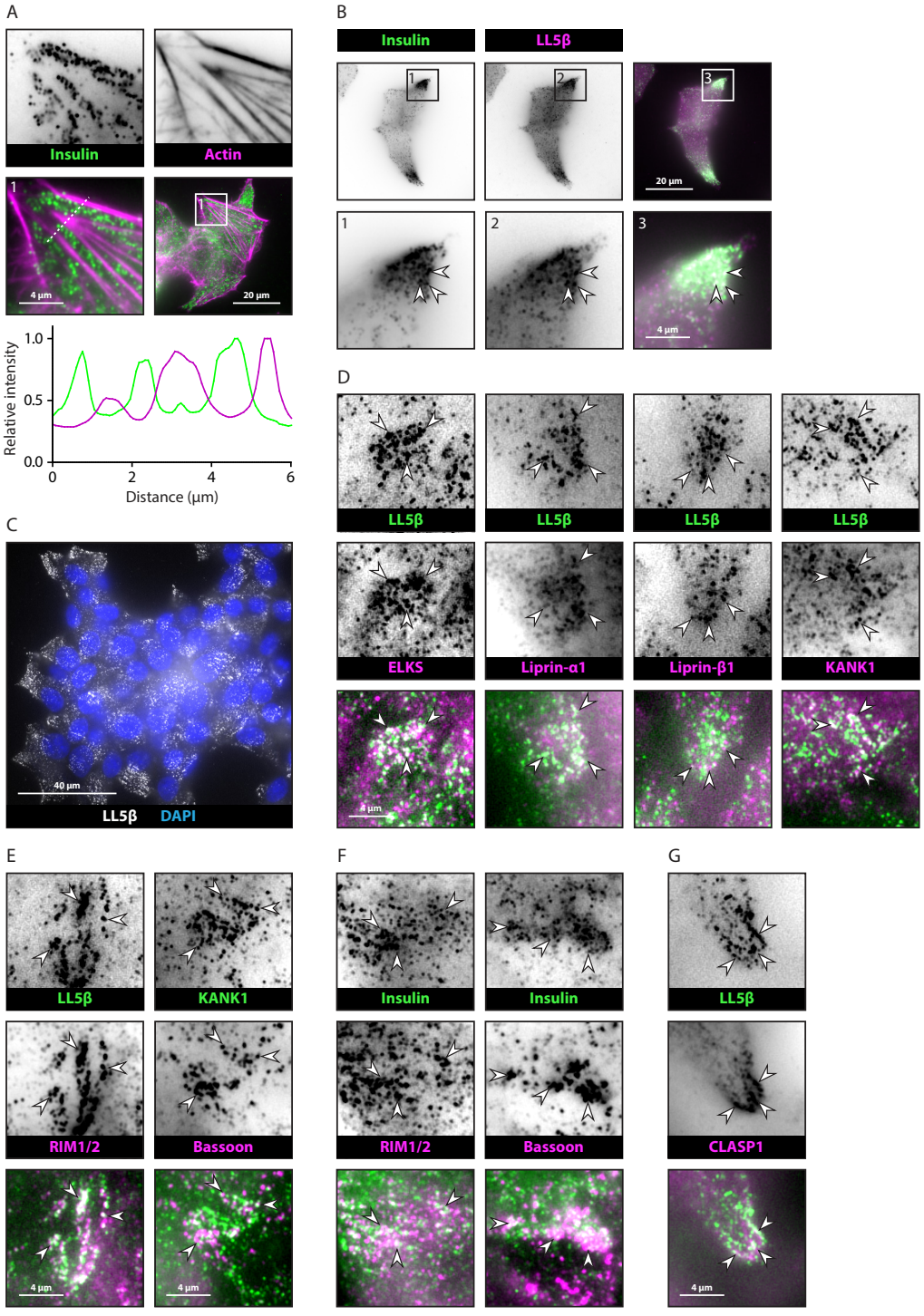

Figure 1. Insulin granules colocalize with a multiprotein docking platform
(A) Staining of insulin (green) and actin (magenta) in INS-1E cells. Intensity profiles along the dotted line are plotted in the graph. **(B)** Staining of insulin (green) and LL5β (magenta) in INS-

1E cells. **(C)** Staining of LL5β (white) and DNA (blue) in INS-1E cells. **(D)** Staining of LL5β (green) and ELKS, Liprin-α1, Liprin-β1, KANK1 (magenta) in INS-1E cells. **(E)** Staining of different CMSC (green) and presynaptic active zone (magenta) proteins in INS-1E cells. Left column, staining of LL5β (green) and RIM1/2 (magenta); Right column, staining of KANK1 (green) and Bassoon (magenta). **(F)** Staining of Insulin (green) and RIM1/2, Bassoon (magenta) in INS-1E cells. **(G)** Staining of LL5β (green) and CLASP1 (magenta) in INS-1E cells.

mM), insulin vesicles dock on protein patches consisting of CMSC proteins and proteins involved in the docking and secretion of neurotransmitters at the active zone of the neuronal presynapse. From now on we will call this complex the insulin docking complex (IDC).

LL5β participates in IDC recruitment to the cell cortex

To gain a better understanding of the subcellular organization of the IDC we combined immunostainings with stimulated emission depletion (STED) microscopy. The high resolution imaging revealed a core of LL5β molecules surrounded by the other members of the CMSC as well RIM1/2 (Figure 2A). SiRNA mediated depletion of LL5β resulted in the relocalization of RIM1/2 from the cortex (Figure 2B), which is consistent with LL5β participating in linking the IDC to the plasma membrane as is the case for the CMSC (Lansbergen et al., 2006).

The insulin docking complex is recruited to focal adhesions upon glucose stimulation

As pancreatic β-cells respond to high glucose levels by secreting insulin, we tested the response to glucose and insulin secretion of the INS-1E cells. Overnight glucose starvation (2 mM glucose) led to accumulation of insulin in the cells (Figures 3A and 3B). After only 2 minutes of glucose stimulation (25 mM glucose), we found an almost 30% reduction of the total insulin pool which kept decreasing for approximately 10 minutes (Figures 3A and 3B). These observations are fully consistent with previous studies showing that insulin secretion occurs in a biphasic manner, with the release of the predocked insulin pool within the first 10 minutes (Seino et al., 2011). After 10 minutes, cellular insulin levels slowly recovered, indicating that the cells shifted to slow and steady secretion of newly formed insulin molecules (Figures 3A and 3B), a process described in literature as the second phase of insulin secretion (Seino et al., 2011).

We then focused on the dynamics of the IDC upon GSIS. After only 2 minutes of GSIS, the IDC patches visualized by LL5β, ELKS and Liprin-α1 immunostaining strongly concentrated into elongated clusters (Figures 3C and 3D), which were often

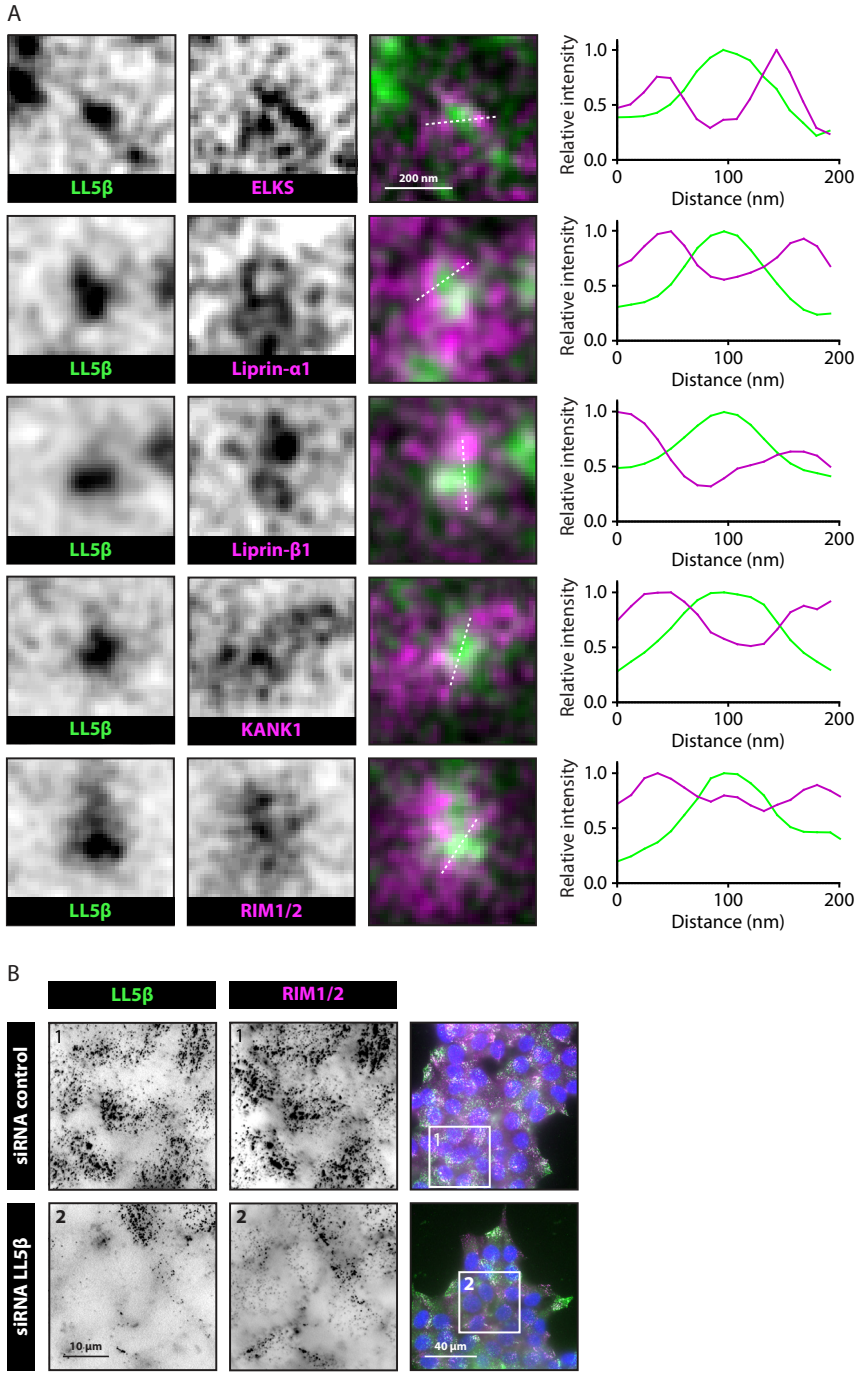

Figure 2. LL5β forms the core of IDCs

(A) Staining of LL5β (green) and ELKS, Liprin-α1, Liprin-β1, KANK1, RIM1/2 (magenta) in INS-1E cells. Intensity profiles along the dotted lines are plotted in the graphs. **(B)** Staining of LL5β (green), RIM1/2 (magenta) and DNA (blue) in INS-1E cells transfected with control siRNA or siRNA against LL5β.

closely apposed but did not overlap with FAs visualized by immunostaining for phosphorylated Focal Adhesion Kinase (pFAK) (Figure 3E).

These results indicate that, upon GSIS, the IDC components change their subcellular distribution and concentrate around FAs.

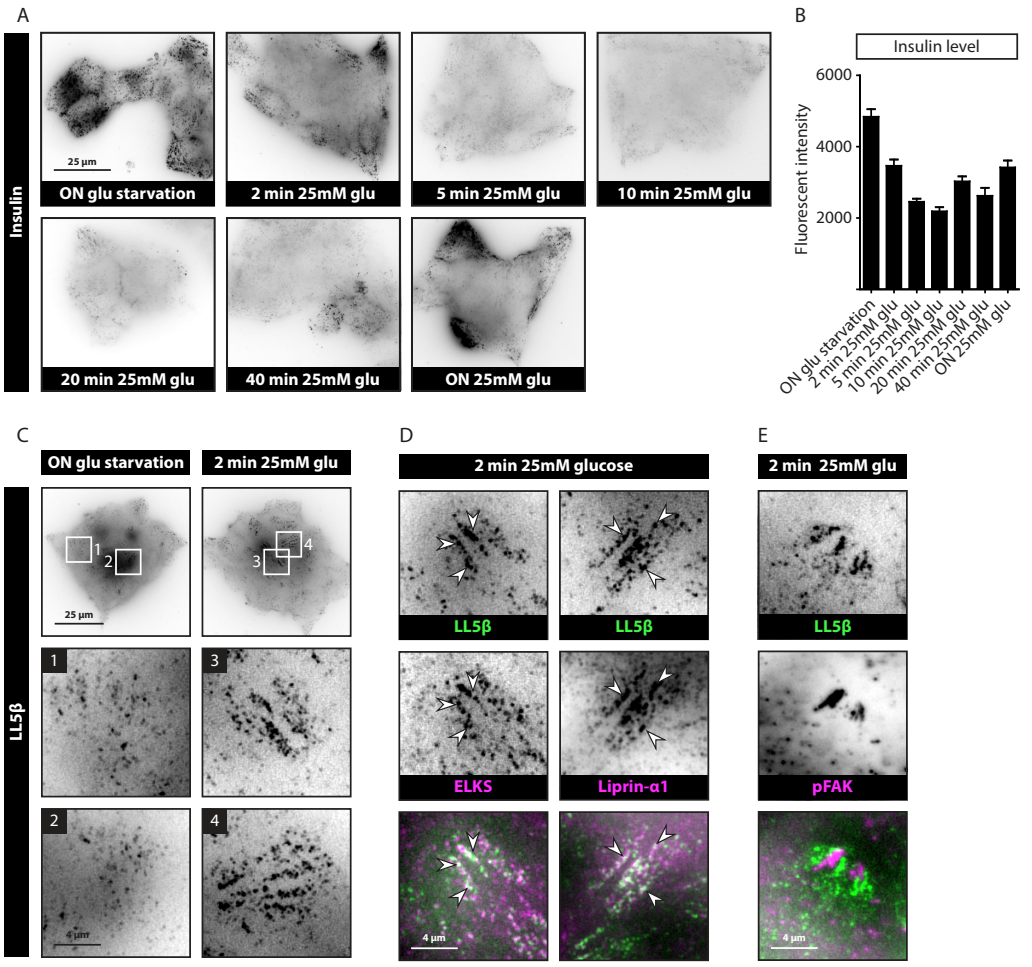

Figure 3. IDCs accumulate around FAs upon glucose stimulation
(A) Staining of insulin in INS-1E cells treated with glucose as indicated. ON=overnight; glu=glucose. **(B)** Quantification of fluorescence intensity of insulin in INS-1E cells treated with glucose as indicated. For all conditions, n=5; error bars, S.E.M. **(C)** Staining of LL5β in INS-1E cells treated with glucose as indicated. **(D)** Staining of LL5β (green) and ELKS, Liprin-α1 (magenta) in INS-1E cells treated with glucose as indicated. **(E)** Staining of LL5β (green) and pFAK (magenta) in INS-1E cells treated with glucose as indicated.

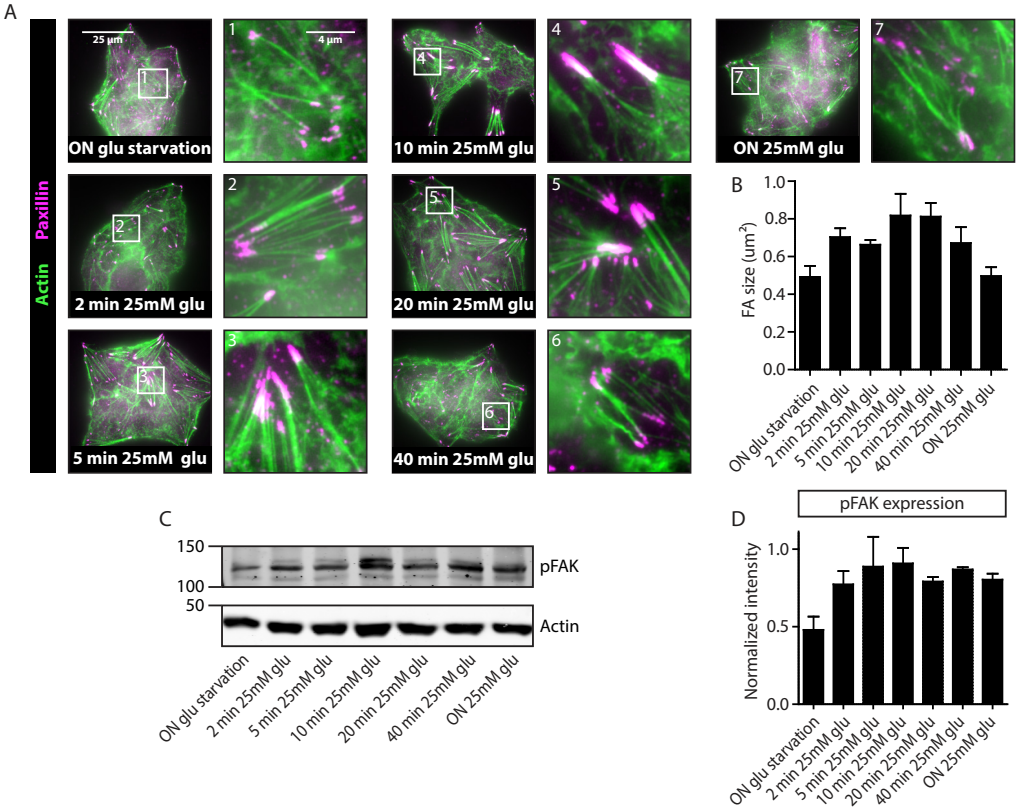
A
Actin Paxillin
25 µm
ON glu starvation
2 min 25mM glu
5 min 25mM glu
10 min 25mM glu
20 min 25mM glu
40 min 25mM glu
ON 25mM glu
4 µm
B
FA size (um²)
1.0
0.8
0.6
0.4
0.2
0.0
ON glu starvation
2 min 25mM glu
5 min 25mM glu
10 min 25mM glu
20 min 25mM glu
40 min 25mM glu
ON 25mM glu
C
150
100
50
pFAK
Actin
ON glu starvation
2 min 25mM glu
5 min 25mM glu
10 min 25mM glu
20 min 25mM glu
40 min 25mM glu
ON 25mM glu
D
pFAK expression
Normalized intensity
1.0
0.5
0.0
ON glu starvation
2 min 25mM glu
5 min 25mM glu
10 min 25mM glu
20 min 25mM glu
40 min 25mM glu
ON 25mM glu

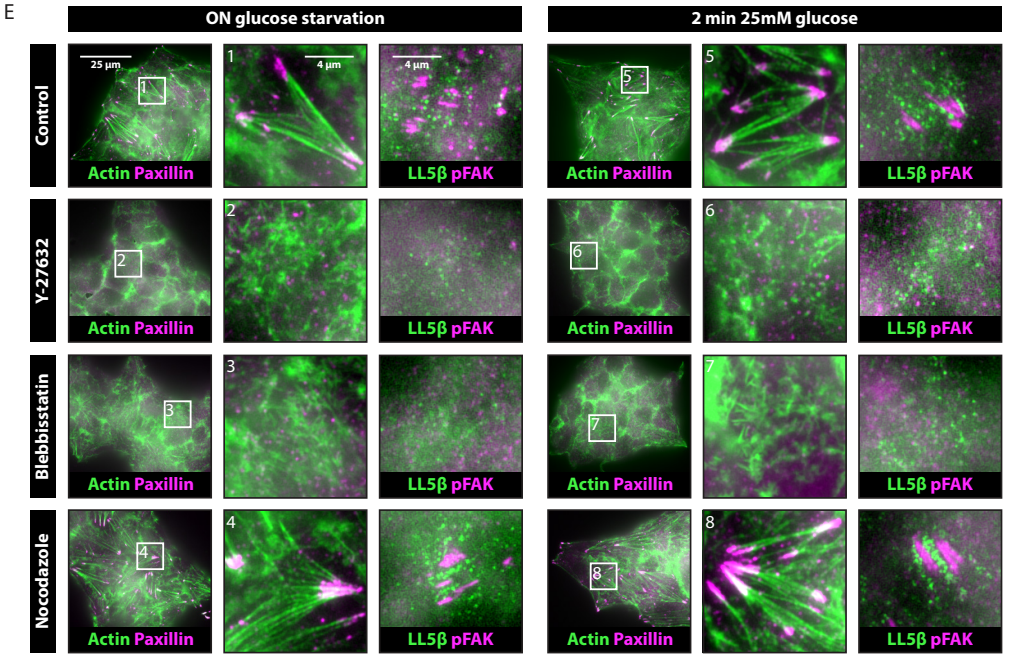
E
ON glucose starvation
2 min 25mM glucose
Control
Y-27632
Blebbistatin
Nocodazole
25 µm
4 µm
Actin Paxillin
LL5β pFAK

Figure 4. Glucose treatment results in FA activation
(A) Staining of actin (green) and paxilin (magenta) in INS-1E cells treated with glucose as indicated. glu=glucose. **(B)** Quantification of FA size in INS-1E cells treated with glucose as indicated. glu=glucose; all conditions, n=5; error bars, S.E.M. **(C)** Western blot analysis of extracts of INS-1E cells treated with glucose as indicated. **(D)** Quantification of Western blot analysis as shown in (C). For all conditions, n=2; error bars, S.E.M. **(E)** Staining of actin (green) and paxillin (magenta) (left and middle column) and LL5β (green) and pFAK (magenta) (right column) in INS-1E cells treated with different drugs and glucose as indicated.

Glucose stimulation increases actomyosin contractility and activates formation of FAs, resulting in IDC recruitment

Increase of actomyosin contractility leads to remodeling of FA complexes (Schwartz, 2010). This process involves the activation and phosphorylation of FAK and Paxillin, two well-studied FA components, which play an important role in cell migration (Hu et al., 2014). Previous work has shown that the activation of FAs results in the recruitment of the CMSC, a process mediated by the interaction of the FA protein Talin and the CMSC component KANK1 (Bouchet et al., 2016). To test whether glucose stimulation could lead to activation of FAs and thus the GSIS specific recruitment of the IDC in INS-1E cells, we induced GSIS and measured the surface area of FAs, a well-known read-out for FA activation (Burridge and Chrzanowska-Wodnicka, 1996). Indeed, upon 10 minutes of glucose stimulation we found thicker and more prominent actin stress fibers, indicating that actomyosin contractility was increased (Figure 4A). This was accompanied by approximately 40% enlargement of the FA areas, which gradually decreased again after 10 minutes (Figures 4A and 4B). In addition, Western blot analysis revealed an increase in the pool of pFAK after 10 minutes of glucose stimulation (Figures 4C and 4D). Together, this temporal profile fits well with the first phase of insulin secretion, which ends after approximately 10 minutes of glucose stimulation (Figures 3A and 3B).

Actomyosin-based contraction is regulated via the Rho/Rho kinase (ROCK) signaling pathway, which drives the formation of actin stress fibers and FAs (Chrzanowska-Wodnicka and Burridge, 1996). To test whether glucose stimulation-induced recruitment of the IDC to FAs depends on actomyosin contractility and FA activation, we tuned this pathway with either blocking or activating drugs. Inhibition of ROCK with Y-27632, or its downstream target myosin II by blebbistatin, induced strong loss of the actin cables and FAs, and abolished specific recruitment of the IDC, independent of glucose concentration (Fig. 4E). In contrast, activation of the Rho/ROCK signaling pathway by nocodazole induced microtubule disassembly (Etienne-Manneville, 2013; Rape et al., 2011) enhanced IDC recruitment even in the absence of glucose, thereby mimicking the effect of glucose-activated actomyosin contractility (Figure 4E).

Taken together, these results show that glucose stimulation induces actomyosin contractility in INS-1E cells. As a result, FAs are enlarged and recruitment of IDC is observed.

The insulin docking complex co-localizes with insulin in β-cells of isolated murine pancreatic islets

To confirm the existence of IDCs consisting of CMSC proteins and presynaptic active zone proteins *in vivo*, we isolated pancreatic islets from adult wild type mice and visualized proteins of interest using immunofluorescence. Co-staining of the α-cell marker glucagon and the β-cell marker insulin revealed two distinct groups of cells within one islet (Figure 5A), indicating that we successfully cultured pancreatic islets isolated from mice. Next, we co-stained insulin with LL5β, RIM1/2 or Bassoon. All three proteins were specifically enriched in β-cells and strongly co-localized with insulin vesicles (Figure 5B). These results clearly indicate that *in vivo*, insulin vesicles dock on protein complexes with the same composition as we described for the pancreatic β-cell line INS-1E.

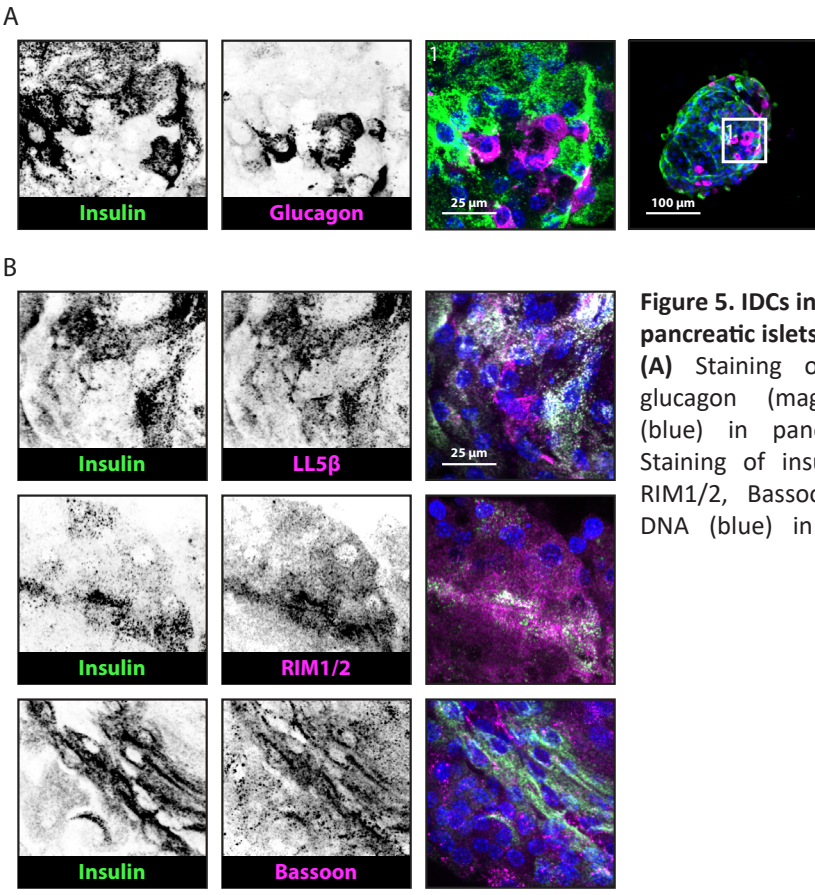

Figure 5. IDCs in isolated murine pancreatic islets

(A) Staining of insulin (green), glucagon (magenta) and DNA (blue) in pancreatic islets. **(B)** Staining of insulin (green), LL5β, RIM1/2, Bassoon (magenta) and DNA (blue) in pancreatic islets.

Discussion

In this study we describe the presence of a multiprotein insulin docking platform in pancreatic β-cells. The complex harbors proteins of the molecular machinery responsible for the exocytosis of neurotransmitters at the presynaptic active zone and proteins previously described as subunits of a CMSC that specifically localizes to the vicinity of FAs (Lansbergen et al., 2006; van der Vaart et al., 2013). We found that upon glucose stimulation, FAs of the β-cells became activated in a myosin II dependent way, resulting in cortical clustering of the IDC around FAs. These IDC clusters could potentially function as docking platforms for insulin granules prior to secretion.

Although neurotransmitter release and synaptic transmission is much faster than insulin secretion upon glucose stimulation, both processes display striking similarities. In both situations the actual release of exocytotic content is activated by depolarization of the membrane, subsequent influx of Ca^{2+} ions through opened voltage-gated Ca^{2+} channels and activation of the exocytotic machinery. Therefore, it is not surprising that both systems rely on comparable exocytotic mechanisms. In fact, it has been shown previously that multiple SNARE isoforms and SNARE-associated proteins including syntaxin 1, VAMP2, SNAP25 and Munc-18 mediate exocytosis in both neurons as well as β-cells (Roder et al., 2016; Sudhof, 2013). In addition, two of the key scaffold proteins of the active zone, ELKS and Bassoon, have been shown to colocalize with docked insulin vesicles (Ohara-Imaizumi et al., 2005).

What might be more surprising is the presence of CMSC proteins in the IDC. Previous studies show that the CMSC accumulates around FAs, thereby facilitating FA turnover in migrating cells. CLASPs bridge microtubule plus-ends with the CMSC, thereby creating transport routes for matrix metalloproteinases that sever extracellular matrix resulting in the disassembly of FAs (Stehbens et al., 2014). Also in pancreatic β-cells, we found CLASP1 to be present at the IDC suggesting a comparable mechanism in which insulin vesicles are transported to IDCs. Although multiple lines of research show that insulin vesicles are transported over microtubules by kinesins (Boyd et al., 1982; Heaslip et al., 2014; Lacy et al., 1968; Suprenant and Dentler, 1982; Varadi et al., 2002), more recent evidence indicates that microtubules negatively regulate insulin secretion by facilitating transport away from insulin secretion sites. In fact, it was shown that high glucose treatment destabilized microtubules, thereby preventing insulin granule withdrawal from the cell periphery. Microtubule depolymerization by nocodazole treatment increased insulin granule concentration at exocytotic sites and dramatically enhanced insulin secretion (Zhu et al., 2015). Whether this is due to blocked granule withdrawal or enhanced actomyosin contractility, activated FAs and recruitment of the IDC as a result of microtubule disassembly and Rho activation (Etienne-Manneville,

2013; Rape et al., 2011) would require further investigation. To better understand the role of microtubules in insulin transport and to determine whether the CMSC functions as a microtubule stabilizing complex in pancreatic β-cells, more detailed cell biological studies are required.

Recent work from our lab and others showed that CMSCs are linked to FAs through members of the KANK protein family (Bouchet et al., 2016; Sun et al., 2016). KANKs directly bind to Talin, a core protein of FAs (Calderwood and Ginsberg, 2003). As Talin forges the direct link between the CMSC and actin, together with KANK it might play a profound role in the mechanisms underlying actomyosin contractility and IDC recruitment to FAs. Interestingly, the connection between actomyosin contractility and FA activation appeared to be key in the regulation of insulin secretion. More specifically, is was shown that the inhibition of myosin II or its upstream regulator myosin light chain kinase associates with shortening of actin stress fibers, reduced numbers of FAs and a decrease in the number of insulin granules in close proximity to the basal membrane in pancreatic β-cells. As a result, GSIS was strongly affected (Arous et al., 2013). Contracting actin stress fibers lead to activation of FAs, a classic example of mechanotransduction (Schwartz, 2010). Detailed analysis revealed that FA activation, and more specifically the phosphorylation of FAK and Paxillin, is crucial for GSIS (Cai et al., 2012; Rondas et al., 2011; Rondas et al., 2012). It was shown that the phosphorylation of these FA components results in remodeling of the actin cytoskeleton (Rondas et al., 2011), a process essential for insulin granule docking and fusion. In addition, FAK and Paxillin phosphorylation activated the MAPK/ERK pathway (Rondas et al., 2012), which on itself has been associated with actin remodeling and insulin secretion (Tomas et al., 2006). These results were confirmed *in vivo* by creating a β-cell specific FAK knockout mouse which exhibited normal glucose sensing and preserved Ca^{2+} influx but significantly impaired insulin secretion (Cai et al., 2012).

Taken together, our results fit well with the idea that FA activation plays a role in insulin secretion upon glucose stimulation. We show that, in addition to actin remodeling, FA activation leads to the assembly of insulin docking platforms that can potentially enhance the secretion of insulin. Our data have broadened our knowledge regarding the mechanisms underlying insulin secretion and could help in understanding the molecular background of diabetes type II that affects hundreds of millions of people around the world.

Experimental procedures

Cell culture and transfection

INS-1E cells were obtained from Eelco de Koning (Hubrecht Institute Utrecht, The Netherlands) and cultured in Roswell Park Memorial Institute (RPMI) medium 1640 (Gibco, Life Technologies) supplemented with 10% fetal calf serum (FCS) (GE Healthcare Life Sciences), 10 mM Hepes pH 7.4, 1 mM Sodium Pyruvate (Gibco, Life Technologies), 55 μM β-mercaptoethanol (Gibco, Life Technologies) and 11 mM glucose. The cells were routinely checked for mycoplasma contamination using the MycoAlert™ Mycoplasma Detection Kit (Lonza). For glucose starvation prior to GSIS induction, INS-1E cells were cultured for 18 hours in culture medium as described above supplemented with 2 mM glucose. GSIS was induced by culturing glucose starved INS-1E cells in culture medium as described above supplemented with 25 mM glucose.

Lipofectamine RNAiMAX (Invitrogen) was used to transfect INS-1E cells with 20 nM siRNAs. Corresponding experiments were performed 72 h after siRNA transfection.

siRNAs

siRNAs targeting the following sequences were purchased from Sigma-Adrich: LL5β, 5'-GGAGATTCTAGATCATCTA-3' and control targeting luciferase 5'-CGTACGCGGAATACTTCGA-3' (Dambournet et al., 2011).

Antibodies, drugs and chemicals

Mouse monoclonal antibodies against the following proteins were used: LL5β (Joshua Sanes, Harvard University Cambridge, USA); Bassoon (Enzo life sciences); Paxillin (BD biosciences) and Glucagon (Abcam). Rabbit polyclonal antibodies against the following proteins were used: ELKS (Proteintech); Liprin-α1 (Spangler et al., 2011); Liprin-β1 (van der Vaart et al., 2013); KANK1 (Atlas antibodies); RIM1/2 (Synaptic systems); CLASP1 (Mimori-Kiyosue et al., 2005) and FAK phospho-tyrosine 397 (pFAK) (Biosource). Guinea pig polyclonal antibody against insulin was purchased from DAKO. Alexa-Fluor-405-, Alexa-Fluor-488- and Alexa-fluor-594-conjugated goat antibodies against mouse, rabbit and guinea pig were purchased from Life Technologies. For Western blotting, IRDye-680LT- and IRDye-800CW-conjugated goat antibodies against mouse and rabbit IgG were purchased from Li-Cor Biosciences.

Alexa-Fluor-488- and Alexa-Fluor-595-conjugated phalloidin were purchased from Life Technologies. Nocodazole was purchased from Sigma-Aldrich and used at a concentration of 10 μM. Blebbistatin was purchased from Enzo Life Sciences and used at a concentration of 50 μM. ROCK1 inhibitor Y-27632 was purchased from Sig-

ma-Aldrich and used at a concentration of 10 μM. Cells were treated with nocodazole, blebbistatin or Y-27632 for 1 h prior to fixation.

Immunofluorescence staining of fixed samples

For immunofluorescence staining, cells were fixed with either 4% PFA for 20 min at room temperature (staining for insulin, LL5β, RIM1/2, Bassoon, Paxillin, Glucagon, phalloidin) or −20°C MeOH for 10 min (staining for LL5β, ELKS, Liprin-α1, Liprin-β1, KANK1, RIM1/2, Bassoon, CLASP1, pFAK) followed by permeabilization with 0.2% Triton X-100 for 2 min. Next, samples were blocked with 1% BSA diluted in PBS supplemented with 0.05% Tween-20 for 45 min and sequentially incubated with primary antibodies for 1 h and fluorescently labeled secondary antibodies for 45 min. Finally, samples were washed, dried and mounted in DAPI-containing Vectashield (Vector laboratories).

Isolation and culture of pancreatic islets

Murine pancreatic islets were isolated from adult 3-6 month old mice that were sacrificed by cervical dislocation. The isolated pancreas was rinsed in PBS cut into small pieces with surgical blades and incubated in 3 mg/ml collagenase (C9263, Sigma) dissolved in RPMI 1640 (Gibco, Life Technologies) in a total volume of 3 ml/pancreas for 20 min at 37°C. During incubation, solution was shaken rigorously. Next, 6 ml of cold RPMI 1640 supplemented with 10% FCS, 10 mM Hepes pH 7.4, 1 mM Sodium Pyruvate, 55 μM β-mercaptoethanol and 11 mM glucose was added to the solution, followed by two wash steps using centrifugation (5 min, 200g, 4°C). After washing, the isolated islets were resuspended in 5ml RPMI 1640 supplemented as described above, handpicked using a pipette and transferred to new culture dishes until almost no exocrine tissue was left. Finally the islets where transferred to culture dishes containing Matrigel-coated coverslips. Coverslips where coated with 388 μg/ml Matrigel (Corning) in PBS for 2 h at 37°C. Isolated islets were cultured in RPMI 1640 supplemented as described above until islets were fully attached to coated coverslips. After 3 days in culture, islets were fixed and immuno-stained for proteins of interest. All animal experiments were performed in compliance with the institutional guidelines for the welfare of experimental animals approved by the Animal Ethical Review Committee (DEC 2014.I.03.020) of Utrecht University, the Netherlands.

Microscopy and image analysis

Fixed and stained cell lines were imaged using widefield fluorescence illumination on a Nikon Eclipse 80i upright microscope equipped with a CoolSNAP HQ2 CCD camera (Photometrics), an Intensilight C-HGFI precentered fiber illuminator (Nikon), ET-DAPI, ET-EGFP and ETmCherry filters (Chroma), controlled by Nikon NIS Br software and

using a Plan Apo VC 23 100x NA 1.4 oil, Plan Apo VC 60x NA 1.4 oil or a Plan Fluor 20x MI NA 0.75 oil objective (Nikon).

For quantification of insulin secretion, fluorescence intensity of insulin signal acquired with the setup described above was measured and corrected for the cell surface area using ImageJ 1.50b. For FA surface area quantification, fluorescent Paxillin signal acquired with microscope system as described above, was subjected to maximum entropy thresholding followed by automated particle analysis, thereby calculating the average FA surface area using ImageJ 1.50b. For presentation, images were adjusted for brightness using ImageJ 1.50b.

Fixed and stained isolated pancreatic islets were imaged using confocal fluorescence illumination on a Nikon Eclipse Ti microscope equipped with a perfect focus system (PFS, Nikon), a spinning-disc-based confocal scanner unit (CSU-X1-A1, Yokogawa), an Evolve 512 EMCCD camera (Photometrics) attached to a 2.0× intermediate lens (Edmund Optics), a super-high-pressure mercury lamp (C-SHG1, Nikon), a Roper Scientific custom-made set of Stradus 405-nm (100 mW, Vortran), Calypso 491-nm (100 mW, Cobolt) and Jive 561-nm (100 mW, Cobolt) lasers, a set of ET-BFP2, ET-EGFP, ET-mCherry and ET-EGFP-mCherry filters (Chroma) for wide-field fluorescence observation, a set of ET460/50m, ET525/50m or ET535/30m (green), ET630/75m (red) and ET-EGFP/mCherry filters (Chroma) for spinning-disc-based confocal imaging and a motorized stage MS-2000-XYZ with Piezo Top Plate (ASI). The microscope setup was controlled by MetaMorph 7.7.11.0 software. Images were acquired using Plan Fluor 10× NA 0.3 air, Plan Fluor 20× MI NA 0.75 oil, Apo LWD λS 40x NA 1.15 water, Plan Apochromat λ 60× NA 1.4 oil and Plan Apo VC 60× NA 1.4 oil objectives. Images are presented as maximum projections of 0.5-µm-step z-scans and adjusted for brightness using ImageJ 1.50b.

Super resolution imaging of CMSC proteins in INS-1E cells was performed using gated confocal fluorescence illumination on a Leica TCS SP8 STED3X SMD FLIM Super Resolution and confocal microscope equipped with Adaptive Focus Control, a filter free Spectral Leica SP detector and an internal Leica GaAsP HyD hybrid detector, a 405 nm DMOD, 440nm pulsed FLIM, Argon laser, a fully tunable supercontinuum white laser (470 to 670 nm) and 592 nm, 660 nm and 775nm STED depletion laser. Images were acquired using a HC PL APO Cs2 100x/1.40 oil objective. Alexa-Fluor-488-conjugated antibodies were excited with the 488 nm supercontinuum white laser (80MHz) and depleted with the CW 592 nm STED depletion laser. Alexa-Fluor-594-conjugated antibodies were excited with the 594 nm super continuum white laser (80MHz) and depleted with the 775 nm STED pulsed depletion laser. For presentation, images were adjusted for brightness using ImageJ 1.50b.

References

Arous, C., and P.A. Halban. 2015. The skeleton in the closet: actin cytoskeletal remodeling in beta-cell function. Am J Physiol Endocrinol Metab. 309:E611-620.

Arous, C., D. Rondas, and P.A. Halban. 2013. Non-muscle myosin IIA is involved in focal adhesion and actin remodelling controlling glucose-stimulated insulin secretion. Diabetologia. 56:792-802.

Asfari, M., D. Janjic, P. Meda, G. Li, P.A. Halban, and C.B. Wollheim. 1992. Establishment of 2-mercaptoethanol-dependent differentiated insulin-secreting cell lines. Endocrinology. 130:167-178.

Ashcroft, F.M., D.E. Harrison, and S.J. Ashcroft. 1984. Glucose induces closure of single potassium channels in isolated rat pancreatic beta-cells. Nature. 312:446-448.

Astro, V., and I. de Curtis. 2015. Plasma membrane-associated platforms: dynamic scaffolds that organize membrane-associated events. Sci Signal. 8:re1.

Barg, S., X. Ma, L. Eliasson, J. Galvanovskis, S.O. Gopel, S. Obermuller, J. Platzer, E. Renstrom, M. Trus, D. Atlas, J. Striessnig, and P. Rorsman. 2001. Fast exocytosis with few Ca(2+) channels in insulin-secreting mouse pancreatic B cells. Biophys J. 81:3308-3323.

Bouchet, B.P., R.E. Gough, Y.C. Ammon, D. van de Willige, H. Post, G. Jacquemet, A.M. Altelaar, A.J. Heck, B.T. Goult, and A. Akhmanova. 2016. Talin-KANK1 interaction controls the recruitment of cortical microtubule stabilizing complexes to focal adhesions. Elife. 5.

Boyd, A.E., 3rd, W.E. Bolton, and B.R. Brinkley. 1982. Microtubules and beta cell function: effect of colchicine on microtubules and insulin secretion in vitro by mouse beta cells. J Cell Biol. 92:425-434.

Burridge, K., and M. Chrzanowska-Wodnicka. 1996. Focal adhesions, contractility, and signaling. Annu Rev Cell Dev Biol. 12:463-518.

Cai, E.P., M. Casimir, S.A. Schroer, C.T. Luk, S.Y. Shi, D. Choi, X.Q. Dai, C. Hajmrle, A.F. Spigelman, D. Zhu, H.Y. Gaisano, P.E. MacDonald, and M. Woo. 2012. In vivo role of focal adhesion kinase in regulating pancreatic beta-cell mass and function through insulin signaling, actin dynamics, and granule trafficking. Diabetes. 61:1708-1718.

Calderwood, D.A., and M.H. Ginsberg. 2003. Talin forges the links between integrins and actin. Nat Cell Biol. 5:694-697.

Chrzanowska-Wodnicka, M., and K. Burridge. 1996. Rho-stimulated contractility drives the formation of stress fibers and focal adhesions. J Cell Biol. 133:1403-1415.

Cook, D.L., and C.N. Hales. 1984. Intracellular ATP directly blocks K+ channels in pancreatic B-cells. Nature. 311:271-273.

Curry, D.L., L.L. Bennett, and G.M. Grodsky. 1968. Dynamics of insulin secretion by the perfused rat pancreas. Endocrinology. 83:572-584.

Dambournet, D., M. Machicoane, L. Chesneau, M. Sachse, M. Rocancourt, A. El Marjou, E. Formstecher, R. Salomon, B. Goud, and A. Echard. 2011. Rab35 GTPase and OCRL phosphatase remodel lipids and F-actin for successful cytokinesis. Nat Cell Biol. 13:981-988.

Daniel, S., M. Noda, S.G. Straub, and G.W. Sharp. 1999. Identification of the docked granule pool responsible for the first phase of glucose-stimulated insulin secretion. Diabetes. 48:1686-1690.

Etienne-Manneville, S. 2013. Microtubules in cell migration. Annu Rev Cell Dev Biol. 29:471-499.

Grodsky, G., H. Landahl, D. Curry, and L. Bennett. 1970. A two-compartmental model for insulin secretion. Adv Metab Disord. 1:Suppl 1:45-50.

Gundelfinger, E.D., and A. Fejtova. 2012. Molecular organization and plasticity of the cytomatrix at the active zone. Curr Opin Neurobiol. 22:423-430.

Heaslip, A.T., S.R. Nelson, A.T. Lombardo, S. Beck Previs, J. Armstrong, and D.M. Warshaw. 2014. Cytoskeletal dependence of insulin granule movement dynamics in INS-1 beta-cells in response to glucose. PLoS One. 9:e109082.

Hida, Y., and T. Ohtsuka. 2010. CAST and ELKS proteins: structural and functional determinants of the presynaptic active zone. J Biochem.

148:131-137.

Hu, Y.L., S. Lu, K.W. Szeto, J. Sun, Y. Wang, J.C. Lasheras, and S. Chien. 2014. FAK and paxillin dynamics at focal adhesions in the protrusions of migrating cells. Sci Rep. 4:6024.

Ko, J., M. Na, S. Kim, J.R. Lee, and E. Kim. 2003. Interaction of the ERC family of RIM-binding proteins with the liprin-alpha family of multidomain proteins. J Biol Chem. 278:42377-42385.

Lacy, P.E., S.L. Howell, D.A. Young, and C.J. Fink. 1968. New hypothesis of insulin secretion. Nature. 219:1177-1179.

Lansbergen, G., I. Grigoriev, Y. Mimori-Kiyosue, T. Ohtsuka, S. Higa, I. Kitajima, J. Demmers, N. Galjart, A.B. Houtsmuller, F. Grosveld, and A. Akhmanova. 2006. CLASPs attach microtubule plus ends to the cell cortex through a complex with LL5beta. Dev Cell. 11:21-32.

Meglasson, M.D., and F.M. Matschinsky. 1986. Pancreatic islet glucose metabolism and regulation of insulin secretion. Diabetes Metab Rev. 2:163-214.

Merglen, A., S. Theander, B. Rubi, G. Chaffard, C.B. Wollheim, and P. Maechler. 2004. Glucose sensitivity and metabolism-secretion coupling studied during two-year continuous culture in INS-1E insulinoma cells. Endocrinology. 145:667-678.

Mimori-Kiyosue, Y., I. Grigoriev, G. Lansbergen, H. Sasaki, C. Matsui, F. Severin, N. Galjart, F. Grosveld, I. Vorobjev, S. Tsukita, and A. Akhmanova. 2005. CLASP1 and CLASP2 bind to EB1 and regulate microtubule plus-end dynamics at the cell cortex. J Cell Biol. 168:141-153.

Noordstra, I., and A. Akhmanova. 2017. Linking cortical microtubule attachment and exocytosis. F1000Res. 6:469.

O'Connor, M.D., H. Landahl, and G.M. Grodsky. 1980. Comparison of storage- and signal-limited models of pancreatic insulin secretion. Am J Physiol. 238:R378-389.

Ohara-Imaizumi, M., T. Ohtsuka, S. Matsushima, Y. Akimoto, C. Nishiwaki, Y. Nakamichi, T. Kikuta, S. Nagai, H. Kawakami, T. Watanabe, and S. Nagamatsu. 2005. ELKS, a protein structurally related to the active zone-associated protein CAST, is expressed in pancreatic beta cells and functions in insulin exocytosis: interaction of ELKS with exocytotic machinery analyzed by total internal reflection fluorescence microscopy. Mol Biol Cell. 16:3289-3300.

Olofsson, C.S., S.O. Gopel, S. Barg, J. Galvanovskis, X. Ma, A. Salehi, P. Rorsman, and L. Eliasson. 2002. Fast insulin secretion reflects exocytosis of docked granules in mouse pancreatic B-cells. Pflugers Arch. 444:43-51.

Orci, L., K.H. Gabbay, and W.J. Malaisse. 1972. Pancreatic beta-cell web: its possible role in insulin secretion. Science. 175:1128-1130.

Prentki, M., and F.M. Matschinsky. 1987. Ca2+, cAMP, and phospholipid-derived messengers in coupling mechanisms of insulin secretion. Physiol Rev. 67:1185-1248.

Rape, A., W.H. Guo, and Y.L. Wang. 2011. Microtubule depolymerization induces traction force increase through two distinct pathways. J Cell Sci. 124:4233-4240.

Roder, P.V., B. Wu, Y. Liu, and W. Han. 2016. Pancreatic regulation of glucose homeostasis. Exp Mol Med. 48:e219.

Rondas, D., A. Tomas, and P.A. Halban. 2011. Focal adhesion remodeling is crucial for glucose-stimulated insulin secretion and involves activation of focal adhesion kinase and paxillin. Diabetes. 60:1146-1157.

Rondas, D., A. Tomas, M. Soto-Ribeiro, B. Wehrle-Haller, and P.A. Halban. 2012. Novel mechanistic link between focal adhesion remodeling and glucose-stimulated insulin secretion. J Biol Chem. 287:2423-2436.

Rorsman, P., L. Eliasson, E. Renstrom, J. Gromada, S. Barg, and S. Gopel. 2000. The Cell Physiology of Biphasic Insulin Secretion. News Physiol Sci. 15:72-77.

Satin, L.S., and D.L. Cook. 1985. Voltage-gated Ca2+ current in pancreatic B-cells. Pflugers Arch. 404:385-387.

Schwartz, M.A. 2010. Integrins and extracellular matrix in mechanotransduction. Cold Spring Harb Perspect Biol. 2:a005066.

Seino, S., T. Shibasaki, and K. Minami. 2011. Dynamics of insulin secretion and the clinical implications for obesity and diabetes. J Clin Invest. 121:2118-2125.

Spangler, S.A., D. Jaarsma, E. De Graaff, P.S. Wulf,

A. Akhmanova, and C.C. Hoogenraad. 2011. Differential expression of liprin-alpha family proteins in the brain suggests functional diversification. J Comp Neurol. 519:3040-3060.

Stehbens, S.J., M. Paszek, H. Pemble, A. Ettinger, S. Gierke, and T. Wittmann. 2014. CLASPs link focal-adhesion-associated microtubule capture to localized exocytosis and adhesion site turnover. Nat Cell Biol. 16:561-573.

Sudhof, T.C. 2012. The presynaptic active zone. Neuron. 75:11-25.

Sudhof, T.C. 2013. A molecular machine for neurotransmitter release: synaptotagmin and beyond. Nat Med. 19:1227-1231.

Sun, Z., H.Y. Tseng, S. Tan, F. Senger, L. Kurzawa, D. Dedden, N. Mizuno, A.A. Wasik, M. Thery, A.R. Dunn, and R. Fassler. 2016. Kank2 activates talin, reduces force transduction across integrins and induces central adhesion formation. Nat Cell Biol. 18:941-953.

Suprenant, K.A., and W.L. Dentler. 1982. Association between endocrine pancreatic secretory granules and in-vitro-assembled microtubules is dependent upon microtubule-associated proteins. J Cell Biol. 93:164-174.

Tomas, A., B. Yermen, L. Min, J.E. Pessin, and P.A. Halban. 2006. Regulation of pancreatic beta-cell insulin secretion by actin cytoskeleton remodelling: role of gelsolin and cooperation with the MAPK signalling pathway. J Cell Sci. 119:2156-2167.

van der Vaart, B., W.E. van Riel, H. Doodhi, J.T. Kevenaar, E.A. Katrukha, L. Gumy, B.P. Bouchet, I. Grigoriev, S.A. Spangler, K.L. Yu, P.S. Wulf, J. Wu, G. Lansbergen, E.Y. van Battum, R.J. Pasterkamp, Y. Mimori-Kiyosue, J. Demmers, N. Olieric, I.V. Maly, C.C. Hoogenraad, and A. Akhmanova. 2013. CFEOM1-associated kinesin KIF21A is a cortical microtubule growth inhibitor. Dev Cell. 27:145-160.

Varadi, A., E.K. Ainscow, V.J. Allan, and G.A. Rutter. 2002. Involvement of conventional kinesin in glucose-stimulated secretory granule movements and exocytosis in clonal pancreatic beta-cells. J Cell Sci. 115:4177-4189.

Zhu, X., R. Hu, M. Brissova, R.W. Stein, A.C. Powers, G. Gu, and I. Kaverina. 2015. Microtubules Negatively Regulate Insulin Secretion in Pancreatic beta Cells. Dev Cell. 34:656-668.

6

General discussion

Ivar Noordstra[1]

[1]Cell Biology, Faculty of Science, Utrecht University, 3584 CH Utrecht, The Netherlands

General discussion

In this thesis, we have focused on the principles of organizing the microtubule network in multiple systems and processes including migrating breast cancer cells (Chapter 3), epithelial cells (Chapter 4) and pancreatic β-cells (Chapter 5). By studying the underlying molecular mechanisms controlling the microtubule organization in these systems, we found both overlapping and system-specific molecular players that are essential for proper cell function. In this chapter, we will combine our findings, place them in a broader context and make suggestions for future research.

Microtubules in cell migration – Breast cancer metastasis

Cell migration through a 3D matrix is required for numerous physiological functions such as tissue morphogenesis, regeneration and immune surveillance (Friedl and Wolf, 2010; Ridley et al., 2003) and is activated in epithelia undergoing malignant transformation as the initial step of metastatic dissemination (Chaffer and Weinberg, 2011). An important player in cell migration is the microtubule cytoskeleton (Etienne-Manneville, 2013; Kaverina and Straube, 2011). The investigation of microtubule function is of particular interest because microtubule-targeting agents (MTAs) are widely used to treat cancer, and their strong antimetastatic action cannot be fully explained by their anti-mitotic effect (Komlodi-Pasztor et al., 2011; Mitchison, 2012). For example, it was shown that treatment with low doses of the microtubule stabilizing drug paclitaxel, which did not block cell proliferation, reduced invasiveness of mesenchymal breast cancer cells (Tran et al., 2009). Complete destruction or strong perturbation of microtubules by stabilizing or destabilizing MTAs indicated that microtubules are required for the formation of invadopodia, endothelial cell branches and pseudopods in 3D (Myers et al., 2011; Oyanagi et al., 2012; Schoumacher et al., 2010), as well as for cell migration in strong confinement (Balzer et al., 2012). 3D cultures of mesenchymal cells showed that long pseudopods contain a microtubule core and are lost after short-term treatments with high doses of nocodazole or paclitaxel (Rhee et al., 2007) or long-term treatments with low doses of paclitaxel (Kikuchi and Takahashi, 2008).

In chapter 3, we have systematically analyzed how one of the most basic properties of cellular microtubules, the ability to grow rapidly and persistently, regulates interstitial invasion of mesenchymal cells. We uncovered a fundamental role for microtubule growth persistence in controlling mesenchymal cell shape and invasiveness in 3D matrix both *in vitro* and *in vivo* (Figure 1). When microtubule growth persistence was inhibited in interphase cells by SLAIN2 inactivation, pseudopod elongation could not take place and 3D motility was suppressed. Because of such a striking defect, we expected to detect alterations in the factors usually associated with both dynamic microtubules and 3D

morphogenesis, such as Rho GTPase activity, vesicle trafficking and focal adhesions (Caswell et al., 2008; Caswell et al., 2007; Friedl and Alexander, 2011; Jacquemet et al., 2013; Sanz-Moreno and Marshall, 2010). Surprisingly, by using biochemical assays and high-resolution imaging, we found no evidence indicating that any of these players were altered in a way that could explain the loss of pseudopod elongation. Besides, we established that microtubule growth at the leading edge persists much longer in 3D than in 2D cell cultures. We found that this was associated with frequent microtubule buckling, a phenomenon previously associated with resistance to compression (Brangwynne et al., 2006; Dogterom et al., 2005; Dogterom and Yurke, 1997; Hotani and Miyamoto, 1990; Ingber, 2003; Waterman-Storer et al., 1995). By depolymerizing actin, we showed that SLAIN2/chTOG-dependent microtubule growth persistence promotes the ability of microtubules to push the plasma membrane. However, in the presence of intact F-actin, not only the SLAIN2/ch-TOG complex but also CLASP1 was essential to prevent microtubule catastrophes at the tips of cell protrusions. It is possible that both SLAIN2/ch-TOG and CLASP1 are needed to stabilize microtubule plus ends, because by stiffening the cortex or inducing retrograde flow, F-actin increases the force applied to microtubule ends, a factor previously shown to be a potent catastrophe inducer (Janson et al., 2003). Another possibility is that F-actin-rich cortex recruits microtubule depolymerases that induce catastrophes. Catastrophe suppression at pseudopod tips likely involves other factors, such as the microtubule-actin crosslinking proteins MACFs, with which CLASPs are known to cooperate (Drabek et al., 2006), and cortical proteins responsible for microtubule capture, such as the CLASP-interacting protein LL5β previously implicated in 3D cell migration (Astro et al., 2014; Lansbergen et al., 2006) and discussed in Chapter 2.

The notion that persistently growing microtubules are the primary driver of cell protrusions in 3D would be inconsistent with a large body of literature demonstrating that membrane protrusions depend on actin polymerization (Friedl and Alexander, 2011; Olson and Sahai, 2009; Sanz-Moreno and Marshall, 2010). Importantly, we found that Rac1 inhibition completely suppressed small protrusions that were still formed in SLAIN2-inactivated cells in 3D. Moreover, our simultaneous imaging of microtubules and membrane dynamics shows that small lamellae first emerge at pseudopod tips and are subsequently populated by microtubules. We therefore favor the idea that the function of persistently growing microtubules is not to initiate protrusions but prevent their retraction. This notion is consistent with our observation that pseudopod retraction occurs gradually upon low-dose MTA treatment, most likely due to the fact that integrin-based adhesions are not detached immediately upon MTA addition. In line with this idea, microtubule stabilization induced by the overexpression of neuronal microtubule associated proteins (MAPs) prevented pseudopod retraction when microtubule growth was suppressed. However, in these conditions, pseudopod dynamics was blocked and

the cells appeared "frozen" in a particular shape. This indicates that dynamic microtubules are required for cell shape remodeling but resistance to depolymerization is sufficient to prevent pseudopod collapse. The importance of microtubules in cell elongations is supported by studies in different model systems, such as astrocytes, neurons, muscle cells and even Hela cells (Etienne-Manneville, 2013; Mogessie et al., 2015; Picone et al., 2010).

We propose a model in which persistently growing microtubules have a load-bearing function in supporting elongation of mesenchymal cells on substrates: persistently growing microtubules populate newly formed protrusions and bias them against retraction (Figure 1). It is possible that intermediate filaments, the distribution of which is microtubule-dependent, contribute to this function, as was proposed for in-

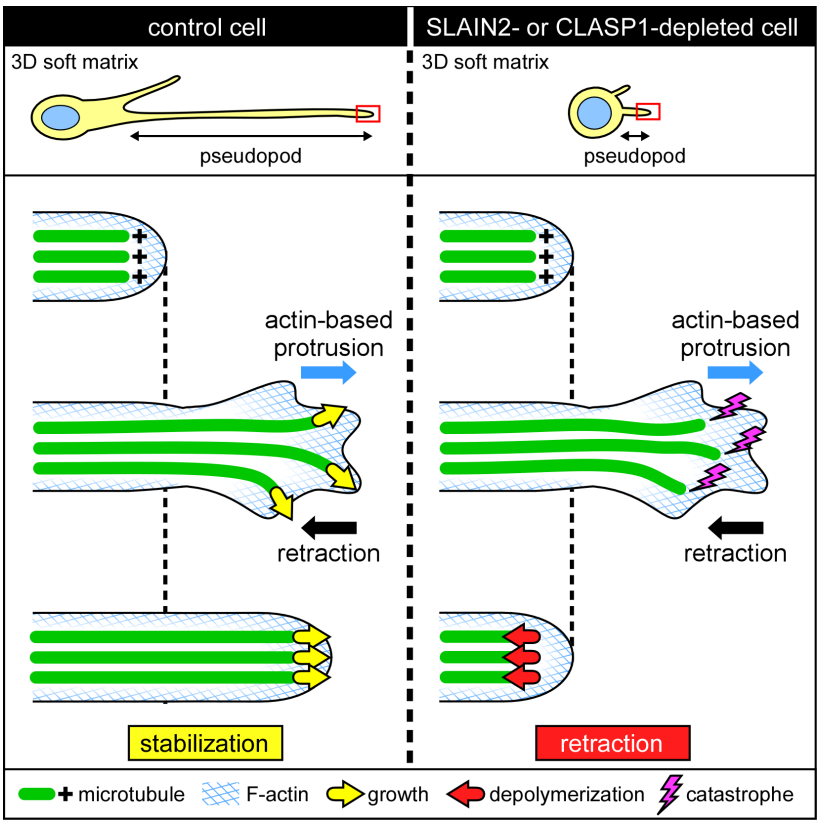

Figure 1. Model for the role of microtubule growth persistence in pseudopod elongation in soft matrix

In control cells persistently growing microtubules populate newly formed actin-based protrusions and bias them against retraction (left). When SLAIN2 or CLASP1 are inactivated, microtubules engaged in the newly formed protrusions undergo catastrophe and are unable to counteract retraction (right).

vadopodia (Schoumacher et al., 2010). As the cell extends, microtubules organize into bundles along the long cell axis and provide physical support for the pseudopod elongation by counteracting membrane contractility. This function is only essential for cell morphology when cells are spread through integrin-based attachment to a soft substrate. On a hard substrate, physical support for the cell spreading is provided by the substrate itself (Ingber, 2003). Of note, cells with attenuated microtubule growth can still efficiently move when cultured on top of a soft matrix, although they cannot form long pseudopods. However, such cells are immobilized when embedded within the same matrix because they cannot form distant adhesions relying on elongated pseudopods (Friedl and Alexander, 2011). Importantly, our study shows for the first time that interphase-specific attenuation of microtubule growth inhibits breast tumor invasion and metastasis, and that this effect does not relate to mitosis or proliferation block. This supports the idea that inhibition of interstitial invasion by MTAs at low concentrations which are clinically relevant (Tredan et al., 2007) is a possible factor of their anti-metastatic effect. Our data directly indicate that not only mitotic but also interphase microtubule dynamics is an important therapeutic target. Based on these findings, one can envisage development of clinical treatment regimens using low dosage adjuvant MTAs to prevent local tumor cell invasion and dissemination.

Microtubules in morphogenesis – Epithelial polarity

The microtubule cytoskeleton regulates cell polarity by spatially organizing membrane trafficking and signaling processes. In living cells, the microtubule minus ends are stabilized by binding to specific molecules or structures, such as the ɣ-tubulin ring complex (ɣ-TuRC) located at the centrosome or other microtubule-organizing centers (Dammermann et al., 2003; Wu and Akhmanova, 2017). Although in many types of cultured cells, microtubules form a radial array organized by the centrosome and the adjacent Golgi apparatus, in polarized epithelial cells most microtubules do not emanate from the centrosome. Instead they are arranged along the apico-basal axis, with the minus ends located at the apical side (Bacallao et al., 1989; Mogensen et al., 1989; Troutt and Burnside, 1988). This specific non-centrosomal microtubule organization can be controlled by moving components of the ɣ-TuRC to the apical regions of the cell. In fact, it has been shown that the centrosomal anchoring protein ninein is released from the centrosome and moves in a microtubule-dependent manner to non-centrosomal apical sites (Moss et al., 2007). More detailed analysis revealed a mechanism in which CLIP-170 and IQGAP1 facilitate the recruitment of ninein to non-centrosomal microtubule organizing centers in a process promoted by active Rac1 (Goldspink et al., 2017). Interestingly, CLIP-170 and IQGAP1 are also involved in capturing and stabilizing microtubule plus ends at the cell cortex, a mechanism important for the regulation of exocytosis as we discussed in Chapter 2. In addition to ɣ-TuRC associated proteins, also proteins that

bind to microtubule minus ends independently of ɣ-tubulin can control and maintain a non-centrosomal microtubule organization. The most notable example of the latter are the members of calmodulin-regulated spectrin associated protein (CAMSAP)/Patronin family which recognize and decorate free microtubule minus ends, thereby protecting them from depolymerization (Goodwin and Vale, 2010; Hendershott and Vale, 2014; Jiang et al., 2014; Tanaka et al., 2012). Detailed analysis in intestinal epithelial layers both *in vitro* and *in vivo* revealed a pivotal role for CAMSAP3 in orienting the apico-basal polarity of microtubules (Toya et al., 2016).

In Chapter 4, we studied the molecular mechanisms underlying the apical localization of CAMSAP3 and analyzed its role in epithelial morphogenesis. We found that the spectraplakin ACF7 interacts with CAMSAP3 and that ACF7 is required for the apical recruitment of CAMSAP3 in polarized epithelial layers. ACF7 has previously been shown to also interact with the microtubule plus-end tracking protein EB1 through its C-terminal SxIP motif and with the microtubule lattice through its GAS2 domain (Alves-Silva et al., 2012; Applewhite et al., 2010; Honnappa et al., 2009; Kodama et al., 2003; Sun et al., 2001). We found that the binding of ACF7 to CAMSAP3 is mediated by a specific set of spectrin repeats in the middle of the molecule. Interestingly, ACF7 does not show an exclusive apical localization in polarized epithelial layers. How is the interaction between CAMSAP3 decorated microtubule minus ends and ACF7 then restricted to the apical side of the cells? A plausible explanation comes from a study performed in Drosophila embryos (Nashchekin et al., 2016). They showed that Par-1 kinase prevents the association of the ACF7 orthologue Shot with the posterior actin cortex, thereby restricting the formation of non-centrosomal microtubule organizing centers to the anterior and lateral cortex. The interaction of Shot with the cortex depends on its N-terminal calponin homology domains, which bind to F-actin (Lee and Kolodziej, 2002; Leung 1999). Despite this interaction, *in vitro* experiments did not reveal any phosphorylation of the actin binding domains by Par-1 (Nashchekin et al., 2016). Therefore, it seems to be more likely that Par-1 acts by modifying the cortex to block the binding of Shot. Par-1, also known as microtubule affinity regulating kinase (MARK), is a protein kinase associated with the phosphorylation of microtubule associated proteins (Drewes et al., 1997). Although there is no direct evidence for CAMSAP3 phosphorylation by MARK, specific phosphorylation at the basal regions of the cell could potentially restrict ACF7-CAMSAP3 interaction to the apical domain of epithelial cells.

In polarized epithelial layers the formation of the actin brush border depends on the dynein-based apical accumulation of Rab11A recycling endosomes. These endosomes are apically captured by myosin VB and carry atypical protein kinase C (aPKC), the aPKC activator phosphoinositide-dependent protein kinase 1 (PDK1) (Dhekne et al., 2014; Kravtsov et al., 2014), and the Ste20-like protein kinase Mst4, which contribute to the structural differentiation of the apical domain by promoting microvilli develop-

ment through phosphorylation of ezrin (Dhekne et al., 2014). In addition to recycling endosome associated phosphorylation, an alternative theory has been proposed in which Lymphocyte-oriented-kinase (LOK) specifically phosphorylates PIP2 bound ezrin to activate it (Pelaseyed et al., 2017). Mutations in the MYO5B gene, encoding myosin VB have been associated with microvillus inclusion disease (MVID), a rare enteropathy that is clinically characterized by severe diarrhea and nutrient malabsorption (Cutz et al., 1989). The disease is caused by mispositioning of Rab11A recycling endosomes, which shift from an apical distribution in normal enterocytes to a subnuclear position in MVID enterocytes. As a result, the formation of apical microvilli is strongly perturbed and microvilli-lined inclusion bodies are formed (Dhekne et al., 2014; Szperl et al., 2011). Although we did not detect any microvilli inclusion bodies, the CRISPR/Cas9-mediated knockout of CAMSAP3 did strongly affected actin brush border formation in epithelial cells. Detailed analysis revealed a conversion of the microtubule network from apico-basal in wild-type cells to centrosomal in CAMSAP3 knockout cells. This led to the dynein driven accumulation of Rab11A vesicles around the centrosome, perturbed apical Rab11A signaling and strongly affected microvilli formation (Figure 2). In contrast to our findings, mice expressing nonfunctional CAMSAP3 displayed a normal actin brush border (Toya et al., 2016). How can this be reconciled with our results? One plausible explanation could be the redundancy of CAMSAP3 with ɣ-tubulin and ninein. In Caenorhabditis elegans it was shown that ɣ-tubulin acts with the ninein homologue NOCA-1 to assemble non-centrosomal microtubule arrays, and that in some cell types this process is redundant with the microtubule minus end stabilization by the CAMSAP3 homologue Patronin (Wang et al., 2015). Another explanation could be the gradual centrosome inactivation during long-term differentiation of epithelial cells, a process that is regulated by biochemically and functionally distinct ɣ-tubulin complexes that are differentially regulated (Muroyama et al.,

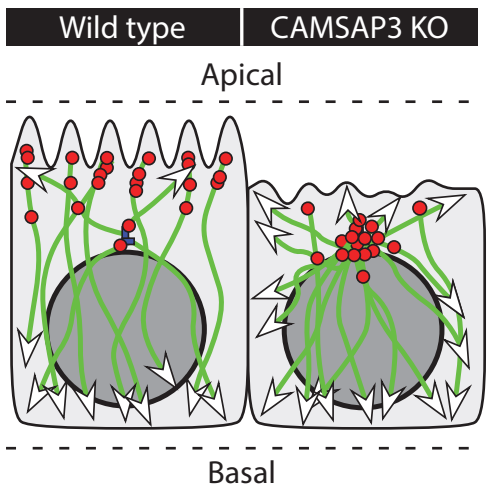

Figure 2. Model of the microtubule organization and Rab11A recycling endosome delivery in wild type and CAMSAP3 knockout epithelial cells

In wild type cells, microtubule minus ends are anchored by CAMSAP3 to the apical side, thereby facilitating the apical delivery of Rab11A recycling endosomes and brush border formation (left). In CAMSAP3 knockout cells, microtubule minus ends are anchored at the centrosome resulting in pericentrosomal delivery of Rab11A recycling endosomes and strongly affected brush border formation (right). KO, knockout.

2016). In line with this idea, the microtubule network in polarized epithelial layers of mice expressing nonfunctional CAMSAP3 became disorganized instead of centrosomal (Toya et al., 2016). This disorganized microtubule organization is likely to delay but not to block apical localization of Rab11A vesicles and microvilli formation.

Our work shows how non-centrosomal microtubules can break symmetry thereby creating polarity that is essential for proper functioning of the cells. Studying defects in microtubule organization can increase our understanding of diseases like MVID that are caused by polarity problems and the mislocalization of cellular cargo.

Microtubules in metabolism – Insulin secretion

As discussed above, the major tracks for vesicular transport are microtubules. Vesicles are transported along microtubules by two types of motors: kinesins, which are mostly plus-end-directed, and cytoplasmic dynein, which moves to microtubule minus ends. In polarized epithelial layers, dynein is responsible for transporting Rab11A recycling endosomes to the microtubule minus ends, located at the apical membrane (Horgan et al., 2010; Khanal et al., 2016; Riggs et al., 2007). Here, Rab11A vesicles activate signaling pathways which ultimately lead to the establishment of microvilli (Dhekne et al., 2014). In Chapter 4, we have shown that the protein CAMSAP3 links the microtubule minus ends to the apical regions of the cell. At the moment, we are only beginning to understand the mechanisms responsible for cortical microtubule minus-end tethering. However, years of research revealed multiple protein complexes responsible for coordinating microtubule plus-end organization with the tethering, docking and secretion of exocytotic vesicles, as discussed in Chapter 2. One of those complexes has been described as the cortical microtubule stabilizing complex (CMSC), a large protein assembly composed of the PIP3 binding protein LL5β, the scaffold proteins ELKS, Liprin-α1 and Liprin-β1, and the focal adhesion interacting protein KANK1 (Bouchet et al., 2016; Lansbergen et al., 2006; van der Vaart et al., 2013). Both ELKS and the members of the Liprin-α1 family are also described as major components of the cytomatrix at the active zone (CAZ), the principle site of Ca^{2+}-dependent exocytosis of neurotransmitters at neuronal synapsis (Gundelfinger and Fejtova, 2012; Hida and Ohtsuka, 2010; Spangler and Hoogenraad, 2007; Sudhof, 2012). Importantly, CMSC and CAZ have multiple non-overlapping components; for example, CAZ does not contain either LL5β or KANK1 and does not appear to be directly connected to microtubules. Interestingly, ELKS has also been shown to participate in the docking and fusion of insulin vesicles in pancreatic β-cells. In fact, docking and secretion of insulin vesicles coincided with cortical clusters of ELKS, and the siRNA-mediated depletion of ELKS strongly abolished glucose stimulated insulin secretion (Ohara-Imaizumi et al., 2005).

In Chapter 5, we focused on the molecular machinery that underlies the docking of insulin vesicles upon glucose stimulation in pancreatic β-cells. Immunofluorescence

staining revealed that insulin vesicles dock on multiprotein complexes that consist of all previously mentioned CMSC proteins and proteins involved in the exocytosis of neurotransmitters at the presynaptic active zone (Figure 3). Since both neurotransmitter release and insulin secretion rely on Ca^{2+}-dependent exocytosis, their overlap in molecular machinery does not come as a big surprise. However, the differences between both systems raise many questions. As mentioned previously, LL5 and KANK homologues are not found at the pre-synapse. However, both proteins fulfill very specialized functions at the CMSC. LL5β links the CMSC to the membrane by interacting with PIP3 (Lansbergen et al., 2006; Paranavitane et al., 2003), but also links the CMSC to microtubule plus ends through a direct interaction with the +TIP CLASP (Hotta et al., 2010; Lansbergen et al., 2006). It has been shown that depletion of LL5β in HeLa cells disrupts the cortical localization of the CMSC (Lansbergen et al., 2006). Also in pancreatic β-cells LL5β depletion led to relocalization of RIM1/2, one of the pre-synaptic proteins present in the insulin docking complex (IDC). In addition, stimulated emission depletion (STED) microscopy showed that LL5β clusters are surrounded by other IDC subunits, indicating that LL5β forms the physical core of the IDC. Are microtubules linked to IDCs through CLASP and LL5β? As is the case for most vascular transport, insulin transport is facilitated by microtubules (Boyd et al., 1982; Heaslip et al., 2014; Lacy et al., 1968; Suprenant and Dentler, 1982; Varadi et al., 2002). Linking microtubules and thus insulin transport to exocytosis sites would therefore significantly increase the efficiency of insulin secretion. Although we have shown co-localization between CLASP and the IDC, more research needs to be done to test this hypothesis.

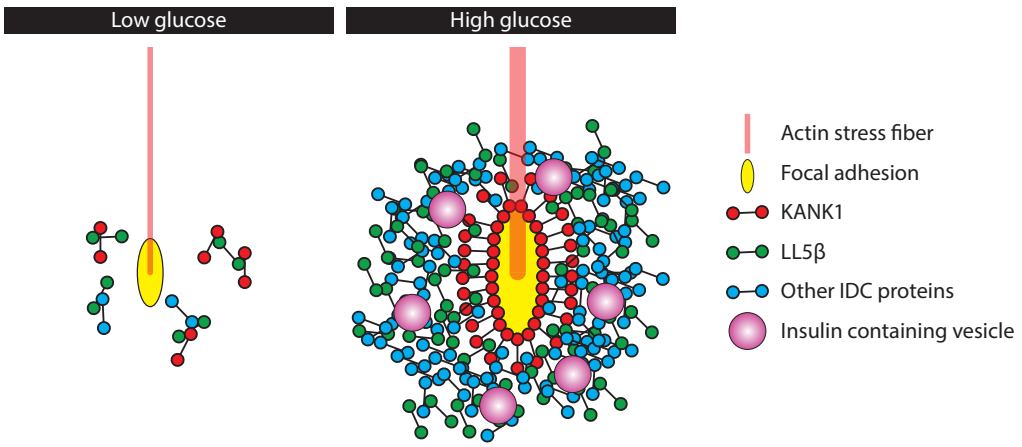

Figure 3. Model for the glucose stimulated recruitment of insulin docking complexes to focal adhesions

High glucose stimulation activates focal adhesions, resulting in the recruitment of KANK1, LL5β and other insulin docking complex proteins. Together these insulin docking complexes form potential hotspots for insulin secretion. IDC, insulin docking complex

CMSCs are linked to focal adhesions by KANK1, which directly interacts with talin, the core focal adhesion protein (Bouchet et al., 2016). KANK1 also binds to Liprin-β1, and the inhibition of either the Liprin-β1-KANK1 or the KANK1-talin interaction disrupts the CMSC localization and cortical microtubule capture around focal adhesions (Bouchet et al., 2016). Interestingly, we found that the IDC gets recruited to focal adhesions upon glucose stimulation. This is caused by an increase in actomyosin contractility which activates focal adhesions as has been shown before in Hela cells (Bouchet et al., 2016; Schwartz, 2010) (Figure 3). Focal adhesion activation upon glucose stimulation is an essential mechanism for insulin secretion (Arous and Halban, 2015; Arous et al., 2013; Cai et al., 2012; Rondas et al., 2011; Rondas et al., 2012). However, till now this was not directly linked to the recruitment of proteins involved in the docking of insulin vesicles. In fact, actomyosin dependent focal adhesion activation was shown to remodel the actin cytoskeleton (Rondas et al., 2011) and activate the MAPK/ERK pathway (Rondas et al., 2012), which on itself has been associated with actin remodeling and insulin secretion (Tomas et al., 2006). Taken together, we think that focal adhesion activation stimulates insulin secretion by remodeling the actin cytoskeleton, activating the MAPK/ERK pathway and recruiting the molecular machinery involved in the exocytosis of insulin vesicles. But why would insulin be secreted around focal adhesions? As β-cells are tightly packed in the pancreatic islets of Langerhans, their basal sides are pointing towards the extracellular matrix and blood vessels that need to drain the insulin from the pancreas. Secreting insulin around focal adhesions would therefore strongly increase the efficiency of draining insulin and transporting it through the body to insulin responsive tissues. Whether this hypothesis holds true should be tested by performing immunohistochemical stainings on isolated pancreas tissue to visualize protein complexes *in vivo*.

Concluding remarks

In this thesis we studied the molecular mechanisms underlying microtubule organization in different systems including 3D migrating breast cancer cells, polarized epithelial cells and pancreatic β-cells. We showed that a wide range of microtubule associated proteins is involved in maintaining polarity thereby securing proper cell functioning. Despite the differences, we also identified multiple common factors indicating that the mechanisms that control microtubule organization are strongly conserved in many biological processes ranging from cell migration and morphogenesis to metabolism. Collectively, our studies demonstrated that the microtubule cytoskeleton and its associated proteins are key-players in maintaining proper functioning of the building blocks of life, our cells.

References

Alves-Silva, J., N. Sanchez-Soriano, R. Beaven, M. Klein, J. Parkin, T.H. Millard, H.J. Bellen, K.J. Venken, C. Ballestrem, R.A. Kammerer, and A. Prokop. 2012. Spectraplakins promote microtubule-mediated axonal growth by functioning as structural microtubule-associated proteins and EB1-dependent +TIPs (tip interacting proteins). J Neurosci. 32:9143-9158.

Applewhite, D.A., K.D. Grode, D. Keller, A.D. Zadeh, K.C. Slep, and S.L. Rogers. 2010. The spectraplakin Short stop is an actin-microtubule cross-linker that contributes to organization of the microtubule network. Mol Biol Cell. 21:1714-1724.

Arous, C., and P.A. Halban. 2015. The skeleton in the closet: actin cytoskeletal remodeling in beta-cell function. Am J Physiol Endocrinol Metab. 309:E611-620.

Arous, C., D. Rondas, and P.A. Halban. 2013. Non-muscle myosin IIA is involved in focal adhesion and actin remodelling controlling glucose-stimulated insulin secretion. Diabetologia. 56:792-802.

Astro, V., S. Chiaretti, E. Magistrati, M. Fivaz, and I. de Curtis. 2014. Liprin-alpha1, ERC1 and LL5 define polarized and dynamic structures that are implicated in cell migration. J Cell Sci. 127:3862-3876.

Bacallao, R., C. Antony, C. Dotti, E. Karsenti, E.H. Stelzer, and K. Simons. 1989. The subcellular organization of Madin-Darby canine kidney cells during the formation of a polarized epithelium. J Cell Biol. 109:2817-2832.

Balzer, E.M., Z. Tong, C.D. Paul, W.C. Hung, K.M. Stroka, A.E. Boggs, S.S. Martin, and K. Konstantopoulos. 2012. Physical confinement alters tumor cell adhesion and migration phenotypes. FASEB J. 26:4045-4056.

Bouchet, B.P., R.E. Gough, Y.C. Ammon, D. van de Willige, H. Post, G. Jacquemet, A.M. Altelaar, A.J. Heck, B.T. Goult, and A. Akhmanova. 2016. Talin-KANK1 interaction controls the recruitment of cortical microtubule stabilizing complexes to focal adhesions. Elife. 5.

Boyd, A.E., 3rd, W.E. Bolton, and B.R. Brinkley. 1982. Microtubules and beta cell function: effect of colchicine on microtubules and insulin secretion in vitro by mouse beta cells. J Cell Biol. 92:425-434.

Brangwynne, C.P., F.C. MacKintosh, S. Kumar, N.A. Geisse, J. Talbot, L. Mahadevan, K.K. Parker, D.E. Ingber, and D.A. Weitz. 2006. Microtubules can bear enhanced compressive loads in living cells because of lateral reinforcement. J Cell Biol. 173:733-741.

Cai, E.P., M. Casimir, S.A. Schroer, C.T. Luk, S.Y. Shi, D. Choi, X.Q. Dai, C. Hajmrle, A.F. Spigelman, D. Zhu, H.Y. Gaisano, P.E. MacDonald, and M. Woo. 2012. In vivo role of focal adhesion kinase in regulating pancreatic beta-cell mass and function through insulin signaling, actin dynamics, and granule trafficking. Diabetes. 61:1708-1718.

Caswell, P.T., M. Chan, A.J. Lindsay, M.W. McCaffrey, D. Boettiger, and J.C. Norman. 2008. Rab-coupling protein coordinates recycling of alpha5beta1 integrin and EGFR1 to promote cell migration in 3D microenvironments. J Cell Biol. 183:143-155.

Caswell, P.T., H.J. Spence, M. Parsons, D.P. White, K. Clark, K.W. Cheng, G.B. Mills, M.J. Humphries, A.J. Messent, K.I. Anderson, M.W. McCaffrey, B.W. Ozanne, and J.C. Norman. 2007. Rab25 associates with alpha5beta1 integrin to promote invasive migration in 3D microenvironments. Dev Cell. 13:496-510.

Chaffer, C.L., and R.A. Weinberg. 2011. A perspective on cancer cell metastasis. Science. 331:1559-1564.

Cutz, E., J.M. Rhoads, B. Drumm, P.M. Sherman, P.R. Durie, and G.G. Forstner. 1989. Microvillus inclusion disease: an inherited defect of brush-border assembly and differentiation. N Engl J Med. 320:646-651.

Dammermann, A., A. Desai, and K. Oegema. 2003. The minus end in sight. Curr Biol. 13:R614-624.

Dhekne, H.S., N.H. Hsiao, P. Roelofs, M. Kumari, C.L. Slim, E.H. Rings, and S.C. van Ijzendoorn. 2014. Myosin Vb and Rab11a regulate phosphorylation of ezrin in enterocytes. J Cell Sci.

127:1007-1017.

Dogterom, M., J.W. Kerssemakers, G. Romet-Lemonne, and M.E. Janson. 2005. Force generation by dynamic microtubules. Curr Opin Cell Biol. 17:67-74.

Dogterom, M., and B. Yurke. 1997. Measurement of the force-velocity relation for growing microtubules. Science. 278:856-860.

Drabek, K., M. van Ham, T. Stepanova, K. Draegestein, R. van Horssen, C.L. Sayas, A. Akhmanova, T. Ten Hagen, R. Smits, R. Fodde, F. Grosveld, and N. Galjart. 2006. Role of CLASP2 in microtubule stabilization and the regulation of persistent motility. Curr Biol. 16:2259-2264.

Drewes, G., A. Ebneth, U. Preuss, E.M. Mandelkow, and E. Mandelkow. 1997. MARK, a novel family of protein kinases that phosphorylate microtubule-associated proteins and trigger microtubule disruption. Cell. 89:297-308.

Etienne-Manneville, S. 2013. Microtubules in cell migration. Annu Rev Cell Dev Biol. 29:471-499.

Friedl, P., and S. Alexander. 2011. Cancer invasion and the microenvironment: plasticity and reciprocity. Cell. 147:992-1009.

Friedl, P., and K. Wolf. 2010. Plasticity of cell migration: a multiscale tuning model. J Cell Biol. 188:11-19.

Goldspink, D.A., C. Rookyard, B.J. Tyrrell, J. Gadsby, J. Perkins, E.K. Lund, N. Galjart, P. Thomas, T. Wileman, and M.M. Mogensen. 2017. Ninein is essential for apico-basal microtubule formation and CLIP-170 facilitates its redeployment to non-centrosomal microtubule organizing centres. Open Biol. 7.

Goodwin, S.S., and R.D. Vale. 2010. Patronin regulates the microtubule network by protecting microtubule minus ends. Cell. 143:263-274.

Gundelfinger, E.D., and A. Fejtova. 2012. Molecular organization and plasticity of the cytomatrix at the active zone. Curr Opin Neurobiol. 22:423-430.

Heaslip, A.T., S.R. Nelson, A.T. Lombardo, S. Beck Previs, J. Armstrong, and D.M. Warshaw. 2014. Cytoskeletal dependence of insulin granule movement dynamics in INS-1 beta-cells in response to glucose. PLoS One. 9:e109082.

Hendershott, M.C., and R.D. Vale. 2014. Regulation of microtubule minus-end dynamics by CAMSAPs and Patronin. Proc Natl Acad Sci U S A. 111:5860-5865.

Hida, Y., and T. Ohtsuka. 2010. CAST and ELKS proteins: structural and functional determinants of the presynaptic active zone. J Biochem. 148:131-137.

Honnappa, S., S.M. Gouveia, A. Weisbrich, F.F. Damberger, N.S. Bhavesh, H. Jawhari, I. Grigoriev, F.J. van Rijssel, R.M. Buey, A. Lawera, I. Jelesarov, F.K. Winkler, K. Wuthrich, A. Akhmanova, and M.O. Steinmetz. 2009. An EB1-binding motif acts as a microtubule tip localization signal. Cell. 138:366-376.

Horgan, C.P., S.R. Hanscom, R.S. Jolly, C.E. Futter, and M.W. McCaffrey. 2010. Rab11-FIP3 links the Rab11 GTPase and cytoplasmic dynein to mediate transport to the endosomal-recycling compartment. J Cell Sci. 123:181-191.

Hotani, H., and H. Miyamoto. 1990. Dynamic features of microtubules as visualized by dark-field microscopy. Adv Biophys. 26:135-156.

Hotta, A., T. Kawakatsu, T. Nakatani, T. Sato, C. Matsui, T. Sukezane, T. Akagi, T. Hamaji, I. Grigoriev, A. Akhmanova, Y. Takai, and Y. Mimori-Kiyosue. 2010. Laminin-based cell adhesion anchors microtubule plus ends to the epithelial cell basal cortex through LL5alpha/beta. J Cell Biol. 189:901-917.

Ingber, D.E. 2003. Tensegrity I. Cell structure and hierarchical systems biology. J Cell Sci. 116:1157-1173.

Jacquemet, G., M.J. Humphries, and P.T. Caswell. 2013. Role of adhesion receptor trafficking in 3D cell migration. Curr Opin Cell Biol. 25:627-632.

Janson, M.E., M.E. de Dood, and M. Dogterom. 2003. Dynamic instability of microtubules is regulated by force. J Cell Biol. 161:1029-1034.

Jiang, K., S. Hua, R. Mohan, I. Grigoriev, K.W. Yau, Q. Liu, E.A. Katrukha, A.F. Altelaar, A.J. Heck, C.C. Hoogenraad, and A. Akhmanova. 2014. Microtubule minus-end stabilization by polymerization-driven CAMSAP deposition. Dev Cell. 28:295-309.

Kaverina, I., and A. Straube. 2011. Regulation of cell migration by dynamic microtubules. Semin Cell Dev Biol. 22:968-974.

Khanal, I., A. Elbediwy, C. Diaz de la Loza Mdel, G.C. Fletcher, and B.J. Thompson. 2016. Shot and Patronin polarise microtubules to direct membrane traffic and biogenesis of microvilli in epithelia. J Cell Sci. 129:2651-2659.

Kikuchi, K., and K. Takahashi. 2008. WAVE2- and microtubule-dependent formation of long protrusions and invasion of cancer cells cultured on three-dimensional extracellular matrices. Cancer Sci. 99:2252-2259.

Kodama, A., I. Karakesisoglou, E. Wong, A. Vaezi, and E. Fuchs. 2003. ACF7: an essential integrator of microtubule dynamics. Cell. 115:343-354.

Komlodi-Pasztor, E., D. Sackett, J. Wilkerson, and T. Fojo. 2011. Mitosis is not a key target of microtubule agents in patient tumors. Nat Rev Clin Oncol. 8:244-250.

Kravtsov, D., A. Mashukova, R. Forteza, M.M. Rodriguez, N.A. Ameen, and P.J. Salas. 2014. Myosin 5b loss of function leads to defects in polarized signaling: implication for microvillus inclusion disease pathogenesis and treatment. Am J Physiol Gastrointest Liver Physiol. 307:G992-G1001.

Lacy, P.E., S.L. Howell, D.A. Young, and C.J. Fink. 1968. New hypothesis of insulin secretion. Nature. 219:1177-1179.

Lansbergen, G., I. Grigoriev, Y. Mimori-Kiyosue, T. Ohtsuka, S. Higa, I. Kitajima, J. Demmers, N. Galjart, A.B. Houtsmuller, F. Grosveld, and A. Akhmanova. 2006. CLASPs attach microtubule plus ends to the cell cortex through a complex with LL5beta. Dev Cell. 11:21-32.

Mitchison, T.J. 2012. The proliferation rate paradox in antimitotic chemotherapy. Mol Biol Cell. 23:1-6.

Mogensen, M.M., J.B. Tucker, and H. Stebbings. 1989. Microtubule polarities indicate that nucleation and capture of microtubules occurs at cell surfaces in Drosophila. J Cell Biol. 108:1445-1452.

Mogessie, B., D. Roth, Z. Rahil, and A. Straube. 2015. A novel isoform of MAP4 organises the paraxial microtubule array required for muscle cell differentiation. Elife. 4:e05697.

Moss, D.K., G. Bellett, J.M. Carter, M. Liovic, J. Keynton, A.R. Prescott, E.B. Lane, and M.M. Mogensen. 2007. Ninein is released from the centrosome and moves bi-directionally along microtubules. J Cell Sci. 120:3064-3074.

Muroyama, A., L. Seldin, and T. Lechler. 2016. Divergent regulation of functionally distinct gamma-tubulin complexes during differentiation. J Cell Biol. 213:679-692.

Myers, K.A., K.T. Applegate, G. Danuser, R.S. Fischer, and C.M. Waterman. 2011. Distinct ECM mechanosensing pathways regulate microtubule dynamics to control endothelial cell branching morphogenesis. J Cell Biol. 192:321-334.

Nashchekin, D., A.R. Fernandes, and D. St Johnston. 2016. Patronin/Shot Cortical Foci Assemble the Noncentrosomal Microtubule Array that Specifies the Drosophila Anterior-Posterior Axis. Dev Cell. 38:61-72.

Ohara-Imaizumi, M., T. Ohtsuka, S. Matsushima, Y. Akimoto, C. Nishiwaki, Y. Nakamichi, T. Kikuta, S. Nagai, H. Kawakami, T. Watanabe, and S. Nagamatsu. 2005. ELKS, a protein structurally related to the active zone-associated protein CAST, is expressed in pancreatic beta cells and functions in insulin exocytosis: interaction of ELKS with exocytotic machinery analyzed by total internal reflection fluorescence microscopy. Mol Biol Cell. 16:3289-3300.

Olson, M.F., and E. Sahai. 2009. The actin cytoskeleton in cancer cell motility. Clin Exp Metastasis. 26:273-287.

Oyanagi, J., T. Ogawa, H. Sato, S. Higashi, and K. Miyazaki. 2012. Epithelial-mesenchymal transition stimulates human cancer cells to extend microtubule-based invasive protrusions and suppresses cell growth in collagen gel. PLoS One. 7:e53209.

Paranavitane, V., W.J. Coadwell, A. Eguinoa, P.T. Hawkins, and L. Stephens. 2003. LL5beta is a phosphatidylinositol (3,4,5)-trisphosphate sensor that can bind the cytoskeletal adaptor, gamma-filamin. J Biol Chem. 278:1328-1335.

Pelaseyed, T., R. Viswanatha, C. Sauvanet, J.J. Filter, M.L. Goldberg, and A. Bretscher. 2017. Ezrin activation by LOK phosphorylation involves a PIP2-dependent wedge mechanism. Elife. 6.

Picone, R., X. Ren, K.D. Ivanovitch, J.D. Clarke, R.A. McKendry, and B. Baum. 2010. A polarised population of dynamic microtubules mediates homeostatic length control in animal cells.

PLoS Biol. 8:e1000542.

Rhee, S., H. Jiang, C.H. Ho, and F. Grinnell. 2007. Microtubule function in fibroblast spreading is modulated according to the tension state of cell-matrix interactions. Proc Natl Acad Sci U S A. 104:5425-5430.

Ridley, A.J., M.A. Schwartz, K. Burridge, R.A. Firtel, M.H. Ginsberg, G. Borisy, J.T. Parsons, and A.R. Horwitz. 2003. Cell migration: integrating signals from front to back. Science. 302:1704-1709.

Riggs, B., B. Fasulo, A. Royou, S. Mische, J. Cao, T.S. Hays, and W. Sullivan. 2007. The concentration of Nuf, a Rab11 effector, at the microtubule-organizing center is cell cycle regulated, dynein-dependent, and coincides with furrow formation. Mol Biol Cell. 18:3313-3322.

Rondas, D., A. Tomas, and P.A. Halban. 2011. Focal adhesion remodeling is crucial for glucose-stimulated insulin secretion and involves activation of focal adhesion kinase and paxillin. Diabetes. 60:1146-1157.

Rondas, D., A. Tomas, M. Soto-Ribeiro, B. Wehrle-Haller, and P.A. Halban. 2012. Novel mechanistic link between focal adhesion remodeling and glucose-stimulated insulin secretion. J Biol Chem. 287:2423-2436.

Sanz-Moreno, V., and C.J. Marshall. 2010. The plasticity of cytoskeletal dynamics underlying neoplastic cell migration. Curr Opin Cell Biol. 22:690-696.

Schoumacher, M., R.D. Goldman, D. Louvard, and D.M. Vignjevic. 2010. Actin, microtubules, and vimentin intermediate filaments cooperate for elongation of invadopodia. J Cell Biol. 189:541-556.

Schwartz, M.A. 2010. Integrins and extracellular matrix in mechanotransduction. Cold Spring Harb Perspect Biol. 2:a005066.

Spangler, S.A., and C.C. Hoogenraad. 2007. Liprin-alpha proteins: scaffold molecules for synapse maturation. Biochem Soc Trans. 35:1278-1282.

Sudhof, T.C. 2012. The presynaptic active zone. Neuron. 75:11-25.

Sun, D., C.L. Leung, and R.K. Liem. 2001. Characterization of the microtubule binding domain of microtubule actin crosslinking factor (MACF): identification of a novel group of microtubule associated proteins. J Cell Sci. 114:161-172.

Suprenant, K.A., and W.L. Dentler. 1982. Association between endocrine pancreatic secretory granules and in-vitro-assembled microtubules is dependent upon microtubule-associated proteins. J Cell Biol. 93:164-174.

Szperl, A.M., M.R. Golachowska, M. Bruinenberg, R. Prekeris, A.M. Thunnissen, A. Karrenbeld, G. Dijkstra, D. Hoekstra, D. Mercer, J. Ksiazyk, C. Wijmenga, M.C. Wapenaar, E.H. Rings, and I.S.C. van. 2011. Functional characterization of mutations in the myosin Vb gene associated with microvillus inclusion disease. J Pediatr Gastroenterol Nutr. 52:307-313.

Tanaka, N., W. Meng, S. Nagae, and M. Takeichi. 2012. Nezha/CAMSAP3 and CAMSAP2 cooperate in epithelial-specific organization of noncentrosomal microtubules. Proc Natl Acad Sci U S A. 109:20029-20034.

Tomas, A., B. Yermen, L. Min, J.E. Pessin, and P.A. Halban. 2006. Regulation of pancreatic beta-cell insulin secretion by actin cytoskeleton remodelling: role of gelsolin and cooperation with the MAPK signalling pathway. J Cell Sci. 119:2156-2167.

Toya, M., S. Kobayashi, M. Kawasaki, G. Shioi, M. Kaneko, T. Ishiuchi, K. Misaki, W. Meng, and M. Takeichi. 2016. CAMSAP3 orients the apical-to-basal polarity of microtubule arrays in epithelial cells. Proc Natl Acad Sci U S A. 113:332-337.

Tran, T.A., L. Gillet, S. Roger, P. Besson, E. White, and J.Y. Le Guennec. 2009. Non-anti-mitotic concentrations of taxol reduce breast cancer cell invasiveness. Biochem Biophys Res Commun. 379:304-308.

Tredan, O., C.M. Galmarini, K. Patel, and I.F. Tannock. 2007. Drug resistance and the solid tumor microenvironment. J Natl Cancer Inst. 99:1441-1454.

Troutt, L.L., and B. Burnside. 1988. The unusual microtubule polarity in teleost retinal pigment epithelial cells. J Cell Biol. 107:1461-1464.

van der Vaart, B., W.E. van Riel, H. Doodhi, J.T. Kevenaar, E.A. Katrukha, L. Gumy, B.P. Bouchet, I. Grigoriev, S.A. Spangler, K.L. Yu, P.S. Wulf, J. Wu, G. Lansbergen, E.Y. van Battum, R.J.

Pasterkamp, Y. Mimori-Kiyosue, J. Demmers, N. Olieric, I.V. Maly, C.C. Hoogenraad, and A. Akhmanova. 2013. CFEOM1-associated kinesin KIF21A is a cortical microtubule growth inhibitor. Dev Cell. 27:145-160.

Varadi, A., E.K. Ainscow, V.J. Allan, and G.A. Rutter. 2002. Involvement of conventional kinesin in glucose-stimulated secretory granule movements and exocytosis in clonal pancreatic beta-cells. J Cell Sci. 115:4177-4189.

Wang, S., D. Wu, S. Quintin, R.A. Green, D.K. Cheerambathur, S.D. Ochoa, A. Desai, and K. Oegema. 2015. NOCA-1 functions with gamma-tubulin and in parallel to Patronin to assemble non-centrosomal microtubule arrays in C. elegans. Elife. 4:e08649.

Waterman-Storer, C.M., J. Gregory, S.F. Parsons, and E.D. Salmon. 1995. Membrane/microtubule tip attachment complexes (TACs) allow the assembly dynamics of plus ends to push and pull membranes into tubulovesicular networks in interphase Xenopus egg extracts. J Cell Biol. 130:1161-1169.

Wu, J., and A. Akhmanova. 2017. Microtubule-Organizing Centers. Annu Rev Cell Dev Biol.

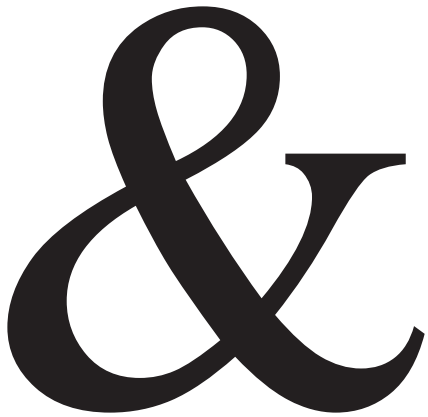

Addendum

Summary

Nederlandse samenvatting

Curriculum Vitae

List of publications

Dankwoord

Summary

Cell polarity refers to a fundamental property of eukaryotic cells, in which cellular components and structures are organized in an asymmetric fashion. In order to control their polarity, cells make use of microtubules, hollow polymers that extend throughout the cytoplasm. Due to the asymmetry of their building blocks, microtubules form polarized structures that play key roles in many biological processes. Their organization is tightly controlled by a wide range of intrinsic properties and associated factors.

In this thesis, we focus on the role of microtubules in three different cellular systems that strongly rely on tightly controlled polarity. We show that a wide range of microtubule associated proteins is involved in maintaining polarity thereby securing proper cell functioning. Despite the differences, we also identified multiple common factors indicating that the mechanisms that control microtubule organization are strongly conserved in many biological processes.

Positioning of the microtubule ends is essential for obtaining and maintaining cellular polarity. Over the years, multiple microtubule-associated and cortical proteins have been discovered that facilitate the interaction between microtubule plus ends and the cell cortex. In Chapter 2, we provide an overview of mammalian protein complexes that have been shown to participate in both cortical microtubule capture and exocytosis, thereby regulating the spatial organization of secretion. These complexes include microtubule plus-end tracking proteins, scaffolding factors, actin-binding proteins, and components of vesicle docking machinery, which together allow efficient coordination of cargo transport and release.

The polarity of migrating cells with ruffling leading lamellipodia and contractile rears is reflected by the asymmetric organization of the underlying microtubule cytoskeleton. The majority of the microtubules are anchored with their minus ends at the centrosome or the Golgi apparatus, which are typically positioned between the nucleus and the leading edge. The density of growing microtubule plus ends is higher in the direction of migration. Despite the fact that most *in vivo* migration occurs in a 3D environment, most studies are performed in 2D in which cells are plated on top of flat glass surfaces. In Chapter 3 we studied the role of microtubules in 3D cell migration and we found that the microtubule plus-end tracking protein SLAIN2, which suppresses catastrophes, is not required for 2D cell migration but is essential for mesenchymal cell invasion in 3D culture and in a mouse cancer model. We show that SLAIN2 inactivation does not affect Rho GTPase activity, trafficking, and focal adhesion formation. However, SLAIN2-dependent catastrophe inhibition determines microtubule resistance to compression and pseudopod elongation. Another plus-end tracking protein, CLASP1, is also needed to form invasive pseudopods because it prevents catastrophes specifically at their tips.

When microtubule growth persistence is reduced, inhibition of microtubule depolymerization is sufficient for pseudopod maintenance but not remodeling. We propose that catastrophe inhibition by SLAIN2 and CLASP1 supports mesenchymal cell shape in soft 3D matrices by enabling microtubules to perform a load-bearing function.

The microtubule cytoskeleton of epithelial cells undergoes a dramatic rearrangement during the cellular morphogenesis in which the cells shift from being unpolarized to an apico-basal polarized organization. In unpolarized cells the microtubule minus ends are clustered in the middle of the cell and the plus ends are pointing towards the cell periphery resulting in a typical radial microtubule array. As cells become polarized, however, the microtubule network changes and becomes arranged along the apico-basal axis, with the minus ends located at the apical side and the plus pointing towards the basal regions of the cell. In Chapter 4, we investigated the molecular mechanisms underlying the specific microtubule organization found in polarized epithelia. We found that in mammalian intestinal epithelial cells, the spectraplakin ACF7 specifically binds to CAMSAP3 and is required for the apical localization of CAMSAP3-decorated microtubule minus ends. Loss of ACF7 but not of CAMSAP3 or its homologue CAMSAP2 affected the formation of polarized epithelial cysts in 3D cultures. In short-term epithelial polarization assays, knockout of CAMSAP3, but not of CAMSAP2, caused microtubule reorganization into a more radial centrosomal array, redistribution of Rab11A-positive endosomes from the apical cell surface to the pericentrosomal region and inhibition of actin brush border formation at the apical side of the cell. We conclude that ACF7 is an important regulator of apico-basal polarity in mammalian intestinal cells and that a radial centrosome-centered microtubule organization can act as an inhibitor of epithelial polarity.

Cortical microtubule interactions are facilitated by the cortical microtubule stabilizing complex (CMSC). This multiprotein complex links microtubules to focal adhesions, thereby promoting the delivery of exocytotic cargo required for the turnover of focal adhesions. In Chapter 5, we describe that, in addition to its role in focal adhesion turnover, the CMSC is part of an insulin docking complex in pancreatic β-cells. We show that glucose dependent activation of focal adhesions leads to the recruitment of insulin docking complexes to focal adhesion rich cortical areas thereby forming potential docking platform for insulin containing granules. These insulin docking complexes consist of CMSC subunits and proteins involved in the exocytosis of neurotransmitters at the presynaptic active zone in neurons. The described experiments give new insights in the molecular machinery underlying the exocytosis of insulin from pancreatic β-cells.

To conclude, this thesis describes multiple mechanisms in which the microtubule cytoskeleton acquires asymmetry and promotes cell polarity, thereby contributing to the proper functioning of cells, tissues and organisms.

Nederlandse samenvatting

Celpolariteit verwijst naar een fundamentele eigenschap van eukaryotische cellen, waarbij cellulaire componenten en structuren op een asymmetrische manier georganiseerd zijn. Om hun polariteit te reguleren, maken cellen gebruik van microtubuli, holle polymeren die zich uitstrekken in het cytoplasma. Doordat de bouwstenen van microtubuli ook asymmetrisch zijn, vormen ze gepolariseerde structuren die sleutelrollen vervullen in meerdere biologische processen. De organisatie van microtubuli wordt strikt gereguleerd door een breed scala aan intrinsieke eigenschappen en geassocieerde factoren.

In dit proefschrift focussen we ons op de rol van microtubuli in drie verschillende cellulaire systemen die sterk afhankelijk zijn van een strikt gereguleerde polariteit. We laten zien dat een grote hoeveelheid microtubuli geassocieerde eiwitten betrokken zijn bij het in stand houden van polariteit, waardoor het functioneren van de cel wordt gewaarborgd. Naast de verschillen, hebben we meerdere overeenkomende factoren geïdentificeerd. Dit toont aan dat de mechanismen die de organisatie van microtubuli reguleren sterk geconserveerd zijn in meerdere biologische processen.

Het positioneren van de microtubuli uiteinden is essentieel voor het verkrijgen en onderhouden van cellulaire polariteit. Door de jaren heen zijn er meerdere microtubuli geassocieerde en corticale eiwitten ontdekt die de interactie tussen plus-einden van microtubuli en de celcortex faciliteren. In hoofdstuk 2 geven we een overzicht van eiwittencomplexen waarvan is aangetoond dat ze betrokken zijn bij zowel corticale microtubuli verankering en exocytose, waardoor ze de ruimtelijke organisatie van secretie reguleren. Deze complexen omvatten eiwitten die binden aan microtubuli plus-einden, verbindende factoren, actine-bindende eiwitten en componenten die betrokken zijn bij het vasthouden van secretie-blaasjes. Tezamen coördineren deze eiwitten transport en secretie van cellulaire lading.

De polariteit van migrerende cellen met plooiende lamellipodia aan de voorkant en samentrekkende achterkant wordt weerspiegeld door de asymmetrische organisatie van het onderliggende microtubuli cytoskelet. De meerderheid van de microtubuli zijn verankerd met de min-einden aan het centrosoom of het Golgi apparaat, welke zich bevinden tussen de celkern en de voorkant van de cel. De dichtheid van groeiende microtubuli plus-einden is groter in de richting van de migratie. Ondanks het feit dat de meeste *in vivo* migratie plaatsvindt in 3D, is het merendeel van de celmigratie onderzoeken uitgevoerd in 2D, waarbij cellen op platte glaasjes worden gekweekt. In hoofdstuk 3 hebben we de rol van microtubuli in 3D celmigratie bestudeerd. Hierbij hebben we ontdekt dat het microtubuli plus-eind bindende eiwit SLAIN2, welke microtubuli catastrofes onderdrukt, niet nodig is voor 2D cel migratie maar essentieel is voor me-

senchymale celinvasie in 3D celkweken en in een muis tumormodel. We laten zien dat SLAIN2 inactivatie geen effect heeft op Rho GTPase activiteit, subcellulair transport en de formatie van focale adhesies. Echter, SLAIN2-afhankelijke catastrofe inhibitie beïnvloed de weerstand van microtubuli tegen compressie en pseudopodie elongatie. Een ander plus-eind bindende eiwit, CLASP1, is ook essentieel voor de formatie van invasieve pseudopodiën omdat het catastrofes voorkomt specifiek in de punt van de pseudopodie. Het verhinderen van microtubuli depolymerisatie is voldoende voor het in stand houden, maar niet voor het remodelleren van pseudopodiën, als de groei van microtubuli wordt geremd. We stellen dat catastrofe inhibitie door SLAIN2 en CLASP1 de vorm van mesenchymale cellen in zachte weefsels ondersteund door microtubuli in staat te stellen weerstand te bieden aan tegenwerkende krachten.

Het microtubuli cytoskelet van epitheelcellen ondergaat een drastische herschikking tijdens de cellulaire morfogenese, waarbij de cellen veranderen van ongepolariseerd naar een apicale-basale polarisatie. In ongepolariseerde cellen komen de microtubuli min-einden samen in het midden van de cel en wijzen de plus-einden richting de cel periferie wat resulteert in een radiale microtubuli organisatie. Als de cellen polariseren, veranderd de microtubuli organisatie in een gepolariseerd netwerk waarbij de min-einden aan de apicale kant lokaliseren en de plus-einden richting de basale kant van de cel wijzen. In hoofdstuk 4 hebben we de moleculaire mechanismen onderzocht die verantwoordelijk zijn voor de specifieke organisatie van microtubuli in gepolariseerd epitheel. We hebben ontdekt dat, in epitheelcellen uit de darm, de spectraplakin ACF7 specifiek aan CAMSAP3 bindt en daarbij de apicale lokalisatie van CAMSAP3 gebonden microtubuli min-einden reguleert. In tegenstelling tot CAMSAP2 en CAMSAP3 leidde het verlies van ACF7 tot afwijkingen in de formatie van gepolariseerde acini in 3D kweken. Daarnaast leidde de afwezigheid van specifiek CAMSAP3 in epitheel polarisatie over een korte termijn tot reorganisatie van de microtubuli in een radiaal centrosomaal netwerk, de redistributie van Rab11A-positieve endosomen van het apicale celoppervlak naar het pericentrosomale gebied en een remming van de aanmaak van microvilli aan de apicale kant van de cel. We concluderen dat ACF7 een belangrijke schakel is in de regulatie van apicale-basale polariteit in darmcellen en dat een centrosomaal microtubuli netwerk de polariteit van epitheel kan verstoren.

Corticale microtubuli interacties worden gefaciliteerd door het corticale microtubuli stabilisatie complex (CMSC). Dit complex, bestaande uit meerdere eiwitten, koppelt microtubuli aan focale adhesies, waardoor het de aanvoer van exocytotische lading die nodig is voor de afbraak van focale adhesies stimuleert. In hoofdstuk 5 beschrijven we dat, naast de rol in de afbraak van focale adhesies, het CMSC onderdeel is van een complex dat betrokken is bij de binding en secretie van insuline in β-cellen van de alvleesklier. We laten zien dat de glucose afhankelijke activatie van focale adhesies leidt tot de rekrutering van deze complexen naar focale adhesie rijke gebieden waarbij ze

potentiele bindings-platformen voor insuline-blaasjes vormen. Deze platformen bestaan uit onderdelen van het CMSC en eiwitten die betrokken zijn bij de exocytose van neurotransmitters in de presynaptische actieve zone van neuronen. De beschreven experimenten geven nieuwe inzichten in de onderliggende moleculaire machinerie die betrokken is bij de exocytose van insuline uit β-cellen van de alvleesklier.

Dit proefschrift beschrijft meerdere mechanismen waarbij het microtubuli cytoskelet asymmetrie verwerft en celpolariteit promoot. Hierbij draagt het bij aan het goed functioneren van cellen, weefsels en organismen.

Curriculum Vitae

Ivar Noordstra was born on the 21st of May 1989 in Kamperzeedijk, a small rural village that is part of Genemuiden, The Netherlands. In 2006 he obtained his high school degree (Havo) from Ichthus College IJsselmuiden/Kampen. Driven by his interest for biology, Ivar continued with the study Biology and Medical Laboratory Research (Biologie en Medisch Laboratorium Onderzoek) at Saxion Hogescholen Deventer, from which he obtained his bachelor's degree in 2010. As part of the bachelor's program, he performed multiple research projects including an internship at the department of Immunology from Erasmus Medisch Centrum (MC) Rotterdam, where he studied the effects of oligopeptides on cell migration in a transwell system in the group of Dr. Wim Dik. During a second internship at the Hubrecht Institute, Utrecht, Ivar focussed on the roll of Glepp1 in zebrafish embryonic development in the group of Prof. Dr. Jeroen den Hertog. After obtaining his bachelor's degree and motivated by his interest in research, Ivar continued his education in the field of life sciences and started the biomedial sciences master Cancer Genomics and Developmental Biology at the University of Utrecht, which he finished in 2012. During this program he joined the group of Dr. Madelon Maurice at the department of Cell Biology from Universitair Medisch Centrum (UMC) Utrecht, to further develop a study regarding internally flag-tagged Wnt3a: A novel tool to study Wnt signaling. A second internship was performed at the department of Cell Biology from Universiteit Utrecht (UU) in the group of Prof. Dr. Anna Akhmanova, in which Ivar analyzed ELKS function and dynamics by high-resolution microscopy. His fascination for the field of cytoskeletal dynamics and his growing interest in fundamental research resulted in the start of a PhD research project in 2012 under the supervision of Prof. Dr. Anna Akhmanova. The results Ivar obtained during his PhD research project are described in this thesis.

List of publications

Linking cortical microtubule attachment and exocytosis
Noordstra I, Akhmanova A.
F1000Res. 2017 Apr 12;6:469

Mesenchymal cell invasion requires cooperative regulation of persistent microtubule growth by SLAIN2 and CLASP1
Bouchet BP*, Noordstra I*, van Amersfoort M, Katrukha EA, Ammon YC, Ter Hoeve ND, Hodgson L, Dogterom M, Derksen PWB, Akhmanova A.
Dev Cell. 2016 Dec 19;39(6):708-723

Control of apico-basal epithelial polarity by the microtubule minus-end-binding protein CAMSAP3 and spectraplakin ACF7
Noordstra I, Liu Q, Nijenhuis W, Hua S, Jiang K, Baars M, Remmelzwaal S, Martin M, Kapitein LC, Akhmanova A.
J Cell Sci. 2016 Nov 15;129(22):4278-4288

Molecular pathway of microtubule organization at the golgi apparatus
Wu J, de Heus C, Liu Q, Bouchet BP, Noordstra I, Jiang K, Hua S, Martin M, Yang C, Grigoriev I, Katrukha EA, Altelaar AF, Hoogenraad CC, Qi RZ, Klumperman J, Akhmanova A.
Dev Cell. 2016 Oct 10;39(1):44-60

*Authors contributed equally

Dankwoord

Wederom een leeg document voor me, maar deze keer als afsluiting van een onvergetelijke periode. Een promotietraject is zoals ze zeggen “een weg van ups-and-downs”, maar zeker de moeite waard! Als ik terugkijk op de afgelopen jaren kan ik alleen maar zeggen dat ik een fantastische tijd heb gehad. Zoveel geleerd, zoveel mooie dingen gedaan en zoveel mensen ontmoet. Kortom: “Time flies when you’re having fun!” Vijf jaar zijn voorbij gevlogen en in deze periode heb ik mij gesteund gevoeld door een groot aantal mensen, zowel op het lab als daarbuiten. Om deze reden wil ik jullie allemaal ongelofelijk bedanken!

Daarbij wil ik beginnen met mijn promotor. Beste Anna, dankjewel dat ik in jouw groep mijn promotietraject heb mogen doorlopen. Een PhD is, zoals velen kunnen beamen, een bewogen rit, maar met jou begeleiding heb ik al die tijd het gevoel gehad dat het goed zou komen. Dit weerspiegelt gelijk één van je grote kwaliteiten: het managen van een groep mensen/wetenschappers en het sturen van meerdere onderzoeken. Daarnaast heb ik ongelofelijk veel respect voor jou als wetenschapper. Je kennis en kwaliteiten wat betreft wetenschappelijk onderzoek en onderwijs hebben mij altijd enorm geïnspireerd en zullen mij ongetwijfeld nog veel vaker inspireren tijdens de rest van mijn carrière. Heel veel dank voor jou supervisie en ik wens je heel veel goeds toe voor de toekomst op zowel wetenschappelijk als persoonlijk vlak.

Casper, bedankt voor al je input tijdens de maandag en vrijdag meetings. Jouw inzichten hebben bijgedragen aan het succesvol afronden van meerdere projecten. Blijkbaar lijken de 3D migrerende cellen toch in meerdere opzichten op neuronen! Ik bewonder jouw werk en manier van kijken naar wetenschap en heb ontzettend veel respect voor hoe jij inmiddels twee labs managet. Ik wens je heel veel succes toe zowel in Utrecht als in San Francisco. Sander, bedankt voor je oprechte interesse en vele vragen tijdens de gezamenlijke celbiologie/ontwikkelingsbiologie meetings. De veelzijdigheid van jullie werk heeft me altijd enorm aangesproken. Daarnaast wil ik je bedanken voor het plaatsnemen in mijn promotiecommissie. Ook de andere leden van mijn promotiecommissie, Madelon Maurice, Judith Klumperman, Paul van Diest en Alessandra Cambi, bedankt voor het lezen en beoordelen van mijn proefschrift.

Dear Amol, about five years ago we started our PhDs around the same time. In those 5 years, you did not only turn out to be a great colleague but also a fantastic friend. From dealing with bears in Yosemite NP to surviving Airbnbs and snowstorms in Harlem, New York, we always had great fun. From getting lost in the forest while training for a half marathon (which made us run even more than the actual race distance), to driving through a ridiculous rain burst in Germany on our way to a historical half-timbered house, we always survived! I cannot count all the awesome activities we did on two

hands but I will never forget one of them. To also end with a crazy activity we decided to defend our PhDs on the same day while being each other's paranymph. I cannot think of a better way to end this period. I wish you all the best for your future career and we will definitely see each other again, somewhere in the world, to do some more great things! Dear Maud, thank you very much for being my second paranymph. I really appreciate the way you are pursuing your scientific career. How you are dealing with your family and work shows of strong perseverance and deserves much respect. Your perseverance is also reflected by our morning swims. While I am completely bored after 30 minutes of swimming up and down the same lane over and over again, you always seem to easily swim close to one hour without losing any speed. With great pleasure I have seen the development of your own story and you can be very proud of it. Without any doubt I can say that your expertise is a great addition to the lab. I also want to wish you all the best for the future and I am glad that you will be standing next to me during my defense!

Lukas, bedankt voor je input tijdens de ontwikkeling en publicatie van de migratie en epitheel projecten. De specialiteiten van jouw lab hebben absoluut bijgedragen aan het publiceren van deze studies. Esther, Dankjewel voor al je hulp bij het managen van de *in vivo* experimenten. Ik wens je ontzettend veel kracht toe voor nu en in de toekomst! Corette, Paul en Harold bedankt voor de belangstelling in onze projecten en de gezelligheid tijdens lunch, borrels en uitjes.

Ben, the first years of my PhD we actively collaborated on the migration project. In fact, you taught me basically everything that has anything to do with cell migration. Thank you very much for all your time and effort. It was great to see how passionate you could be about completely different things. Whether you were talking about science, building guitars or diving, the stories were always amazing. I wish you all the best for the future and good luck doing science, music or maybe something completely different (I also heard you talking about a goat farm once?). Eugene, the link in so many different publications of the department. Your expertise is absolutely indispensable. Thank you very much for all your help regarding biophysics, modeling, microscopy, programming etc. etc. etc. etc. And of course many thanks for being a great roomie!

Jingchao, the one and only Dr. Wu! It was great to spend the biggest time of our PhDs together in the lab. All the time I greatly appreciated you as a scientist but even more as a true friend. The trip we made to Heidelberg and later on to the Eifel to do some hiking was absolutely awesome. Amol and I got to know you as a true animal lover. We also had great fun in Giethoorn and I will never forget the moment that you steered our boat right in to a group of innocent canoeing tourists. Luckily everybody survived. I wish you all the best in your scientific and personal life and I am sure we will see each other again. Qingyang, first of all I would like to thank you for your contribution to the epithelial paper. Your work greatly helped to publish the study. Secondly, and even more important, I would like to thank you for being such a nice colleague. It was great

to share the lab with you and I wish you all the best for the future together with Stefan. Helma, bedankt voor de mooie tijd die we zowel binnen als buiten het lab hebben gehad. Het was geweldig dat we mee mochten genieten van jullie bruiloft. Echt een top feestje! Ook de fotografiecursus van Roel bij jullie thuis was ontzettend leuk en erg leerzaam. Ik wens jullie, met z'n drietjes (Wat super leuk!!), een geweldige toekomst toe! Peter Jan, mr. IT-wannabe-oftochlievernie. Als student bij Helma heb je al laten zien dat je over een groot doorzettingsvermogen beschikt. Bij niemand anders heb ik pull downs en western blots zo zien evolueren als bij jou. Nu je aan je eigen promotie begonnen bent, zie ik dezelfde eigenschappen weer terug die ongetwijfeld zullen leiden tot een zeer succesvolle periode. Ik wil je bedanken voor de tijd samen op het lab en mocht het uiteindelijk toch niet helemaal lekker lopen, dan kun je altijd nog een carrière in de IT overwegen. Ik weet in ieder geval bij wie ik moet zijn als ik problemen met mijn computer heb. York, mijn tweede bench-buurman. Als ik alles met jouw naam erop niet meer aan zou mogen raken, dan zou er niet veel meer voor mij overblijven. Gelukkig sta jij altijd klaar om je spullen uit te lenen en anderen te helpen. Keurig georganiseerd en dat zie je terug in je werk. Heel erg bedankt voor je hulp tijdens de afronding van het migratie project. Ik wens je heel veel fijne uren toe in je auto (of weinig uren op de fiets), heel veel mooie kuilen in het strand en bovendien een hele succesvolle PhD en een mooie toekomst! Chao, probably the biggest FC Utrecht fan of the department. It was great to visit a match with you and the others. Thank you for the nice time in the lab and good luck with your projects (with or without EB's). Fangrui, from the moment you entered the lab I noticed that you really like singing. Keep this cheerful attitude and you will definitely have a good time in the lab. Dieudonnée, Ruben and Chiung-Yi, maybe not fulltime but definitely part of the Akhmanova lab. Thank you very much for all the nice conversations and I wish you all the best for your PhD projects. Andrea and Carol, although it is already quite some time ago that both of you left the lab, I really would like to thank you for the great time we had in my first years. Good luck with your post-docs and I am sure we will see each other again in the future.

Ilya, I cannot remember how often I entered your office with a microscopy problem that you could solve by pressing a button that I tried at least twenty times before. Thank you very much for your magic microscopy hands and all your help regarding imaging. Ruddi, thank you for being such a nice roomie. It was great to see that you happily stick to your siesta tradition in the afternoon. Good luck with you liposomes and I wish you and your family all the best. Ankit, visiting you and your family at your place was absolutely amazing. I think we, Dutch people, can learn a lot from the cooking abilities of your wife. Good luck with your post-doc and I wish you and your family all the best for the future. Kai and Shasha, incredible sources of constructs and knowledge. The amount of data you guys generate and the high quality of your work is just amazing. Thank you very much for all your help and all the materials you provided. I wish you all

the best running your own lab back in China and of course a fantastic time as a reunited family. Hari and Renu, although you guys also left some time ago I would still like to thank you for your help in the first year of my PhD. Good luck with your careers!

Je leert nog verrassend veel bij, als je zelf iemand iets moet leren. Jan, Heleen, Jessie, Jooske, Matthijs en Bas. Het was me een waar genoegen om jullie tijdens je stages te mogen begeleiden. Ontzettend bedankt voor al jullie hulp! Het vervult me toch wel een beetje met trots als ik zie hoe jullie carrières zich ontwikkelen. Heel veel succes en ik weet zeker dat we elkaar vaker gaan zien.

Fons, officieel met pensioen maar eigenlijk nooit echt weg. Een aantal jaar heb ik, samen met jou, de microtubuli module voor het JCU begeleidt. Dit heb ik altijd met ontzettend veel plezier gedaan. Bedankt voor je aanstekelijke vrolijkheid en geniet van je welverdiende vrije dagen. Laurens, inmiddels hebben wij ook een aantal keer samen gewerkt aan onderwijs gerelateerde zaken. Bedankt voor de mooie tijd en ik wens je heel veel succes toe voor de toekomst.

Max, vanaf onze masters heb ik jou leren kennen als een zeer betrokken en gepassioneerd persoon. Bedankt voor de mooie tijd die we hebben gehad zowel op het lab als daarbuiten. Het was super om mee te mogen genieten van jullie bruiloft en ik wens jou en Jasmijn een fantastische tijd toe in de VS! Lars, ook jou ken ik al vanaf onze masters en we zijn op hetzelfde moment onze promotietrajecten ingegaan. Jouw passie voor en kijk op wetenschap heeft me altijd enorm aangesproken! Naast wetenschap is ook het fietsen een gedeelde passie, wat heeft geleid tot één van de sportieve hoogtepunten van de afgelopen jaren: De kersentocht! Ontzettend leuk om dat samen met jullie te doen. Ik wens jou en je familie een fantastische toekomst toe en we komen elkaar ongetwijfeld nog weer tegen. Riccardo, another bicycle fan. Doing the cherry tour with Lars and you was awesome. Good luck finishing your PhD and climbing many more mountains in the future. Wilco, ontzettend bedankt voor je hulp tijdens het afronden van het epitheel project. Jouw stabiele lijnen en feedback hebben enorm bijgedragen aan deze publicatie. Ik wens je heel veel succes toe voor het vervolg van je carrière. Roderick, de man van de mooiste plaatjes. Ik denk dat je bijna elke image competition wel zou kunnen winnen! Ik vind het ontzettend gaaf dat we de door jullie geoptimaliseerde superresolutie technieken nu toe kunnen passen op ons insuline secretie project. Heel veel succes in de toekomst en we gaan elkaar ongetwijfeld nog weer tegenkomen op meetings waar dan ook ter wereld. Sybren, bedankt voor je hulp met de *in vivo* experimenten. Het duurde even voor we doorhadden hoe we de pancreas moesten isoleren maar mede dankzij jou hulp is het uiteindelijk toch gelukt. Ik wens je veel succes toe bij het afronden van je PhD. Bas, Suzanne and Marina, organizing a lab outing with you guys was a lot of fun! I wish you all the best for the future. Bart, altijd vrolijk en altijd in voor een grap. Samen met jou, Ben en Aron naar Neil Young was echt te gek! Ik wil je ontzettend bedanken voor al je hulp op het lab! Phebe, wat zou het een zooitje zijn zonder jou. Absoluut onmisbaar op

zoveel fronten. Heel erg bedankt voor al je hulp op de voor- en achtergrond! Margriet, Sofia and René, thank you very much for the technical support and the great time in the lab. Cátia, Thanks to you I will never forget the meaning of the word 'bouton'. You did a great job during your PhD and I wish you and Reinier all the best for the future. We might see each other again during one of the PEC Zwolle matches! Hai Yin, ik heb ongelofelijk veel respect voor hoe jij bent teruggekomen. Heel veel succes bij het afronden van je PhD en ik wens je een fantastische toekomst toe.

Josta, Petra, Mariella, Marta, Marleen, Sam, Marijn, Kah Wai, Robert and Joanna, it is great to see that you all successfully finished your PhDs. Thank you very much for the great time we had together and lots of success for the next steps in your careers. Anne, Yujie, Feline, Xingxiu, Dennis, Elske, Robin, Lisa, Jessica, Jian and Nicky, keep up the PhD smile and I am sure you will all finish successfully! Thank you very much for the great time and we will see each other again. Phil, Laura, Anaël, Karin, Elena, Gabi, Amélie, Martin, Lena, Inês, Mithila, Olga, Desiree, Eliana and Eitan. It was great to have you as colleagues. Thank you very much for the nice time in the lab and good luck with your future careers. Sabrina, Raimond, Bram, Purvi, Marta, Katerina, Dusan, Rachid, Vida and Sara, it is truly amazing what you can do with nanobodies. I will not forget the always returning lama smile during your talks on Mondays. Keep up the good work! Inge, Mike, Adri, Aniek, Juliane, Helena, Molly, Vincent, João, Janine, Amalia, Victoria, Amir, Jana, Thijs, Suzan and Selma, the awesome neighbors from the east wing. Thank you very much for all your input during the combined Monday meetings. I really enjoyed the diversity in different topics (worms are cool!) and I wish you all the best for the future.

Aan alle vrienden van de Kamperzeedijk en omstreken. Soms is het heerlijk om gewoon even uit het academische wereldje te kunnen stappen. De Kamperzeedijk is bij uitstek de plek om dit te doen. Inmiddels kennen we elkaar al bijna 25 jaar en nog steeds zijn we een hechte groep vrienden. Het is fantastisch om te zien hoe iedereen zijn leven invult op zijn of haar eigen manier. Heel erg bedankt voor jullie welgemeende interesse in ons werk, maar bovenal: heel erg bedankt dat jullie nog steeds dezelfde groep vrienden zijn!

3 broers, zo verschillend maar toch ook zo hetzelfde. Aron en Niels, jullie zijn niet alleen mijn broers maar ook mijn beste vrienden. Ik ben ongelofelijk trots op wat jullie allemaal al hebben bereikt! Bedankt dat jullie altijd voor Lilian en mij klaarstaan en bedankt voor de interesse die jullie altijd hebben getoond. De momenten dat wij samen zijn, zijn voor mij enorm dierbaar en ik weet zeker dat er nog heel veel bijzondere momenten bij gaan komen.

Pap en mam, waar moet ik beginnen? Ik kan jullie niet genoeg bedanken voor jullie steun. Het is zo ontzettend belangrijk geweest de afgelopen jaren. Het gevoel dat er altijd mensen zijn die achter je staan, no matter what! Bedankt dat jullie ons de vrijheid

hebben gegeven om ons eigen plan te trekken en te ontwikkelen tot wie we nu zijn. Bij jullie zullen we nooit voor een gesloten deur komen te staan. Niet naar binnen en niet naar buiten.

Lieve Lilian, 5 jaar geleden kwamen we net terug uit Australië. Een onvergetelijke reis en het begin van iets heel bijzonders. Inmiddels zijn we alweer zes jaar samen en ik ben er ongelofelijk trots op dat ik je nu mijn vrouw mag noemen. Heel erg bedankt voor al je steun de afgelopen jaren en ik kijk ontzettend uit naar alle avonturen die we samen gaan beleven. Ik hou van jou!